Investigating the Effect of Cell Culture Compositions on Mitochondrial Metabolism, Dynamics, and Transcriptome and Proteome of cells

Fereshteh Moradi, MSc. MBS

Biological Sciences

Submitted in partial fulfillment
of the requirements for the degree of

Doctor of Philosophy

Faculty of Mathematics and Science, Brock University

St. Catharines, Ontario

ABSTRACT

The phytoestrogen Resveratrol (RES) is a natural polyphenol that has been detected in more than 70 plant species. RES has structural similarity to mammalian estrogens and can bind to estrogen receptors, eliciting genomic and non-genomic effects. Both RES and physiological estrogens like 17-β-estradiol (E_2) have wide-ranging effects on mitochondria. In this thesis, I began by investigating RES's effects on mitochondrial network dynamics (Chapter 2) and discovered a pro-fusion activity apparently mediated by the mitofusin enzyme Mfn2. RES stimulated mitochondrial network hyper-fusion morphology in all three cell lines investigated (C2C12 (mouse myoblast), PC3 (prostate cancer), and MEFs (mouse embryonic fibroblast)), but the effect was absent in Mfn2-null MEFs. As this work was being completed; several research groups introduced 'physiologic cell culture media' that are modeled on the human plasma metabolome. I co-authored a study (not in this thesis) demonstrating that RES's effects on mitochondrial dynamics are dependent on cell culture conditions. To follow up on this, I investigated whether E_2's mitochondrial effects might also be dependent on the cell culture environment, and showed conclusively that this is indeed the case, using C2C12 cells as a model system (Chapter 3). These results and those published by others in 2017-2019 suggested that medium composition can profoundly affect cellular functions. In Chapter 4, I followed this up by studying how culture conditions affect mitochondrial bioenergetics and network morphology using four cancer cell lines and showed that this is a significant issue. Finally, to gain a more complete understanding of this phenomenon, I completed a full transcriptomic and proteomic analysis of media effects using MCF7 breast cancer cells as a model (Chapter 5). I showed that hundreds of transcripts and proteins are affected according to culture conditions. Taken together, the results presented in this thesis emphasize the significant extent to which the cell culture environment affects experimental outcomes, particularly with respect to mitochondrial bioenergetics and dynamics. This information contributes to the development of cell culture experiments providing results that can be translated *in vivo*.

ACKNOWLEDGEMENTS

First and foremost, I would like to express my sincere gratitude to my supervisor, Dr. Jeff Stuart, for the invaluable expertise, support, and constant guidance he gave me through my research project and thesis writing. His passion for science and his optimism are truly inspiring! Dr. Stuart- you have been a great mentor and I am grateful for allowing me to experience this incredible journey in your lab. You have made a profound impact on my professional life, and I cannot thank you enough. I would not have been able to complete this degree without you.

I would like to thank my thesis advisory committee members, Dr. Gaynor Spencer and Dr. Rebecca MacPherson for the time they dedicated and their recommendations on the progress of my project. I would also like to thank Dr. Ping Liang and Dr. Sarah Alderman for their collaborations. I acknowledge Dr. Val Andrew Fajardo for all his support and guidance over the course of my study at Brock University; he has done instrumental contributions toward my success. I must express my heartfelt gratitude to all past and present members of the Dr. Stuart's lab for fostering an extremely positive friendly work environment. Specifically, I would like to extend a special thank you to Joao Fonseca, Andrew Valente, Olivia Bagshaw, Christopher Moffatt, Holt Messner, and Georgina Gardner for all their support as colleagues and most importantly as friends. I will never forget our lab lunches and talking! I would express my thank you to Lucas Maddalena for being an incredible senior colleague; he trained me patiently when I joined the lab. I also like to thank Ilona Hilson for her collaboration with RNA-seq data analysis, and Eric De Hoog for being always available to help.

To Dr. Aleksandar Necakov (Sasha), your passion and excitement for science and your extremely caring attitude toward people around you have been truly inspirational to me. I also like to thank Sasha's lab members (Marvel Megaly, Anel Turgambayeva, Gregory Foran, Ryan Hallam) for all the great fun we had. Specifically, I thank Gregory for his always readiness to assist and troubleshoot techniques. Finally, I cannot find any words to express my gratitude to my incredible family for their love and always supporting my decisions even when I left them and came to Canada. I would not finish this endeavour without their constant support.

TABLE OF CONTENTS

List of figures

CHAPTER1

CHAPTER 2

CHAPTER 3

CHAPTER 4

CHAPTER 5

APPENDIX

List of tables

CHAPTER 1

CHAPTER 5

APPENDIX

List of Abbreviations

ANOVA	Analysis of variance
ATP	Adenosine triphosphate
BSA	Bovine serum albumin
CLAHE	Contrast limited adaptive histogram equalization
CREB	cAMP response element binding protein
DAVID	Database for Annotation**,** Visualization and Integrated Discovery
DEGs	Differentially expressed genes
DEPs	Differentially expressed proteins
DMEM	Dulbecco's modified eagle medium
DMSO	Dimethyl sulfoxide
DPN	Diaryl propionitrile
DRP1	Dynamin-related protein 1
DTT	DL-dithiothreitol
E_2	17-β estradiol
EDTA	Ethylenediaminetetraacetic acid
ECAR	Extra cellular acidification
ER	Estrogen receptor
ETC	Electron transport chain
FBS	Fetal bovine serum
FC	Fold Change
FCCP	Carbonyl cyanide-p-trifluoromethoxy phenyl hydrazone
FIH	Factor inhibiting HIF
FIJI	FIJI is just ImageJ
FMN	Flavin mononucleotide
FOXO1	Fork head box class-O

FPRKM	Fragments Per Kilobase of transcript per Million mapped reads
G418	Geneticin
GO	Gene Ontology
GPx	Glutathione peroxidase
GR	Glutathione reductase
GRx	Glutaredoxin
GSH	Glutathione
H_2O_2	Hydrogen peroxide
HEPES	(4-(2-hydroxyethyl)-1-piperazineethanesulfonic acid
HIF-1α	Hypoxia inducible factor-1α
HPLM	Human plasma like medium
HRE	Hypoxia response elements
HRP	Horseradish peroxidase
IMM	Inner mitochondrial membrane
iTRAQ	Isobaric tags for relative and absolute quantification
KEGG	Kyoto Encyclopedia of Genes and Genomes
LDH	Lactate dehydrogenase
mEFP	Modified emerald fluorescent protein
MEM	Modified eagle medium
MiNA	Mitochondrial network analysis tool
Mfn2	Mitofusin2
MPP	Mitochondrial processed peptidase
NAD+	Nicotinamide adenine dinucleotide (oxidized)
NADH	Nicotinamide adenine dinucleotide (reduced)
NADPH	Nicotinamide adenine dinucleotide phosphate
NO	Nitric oxide
NOX	NADPH oxidase

NRF	Nuclear respiratory factor
Nrf2	Nuclear factor (erythroid derived 2) related factor 2
O_2	Oxygen
$O^{2\bullet-}$	Superoxide onion
OCR	Oxygen consumption rate
•OH	Hydroxyl radical
OMM	Outer mitochondrial membrane
ONOO-	Peroxynitrite
OPA1	Optic trophic 1
OXPHOS	Oxidative phosphorylation
PARL	Presenilin-associated rhomboid-like protein
PBS	Phosphate-buffered saline
PDH	Pyruvate dehydrogenase
PGC-1α	Peroxisome proliferator-activated γ receptor coactivator 1α
PHD	Prolyl hydroxylase domain
PINK1	PTEN-induced kinase 1
Plasmax	Plasma like medium
PPT	1,3,5-tris (4-hydroxyphenyl)-4-propyl-1H-pyrazole
PPP	Pentose phosphate pathway
Prx	Peroxiredoxin
RES	Resveratrol
ROS	Reactive oxygen species
SEM	Standard error of the mean
SIRT1	NAD+-dependent protein deacetylase Sirtuin 1
SOD	Superoxide dismutase
MnSOD	Manganese superoxide dismutase

TCA	Tricarboxylic acid
TFAM	Transcription factor A mitochondrial
TMRM	Tetramethyl rhodamine, methyl ester
Trx	Thioredoxin
TrxR	Thioredoxin reductase
VHL	Von Hippel-Lindau
ΔΨm	Mitochondrial membrane potential

CHAPTER 1: Introduction and Literature Review

GENERAL INTRODUCTION

Resveratrol (trans-, 3 ,4′ ,5-trihydroxystilbene; RES) is a phytochemical belonging to the structural class of polyphenols, which constitute one of the most abundant and widely distributed groups of natural products in plants. Polyphenols are derived from a common intermediate, phenylalanine, or a similar precursor, shikimic acid. Polyphenols are abundant in a wide variety of edible plants that are consumed as food (e.g., vegetables, cereals, legumes, fruits, nuts) and beverages (e.g., wine, cider, beer, tea, cocoa). These phytochemicals are secondary metabolites with integral functions in plant physiology, including the inhibition of pathogen growth and protection against ultraviolet (UV) radiation (Lagouge et al., 2006; Wu and Hsieh, 2011; Stuart and Robb, 2011). In mammalian cells, this compound shows a wide range of beneficial effects, including activity against glycation, oxidative stress, inflammation, neurodegeneration, and cancer (reviewed in Galiniak et al., 2019).

RES was first isolated in 1939 by Takaoka from *Veratrum grandiflorum* and appears as two isomeric types (cis and trans); the trans isoform is more abundant and has the most potent therapeutic benefits (see below in Figure1.1) (Cardile et al., 2007; Weiskirchen and Weiskirchen, 2016). Epidemiological research supporting the positive correlation between a high dietary consumption of polyphenols and the reduced risk of developing numerous chronic diseases and cancers, has markedly increased interest in the investigation of such molecules (reviewed in De Paepe and Van Coster, 2017). Most notably, RES gained a resurgence of interest in the scientific community following its identification as a powerful activator of SIRT1, an NAD+-dependent protein lysine deacetylase of the Sirtuin family. Sirtuins regulate a wide range of physiological functions, from energy metabolism to stress responses (Howitz et al., 2003).

Prior to its identification as an activator of SIRT1, RES had been noted for its chemical antioxidant properties as well as its estrogen mimetic properties. Indeed, many of the cellular effects of RES are related to its ability to affect reactive oxygen species (ROS) homeostasis via either inhibiting ROS production (e.g., NADPH oxidases, mitochondria) and /or upregulating removal processes (e.g., chemical scavenger of free radicals, Mn–superoxide dismutase (MnSOD) (Gertz et al., 2012; reviewed in Truong et al., 2018). However, the exact underlying mechanisms mediating these effects are not clear. Notably, RES and 17β-estradiol (E_2) have proven to induce similar biological effects, including observations of increased MnSOD activities, promoting

mitochondrial biogenesis. Indeed, some of RES's cellular effects require its ability to modulate estrogen receptor (ER)-mediated signaling, reviewed in (Cipolletti et al., 2018; Stuart and Robb, 2013; Robb and Stuart, 2014).

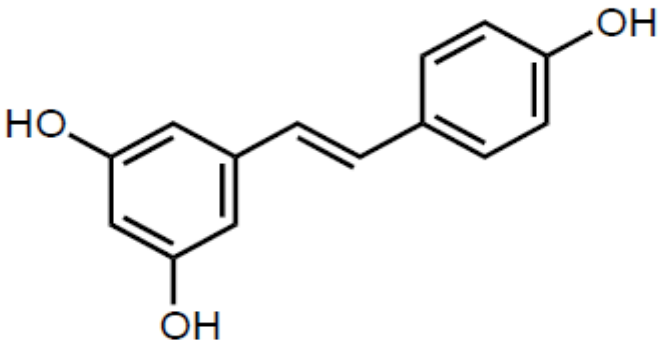

Figure 1.1. Chemical structure of *trans*-Resveratrol. RES basic structure consists of two phenolic rings bonded together by a double styrene bond. The *trans*-isomer is the most stable from the steric point of view which has been shown to exert anti-tumor, longevity promoting, anti-diabetes, cardio- protection, and antimicrobial effects.

RESVERATROL AND ESTROGEN RECEPTORS

ERs are steroid hormone receptors belonging to the superfamily of ligand-activated transcription factors. Three estrogen-receptors have been identified so far: estrogen-receptor alpha (ERα); estrogen receptor beta (ERβ); and the G-protein coupled estrogen receptor (GPER). These ERs have cell-type specific patterns of expression and different intracellular locations. ERs mediate most of the biological effects of estrogens at the level of gene regulation by interacting through its site-specific target DNA and with other coregulatory proteins (reviewed in Kumar et al., 2011). RES binds ERα and ERβ with a K_d in the micromolar range and the EC50 for RES activation of estrogen response element (ERE)-driven reporter gene activity has been reported to be 10 μM (Bowers et al., 2000).

Many nuclear receptors are activated by specific ligands and generally function as transcription factors by binding to specific DNA sequences in the genome. Similar to the other nuclear receptors, ERs act as modular proteins that consist of distinct structural and functional

domains. Starting from NH2- to COO-terminus, the principal domains are: (1) the N-terminal domain (NTD); (2) DNA-binding domain (DBD); (3) ligand-binding domain (LBD) (Tremblay et al., 1999). Two activation function (AF) domains, AF1 and AF2, located within the NTD and LBD, respectively, are responsible for regulating the transcriptional activity of ERs (reviewed in Kumar et al., 2011) (Figure 1.2).

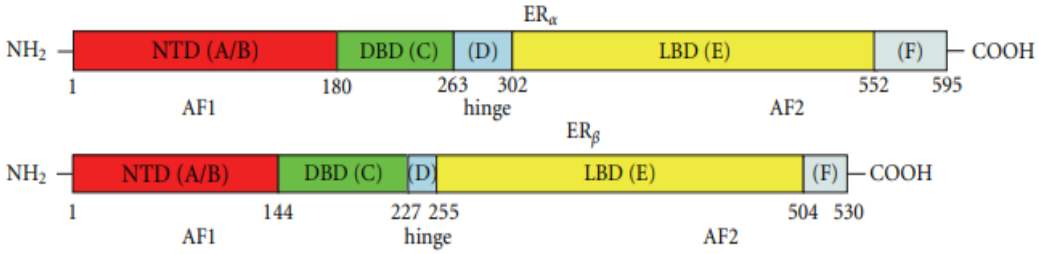

Figure 1.2. Depiction of different domains of ERα and ERβ. NTD—amino terminal domain—in red; DBD—DNA binding domain—in green; hinge region—in blue; LBD—ligand binding domain—in yellow; F region located towards the C-terminal end—in grey. Amino acid sequence position is given for each domain. The structurally distinct amino terminal A/B domains share a 17% amino-acid identity between the ERs. The near-identical central C region (97%) is the DNA-binding domain. The flexible hinge, or D, domain (36%) contains a nuclear localization signal and links the C domain to the carboxyl terminal (E) domain, which has 56% amino-acid homology between the ERs. The carboxyl-terminal F domain shares an 18% amino-acid identity. Adapted from Kumar et al., 2011.

In addition to the classical ER functions as transcription factors, these hormone receptors exert effects via non-classical mechanisms as well. Classical ER (genomic) functions rely on their capacity to modulate the transcription of specific target genes by binding to the estrogen response elements (EREs), 5′AGGTCAnnnTGACCT-3’and recruiting a variety of co-regulators that are required for the transcription induction (Lecomte et al., 2017). With classical signalling binding of ERs to EREs leads to DNA bending and looping, thus allowing interaction with the transcriptional machinery and co-regulator proteins (Simplified in Figure1.3). In the non-classical transcriptional mechanism (tethered), ERs modulate gene transcription without interacting directly with the ERE sequences by binding to specific transcription factors, such as CREB or Fos and Jun proteins, which activate the activator protein 1 (AP-1) and the stimulating protein 1 (Sp1), causing transcriptional activation of multiple growth regulatory genes (Kling, 2001; Lin et al., 2007).

Non-genomic actions of estrogen often involve extranuclear-initiated kinase signaling - transduction mechanisms with the subsequent production of intracellular second messengers, cAMP regulation and protein-kinase activation of signaling cascades that result in indirect changes in gene expression. This mode of action is often related to cytoskeleton remodeling, cell proliferation, and cell survival mechanisms. An interesting phenomenon observed in many cells is that ERs can be activated in the absence of estrogens or other receptor agonists. This ligand-independent ER activation mechanism is mainly triggered by other molecules such as epidermal growth factor (EFG), IGF-1, and neurotransmitters like dopamine, or activation by phosphorylation on specific residues (reviewed in Levin 2009). This mode of activation might fulfill a variety of cell-specific functions of ERs. In addition to nucleus and plasma membrane, ERα and ERβ have been also identified in mitochondria, endoplasmic reticulum, and Golgi (Monje and Boland, 2001; Yang et al., 2009; reviewed in Levin 2009). The presence of ERs on mitochondrion and estrogen responsive elements on the mitochondrial DNA indicates a role for estrogens in regulating the structure and/or function of this organelle.

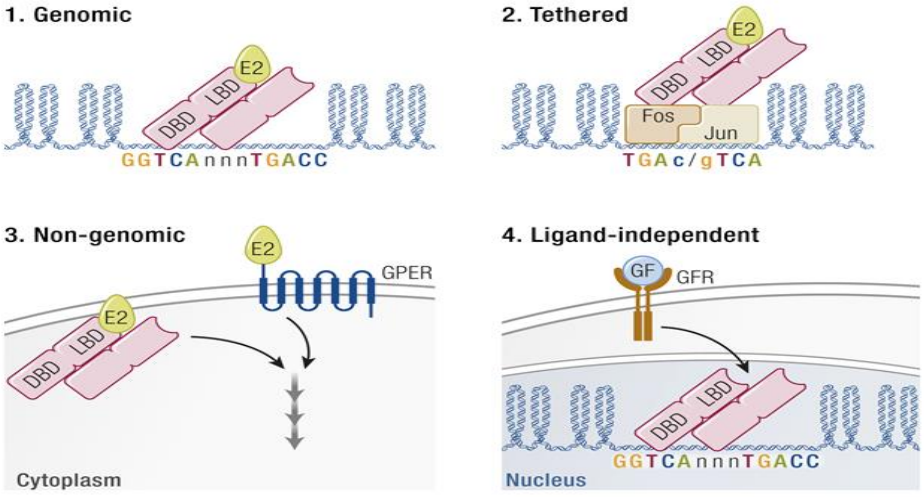

Figure1.3. **Various identified E_2 response mechanism.** (1) **The genomic** mode where interaction between ER and ERE DNA motifs occurs. (2) **The tethered** mode where indirect interaction between ER and other transcriptional regulators occurs, for example, ER is "tethered" to the DNA via FOS/JUN binding to its AP-1 DNA motif. (3) **The nongenomic** mode where the response does not involve interaction with genomic features and initiates a signal from extracellular E_2 that results in rapid signal cascades in the cytoplasm. The responses are mediated by membrane-associated ER, or by GPER, a G protein–coupled receptor. (4**) The ligand-independent** mode where initiates from stimuli such as extracellular growth factor (GF) activation of cell membrane GF receptor (GFR),

which triggers signaling cascades, such as MAPK. The signal is then received by the ER thus regulating its transcriptional modulation of target genes in the absence of E_2. DBD (DNA binding domain); LBD (ligand binding domain). Adapted from Hewitt and Korach, 2018.

ESTROGENS

The human body synthesizes three main estrogens: 17β-estradiol (E_2), estrone (E_1) and estriol (E_3), each of which is C18 steroids derived from cholesterol. Estrogens, the main ER ligands, are lipophilic hormones that diffuse freely into cells. E_2 has the highest affinity for ERα and is the predominant estrogen in circulation in premenopausal women (high pM to nM range). The lower ERα affinity estrogens are E_1 and E_3; E_1 is synthesized from androstenedione in the adrenal cortex and E_3 is primarily produced in the placenta (Gruber et al., 2002).

A comprehensive history on the discovery and characterization of E_2 was published by Evan Simpson and Richard J. Briefly, Edward A. Doisy in 1931 isolated both E_1 and E_3 from the urine of pregnant women and afterward E_2 from pig follicular fluid. Subsequently, our understanding of estrogen actions has greatly improved owing to discovery of E_2's metabolism, tissue-specific uptake, cellular activities, and E_2-dependent changes in the subcellular distribution of ERα. Notably, cloning of ERα from MCF7 human breast cancer cells and the discovery and cloning of ERβ have remarkably contributed to the field of breast cancer biology including development of treatments (reviewed in Simpson and Santen, 2015). Moreover, investigation of the genomic binding distribution of ERα and ERβ in chromatin immunoprecipitation (ChIP) studies indicated the diversity of genes targeted (eg., low-density lipoprotein (LDL) receptor, Nuclear Respiratory Factor-1 (NRF-1, *NRF1*)), by these receptors in response to E_2 (reviewed in Hewitt and Korach, 2018).

O_2 AND REACTIVE OXYGEN SPECIES

There is evidence indicating that phytoestrogens such as RES and estrogens modify ROS production and metabolism (Okoh et al., 2013; reviewed in Liu et al., 2020). ROS affect several intracellular signalling pathways (Sena and Chandel, 2012; Sies and Jones, 2020), including those regulating differentiation (Tormos et al., 2011) and apoptosis (Circu and Aw, 2010; Giorgio et al., 2005). Furthermore, the hypoxia transcriptional response may be modulated by ROS (eg., Chandel

et al., 2002; Brunelle et al., 2005; Lin et al., 2008). Substantial amounts of O_2 initially appeared on Earth around 2.2 billion years ago due to the activity of photo-synthesizing cyanobacteria. Primarily, most of the O_2 reacted with solubilized iron (Fe) generating insoluble oxide minerals. This is referred to as the Great Oxygenation Event (GOE). This is also referred to as the Great Oxygen Catastrophe (GOC) since the rise in O_2 levels resulted in the first mass extinction on Earth (Holland, 2006).

Since the ground state of O_2 contains two unpaired electrons in its outermost orbital, it can thus be considered a free radical. These two electrons have the same quantum spin number and thus can accept only one electron at a time, leading to generation of multiple free radical intermediates. Adaptation to an oxidizing environment provided a selective advantage for organisms capable of coupling enzyme activities to O_2 utilization. In aerobic cells, O_2 is employed by various enzymes but is primarily the driving force underlying aerobic ATP production (Halliwell and Gutteridge, 2015).

In biology and medicine, several types of 'reactive species' are named based on the reactive atom: reactive oxygen species (ROS), reactive nitrogen species (RNS) and reactive sulfur species (RSS). ROS is an umbrella term that refers to a family of O_2 -containing molecules including the superoxide radical anion ($O_2^{\bullet -}$) and hydrogen peroxide (H_2O_2) (Figure. 1.4). ROS can also undergo various chemical reactions to produce secondary oxidative species. For instance, $O_2^{\bullet -}$ can react with nitric oxide ($NO^{\bullet}$) to generate peroxynitrite ($ONOO^-$) and $O_2^{\bullet -}$ and H_2O_2 can generate the highly reactive hydroxyl radical ($OH^{\bullet}$) in the presence of trace metals via Fenton/Haber-Weiss reactions. Importantly, methodological advances in the study of specific ROS molecules by various chemical detectors and by imaging techniques allow better characterization of the individual species. This has resulted in a better appreciation of the biological significance of specific ROS in both physiology and pathology (reviewed in Mailloux, 2015; Hayes et al., 2020). ROS at physiological levels play redox signalling role via different post-translational modifications, denoted as 'oxidative eustress'. Redox signalling influences a wide range of cellular and molecular processes, including protein function, enzyme activity, gene transcription and membrane and genome integrity (reviewed in Sies and Jones, 2020). ROS are short-lived, highly electrophilic molecules generated by the partial reduction of O_2 that regulate cellular homeostasis, but also are primary modulators of cellular dysfunction contributing to disease pathophysiology. ROS are by-

products of numerous enzymatic reactions in various cell compartments, such as the cytoplasm, plasma membrane, endoplasmic reticulum (ER), mitochondria, and peroxisomes (Ye et al., 2017).

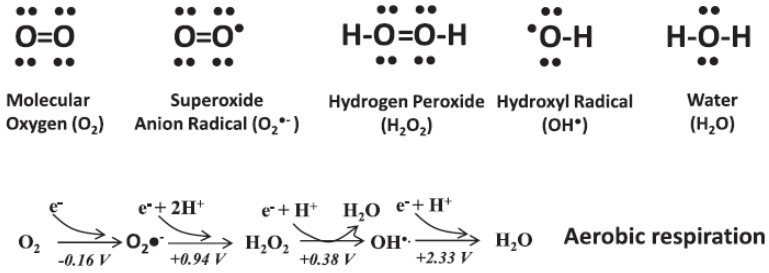

Figure1. 4. Reduction process of O_2 to H_2O and its free radical intermediates species. **Top.** Lewis structures for O_2 and its singlet electron derivatives superoxide ($O^{2\bullet-}$) and hydrogen peroxide (H_2O_2), and hydroxyl radical ($OH^{\bullet}$). **Bottom.** The pathway of O_2 reduction to H_2O during aerobic respiration. Adapted from Mailloux, 2015.

Hydrogen peroxide (H_2O_2)

About 50 years ago, H_2O_2 was initially identified as a product of normal eukaryotic cell respiration. More recently, a variety of tools have allowed the measurement of its intracellular concentration, which is reported to be in the nanomolar range (approximately 1–100 nM) depending on sub-cellular localizations. The generation of H_2O_2 is initiated by various stimuli such as metabolic cues, physiological, pathological stressors, growth factors, and chemokines. Steady-state physiological flux of H_2O_2 toward specific protein targets can cause their reversible oxidation, thus modifying protein activity and subsequently their localization and interactions. Consequently, these modifications impact various downstream processes such as cell proliferation, differentiation, migration, and angiogenesis. Indeed, H_2O_2 is a non- radical oxidant with relatively low reactivity, and thus a long half-life and large diffusion distance, making it an effective signaling molecule. Notably, it reacts very slowly and specifically with glutathione, cysteine and methionine amino acids leading to redox signalling. H_2O_2 reacts also moderately with iron–sulfur (Fe–S) clusters and loosely bound metals. Here I only elaborate on mitochondrial and main non-mitochondrial sources of ROS. However, less significant sources of ROS ensue from the activities of cytochrome P450 (CYP), monoamine oxidase, xanthine oxidase, cyclo-oxygenase (COX), glycolate oxidase, hydroxy acid oxidase, aldehyde oxidase, and amino acid oxidase (Radi, 2018; Jones and Sies, 2015).

Non- mitochondrial ROS

NADPH oxidases

The production of ROS from various cytoplasmic enzymes is of fundamental importance to cellular signalling and disease pathophysiology. The NOX family of nicotinamide adenine dinucleotide phosphate (NADPH) oxidases reduces molecular O_2 via the transfer of electrons from NADPH to form ROS as their sole known enzymatic function. NOX enzymes mediate diverse functions through redox signaling (Bedard and Krause, 2007; Brown and Griendling, 2009), including cell growth, differentiation, and death. Furthermore, NOXs are implicated in pathophysiological mechanisms underlying apoptosis resistance, tumor cell proliferation and metastasis, and angiogenesis (Block and Gorin, 2012; Kamata, 2009; Meitzler et al., 2014).

There are seven members of the NOX family (NOX 1–5 and Duox 1 and 2) (Pandy et al., 2015). NOXs are multi subunit membrane-spanning enzymes that transport electrons from NADPH across biological membranes (Bedard and Krause 2007). While these enzymes localize to a variety of cellular membranes, all can be found in the plasma membrane, where they transport electrons to external O_2, thus leading to the generation of $O^{2\bullet-}$ in the extracellular space (Pandy et al., 2015) (Figure 1.5 depicts these enzymes).

Initially speculated to be exclusively present in phagocytic cells, NOXs are broadly expressed in most cell types and evolutionarily conserved. NOX proteins comprise of NADPH-binding site at the C-terminus, the flavin adenine dinucleotide (FAD)-binding region located proximal to the C-terminal transmembrane domain, six conserved transmembrane domains, and four conserved heme-binding histidines (reviewed in Brown and Griendling, 2009). Upon activation, a catalytic subunit transfers electron across biological membranes from the NADPH substrate to flavin adenine dinucleotide (FAD), and then to heme co-factors located within its membrane-bound subunit, and finally to extracellular O_2, generating either $O_2^{\bullet-}$ (which is rapidly converted into H_2O_2) or H_2O_2 (e.g., NOX4) (Bedard and Krause, 2007). NOX family members differ in their tissue distribution, structure, and regulation.

In addition to their localization to the plasma membrane, some NOX isoforms localize to various organelles. NOX4, for instance, has been identified in membranes of the endoplasmic reticulum (Van Buul et al., 2005), mitochondria (Block et al., 2009; Graham et al., 2010; Shanmugasundaram et al., 2017), and nucleus (Hilenski et al., 2004; Kuroda et al., 2005).

NOS enzymes

In addition to NOX, the nitric oxide synthase (NOS) enzymes also contribute to cytosolic ROS production. In mammals, three NOS isoforms have been characterized so far: neuronal NOS (nNOS; NOS1), endothelial NOS (eNOS; NOS III), and inducible NOS (iNOS; NOS II) (Alderton et al., 2001). While nNOS, eNOS, and iNOS were initially discovered and characterized in the nervous system, epithelium, and macrophages, respectively, they are in fact widely expressed in many cell types (Bachetti et al., 2004; Kroncke et al., 1998). NOS catalyzes the mono-oxygenation reaction of L-arginine to an intermediate, N-ω-hydroxy-L-arginine, followed by a subsequent second mono-oxygenation reaction converting it into L-citrulline and nitric oxide (•NO) with NADPH functioning as the electron donor (Daff, 2010). •NO is an important signaling molecule with roles in numerous biological processes, including endothelial function, vascular smooth muscle cell contraction/dilation, inflammation, neuroplasticity, and cytotoxicity(Griendling et al., 2016) (Figure 1.5 depicts these enzymes) .

Notably, neurotransmission and vascular tone regulation are regulated by stimulating •NO-sensitive guanylyl cyclase and generation of cyclic GMP. •NO is comparatively unreactive and can react with O2−• to form RNS (e.g., peroxynitrite (ONOO−)), a strong oxidant that can cause oxidative damage, nitration, and S-nitrosylation of biomolecules including proteins, lipids, and DNA. Under physiologic conditions, NOS are homodimeric heme-containing enzymes that catalyze the conversion of L-arginine to NO. However, under some conditions, including transient anoxia/ reoxygenation, NOS can become 'uncoupled', generating predominantly $O_2^{-\bullet}$ rather than •NO. This is important because uncoupled NOS not only leads to reduction of the NO availability and also triggers oxidative stress, which contributes significantly to many pathologies (Förstermann and Sessa, 2012).

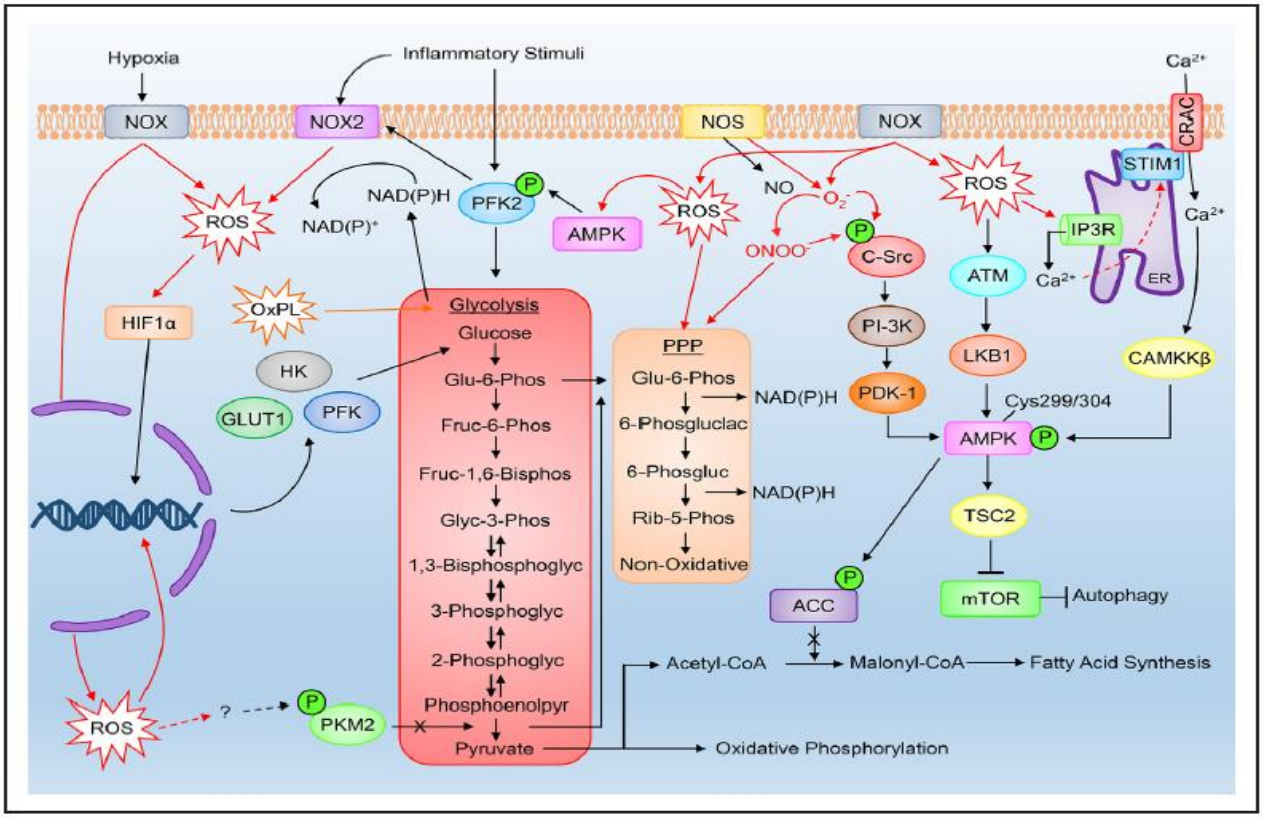

Figure 1.5. Non-mitochondrial source of reactive oxygen species (ROS) and the regulation of cytosolic metabolic pathways. This source of ROS is formed mostly through NADPH oxidase (NOXs) activity and target various metabolic pathways including glycolysis, oxidative phosphorylation, pentose phosphate pathway, and autophagy, to name a few. ACC, acetyl-CoA carboxylase; AMPK, AMP-activated protein kinase; ATM, ataxia-telangiectasia mutated; CAMKKβ, Ca2+/calmodulin dependent protein kinase β; CoA, coenzyme A; CRAC, calcium release–activated channel; ER, endoplasmic reticulum; GLUT1,glucose transporter 1; HIF1α, hypoxia-inducible factor 1α; HK, hexokinase; IP3R, inositol 1,4,5-trisphosphate receptor; LKB1, liver kinase B1; mTOR, mammalian target of rapamycin; NADPH, nicotinamide adenine dinucleotide phosphate; NOS, nitric oxide synthase; OONO, peroxynitrite; OxPL, oxidized phospholipid; PDK-1, phosphoinositide-dependent kinase-1; PFK, phosphor fructo kinase; PI3K, phosphoinositide 3-kinase; PKM2, pyruvate kinase 2; PPP, pentose phosphate pathway; STIM1, stromal interaction molecule 1; and TSC2, tuberous sclerosis protein 2. Adapted from Forrester et al., 2018.

Mitochondrial sources of ROS

In 1957, Peter Siekevitz named the mitochondrion the "powerhouse" of the cell (Siekevitz, 1957). Less than a decade later the first findings indicated that the organelle generated ROS as a by-product of cellular respiration (Jensen, 1966). Since then, the production of these species and their various roles in signaling and disease have been extensively studied such that mitochondria are widely recognized as a source of ROS in animal cells. So far, 11 different sites associated with substrate catabolism and the electron transport chain have been identified to produce ROS in mitochondria (reviewed in Mailloux, 2018) (Figure 1.6). The ROS-producing capabilities of these different enzymes have been reviewed comprehensively in (Brand, 2016; Wong, 2017; Munro and Treberg, 2017).

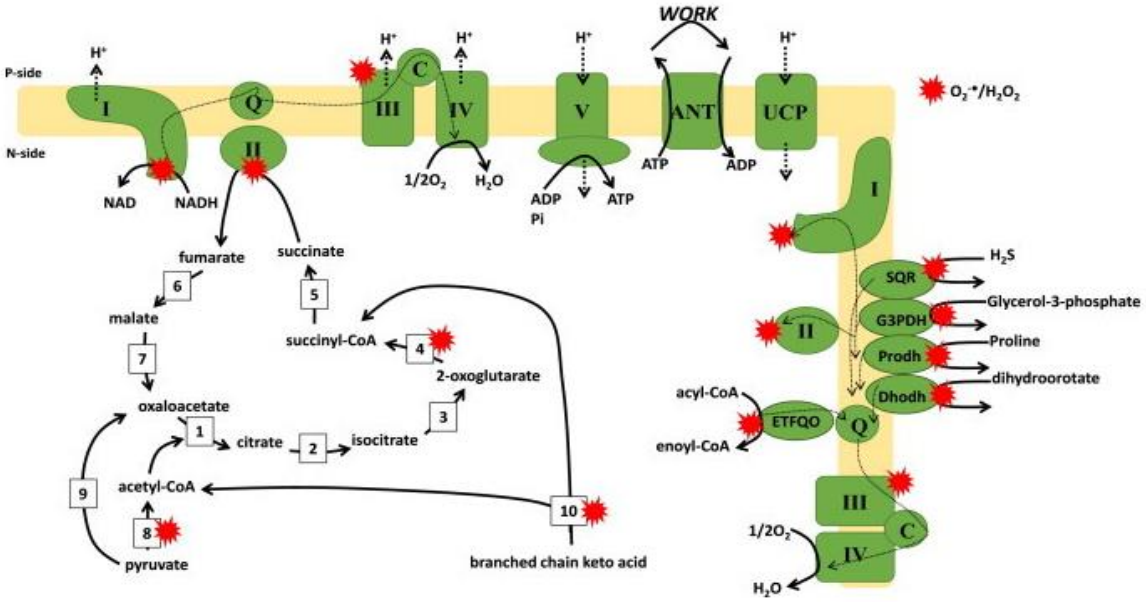

Figure 1.6. Major sites of superoxide and H_2O_2 generation in enzyme complexes of the electron transport system and the Krebs cycle. Notably, the distinct sites of ROS production contribute differently to overall ROS release in different tissues. Ubiquinone (Q) and cytochrome C (C) function as electron carriers between the respiratory complexes. Electron transfer flavoprotein oxidoreductase (ETFQO), dihydroorotate dehydrogenase (Dhodh), proline dehydrogenase (Prodh), succinate: quinone reductase (SQR), sn-glycerol-3-phosphate dehydrogenase (G3PDH) can also release electrons into the Q pool following oxidation of their cognate substrates. Red stars show that 11 potential sources of $O_2^{-\cdot}/H_2O_2$. Dotted lines indicate flow of electrons. Bold dotted lines show flow of protons (H^+). Kreb cycle enzymes are shown: (1) Citrate synthase, (2) aconitase, (3) NAD(P)$^+$-isocitrate dehydrogenase, (4) 2-oxoglutarate dehydrogenase, (5) succinyl-CoA synthase, (6) fumarase, (7) malate dehydrogenase, (8) pyruvate dehydrogenase, (9) pyruvate carboxylase, (10) branched chain keto acid dehydrogenase. Adapted from Mailloux, 2015.

Cellular metabolism consists of the catabolism of glucose (via glycolysis and subsequent pyruvate oxidation), fatty acids (via fatty acid β-oxidation), and amino acids (via oxidative deamination and transamination). The molecules derived from these processes are used in the tricarboxylic acid (TCA) cycle to generate substrates that enter the ETC for oxidative phosphorylation (reviewed in Zhao et al., 2019). The ETC is embedded within the extensive inner membrane of the mitochondrion, in close proximity to the mitochondrial matrix in which the TCA cycle is localized (Figure 1.7). NADH and FADH2 generated by the TCA cycle donate electrons to the ETC at either Complex I (NADH: ubiquinone oxidoreductase) or Complex II (succinate dehydrogenase, SDH), respectively (Figure 1.7). Subsequently Complex I oxidizes NADH and the released electrons are transferred to ubiquinone (Q), generating ubiquinol (QH2). Of note, other different sources also supply electrons into the ubiquinone (Q) pool: Complex II; electron transfer flavoprotein oxidoreductase (ETF-QO), dihydroorotate dehydrogenase, and FAD-linked glycerol phosphate dehydrogenase. The electrons are then passed to Complex III (ubiquinol-cytochrome C reductase) via cytochrome c and ultimately onto Complex IV (cytochrome C oxidase) where they finally reduce O_2 as the last electron acceptor into H_2O (Nicholls, 2008; Klingenberg, 2008).

The electron transfer from mitochondrial respiratory complexes is principally affected by the existence of the substantial redox potential differences between NADH (E^o = -340mV), and O_2 (E^o= 810mV) (Nicholls and Ferguson, 2013). According to Peter Mitchell's Chemiosmotic Theory, the energetically favorable transfer of electrons from NADH to O_2 through the mitochondrial respiratory complexes is coupled to the pumping of protons through Complexes I, III, and IV into the intermembrane space (Mitchell, 1966). In fact, in response to electron transport, a total of ten protons (H+) (two from Complex III, and four from each Complex I and Complex IV) are pumped from the matrix into the intermembrane space which generates an electrochemical proton gradient referred to as the mitochondrial membrane potential ($\Delta\Psi$). $\Delta\Psi$ in combination with proton concentration (pH) generates a protonmotive force (Δp) which is essential for OXPHOS since it couples electron transport (complexes I-IV) (and O_2 consumption) to the function of Complex V (ATP synthase), where protons re-enter the matrix to dissipate the proton gradient allowing for ATP production (reviewed in Nolfi-Donegan et al., 2020).

The predominant route of ROS production by the ETC is the premature leak of electrons from complexes I, II, and III to mediate the one electron reduction of O_2 to superoxide ($O^{2\bullet-}$), ROS generation can happen when single electrons from Complexes I and III react with O_2 to produce $O_2^{-\bullet}$. Also, complex II has been shown to generate $O_2^{-\bullet}$. Complex II oxidizes succinate to fumarate and transfers two electrons onto ubiquinone that fuels the TCA cycle. Indeed, Complex II can generate ROS, mainly from its flavin site, through two mechanisms: a forward mechanism involves electron transfer from succinate when Complexes I and III are inhibited; in a reverse mechanism, electrons are provided through the reduced ubiquinone pool (Buettner, 1993; Murphy, 2009; Mailloux et al., 2013). While initial studies estimated that 1–2% of electrons fluxing to the ETC contributed to $O^{2\bullet-}$generation (Boveris and Chance,1973), it is currently appreciated that the rate of mitochondrial ROS generation is likely lower than this value *in vivo* and differs depending on ETC function. In addition to respiratory complex-derived mitochondrial ROS, other enzymes involved in metabolic reactions are also involved, including 2 -Oxoglutarate dehydrogenase (ODH), pyruvate dehydrogenase (PDH), sn-glycerol-3-phosphate dehydrogenase (mGPDH) (reviewed in Starkov et al., 2004). These enzymes can produce $O_2^{-\bullet}$ / H_2O_2 or both depending on experimental conditions and the energetic substrates used (Quinlan et al., 2013; reviewed in Starkov et al., 2004).

Whereas $O_2^{-\bullet}$ is the proximal ROS produced by the mitochondrial respiratory chain and several localized enzymes, it only interacts significantly with a few biologically relevant targets, notably iron–sulfur proteins, •NO, and quinones. $O_2-\bullet$ is dismutated to H_2O_2 either spontaneously or by SOD (more than 1,000-fold (reviewed in Parascandolo and Laukkanen, 2019). There are three SOD forms in mammalian cells, and two of these localize to mitochondria. Cu,Zn-dependent isoform (Cu,Zn SOD, SOD1), is found in the mitochondrial intermembrane space (and cytosol); the Mn-dependent isoform (Mn SOD, SOD2), is found exclusively in the mitochondrial matrix (Sheng et al., 2014).

H_2O_2 exerts its physiological effects mainly through reversibly oxidizing protein cysteine thiols (–SH) to sulfenic acid (–SOH), referred to as a “redox switch”. Its steady state concentration is therefore relevant to mitochondrial and cytosolic protein function. Reduction of H_2O_2 into H_2O and O_2 is regulated by multiple enzymes such as catalase (Kirkman and Gaetani, 2007) glutathione/glutathione peroxidase (GSH/GPx) and thioredoxin/thioredoxin reductase/peroxiredoxin (Trx/TrxR/Prx) (Trevisan et al., 2014). In mitochondria, GSH and Trx

systems are the major H_2O_2 degrading pathways (Handy and Loscalzo, 2012). In addition, non-catalytic small molecules scavenge ROS and RNS which include endogenously synthesized bilirubin, a-lipoic acid, melatonin, melanin, GSH, and uric acid, as well as exogenously derived vitamin E, vitamin C, b-carotene, and plant polyphenols such as RES (Halliwell and Gutteridge, 2015). Mitochondrial -derived ROS and their downstream targets are shown in Figure1.7.

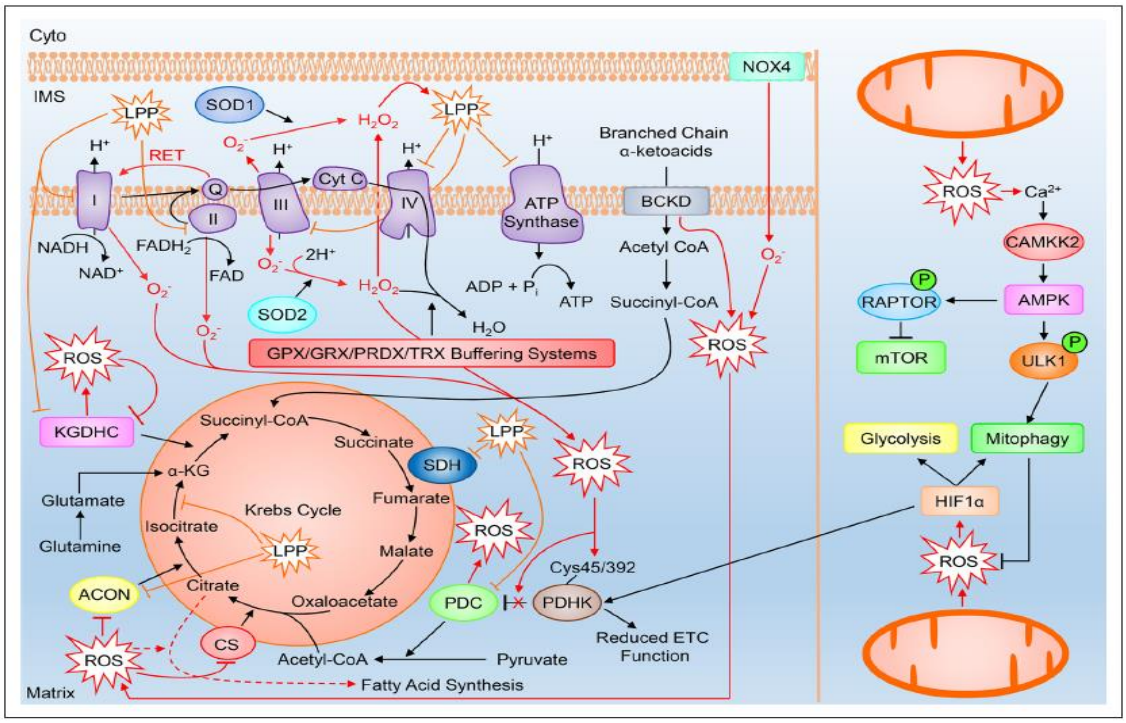

Figure 1.7. Mitochondrial source of reactive oxygen species (ROS) and hypothetical downstream targets. This source of ROS is by-product of mitochondrial respiration (via electron transport chain complexes I, II, III) and various metabolic enzymatic activity which influence metabolic pathways including the Krebs cycle, ATP generation, fatty acid synthesis, glycolysis, and mitophagy. AMPK, AMP-activated protein, kinase α-KG, α-ketoglutarate; ACON, aconitase; BCKD, branched chain keto acid dehydrogenase; CAMKK2, Ca2+/calmodulin-dependent protein kinase 2; CoA, coenzyme A; CS, citrate synthase; ETC, electron transport chain; GPX, glutathione peroxidase; GRX, gluta redoxin; HIF1α, hypoxia-inducible factor 1α; IMS, intermembrane space; KGDHC, α- ketoglutarate dehydrogenase; LPP, lipid peroxidation product; NOX, nicotinamide adenine dinucleotide phosphate (NADPH) oxidase; PDC, pyruvate dehydrogenase; mTOR, mammalian target of rapamycin ; PDHK, pyruvate dehydrogenase kinase; PRDX, peroxiredoxin; RET, reverse electron transfer; SDH, succinate dehydrogenase; SOD, superoxide dismutase; TRX, thioredoxin; and ULK1, uncoordinated 51-like kinase 1. Adapted from Forrester et al., 2018.

RES AND E_2 EFFECTS ON ROS PRODUCTION

There is mounting evidence indicating the effects of RES and E_2 on the expression and function of ROS producing and neutralizing enzymes. Notably, RES has been shown by several studies to modulate NOX (specifically NOX1 and NOX4) expression levels and activity (Schilder et al., 2009; Zhang et al., 2012; Chen et al., 2013). Park et al. (2009) demonstrated that RES treatment of macrophages inhibits LPS-induced NOX1 mRNA expression as well as ROS generation. Consistently, RES is shown to reduce ROS derived from NOX4 in renal fibroblast cells. In fact, the up-regulated NOX family constitute an important source of the intracellular ROS in the kidney which is proposed to be the underlying cause of diabetic nephropathy (reviewed in Lee et al., 2020). Similarly, RES prevents eNOS uncoupling in cardiovascular tissues which provides a protective role. In the same line, treatment of cultured human endothelial cells with RES (Wallerath et al., 2002) or red wines rich in RES, increased the mRNA and protein expression of eNOS (Wallerath et al., 2003; Walerath et al., 2005).

Likewise, E_2 exhibits ROS-modulatory roles in various cell types. For example, E_2 treatment for 11 days in neurons, suppressed oxidative stress via SOD1 and SOD2 upregulation (Rap et al., 2011). Oxidative stress and neuronal cell death induced by O_2-glucose deprivation in mouse brain slices were also ameliorated by E_2 treatment via upregulation of SOD1 (Rao et al., 2013). However, in breast cancer cells E_2 is shown to induce mitochondrial- derived ROS (Felty et al., 2005; Parkash et al., 2006). There are also *in vivo* results showing the regulatory effects of estrogens on ROS; following ovariectomy in rats, NADPH-stimulated H_2O_2 production by the basilar artery was approximately 3-fold higher than levels generated by arteries from control females, indicating that estrogen deficiency causes greater NADPH-oxidase activity in cerebral arteries (Miller et al., 2007). Altogether, these findings indicate the important role of RES and estrogens in modulating ROS metabolism in various contexts, and I discuss them in more details in the corresponding chapters.

MITOCHONDRIAL STRUCTURE AND FUNCTION

Mitochondria, present within almost every eukaryotic cell type, are multifaceted organelles required for signaling and metabolic processes. Beyond their well-understood role in the production of ATP through oxidative phosphorylation (OXPHOS), mitochondria play key roles in biosynthesis, ion homeostasis, redox signaling, apoptotic cell death, and innate and adaptive immunity-activities that must be adjusted to changing cellular needs (Sena and Chandel, 2012; reviewed in Checa and Aran, 2020).

Mitochondria are organized into two phospholipid bilayers: the outer mitochondrial membrane (OMM), which separates the intermembrane space from the cytosol, and the inner mitochondrial membrane (IMM), which has multiple projections deep into the matrix to form cristae (Tilokani et al., 2018). Whereas the OMM is porous to ions and molecules with molecular weight < 2500 Da, the IMM must be relatively impermeable to maintain its electrochemical gradient. Mitochondria are dynamically interconnected organelles, allowing them to share electrochemical gradients and mtDNA. Individual mitochondria fuse together into extensive tubular networks or divide into small rod-shaped or punctate structures. Indeed, mitochondria are highly plastic organelles, constantly changing their distribution, morphology, and connectivity in response to cellular conditions. Collectively, all these processes are referred to as mitochondrial dynamics, which is a tightly regulated balance between mitochondrial fusion and fission. Shifts in the opposing forces of fusion and fission determine changes in mitochondrial network morphology. Mitochondria may also dynamically tether to, and exchange materials with, other cellular organelles such as the endoplasmic reticulum (ER) and lysosomes (Elbaz-Alon, 2015; Murley and Nunnari, 2016). Figure1.8. demonstrates mitochondrial fusion and fission process and the main regulating enzymes.

Mitochondrial fusion

Mitochondrial fusion is a process by which two adjacent mitochondria are fused to form larger elongated and/or branched structures. Content mixing that occurs with fusion can equilibrate mitochondrial proteins, lipids, and metabolites and thus may neutralize local dysfunction. In mammals, this process is regulated by three dynamin-like large GTPases, mitofusin 1 (Mfn1), mitofusin 2 (Mfn2) and optic atrophy gene 1 (OPA1). Mfn1 and Mfn2 are in the OMM and OPA1

is in the IMM. Mfn1/2 share (in humans) approximately 80% amino acid sequence similarity. Overexpression of either Mfn1/2 leads to mitochondrial aggregation around the nucleus (Eura et al., 2003; Tilokani et al., 2018). Whereas, in mouse embryonic fibroblast knockout of Mfn1/2 results in mitochondrial fragmentation, though the morphology varies between Mfn1 and Mfn2 knockouts. This difference between Mfn1 and Mfn2 knockouts can be related to greater GTP-dependent membrane tethering efficiency demonstrated by Mfn1 compared to Mfn2. Nonetheless, when overexpressed, each protein can compensate for the loss of the other to promote fusion, indicating some overlapping functions. Mfn1 and Mfn2 are also required for embryonic development as ablation of either gene is embryonically fatal (Chen et al., 2003). In addition to involvement in mitochondrial fusion, Mfn2 also plays a role in calcium homeostasis, ER- mitochondria contact and cell cycle regulation. Emerging evidence also indicates that Mfn2 inhibits proliferative cell growth and causes apoptosis, for example in Hela cells Mfn2 inhibits the Ras-NF-kB signalling pathway, slowing cell cycle progression (Liu et al., 2019).

Mutations in Mfn2 can result in Charcot-Marie Tooth 2A (CMT2A) and familial Parkinson's disease, both of which are associated with progressive neurodegeneration (Chen and Dorn, 2013; Engelfried et al., 2006; Tanaka et al., 2010). So far over a hundred Mfn2 mutations in various protein domains have been identified in CMT2A (Larrea et al., 2019). However, how Mfn2 mutations lead to CMT2A is controversial and several mechanisms are speculated to play key roles in pathogenesis, including defective mitochondrial fusion, loss of mtDNA integrity, defective mitochondrial transport, and loss of mitochondrial-ER contact sites (Filadi et al., 2018).

Mitochondrial fusion is a highly complex process catalyzed principally by Mfn1 and Mfn2, which have the capacity to homo-dimerize or hetero-dimerize and to prime mitochondrial tethering. Recently it has been proposed that this dimerization occurs through the GTPase domains of mitofusins on opposing mitochondria upon GTP binding. Subsequent GTP hydrolysis causes a conformational change which brings the opposing membranes into close contact to facilitate OMM fusion. Notably, mitofusins' intramolecular binding interactions have been suggested to allow a permissive or restrictive conformation for fusion (Franco et al., 2016).

While the mechanism of IMM fusion is less clear, it is regulated by OPA1 which is anchored to the IMM by an N terminal transmembrane domain (Delettre et al., 2001; Olichon et al.,

2003; Cipolat et al., 2004). OPA1 is a unique dynamin family GTPase in that it is subjected to significant proteolytic processing. Alternative splicing of OPA1 generates long forms (L-OPA1) that can be proteolytically cleaved to short forms (S-OPA1). This cleavage is executed by two mitochondrial peptidases: OMA1 and YME1L (Anand et al., 2014; Olichon et al., 2003). OPA1 is found as both a membrane-spanning inner mitochondrial membrane protein and a soluble form in the IMS (Alexander et al., 2000). In addition to OPA1, cardiolipin, a mitochondria-specific phospholipid, is important for IMM fusion (Ban et al., 2017; Tilokani et al., 2018). The interaction between L-OPA1 and cardiolipin on either side of the membrane tethers the two IMM, which fuse following OPA1-dependent GTP hydrolysis (Liesa et al., 2009). Indeed, S-OPA1 has been proposed to function as a facilitator of OPA1-cardiolipin interaction and subsequent IMM fusion (DeVay et al., 2009; Rujiviphat et al., 2009). Using liposomes reconstituted with recombinant full-length OPA1, OPA1 reconstituted on one set of liposomes was sufficient in fusing the membranes with "naked" liposomes (without OPA1), when the second set of liposomes contained cardiolipin (Ban et al., 2017).

Cells lacking OPA1 demonstrate outer membrane fusion, however, full fusion does not occur, and mitochondria ultimately undergo fission. Interestingly, apart from fusion, OPA1 has been implicated in the maintenance of cristae organization, respiratory chain function, and mitochondrial DNA (Frezza et al., 2006; Cipolat et al., 2006; Anand et al., 2014). OPA1 upregulation in mice causes significant protection against muscular atrophy, ischemic damage in the heart and brain and hepatocyte death which can be explained by the key role of OPA-1 in preventing the release of pro-apoptotic signals (Civiletto et al., 2015; Varanita et al., 2015). Altogether, there is evidence for several other cytosolic and mitochondrial accessory proteins that regulate mitochondrial fusion in mammalian cells (reviewed in Saboury and Shut, 2020).

Mitochondrial fission

The central player in mitochondrial fission is Drp1 (dynamin related protein 1), a large GTPase (Chan, 2012; Labbe´ et al., 2014). Drp1 is mainly localized in the cytosol; upon some modifications such as Ser616 phosphorylation DRP1 translocate from the cytosol to the mitochondrial outer membrane. Drp1 is phosphorylated by specific kinases and signaling pathways during mitochondrial fission, including AMPK, and cyclin-dependent kinase 1/cyclin B1 (Cdk1/cyclin B1). Mitochondrial localized Drp1 functions as a mechano-chemical enzyme that forms helical assemblies that constrict the mitochondrial tubule. Its mechanism of action is

conceptually like the role of classical dynamins in constricting the endocytic vesicles at the cell surface (Ferguson and De Camilli, 2012; Schmid and Frolov, 2011; Lewis et al., 2016). However, emerging evidence suggest that the mechanical properties of Drp1 may be insufficient to complete the scission process indicating the existence of other mediators (Lee et al., 2016).

Other factors such as phospholipids, calcium, and lysosomes have been implicated at different stages of mitochondrial fission, showing the contribution of additional organelles is critical for fragmentation of the mitochondrial network (Nagashima, et al., 2020). Notably, OMM constriction initiates at the mitochondria-ER contact sites, prior to the oligomerization of Drp1. Furthermore, the recruitment of Drp1 to mitochondria is aided by several mitochondrial-bound proteins, including FIS1, MFF, MiD49, and MiD51, where some of these proteins have overlapping functions. In addition, evidence indicates that FIS1 promotes mitochondrial fragmentation both by activating fission and inhibiting fusion by inhibiting the GTPase activity of Mfn1, Mfn2, and OPA1 (Bagshaw et al., 2021). Apart from Drp1, the GTPases dynamins are speculated to be involved in mitochondrial fission, however, this role of dynamin has been recently challenged (Lee et al. 2016; Kamerkar et al., 2018). However, the mechanisms driving the final steps of mitochondrial division are not entirely known.

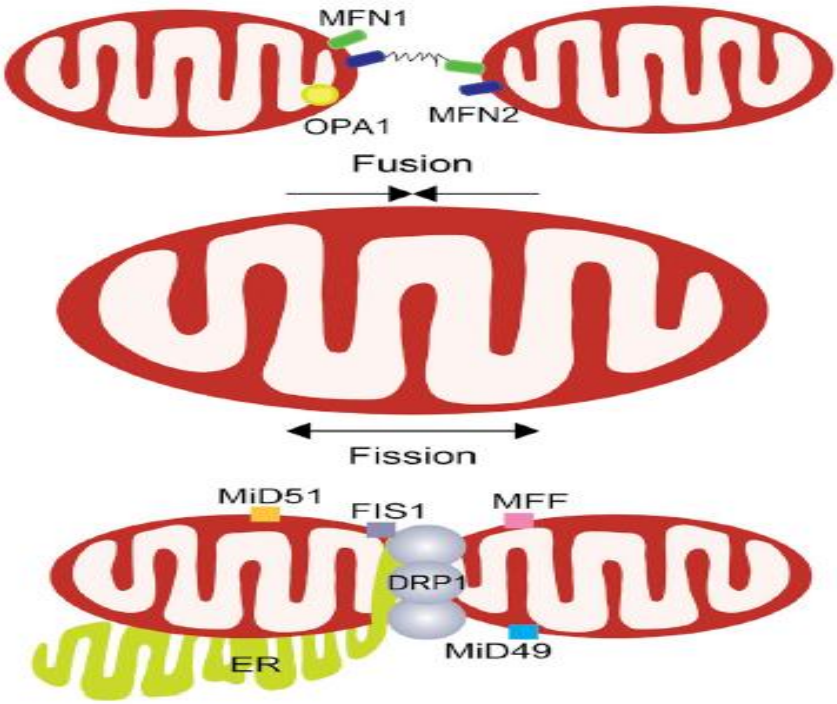

Figure 1.8. Shown are simplified machineries mediating mitochondrial fusion and fission. Mitochondrial fusion requires the action of fusion proteins, OPA1 at the IMM and MFN1 and MFN2 at the OMM inducing the fusion of membranes of juxtaposed mitochondria. Mitochondrial fission instead is promoted by the GTPase activity of DRP1 that is recruited to mitochondria where it interacts with its mitochondrial receptors (MFF, FIS1, MiD51, and MiD51) to pinch off mitochondria into smaller units. Endoplasmic reticulum (ER) determines the sites at which fission happens. Adapted from Liu et al., 2020.

Mitochondrial fission may be partnered with mitophagy. Mitophagy is an essential maintenance mechanism used to continually remove and recycle damaged mitochondrial components (Eiyama and Okamoto, 2015; Narendra et al., 2008). The canonical mitophagy pathway is controlled by PTEN -Induced Kinase 1 (PINK1) and the cytosolic E3 ubiquitin ligase Parkin. The PINK1/Parkin system functions through a ubiquitin-dependent mechanism. Briefly, under normal conditions, PINK1 is translocated to the mitochondrial matrix, and rapidly cleaved by the mitochondrial processing peptidase (MPP) and by the presenilin-associated rhomboid-like (PARL) protease. However, in damaged mitochondria with dissipated membrane potential, PINK1

stabilizes on the OMM, where it facilitates recruitment of cytosolic Parkin. Parkin catalyzes the polyubiquitination of OMM proteins such as mitofusins, which promotes mitochondrial fragmentation and mitochondrial engulfment by an active autophagosome and subsequent degradation in lysosome (Narendra et al., 2008).

Mitophagy can stimulate mitochondrial biogenesis to maintain the remaining population. Mitochondrial biogenesis is a complicated process that involves the coordinated expression of both nuclear and mitochondrial genes (reviewed in Hock and Kralli, 2009). Peroxisome proliferator-activated receptor-γ-coactivator-1 α (PGC-1α) is the master regulator of mitochondrial biogenesis that coactivates the nuclear respiratory factor 1 and/or 2 (NRF-1 and NRF-2), and estrogen related receptors (ERR-α, ERR-β, and ERR-γ), which stimulate the transcription of several nuclear-encoded genes whose protein products localize to mitochondria (Yang et al., 2009). In addition to these nuclear-specific regulatory mechanisms, mitochondria-related mechanisms, such as mtDNA transcription have an integral role in mitochondrial biogenesis. In mammals, mitochondrial transcription requires the mitochondrial RNA polymerase and the transcription factor A mitochondrial (TFAM) (Kanki et al., 2004). PGC-1α expression is regulated by the transcription factors cAMP response element-binding protein (CREB) and fork head box class-O (FoxO1) (reviewed in Hock and Kralli, 2009), while its activity is regulated by reversible phosphorylation and reversible acetylation/deacetylation (Aquilano et al., 2010; Fernandez-Marcos and Auwerx, 2011).

RES has been shown to target mitochondria in various tissues and cell types (reviewed in Stuart and Robb, 2013). Sebastian et al. (2012) showed that the expression of the profusion protein Mfn2 is downregulated in skeletal muscles of adult rats fed high fat diet (HFD). Consistently, with the use of a HFD diet as a trigger for metabolic stress, RES is shown to increase Mfn2 and OPA1 protein expression and mitochondrial fusion and biogenesis *in vivo*. In fact, RES played a preventative role against the consequences of HF diet on mitochondrial dynamics regulators (Palomera-Avalos et al., 2016). Furthermore, the protective role of RES in rotenone-induced neurotoxicity was associated with pro-mitochondrial fusion and biogenesis effects in PC12 (pheochromocytoma of the rat adrenal medulla) cells (Peng et al., 2015). Similarly, E_2 has been shown to interact with mitochondria in various contexts. Mitochondrial morphology and

biogenesis are suggested to be targeted via E_2, these researchers have demonstrated that E_2 increases the transcription and protein expression of nuclear respiratory factor-1 (NRF-1) and upregulates mitochondrial biogenesis in MCF-7 cells (Kelly and Scarpulla, 2004 ; Mattingly et al., 2008). Nonetheless, while RES and E_2 have been shown to target various aspects of mitochondrial physiology in both *in vivo* and *in vitro*, the exact nature of these interactions is controversial.

CELL CULTURE

Biomedical researchers have been using *in vitro* cell culture as a core technique to study cell biology since the 1960s, with the goal of elucidating the cellular mechanisms underlying biological processes. Cell culture is widely used in the medical and industrial sectors for purposes such as the production of recombinant proteins (e.g., monoclonal antibodies), vaccine manufacturing, and assisted reproductive technology. The historical development of animal cell culture *in vitro* dates to 1907, when Ross G. Harrison successfully managed an outgrowth of nerve fibers from a frog for several weeks in lymph (reviewed in Yao and Asayama, 2017).

Healthy somatic cells stop dividing after a certain number of divisions and become senescent, a phenomenon later called the Hayflick limit (Hayflick and Moorhead, 1961). To surpass this limitation, researchers used carcinogens to create an immortal cell line from mouse fibroblasts (Earle et al., 1943). Subsequently, George O. Gey and his coworkers developed an immortal cell line from a tissue of a patient diagnosed with uterine cervical cancer, well known as HeLa cells (reviewed in Lucey et al., 2009).

Following the successful development of an immortal human cell line, the paramount importance of cell culture media became more evident. In the 1950's, Harry Eagle developed the minimum essential medium (MEM) which is composed of the minimal essential components (glucose, six inorganic salts, 13 amino acids, eight water-soluble vitamins, and dialyzed serum) required for proper cell growth (Eagle, 1955). MEM was modified and optimized later by increasing the concentration of certain micronutrients, such as glucose and glutamine, to prevent nutrient exhaustion. One such example is the Dulbecco's modified Eagle's medium (DMEM), a standard cell culture media widely used in research labs (reviewed in Abbas et al., 2021).

While the initial purpose of cell culture was to ensure optimal cell growth, recently, the scientific community has come to appreciate maintaining an environment that mimics the physicochemical milieu of the tissue of origin. To achieve that, various aspects of the cell's microenvironment including pH, osmolarity, temperature, viscosity, and the concentrations of amino acids, vitamins, hormones, growth factors, glucose, and O_2 must be taken into consideration. However, standard cell culture practice does not come close to replicating the physiological conditions that cells are experiencing *in vivo*.

Despite the remarkable developments in cell culture over the last decades many discrepancies between *in vivo* biology and cell-based models (e.g., non physiological media composition, the often hyperoxic environment) have not been fully addressed. In addition to providing ample micronutrients to the cells as the main goal, lack of understanding of how physiological conditions are important contributors to this lack of attention. Notably, the field suffers from the lack of suitable methods for precise regulation of pericellular O_2 levels over the course of a cell culture experiment.

The primary desire for the development of traditional synthetic cell culture media was not mimicking human plasma. Indeed, it addresses the need for production of huge amounts of medium with minimal inherent variability than natural media such as tissue extracts biological fluids (Freshney, 2010). Furthermore, depending on cell metabolic activity and proliferative rate, some cell types require higher/lower levels of nutrients than others do. Not only does traditional synthetic cell culture not take that into account, but it also does not replicate human plasma (reviewed in McKee and Komarova, 2017). For example, one of the neglected components is glucose concentrations (25 mM) in common cell culture practices, which is approximately five-times higher than what normal healthy cells experience *in vivo*. This common choice of culturing cells in hyperglycemic condition is to avoid glucose depletion in culture. This poses a huge challenge in various aspects of cell physiology such as cell metabolism. Cell metabolism is highly flexible (reviewed in Cantor and Sabatini, 2012) and greatly impacted by environmental metabolites and stimuli (reviewed in DeBerardinis et al., 2015). Thus, it is not surprising that several recent findings revealed discrepancies between *in vitro* and *in vivo* cancer cell metabolism (Davidson et al., 2017; Biancur et al., 2017). Furthermore, high glucose levels are shown to cause lactate accumulation and pH changes (reviewed in Yao and Asayama, 2017). In the same line,

Elkalaf et al. (2013) reported that C2C12 cells grown and differentiated in a high glucose media have lower capacity for oxidative phosphorylation than cells grown in 5 mM glucose.

Although the nutrient composition of the culture medium influences the phenotypic behavior of cells, their response to stresses and stimuli, transcriptome, and epigenotype, formulating the commercial media to plasma has been largely neglected, until recently (Schug et al., 2015; Tardito et al., 2015; Cantor et al., 2017; Muir et al; 2017; Muir and Vander Heiden, 2018; Vande Voorde et al., 2019). Recently, a physiologic media was developed based on the metabolites and salts at the concentrations reported for healthy adult human plasma referred to as human plasma-like medium [HPLM] (Cantor et al., 2017). Indeed, they observed that culture in HPLM changes the metabolism of cells compared to that in traditional established media. Among its most observed significant effects is inhibition of de novo pyrimidine synthesis, which is related to uric acid (A´lvarez-Lario and Macarro´n-Vicente, 2010; Kratzer et al., 2014). They found that uric acid directly inhibits uridine monophosphate synthase and consequently, lowers the sensitivity of cancer cells to the chemotherapeutic agent 5-fluorouracil (Cantor et al., 2017).

Likewise, to investigate and reduce the gap between *in vitro* observations and tumor biology *in vivo*, Vande Voorde et al., 2019 formulated a complex culture medium, Plasmax, which is composed of more than 50 nutrients and metabolites within the ranges of individual concentrations measured in human blood. The formulations and ingredients of well-established commercial media versus the physiological media (Plasmax) are outlined in Table 1.1. In this study, authors compared triple-negative breast cancer (TNBC) cell lines cultured in Plasmax or in DMEM-F12, a commercially available medium. Their findings demonstrate that the results obtained in commonly used cell biology assays, such as those testing colony formation and gene expression can be significantly affected by media formulation (Vande Voorde et al., 2019). These studies (Vande Voorde et al, 2019; Cantor et al., 2017) reveal that the non-physiological concentrations of nutrients typically included in commercial media affect the metabolism of cancer cells at various levels (Table1.1 shows the constitutes of HPLM, Plasmax and DMEM).

Given that current cancer research largely depends on results obtained using cell culture models, addressing the many inconsistencies between *in vivo* biology and cell-based models (e.g.,

nonphysiological media constituents, absence of waste product removal, and the often hyperoxic environment) may increase the reliability and robustness of results obtained *in vitro*.

Table 1.1. Comparisons between conventionally used medium (DMEM) with newly developed physiological medium (Plasmax). More than 35% of total micronutrients included in Plasmax is made up of components that are absent in DMEM, this allows for more nutritional options for cells to utilize. The values are based off the table from Tobias Ackerman and Saverio Tardido Cell culture medium formulation and its implications in cell metabolism. Not all media constituents are included in this table. Only constituents that had recorded concentrations were included in this table. All values are in µM. ** indicates components that are released from cells.

Proteogenic Amino acids	**Human Plasma**	**DMEM**	**Plasmax**
Alanine **	230-510	-	510
Arginine	13-64	398	64
Asparagine **	45-130	-	41
Aspartic acid	0-6	-	6
Cysteine	23.2-43.8	-	33
Glutamic acid**	32-140	-	98
Glutamine	420-720	4000	650
Glycine **	170-330	400	330
Histidine	26-120	200	120
Isoleucine	42-100	802	140
Leucine	66-170	802	170
Lysine	150-220	798	220
Methionine	16-30	201	30
Phenylalanine	41-68	400	68
Proline **	110-360	-	360
Serine	56-140	400	140
Threonine	92-240	798	240
Tryptophan	44.8-64.2	78	78
Tyrosine	45-74	399	74
Valine	150-310	803	230
Other components	**Human Plasma**	**DMEM**	**Plasmax**
D- glucose	4598.5 - 5344.1	25000	5560
Lactate**	1118.2 - 1860.6	-	500
Urea	3920.4 - 8228.8	-	3000
Inorganic Salts	**Human Plasma**	**DMEM**	**Plasmax**

Calcium Chloride	1100-1320	1802	1899
Sodium Chloride	136000–145000	110345	118706
Potassium Chloride	3500–5600	5333	5330
Sodium Bicarbonate	23000–28000	44048	26191
Vitamins	**Human Plasma**	**DMEM**	**Plasmax**
p- Aminobenzoate	5.0 - 32.0	-	-
Ascorbate	57.9 - 67.3	-	62
D- Biotin	0.0006 - 0.0019	-	4.1
Choline	9.2 - 19.8	28.6	7.1
Folate	0.017 - 0.025	9.10	2.30
Myo- Inositol	17.1	40	11.1
Niacinamide	0.435 - 0.445	32.8	8.2
D- Calcium Pantothenate	4.5 - 5.3	8.40	2.10
Pyridoxine	0.007 - 0.060	19.40	4.90
Riboflavin	0.0054 - 0.028	1.10	0.30
Thiamine	0.078 - 0.114	11.2	3.0
Vitamin B-12	0.00017 - 0.00033	-	0.0050

In addition to the importance of medium formulation in designing the interpretation of biological research, O_2 is another important, often neglected variable. In fact, one of the most salient discrepancies between routine mammalian cell culture and the *in vivo* environment is the O_2 tensions to which cells are exposed. Room air at sea level contains 160 mmHg O_2, and the air in a humidified CO_2 cell culture incubator commonly consists of 140 mmHg O_2 (20.9% and 18.5% O_2, respectively) (Shown in Figure 1.9). In contrast, most cells in healthy human tissues are exposed to the far lower O_2 tensions ranging from ~5–100 mmHg (0.5 - 10% (physioxia) (reviewed in Carreau et al., 2011) (see Table 1.2). O_2 tensions within a given tissue can also fluctuate according to the metabolic demand. For example, during intense exercise, skeletal muscle oxygenation levels decrease from 30 mmHg O_2 to 7.5 mmHg O_2 (Bylund-Fellenius et al., 1981). O_2 tensions also significantly decrease in cancer and could be as low as 2 mmHg within the cores of tumors (McKeown, 2014). Undoubtedly, mammalian cell culture models, even with supraphysiological O_2 tensions, have resulted in important discoveries; however, investigators must be mindful of how certain facets of biology can be obscured by non-physiologic O_2.

Notably, standard tissue culture conditions (140 mm Hg) expose cells to a partial pressure of O_2 that is even higher than that experienced by the lung alveoli (~110 mm Hg), which are exposed to the highest partial pressure of O_2 of any tissue in the human body (Carreau et al., 2011). Cell culture is typically conducted in the absence of O_2 regulation, resulting in a hyperoxic (~18% O_2 in gas phase) environment (Figure 1.9) (reviewed in Keeley and Mann, 2019). In fact, virtually all modern cell culture laboratories fail to maintain O_2 levels within physiological "normoxic" limits (1 and 6%) (reviewed in Keeley and Mann, 2019), which has effects on culture viability, experimental validity, and reproducibility. While various categories of cellular processes known to be affected by O_2, there is a limited mechanistic understanding of how supraphysiological O_2 levels modulate specific O_2 dependent processes.

Cultivating cells at ambient O_2 levels has been shown to affect several cellular processes, such as cell metabolism, cell replicative growth and apoptosis (reviewed in Al-Ani et al., 2018)) amongst a wide range of other less well-characterized effects. Specifically, applying multiple human cell lines, Timpano et al. (2019) recently have shown that different O_2 tension exposure (ranging from 1%-21%) can significantly modify oxidative lesions to macromolecules (eg., DNA,

RNA), the expression of DNA damage and antioxidant genes, cellular viability and metabolism, and mitochondrial networks and morphology (Timpano et al., 2019). Consistently, several studies show that human mesenchymal stem cells cultured at atmospheric O_2tension (21% O_2) undergo an enhancement in cell senescence markers compared to those cultured at low physiological *in vivo* O_2 tension (Tsai et al., 2011; Kim et al., 2016; Vono et al., 2018). For instance, culturing human dental pulp stem cells under 21% O_2 level led to increased levels of p16 mRNA expression and senescence associated-β-galactosidase activity compared to those cultured at 5% O_2. In this same study, cells cultured at 21% O_2 demonstrated a significant decrease in mitochondria membrane potential and higher levels of ROS in comparison with cells cultured at 5% O_2 (Mas-Bargues et al., 2017). However, they did not attempt to identify the mechanism(s) underlying this effect of O_2 on ROS production. This evidence indicates the dramatic impact that commonly used environmental O_2 level might impose on the highly regulated network of signalling pathways explored under *in vitro* conditions. Moreover, this evidence is compelling enough to state that mammalian cells benefit from being cultured in more physiologic conditions with respect to O_2 tension.

One potential consequence of elevated O_2 in cell culture media is the enhanced cellular production of reactive oxygen and nitrogen species (ROS and RNS) (Halliwell, 2003). Notably, the Michaelis-Menten constant (Km (O_2)) of many ROS and RNS producing enzymes strongly suggest that they can be affected by the O_2 levels (reviewed in Stuart et al., 2018). Consistently, using Amplex Red/horseradish peroxidase assay, H_2O_2 efflux rate was higher for all cell lines growing at 18% O_2, when compared to a more physiological relevant O_2 level (5% O_2) (Maddalena et al., (2017). This oxidative stress observed *in vitro* can influence many important cellular functions and pathways (Holmström and Finkel, 2014).

The main initial reason for maintaining atmospheric O_2 levels in cell culture conditions was to ensure that O_2 availability does not become a limiting factor for cytochrome c oxidase (Complex IV) of the mitochondrial electron transport chain respiration. However, typical cell culture O_2 levels are remarkably higher (approximately 10-fold) than what is required for maximal mitochondrial respiration rates (Gnaiger, 2001; Marcinek et al., 2003; Hoffman et al., 2007). Interestingly, the affinity for O_2 by cytochrome c oxidase (½ maximal (P50/KM) is 0.075 − 0.75 mmHg (0.0097 − 0.097 mM) is exceptionally high compared to other O_2 consuming reactions in

the cell. Due to this high affinity, the mitochondrial respiration can continue until the local concentration of O_2 is very low, so long as the delivery of new O_2 (flux) meets the demands of respiration (reviewed in Place et al., 2017). Moreover, while no scientists would disagree that O_2 tensions alter cell biology, the convenience of culturing cells in ambient O_2 is tempting enough to maintain this widespread approach. In fact, the workstations with glove ports required for appropriate cell culture at physioxic O_2 tensions (e.g., long-term cell maintenance, passaging, and treatment at desired O_2) are expensive in comparison to common cell culture incubators.

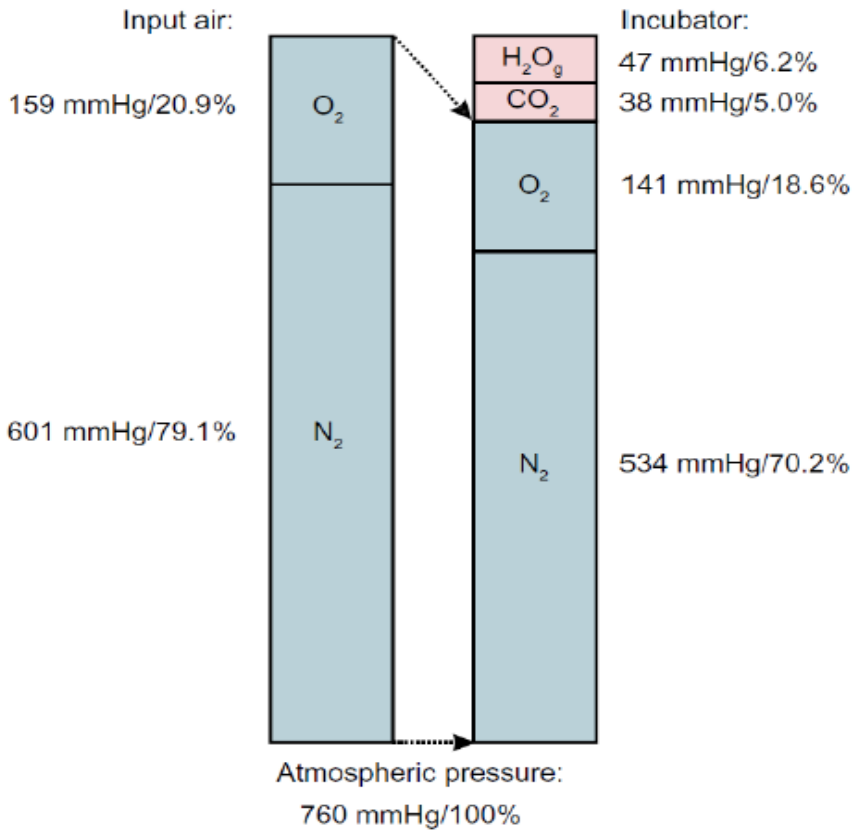

Figure 1.9. Gas phase composition in a common cell culture incubator. Dry air relative gas concentrations are depicted in the left bar. The bar on the right demonstrates the relative gas concentrations in a typical incubator. Gaseous O_2 concentration in the context of cell culture is often cited as 21%. Whereas 21% does show the volume/volume fraction of O_2 in dry air (78.09% nitrogen, 20.95% O_2, 0.93% argon, and 0.039% carbon dioxide), conventional cell culture incubators have additional volumes of both water vapor and CO_2 gas. Adapted from Wenger et al., 2015.

Table 1.2. Mean values of pO_2 in several human tissues are shown. pO_2 value is defined as the balance between O_2 delivery and its consumption, range from as low as 1% O_2 (e.g., mitochondria) to ~15% O_2 (e.g., alveoli). These values are expressed in mmHg and in percentage of O_2 in the microenvironment. Reproduced from Carreau et al., 2011.

	Average mmHg	**Average % pO_2**
Atmospheric air	160	~20.9
Inspired air (in the trachea)	150	19.7
Air in the alveoli	110	14.5
Arterial blood	100	13.2
Kidney	72	9.5
Intestinal tissue	57.6	7.6
Liver	40.6	5.4
Venous blood	40	5.3
Skin (sub-papillary plexus)	35.2	4.6
Brain	33.8	4.4
Muscle	29.2	3.8
Bone marrow	14.5	2
Skin (superficial region)	8	1.1
Mitochondria	<9.9	<1.3

As previously described, ROS are produced by a wide range of organelles and enzymes. A few important producers are the mitochondria, NOXs, xanthine oxidase/oxidoreductase, uncoupled nitric oxidase synthase, trans-plasma membrane redox system, cyclooxygenase, cytochrome P450 enzymes, monoamine oxidase and lipoxygenase. The oxygen-dependence of ROS production by these enzymes and organelles vary widely. Thus, it is expected that their activity will differ widely in the range between physioxia and 18% O_2. For example, in mitochondria complex I FMN site and complex III Q0 site, considered the main sites of ROS production in culture cells, are both saturated at low O_2 levels (Hoffman and Brookes, 2009; Hoffman et al., 2007). Based on this observation, it can be logical to conclude that the rate of mitochondrial ROS production is not O_2-limited in cell culture, and therefore no significant difference is expected to be seen between physioxia and hyperoxia conditions. However, Grivennikova et al. (2018) have shown that ROS production from heart mitochondrial respiratory chains is linearly correlated to O_2 levels. The emergence of contradictory findings might be partially attributed to the fact that different laboratories employ different techniques to measure ROS. In addition to that, determining the concentration of different ROS species is notoriously known to be challenging and error-prone (Beijing and Huang, 2014). Most importantly, it could be related to context-dependency of mitochondrial complex IV in terms of its sensitivity to O_2 levels.

There is a lack of data on Km (O_2) for any of the NOX isoforms. Moreover, some doubt exists regarding the validity and reliability of some assays of NOX activity using isolated membrane fractions (Rezende et al., 2016; Rezende et al., 2017). Nonetheless, O_2 levels in cell culture have been reported to modulate NOX protein activity; the available data indicate that the activities of NOX1, NOX2, and NOX4 are all sensitive to O_2 levels in the range from 5% to 18% (Diebold et al., 2010; Gregg et al., 2014; Stuart et al., 2018). NOX4, with a Km (O_2) value~18%, is particularly sensitive over this range; NOX4 activity triples between 3% and 12% O_2 (Dmitriev et al., 2016). In the same line, NOX4 activity shows a 300% increment in cells cultured at 12% O_2, in comparison to 3% (Nisimoto et al., 2014). Consistently, using a specific inhibitor against both NOX1 and NOX4 isoforms, referred to as GKTT138731, H_2O_2 efflux rate at 18% O_2 was significantly lowered in C2C12 and PC3 cells. However, when cells were grown at 5% O_2 such an inhibitory effect disappeared (Maddalena et al., 2017). Similarly, H_2O_2 efflux rate at 18% O_2 in NOX knock-out mouse models (e.g., NOX1/2/4 triple knockout mouse dermal fibroblasts) is reduced when compared to their wild-type counterparts (Stuart et al., 2018). In addition, there is

evidence showing NOX protein expression levels can be affected by O_2 concentration. We have recently shown that both NOX1 and NOX4 protein expression levels show a reduction pattern at 18% O_2 versus 5% O_2 (Stuart et al., 2018). In addition, there are evidence showing that O_2 affinities of nNOS and iNOS are found relatively consistently to be within a range that is sensitive to changes in O_2 levels between physioxia and 18% O_2 (Rengasamy and Jonhs, 1996). Indeed, cell lines with high expression levels of these isoforms are likely to generate more NO under standard cell culture conditions than *in vivo* (reviewed in Stuart et al., 2018).

Cell culture is an important approach for understanding the cellular and molecular bases of biological phenomena. However, several aspects of traditional cell culture practices limit the accuracy of data collected. Using physiological media and O_2 levels will improve the accuracy, robustness, and reproducibility of obtained results. Finally, such a shift remarkably facilitates extrapolating results from *in vitro* findings to *in vivo* which has lagged various aspects of biomedical research such as drug development.

THESIS OUTLINE

In the first data Chapter, I explore the effects of RES on mitochondrial network dynamics; proliferative cell growth and cellular respiration, more specifically I investigate the role of Mfn2. However, we found out that many effects of RES depend on glucose and O_2 concentrations in cell culture (Fonseca et al., 2018). Since E_2 and the RES have been shown to have overlapping effects on many aspects of mitochondrial functions, I hypothesized that like the dependency of the effects of RES on cell culture condition, E_2 would behave consistently. Thus, in the second data Chapter, I explore the impacts of cell culture conditions on the effects of E_2 on mitochondrial network dynamics, cellular H_2O_2 release and cellular respiration. To expand our understanding, in the third data Chapter, I explore how mitochondrial function and morphology of human cancer cells might be distinct based on the cell culture conditions. Given that, I observed the pervasive effects of cell culture conditions on a broad range of cellular phenotypes, I set out to explore how transcriptomes and proteomes of MCF7 breast cancer cells might be affected by various media conditions in the fourth data Chapter.

CHAPTER 2: Resveratrol stimulates mitochondrial fusion by a mechanism requiring mitofusin-2

This chapter is published as: Robb, E. L., Moradi, F., Maddalena, L. A., Valente, A. J., Fonseca, J., & Stuart, J. A. (2017). Resveratrol stimulates mitochondrial fusion by a mechanism requiring mitofusin-2. *Biochemical and biophysical research communications*, 485(2), 249-254. Robb and Moradi are co-first authors.

Author Contributions

I performed all experiments on MEF and Mfn2-null cells, and Ellen Robb performed the remaining experiments. Lucas Maddalena and Andrew Valente assisted with data analysis and confocal microscopy experiments. Joao Fonseca contributed to cell culture experiments. I, Ellen Robb, Lucas Maddalena and Jeff Stuart wrote the manuscript.

ABSTRACT

Resveratrol (RES) is a plant-derived stilbene associated with a wide range of health benefits. Mitochondria are a key downstream target of RES, and in some cell types RES promotes mitochondrial biogenesis, altered cellular redox status, and a shift toward oxidative metabolism. Mitochondria exist as a dynamic network that continually remodels via fusion and fission processes, and the extent of fusion is related to cellular redox status and metabolism. We investigated RES's effects on mitochondrial network morphology in several cell lines using a quantitative approach to measure the extent of network fusion. 48 h continuous treatment with 10-20 μM RES stimulated mitochondrial fusion in C2C12 myoblasts, PC3 cancer cells, and mouse embryonic fibroblasts in all instances, resulting in larger and more highly branched mitochondrial networks. Mitofusin-2 (Mfn2) is a key protein facilitating mitochondrial fusion, and its expression was also stimulated by RES. Using Mfn2-null cells we demonstrated that RES's effects on mitochondrial fusion, cellular respiration rates, and cell growth are all dependent upon the presence of Mfn2. Taken together, these results demonstrate that Mfn2 and mitochondrial fusion are affected by RES in ways that appear to relate to RES's known effects on cellular metabolism and growth.

INTRODUCTION

Resveratrol (trans-3,4,5 trihydroxystilbene; RES) is a plantderived stilbene associated with protection from a battery of seemingly unrelated diseases (reviewed in Stuart et al., 2013). Aberrant cellular metabolism (either acute or chronic) is implicated in the aetiology of many disorders ameliorated by RES. RES exerts metabolic effects in many cell types, promoting mitochondrial biogenesis and a shift toward a more oxidative phenotype (Lagouge et al., 2003; Sheu et al., 2013; de Oliveira et al., 2016; del Mar Blanquer-Rosselló et al., 2017).

Mitochondria are thus an important target of RES (reviewed in de Oliveira et al., 2016) which has been shown to stimulate mitochondrial biogenesis and altered redox status in skeletal muscle, cardiac and brain tissue, and in many cultured cell lines (Lagouge et al., 2003; López-Lluch et al., 2003; Zhao et al., 2012; Dolinsky et al., 2013). These RES induced effects on mitochondrial metabolism may be central to its many cellular effects. Mitochondrial dynamics are an important aspect of mitochondrial and cell physiology that has not been thoroughly explored in the context of RES. Within cells, mitochondria exist in a dynamic equilibrium between fusion and fission, to form highly connected and independent mitochondrial structures, respectively. This equilibrium is highly malleable, shifting in response to changes in nutrient availability, redox state and the activities of intracellular signalling cascades (reviewed in Youle et al., 2012). Architectural changes in the mitochondrial network are thought to contribute to the 'metabolic efficiency' of the cell, with a more fused, interconnected network associated with increased oxidative metabolism. In contrast, a fragmented network is commonly observed in primarily glycolytic cells (Gomes et al., 2011; Jheng et al., 2012).

Mitochondrial network dynamics are also related to cell division. Mitochondria typically elongate and fuse during G1/S, and fragment during G2/M in a process known as mitotic fission. Interestingly, a highly fused mitochondrial network achieved by either the stimulation of fusion or inhibition of fission (Rehman et al., 2012) can impede progression through the cell cycle, while fragmentation of the mitochondrial network appears to be permissive of rapid proliferation (Taguchi et al., 2007; Mitra et al., 2009; Zhao et al., 2012). In support of the central role of mitochondrial morphology in cell physiology, pharmacological manipulation of the mitochondrial fusion state can directly affect proliferation. Stimulation of network hyperfusion by inhibition of the

fission enzyme dynamin-related protein 1 (Drp1) with the compound mdivi-1 is sufficient to slow the growth of cancer cells (Thomas and Jacobson et al., 2012; Rehman et al., 2012).

Gene knockout of the fusion enzyme mitofusin2 (Mfn2) to produce a fragmented mitochondrial population significantly increases proliferative growth rate in B-cell lymphocytes and mouse embryonic fibroblasts (MEFs), while Mfn2 overexpression slows growth (Rehman et al., 2012; Chen et al., 2014). The slowed cell growth associated with mitochondrial hyperfusion is strikingly similar to the slowed cell growth elicited by RES in multiple cell lines and *in vivo* (Janig et al., 1997; Baur and Sinclair, 2006; Motylewska et al., 2009). Given that changes in both mitochondrial turnover and redox state impact upon the morphology of the mitochondrial network (Youle et al., 2012; Shutt et al., 2012); it is plausible that RES alters mitochondrial dynamics to affect cell proliferation. Two recent studies have shown that RES treatment is associated with changes in the levels of mitochondrial fusion/fission proteins under conditions of metabolic stress (Peng et al., 2016; Palomera-Avalos et al., 2017).

However, there are no reports of RES effects on mitochondrial dynamics under non-stressed conditions nor has the fusion state of mitochondrial networks been quantitatively analysed in RES-treated cells. Here we use MiNA, a mitochondrial network morphology analysis tool (Valente et al., 2017) to determine features of the mitochondrial network in cells following treatment with RES. We demonstrate that RES stimulates mitochondrial fusion that is associated with increased Mfn2 expression and, using Mfn2-null cells, further show that Mfn2 is required for this increased fusion. We further show that RES's effects on cell growth are dependent on Mfn2.

EXPERIMENTAL PROCEDURES

Materials

Modified Eagle Medium with Earl salts, L-glutamine and sodium bicarbonate, Dulbecco's Modified Eagle Medium with high glucose (25 mM), L-glutamine and sodium bicarbonate and Dulbecco's Modified Eagle Medium were obtained from Sigma Aldrich (St. Louis, MO). Penicillin/streptomycin, non-essential amino acids, and fetal bovine serum were obtained from Hyclone (Logan, UTtah). RES was obtained from A.G. Scientific (San Diego, CA). BioRad protein dye was purchased from BioRad laboratories (Hercules, CA). Prestained broad range protein marker was purchased from BioLabs (New England, MA). Pierce Memcode Reversible Protein Stain Kit™ was obtained from Thermo Fisher Scientific (Mississauga, Canada). Mfn2 antibody was purchased from Abnova (Walnut, CA). Infrared dye-conjugated secondary antibody to mouse was purchased from Rockland Immunochemicals (Gilbertsville, PA). Renilla luciferase kit was purchased from Promega (Madison, WI). CellLight mtGFP and MitoTracker Red CMXRos dye were purchased from Life Technologies (Burlington, ON). All other chemicals and purified enzymes were obtained either from SigmaeAldrich (St. Louis, MO), BioShop (Burlington, Canada) or Fisher Scientific (Mississauga, Canada) unless otherwise stated.

Cell lines and culture conditions

C2C12 (Sigma) and PC3 (ATCC) cell lines were cultured in accordance with the distributor's protocol. HeLa cell lines expressing N or C Mito venus-zipper-luciferase (mitoVZL) were a gift from Dr. Heidi McBride at McGill University. They were generated and cultured as described in Ref. (Schauss et al., 2010). Mfn2-null and wt MEFs were purchased from the Jackson Laboratory (Bar Harbor, Maine, USA). All cell lines were cultured at 37 ^{o}C in humidified 5% CO_2, 18% O_2 atmosphere. Cell density and population doubling time were determined by direct counting. Treatments were added directly to culture media and refreshed daily until cells were harvested.

Microscopy

Mitochondria were imaged following transfection with the mitochondrial targeted GFP probe CellLight mtGFP, as per the manufacturer's protocol, or following 15 min incubation with 50 nM MitoTracker Red in a 37°C, 5% CO_2 humidified incubator, as indicated in Results section. Cells were washed with warmed PBS and imaged immediately with either an Olympus Fluoview 300 confocal microscope or Zeiss Axio Observer. Z1 inverted epifluorescence microscope equipped with ApoTome.2 optical sectioning, with a 63 1.4NA oil immersion lens. Analysis of mitochondrial morphology Mitochondrial morphology was analysed using the Mitochondrial Network Analysis tool (MiNA) a macro tool developed for use with the FIJI distribution of ImageJ (Valente et al., 2017). Briefly, fluorescence images were loaded into the program in their native format using BioFormats plugin (Linkert et al., 2010). Images were prepared for analysis through the application of an unsharp mask with a 2 pixel radius to sharpen the image. A median filter was then applied using a 2 pixel radius to remove spurious features without causing a significant loss to high frequency information. The image was then skeletonized, and the skeleton analysed using the Analyse Skeleton plugin included in the FIJI distribution (Arganda-Carreras et al., 2010). Structures containing at least one branch point were considered networks (Leonard et al., 2015).

Cell free mitochondrial fusion assay

Cells (including N and C mitoVZL expressing HeLa) were harvested by trypsinization, and mitochondrial isolation was performed at described in Ref. (Peng et al., 2016). Briefly, 50 mg of C and N mitoVZL mitochondria were incubated in a reaction containing 10 mM HEPES pH7.4, 110 mM mannitol, 68 mM sucrose, 80 mM KCl, 0.5 mM EGTA, 2 mM Mg (CH3COO)2, 0.5 mM GTP, 2 mM K2HPO4, 1 mM ATP, 0.08 mM ADP, 5 mM Na succinate, 1 mM DTT and 5 mg/ mL cytosol. The mitochondria were concentrated by centrifugation, and then incubated on ice for 30 min. The mitochondria were resuspended and incubated in a 37 °C water bath for 30 min. Signal arising from ruptured mitochondria was quenched by incubation with 25 mg trypsin for 15 min on ice, after which trypsin activity was inhibited by incubation with 500 mg soybean trypsin inhibitor for 15 min on ice. Mitochondria were concentrated by centrifugation at 9000g for 1 min and solubilized by 1 h incubation with 50 mL of lysis buffer (Promega) on ice. Luciferase activity was

detected using a commercially available Renilla luciferase kit (Promega) and fluorescence was detected using a Varian Cary Eclipse fluorescence spectrometer.

Cell cycle analysis

Cells were harvested via trypsinization and centrifugation (5 min at 240g), washed once with PBS and then fixed via drop-wise addition of ice-cold ethanol (75% v/v) with routine vortexing. The cell suspensions were then kept at -20 ^{o}C for 2 h before undergoing centrifugation (5 min at 240g) and two washes with ice-cold PBS. Fixed cells were incubated with 0.5 mL Propidium Iodide (PI)/RNase Staining Buffer (BD Pharmingen, USA) in darkness at room temperature for 15 min. The DNA content was measured using a BD Accuri C6 flow cytometer (BD Biosciences, USA). PI signal was detected in the orange range of the spectrum using a 562-588 nm band pass filter. For each sample, 100,000 events were recorded using a medium data acquisition rate, as per the manufacturer guidelines. The percentages of cells in G0-G1, S, and G2-M phases were determined using the CFlow Plus software (BD Biosciences, USA).

Cellular respiration measurements

Oxygen consumption rates of intact cells were measured using a Clark-type O_2 electrode (Rank Brothers Dual Digital Model 20 Respirometer; Bottisham, UK) within a thermostatically-controlled chamber. Cells were harvested via trypsinization and centrifugation (240g for 3 min) before being re-suspended in 1 mL of complete culture media (serving as respiration buffer) and placed into the chamber maintained at 37 ^{o}C. Following the recording, the cell suspension was centrifuged (2200 g for 3 min) and the supernatant discarded.

Preparation of whole cell lysates

Cells were lysed by incubation for 1 h in ice cold lysis buffer (10 mM) Tris pH 8.0, 150 mM NaCl, 2 mM EDTA, 2 mM dithiothreitol, 0.4 mM PMSF, 40% (v/v) glycerol, 0.5% (v/v) NP40 with periodic sonication (Ultrasonic Inc., Sonicator W-375; setting 3). Cell lysates were then centrifuged at 10 000 g (4 C) for 10 min (Thermo Scientific, IEC Micromax/Micromax RF) and the pellet discarded. Protein concentration of the supernatant was determined by the Bradford method with bovine serum albumin as the protein standard.

Western blots

For western blots, Memcode Reversible Protein Stain Kit™ was used to stain PVDF membranes to verify equal protein loading/ transfer. Following blocking, membranes were incubated with antiMfn2 or anti-Drp1 (both at 1:1000 dilution) for 1 hr at room temperature. Following incubation with appropriate secondary antibody, membranes were imaged using the LiCOR Odyssey system.

STATISTICAL ANALYSIS

Data were analysed by t-tests, one-way ANOVA, or repeated measures two-factor ANOVA (as stated in Results section) using either Systat v.12 or GraphPad Prism 5 software. Post-hoc comparisons between means were done by Tukey's test. All data are presented as means ± standard error of the mean (SEM). A p-value of <0.05 was considered significant.

RESULTS

Mitochondrial network morphology was initially assessed in C2C12 and PC3 cells. Cultured cells were treated with 20 μM RES continuously for 48 h then either transfected with a mitochondrial targeted green fluorescent protein (mtGFP) or loaded with Mito Tracker Red and imaged (Figure 2.1A). Mitochondrial morphology was analysed using MiNA to determine the number (structures with at least one branch) and size (number of branches) of mitochondrial networks in both cell lines (Figure 2.1B). Consistent with RES's previously reported stimulation of mitochondrial biogenesis, there were significantly more mitochondrial networks in both cell types following RES treatment. RES also increased the average number of branches per network in both cell lines indicating that, in addition to there being more mitochondrial networks, these networks tended to be more highly fused. As an orthogonal approach to assess the effect of RES on mitochondrial fusion, we employed the cell-free biocomplementation assay developed by Schauss et al., (2010). In this *in vitro* fusion assay, luciferase-catalyzed luminescence can be detected when two populations of mitochondria, each with one half of a luciferase protein, fuse and share contents to make a single functional luciferase.

Cytosol extracts from RES-treated C2C12 cells showed increased stimulation of mitochondrial fusion in this assay compared to those treated with the vehicle control (Figure 2.1C). The direct addition of RES to the reaction had no effect on fusion (not shown), indicating no direct effect of RES on the assay. We quantified the levels of two major fission and fusion proteins, Drp1 and Mfn2, respectively, in C2C12 cells treated with RES or vehicle control (DMSO). Whereas Mfn2 protein levels were elevated in cells treated with RES, no effect on Drp1 levels were observed (Figure 2.1D). This, combined with the RES-stimulation of fusion in the luciferase assay (which is independent of fission), suggested that the increased mitochondrial network size was related specifically to a pro-fusion effect of RES.

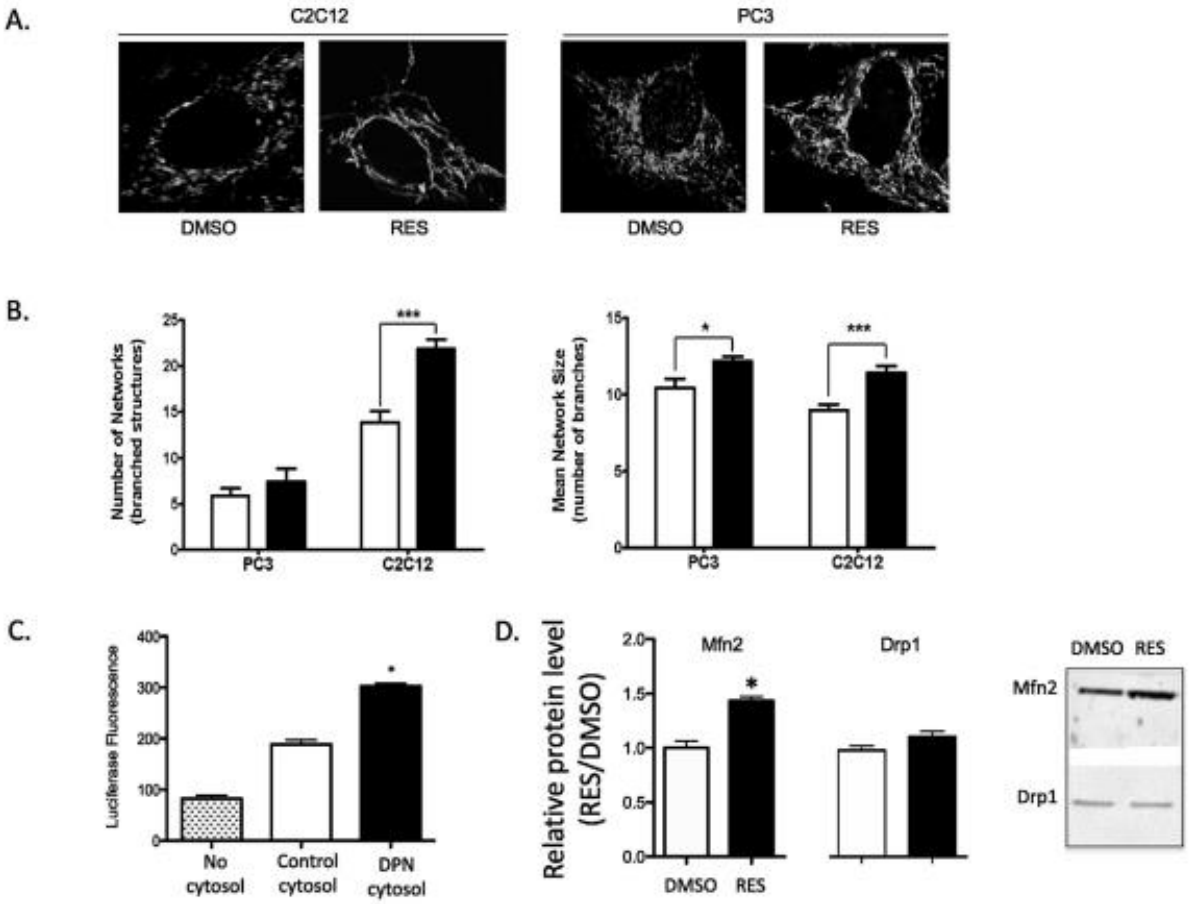

Figure 2.1. Resveratrol stimulates mitochondrial fusion. (**A)** Representative images showing the effect of treatment for 48 h with 20 µM RES on mitochondrial network morphology in C2C12 and PC3 cells treated. (**B)** RES treatment increases number of networks (branched structures), and the mean size of individual networks (number of branches) in both cell types. Data shown are means ± SEM of 30 individual cells from three independent experiments for each cell line and condition. (**C)** RES stimulates mitochondrial fusion as measured in a cell-free fusion assay. Graph shows luciferase fluorescence resulting from *in vitro* mitochondrial fusion in the presence of cytosolic extracts from C2C12 cells treated with either vehicle control or 20 µM RES for 48 h. Data shown are the means ± SEM of three independent experiments. *=$p < 0.05$, ***=$p < 0.001$ compared to vehicle control. (**D)** RES treatment elevates Mfn2, but not Drp1, levels in C2C12 cells. Data shown are the means ± SEM of three independent measurements. *=$p < 0.05$.

To explore the role of Mfn2 in RES's effects on mitochondrial network fusion we used wild type (wt) and Mfn2-null MEFs (Mouse embryonic fibroblast) (Chen et al., 2005). MEFs were treated with either 10 mM RES or vehicle control (DMSO) for 48 h. As in C2C12 and PC3 cells, RES had significant effects on network morphology in both wt (Figure 2.2A) and Mfn2-null (Figure 2.2B) MEFs. In wt MEFs, RES treatment increased the number and size (number of

branches) of mitochondrial networks (Figure 2.2C). In contrast, while RES treatment increased the number of networks in Mfn2-null MEFs, it had no effect on network size in these cells (Figure 2.2D). The continued stimulation of network number suggested that Mfn2 is not necessary for the effect of RES on mitochondrial biogenesis. The morphology of the mitochondrial network is related to the cell's reliance on oxidative metabolism, and RES has been reported to stimulate oxidative metabolism in various cell types (de Oliveira et al., 2016).

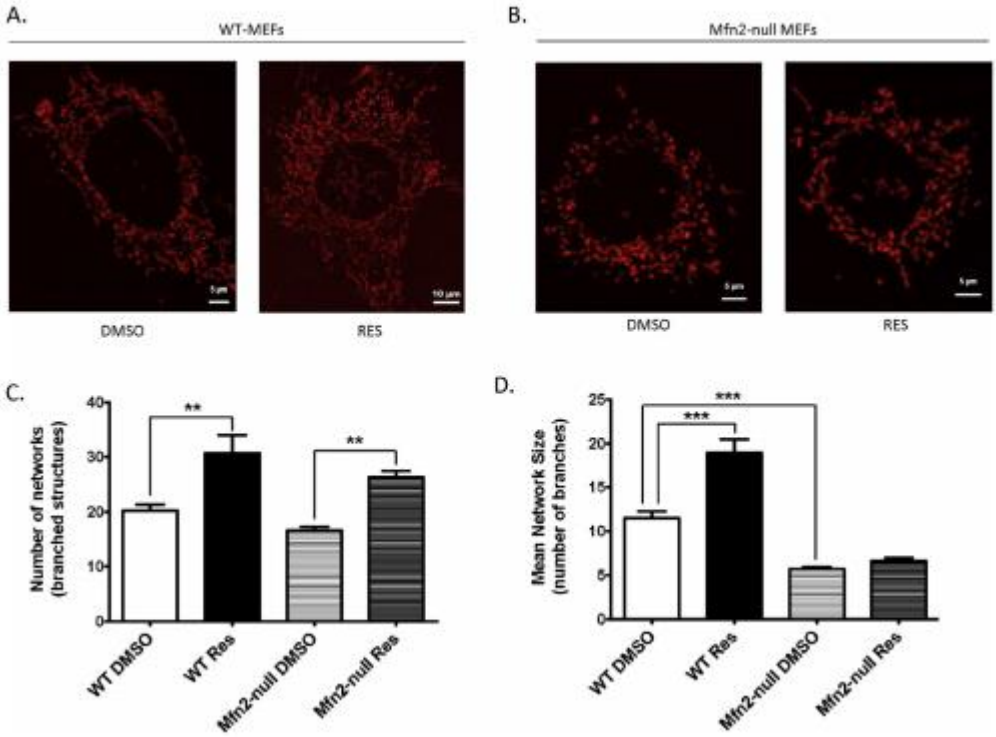

Figure 2.2. RES does not stimulate mitochondrial fusion in Mfn2-null MEFs. **A.** and **B.** Representative Images of wt **(A)** and Mfn2-null **(B)** MEFs treated with 10 µM RES for 48 h. **(C)** RES increased the number of networks in both genotypes. **(D)** RES increased mean network size (number of branches) in wtMEFs but not in Mfn2-null MEFS. Data shown are the means ± SEM of measurements taken from 75 to 125 individual cells over 3-4 independent experiments. *=$p < 0.05$, **=p-value< 0.001 compared to vehicle control.

Consistent with this, RES stimulated a significant increase in both basal and uncoupled O_2 consumption rates in wtMEFs (Figure 2.3). This effect was absent in the Mfn2-null MEFs, which had lower rates of O_2 consumption per cell than wtMEFs. Thus, Mfn2 is required for the RES-stimulated shift toward increased respiration in MEFs. Mitochondrial metabolism is thought to contribute to the regulation of cell cycle progression (Detmer and Chan, 2007) and RES has been widely reported to affect cell cycle progression and cell growth (reviewed in de Oliveira et al., 2016). We therefore investigated whether the ability of RES to affect cell growth was dependent upon Mfn2. Interestingly, although RES increased population doubling time of wt MEFs (Figure 2.4A) and increased the proportion of cells in G0/G1 phase (Figure 2.4B), it had no effect on growth (Figure 2.4A) or cell cycle distribution (Figure 2.4C) of Mfn2-null cells. Together, these data support the hypothesis that RES promotes an Mfn2-dependent increase in mitochondrial network fusion that is associated with a shift toward a more oxidative phenotype and slowed growth.

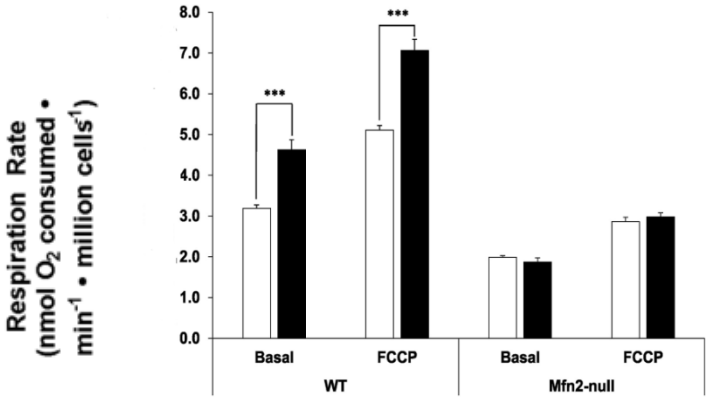

Figure 2.3. RES stimulates respiration in wt but not Mfn2-null MEFs. RES increases basal and FCCP uncoupled respiration rates in wtMEFs but has no effect on Mfn2-null MEFs. Data shown are means ±SEM of 5-12 independent measurements. *** = $p < 0.001$.

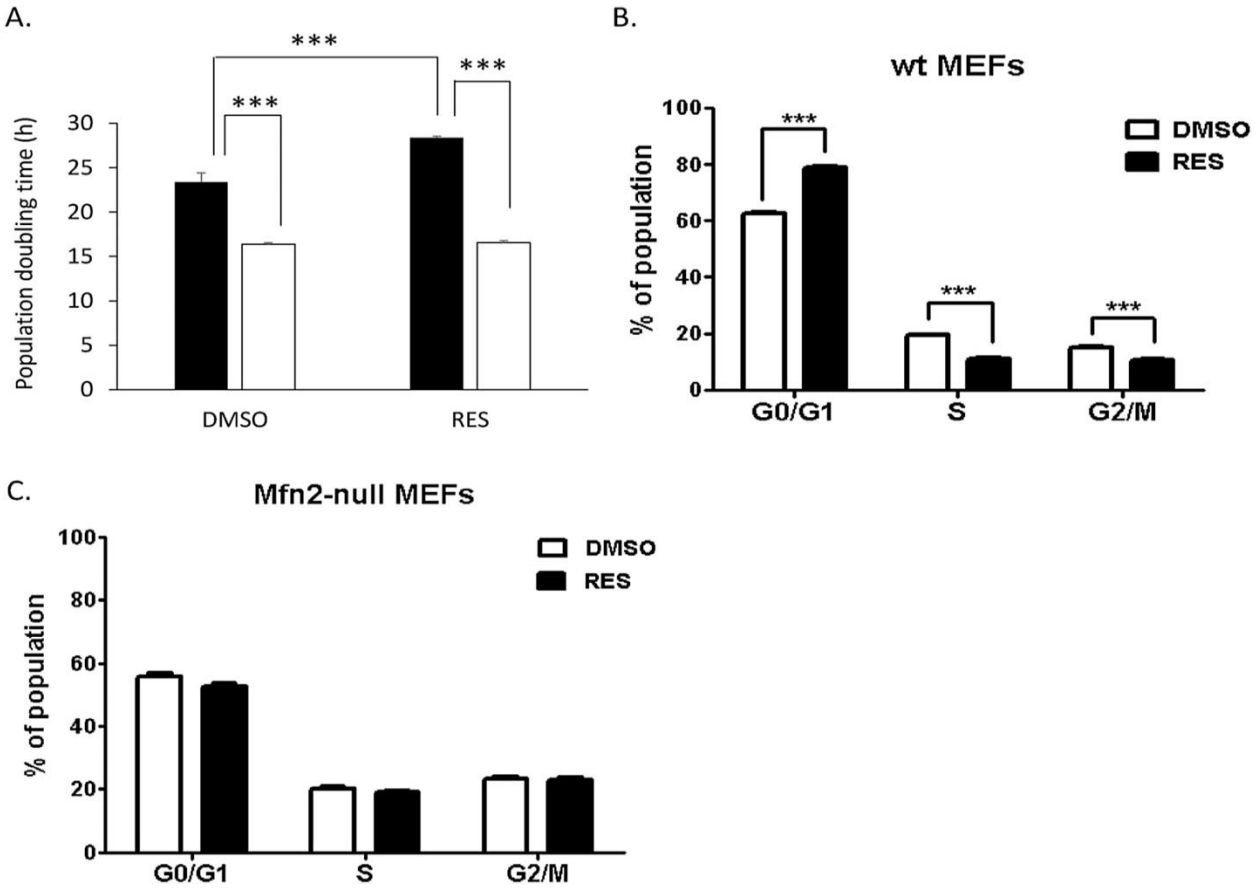

Figure 2.4. No effect of RES on cell growth in Mfn2-null MEFs. (A) 48 h treatment with 10 μM RES inhibits proliferative growth in wtMEFs (filled bars) but has no effect on Mfn2-null MEFs (open bars). ***=$p < 0.001$ compared to vehicle control. RES increases the proportion of wtMEFs in G0/G1 **(B)** but has no effect on cell cycle distribution in Mfn2-null MEFs **(C)** Data shown are means ±SEM of 3-5 independent experiments. *** = $p < 0.001$.

DISCUSSION

In many cell types and tissues, mitochondria are the important downstream targets of RES (reviewed in Stuart et al., 2013), and two recent publications indicate that RES can affect mitochondrial fusion and fission under conditions of metabolic stress *in vitro* (Peng et al., 2016) and *in vivo* (Palomera-Avalos et al., 2017). The results presented here represent the first analysis of RES's effects on mitochondrial network morphology under basal, non-stressed conditions. RES stimulated mitochondrial fusion in all three cell lines we investigated: C2C12 myoblasts, PC3 prostate cancer cells, and MEFs. Given the consistency of effects on these three cell lines, and previous reports of RES affecting mitochondrial fusion machinery under metabolic stress in PC12 cells (Peng et al., 2016) and mouse brain (Palomera-Avalos et al., 2017), it appears that RES can stimulate mitochondrial fusion in many mammalians cell types.

The pro-mitochondrial fusion effect of RES may contribute to its ability to ameliorate the negative effects of various diseases associated with metabolic stress, since fusion of the mitochondrial network is recognized for its role in maintaining mitochondrial and cellular functions (eg., Detmer et al., 2007; Salazar-Roa et al.,2017). Whereas fragmented mitochondria are predisposed to heterogeneity and have diminished respiratory capacity (Cassidy-Stone et al., 2008), elongation and interconnection of the mitochondrial network promotes the sharing of matrix constituents, maintenance of mitochondrial DNA integrity, and overall 'efficiency' of oxidative phosphorylation (Schieke et al., 2008). Small molecules like RES with the capacity to promote mitochondrial fusion are therefore of great interest for their potential as disease treatments. The stimulation of Mfn2 expression and promotion of mitochondrial fusion may also contribute to RES's growth inhibitory effects on some cancer cell lines *in vitro* and tumours *in vivo*. Many cancer cells are typified by their reliance on aerobic glycolysis, with reorganization of cellular metabolism to support the increased anabolic needs of the dividing cell (Lu et al., 2015). Strategies that prevent, or revert, this metabolic transition and promote oxidative metabolism are associated with slowed cancer cell growth (reviewed in Lu et al., 2015; Hirschey et al., 2015).

Changes to the architecture of the mitochondrial network that promote increased oxidative metabolism can therefore play a role in facilitating this metabolic shift and subsequent growth inhibition. Small molecules that promote increased fusion by inhibiting Drp1-mediated fission have been shown to slow cancer growth. Similarly, Mfn2 overexpression is sufficient to slow growth in

multiple cell lines, while Mfn2 knockout accelerates growth (Rehman et al., 2012; Chen et al., 2014).

Although RES may affect the expression and/or activities of multiple proteins impinging upon mitochondrial network morphology our results indicate that Mfn2 is playing a key role, since its absence abolished the growth inhibitory effect of RES in MEFs. In summary, our results indicate that RES stimulates mitochondrial fusion into large, highly branched networks that are associated with increased cellular respiration and reduced growth rates. The pro-fusion protein Mfn2 appears to play a key role in this phenomenon, since effects of RES on fusion, respiration, and growth are all absent in Mfn2-null cells. These observations add to our growing knowledge of how RES targets mitochondrial function to regulate growth, metabolism, and stress resistance.

CHAPTER 3: The effects of media composition and O_2 levels on the effects of 17β-estradiol and selective estrogen receptor modulators on mitochondrial bioenergetics and cellular reactive oxygen species

This chapter is published as: Moradi, F., Fiocchetti, M., Marino, M., Moffatt, C., & Stuart, J. A. (2021). Media composition and O_2 levels determine effects of 17β-estradiol and selective estrogen receptor modulators on mitochondrial bioenergetics and cellular reactive oxygen species. *American journal of physiology. Cell physiology*, *321*(1), C72–C81. https://doi.org/10.1152/ajpcell.00080.2021

Author Contributions

Study conceptualization: FM and JAS. All cell culture, Bradford assay, ROS, and confocal microscopy were done by FM. CM assisted with Seahorse Bioanalyzer flux assay. MF helped with imaging. MM contributed to manuscript writing. All data analysis has been performed by FM. FM and JAS have written the manuscript.

ABSTRACT

Estradiol (E_2) and selective estrogen receptor modulators (SERMs) have broad-ranging cellular effects that include mitochondrial respiration and reactive oxygen species (ROS) metabolism. Many of these effects have been studied using cell culture models. Recent advances have revealed the extent to which cellular metabolism is affected by the culture environment. Cell culture media with metabolite composition similar to blood plasma [e.g., Plasmax, Human Plasma-Like Medium (HPLM)] alter cellular behaviors including responses to drugs. Similar effects have been observed with respect to O_2 levels in cell culture. Given these observations, we investigated whether the effects of E_2 and SERMs are also influenced by media composition and O_2 level during cell culture experiments. We analyzed mitochondrial network characteristics, cellular oxidative metabolism, and H_2O_2 production in C2C12 myoblasts growing in physiological (5%) or standard cell culture (18%) O_2 and in physiological (Plasmax) or standard cell culture [Dulbecco's modified Eagle's medium (DMEM)] media. Although E_2 significantly lowered H_2O_2 production from cells growing in 18% O_2/DMEM (standard cell culture), it had no effect on cells growing in Plasmax. Moreover, culture conditions significantly altered the effects of E_2 and SERMs on mitochondrial abundance and network characteristics. These results indicate that the effects of E_2 and SERMs on various aspects of cell physiology strongly depends on growth conditions, which in turn emphasizes the need to consider this carefully in cell culture experiments.

INTRODUCTION

17β-Estradiol (E_2) affects a wide range of mammalian cellular and physiological processes beyond reproduction (Klinge, 2008; Lagranha et al., 2017). E_2 mediates both genomic and non-genomic actions through estrogen receptors (ERα, ERβ, G protein-coupled ER (GPER) that activate nuclear gene transcription, cellular signal transduction pathways (Fiocchetti et al., 2012; Gupte et al., 2015; Villa et al., 2016), and mitochondrial biogenesis (Mattingly et al., 2008) including processing of RNA transcripts that encode components of the electron transport system (ETS) (Sanchez et al., 2015). E_2 has also been implicated in the regulation of various mitochondrial functions, including basal ATP production (Moreno et al., 2013), maintenance of mitochondrial membrane potential during exposure to physiological stressors (Wang et al., 2001; Nilsen and Briton 2004), and modulating membrane biophysical properties and bioenergetic function (Torres et al., 2018). Reactive oxygen species (ROS) metabolism in various cell types is also affected by E_2 (Borrás et al., 2003; Strehlow et al., 2003; Razmara et al., 2007; Yao et al., 2014; Hima and Sreeja, 2015; Panza et al., 2017) via effects on ROS producing and ROS neutralizing enzymes.

More recently, E_2 has been shown to affect the expression of mitochondrial fusion and fission enzymes (Arnold et al., 2008; Sastre-Serra et al., 2013). Regulation of mitochondrial dynamics via fusion and fission processes is important for mitochondrial DNA maintenance, respiration, the cellular stress response, ROS production (Willems et al., 2015), cell cycle regulation (Mitra et al., 2009), mitophagy (Li et al., 2018), and apoptosis (Grandemange et al., 2009; Cho et al., 2010; Westermann, 2010). Maintenance of functional mitochondrial networks is particularly critical in cell types with high energy demands, including neurons, skeletal muscle, and cardiomyocytes. E_2 has been shown to affect the mRNA and protein levels of key fusion/fission proteins including Mitofusins and Dynamin related protein 1 in MCF7 and other breast cancer cells (Sastre-Serra et al., 2012). There is evidence that ERβ in particular plays a key role in this regulation (Sastre-Serra et al., 2013). Arnold et al. (2008) demonstrated that E_2 stimulates transcription of mitochondrial fusion and fission genes in primary mouse astrocytes, and suggests that mitochondrial dynamics, and other mitochondrial effects of E_2, contribute to the neuroprotection associated with this hormone.

E_2 effects at the cellular level are virtually always studied under standard cell culture conditions in which incubator O_2 levels are not regulated, and headspace O_2 is ~18%. This O_2 level is hyperoxic compared to *in vivo* (Habler and Messmer, 1997), where the O_2 levels experienced by cells in most tissues are in the range of 1–6% (reviewed in Keeley and Mann, 2019). 18% O_2 increases cellular release of H_2O_2 compared to 5% O_2 (Maddalena et al., 2017; Fonseca et al., 2018). H_2O_2 has well characterized and concentration dependent effects on redox regulated signaling pathways and macromolecular damage (Sies et al., 2020).

In addition to nonphysiologic O_2 levels, virtually all cell culture is done in cell culture media (e.g., DMEM, RPMI) whose composition does not resemble that of extracellular fluid that surrounds cells *in vivo*. For example, commonly used cell culture media like DMEM lack some metabolites normally found in human plasma and contain other components, such as glucose, glutamine, or pyruvate, at superphysiological concentrations. This discrepancy has recently gained attention, motivating the development of more physiologically representative media like Human Plasma-Like Medium (HPLM) (Cantor et al., 2017) and Plasmax (Vande Voorde et al., 2019). There is evidence that media composition affects important aspects of cell physiology and alters experimental outcomes (Cantor et al., 2017; Vande Voorde et al., 2019). For example, Fonseca et al. (2018) observed that many of resveratrol's effects on mitochondrial dynamics, cell replicative growth, and ROS production depended on growth media glucose concentration and O_2 levels.

We previously showed that E_2 and ERβ-specific agonist diarylpropionitrile (DPN) modulate mitochondrial morphology in C2C12 mouse skeletal myoblasts (Robb et al., 2017), however, these experiments were performed under standard cell culture conditions: DMEM and 18% O_2. Here, we set out to determine the extent to which cell culture conditions influence E_2's effects on mitochondria and cellular ROS metabolism. We cultured C2C12 cells under four conditions: physiologic O_2 (5%) and physiologic medium (Plasmax); physiologic O_2 and standard medium (DMEM); standard O_2 (18%) and Plasmax; standard O_2 and DMEM. Under these conditions we assessed the effects of E_2, DPN, and the ERα-specific agonist propylpyrazole triol (PPT) on the mitochondrial network, cellular oxidative metabolism, and cellular H_2O_2 production. These experiments demonstrate that culture conditions interact with E_2 (or the ER-specific agonists) to produce different outcomes.

EXPERIMENTAL PROCEDURES

Materials

Diarylpropionitrile (DPN) was obtained from Tocris Bioscience (Ellisville, MO). Propylpyrazole triol (PPT) was obtained from Cayman Chemicals (Ann Arbor, MI). 17β-Estradiol-3 benzoate, Dulbecco's modified Eagle medium with glucose (4,500 mg/L), l-glutamine, and sodium pyruvate (Cat. No. D6429), and supplement-free Dulbecco's modified Eagle medium powdered media (Cat. No. 5030) were purchased from Sigma-Aldrich (St. Louis, MO). Dimethylsufoxide (DMSO), l-glutamine, HEPES [(4-(2-hydroxyethyl)-1 piperazineethane-sulfonic acid], dl-dithiothreitol (DTT), Bradford reagent, and Trypan Blue were obtained from BioShop (Burlington, ON, Canada). Amplex Red reagent (10-acetyl-3, 7-dehydroxyphenoxazine; item 10010469) was purchased from Cayman Chemical (Ann Arbor, MI). Fetal bovine serum (Cat. No. F1051), minimal Eagles' medium (MEM) nonessential amino acid solution, penicillin/streptomycin solution, 0.25% trypsin/EDTA solution were obtained from Sigma-Aldrich (St. Louis). Lipofectamine 2000 transfection reagent was purchased from Life Technologies Incorporated (Burlington, ON, Canada). Tissue culture dishes (100 × 20 mm and 60 × 15 mm) were obtained from Sarstedt, Inc (Newton, SC). C2C12 cell lines were purchased from American Type Culture Collection (Manassas, VA). Plasmax media constituents are exactly adapted from Vande Voorde et al. 2019. α-Aminobutyrate (l-2-Aminobutyric acid; Cat. No. 438371), l-carnosine (Cat. No. 535080), and dl-3-hydroxybutyric acid sodium salt (Cat. No. A 11613-06) were purchased from CEDARLANE (Burlington, ON, Canada). 2-Hydroxybutyrate (2-hydroxybutyric acid sodium salt; Cat. No. S509425) and ammonium metavanadate (Cat. No. A634095) were purchased from Toronto Research Chemicals Inc. (Toronto, ON, Canada). Agilent Seahorse Calibrant XF (Cat. No. 100840-000), XFe 96 Extracellular Flux assay kit (Cat. No. W17619), and XFe 96 cell culture microplate (Cat. No. 101085-004) were purchased from Agilent Technologies (Mississauga, ON, Canada). Carbonyl cyanide-4-(trifluoromethoxy) phenylhydrazone (FCCP) (Cat. No. C2920), Oligomycin (Cat. No. 579-13-5), Rotenone (Cat. No. 83-79-4), and Antimycin A (Cat. No. 1397-94-0) were purchased from Sigma-Aldrich (St. Louis, MO). Unless otherwise stated, all other chemicals, reagents, and solutions (mainly used to make Plasmax) were purchased from Sigma-Aldrich (St. Louis, MO), BioShop (Burlington, ON, Canada), or Fisher Scientific (Mississauga, ON, Canada).

Cell Culture

C2C12 cells were acquired from American Type Culture Collection and initially cultured according to the provider to expand the population. Cells were thereafter cultured in either high-glucose DMEM supplemented with 10% fetal bovine serum (FBS), 2× minimal Eagles' medium (MEM) nonessential amino acid solution, and penicillin (50 IU/mL)/streptomycin (50 μg/mL) solution (Diokmetzidou et al., 2016) or in Plasmax media supplemented with 2.5% FBS and penicillin (50 IU/mL)/streptomycin (50 μg/mL) solution for 2 wk before initiation of experiments. Cells were seeded at a density of 1×10^6 cells in 10-cm plates. Cells were maintained within a humidified 5% CO_2 atmosphere at 37°C inside one of two Forma 3110 water-jacketed incubators with O_2 control (Thermo Fisher, Waltham, MA). In one incubator, O_2 was not regulated (standard cell culture approach) and thus equilibrated to ∼18% O_2 (superphysiological). In the other incubator, O_2 was regulated at 5% (physiological). All media were conditioned in the corresponding incubator for 24 h before use to ensure equilibration with the ambient condition. To avoid effects of molecules with estrogenic activity such as phenol red or serum protein-bound estrogens and growth factors, cells were transferred to either phenol red-free DMEM containing 10% charcoal-stripped FBS or phenol red-free Plasmax containing 2.5% charcoal-stripped FBS 96 h before treatment with E_2, DPN, PPT (each at 10 nM, 48 h), or vehicle control (DMSO). All treatments were delivered directly to the culture media and were refreshed daily.

Sample Preparation for Measuring Cellular Respiration at 18% O_2

C2C12 cells were seeded at a concentration of 15×10^3/well on a XF96-well microplate 14 h before oxygen consumption rate (OCR) measurements according to the study by Nicholls et al. (2010) with cell concentration modification following titration assay. Cells were seeded in a 80 μL final volume of media. Wells on the four corners of the plate were medium-only to serve as background correction wells. When cells are seeded at room temperature and then transferred immediately into a tissue culture incubator (∼37°C), the environmental condition of the edge wells change more rapidly than the environmental conditions of the interior wells with respect to temperature, humidity, and % CO_2. Thus, to avoid the effect of edge effect on cell growth, cells were left at room temperature for 60 min before transferring them to the incubator. Hydration of a flux analyzer sensor cartridge probe plate was done by adding 200 μL milli Q water into each well of the utility plate and putting the cartridge back onto the utility microplate. The utility plate was then placed in

a non-CO_2 incubator at 37°C overnight. At least 1 h before commencing the assay, 200 µL of the Seahorse Bioscience XF96 Calibrant pH 7.4 solution was added to each well of the utility plate (after removing the milliQ water from the wells). Before analysis, the culture media was replaced with either unbuffered (lacking sodium bicarbonate) DMEM pH 7.4 or Plasmax pH 7.4 and cells were then allowed to equilibrate in a non-CO_2, at 37°C incubator to allow for precise measurement (45 min). One hour before measurement, the following compounds were added to the hydrated sensor cartridges: Oligomycin (1.0 µM), FCCP (1.0 µM), and rotenone/antimycin A (0.5 µM). These concentrations are selected following titration experiments (according to Agilent Seahorse XF Cell Mito Stress guidelines). Then, the sensor cartridges were loaded into the Seahorse Analyzer. After calibration, the sensor cartridges were replaced with the XF96 microplates and the measurement program was resumed to obtain the following OCR parameters: Basal OCR, maximal OCR, and spare respiratory capacity. Wave Desktop 2.6 Software (Agilent) was used for data acquisition and data analysis for assays. The OCR values were normalized to the protein concentration per well and were presented as pmol/min/µg protein.

Hydrogen Peroxide Determination

Cellular hydrogen peroxide (H_2O_2) efflux was measured as in the study by Maddalena et al. (2017), using an Amplex Red reagent (10-acetyl-3,7-dihydroxyphenoxazine)-based assay, in which the fluorescent oxidation product resorufin serves as a readout for H_2O_2 levels (Zhou et al., 1997). C2C12 cells (from the cells adapted to the described experimental conditions) were seeded at a density of 3×10^3/well in 6-well plates. E_2, DPN, PPT (each at 10 nM, 48 h), or vehicle control (DMSO) were added to the plates with daily refreshing the media and treatment. Krebs–Ringer buffer (KRB: 135 mM NaCl, 5 mM KCl, 1 mM $MgSO_4$, 0.4 mM K_2HPO_4, 20 mM HEPES, 5.5 mM glucose, pH ~7.4) supplemented with either 10% FBS (for DMEM) or 2.5% FBS (for Plasmax) were incubated overnight at either 18% O_2 or 5% O_2 incubator to reach equilibration with headspace gases. Immediately before experiments, cells were washed and then incubated in the prepared KRB (1 mL, 2 h) containing freshly added Amplex Red reagent (50 µM) and horseradish peroxidase (0.1 U/mL). A standard curve for H_2O_2 (0 to 3 µM) was created with each experiment. Following 2-h incubation, KRB buffer was collected from the plates and resorufin fluorescence was measured using excitation and emission wavelengths of 535 nm and 595 nm, respectively (Cary

Eclipse fluorescence spectrophotometer, Agilent Technologies, Santa Clara, CA). Cells were then trypsinized and counted with a hemocytometer. H_2O_2 efflux rates (μmol/h) were standardized to cell number.

Establishment of a Stable C2C12 Cell Line Expressing Modified Emerald Fluorescent Protein-in Mitochondria

The plasmid mEmerald-Mito-7 encoding a gene for modified emerald fluorescent protein (mEFP) targeted to the mitochondrial matrix compartment via N-terminal mitochondrial targeting sequence from subunit VIII of human Complex IV/cytochrome C oxidase (Planchon et al., 2011) was a gift from Michael Davidson (Florida State University). The plasmid carries a kanamycin-resistance gene for bacterial selection and geneticin (G418) resistance gene for mammalian cell selection. Plasmid DNA was isolated and purified from bacterial cultures via a plasmid DNA Miniprep Kit (Norgen Biotek, Thorold, ON, Canada). Plasmid DNA purity and concentration were assessed by using a Nanodrop Spectrophometer (Thermo Fisher). To create stable cell lines, C2C12 cells were plated in a 24-well plate with a cell density that allows cells to reach ~80% confluency 24 h later. Briefly, cells were transfected with Lipofectamine 2000 reagent and different combinations of plasmid DNA: Lipofectamine reagents were used. After 24 h, stable transfected cells were selected with G418 for 10 days (G418 concentration was determined in a prior screening experiment). After 10 days of selection, the concentration of G418 in culture media was lowered to a maintenance concentration. Mitochondrial localization of the mEFP was confirmed by detecting colocalization of mEFP signal with the mitochondrial targeted fluorescent dye Mito Tracker Red CMXRos. The transfected cells are referred to as mEFP-C2C12 afterward.

Fluorescence Microscopy

Fluorescence micrographs of live cells were obtained using a Carl Zeiss Axio Observer. Z1 inverted light/epifluorescence microscope was equipped with ApoTome.2 optical sectioning and a Hamamatsu ORCA-Flash 4.0 V2 digital camera. mEFP-C2C12 cells (1×10^3) were cultured on Matek 35 mm poly-D-lysine-coated glass bottom culture dishes for 48 h. Media and treatments were refreshed every 24 h. Images were collected with a Plan-Apochromat ×63/1.40 Oil DIC M27 microscope objective. The microscope stage and objective were maintained with temperature control achieved through Temp Module S-controlled stage heater and objective heater (PeCon, Erbach, Germany) at 37°C, and a humidified 5% CO_2 environment with either 18% or 5%

O_2 throughout the experiments. During experiments conducted at 5% O_2, a humidified 5% O_2-5% CO_2-90% N_2 gas mix was continuously delivered through the Temp Module on-stage heater. Green fluorescence was detected using a fluorescence channel possessing excitation and emission wavelength filter sets of 450–490 nm and 500–550 nm, respectively with set excitation and emission wavelengths of 488 nm and 509 nm, respectively. The intensity of fluorescence illumination by an X-Cite 120LED light source and camera exposure times were both held constant across experiments. Z-stack series were rendered into single two-dimensional (2-D) images using the "extended depth of focus" processing tool in the Zeiss Zen 2 software. Z-stacks consisted of 20 slices, each 0.25 μm apart. Maximum intensity projections were generated for each stack using the Fiji distribution of ImageJ.

Image Analysis

Mitochondrial morphology was analyzed and quantified using the Mitochondrial Network Analysis tool (MiNA), a macro tool developed for use with the FIJI distribution of ImageJ (Valente et al., 2017). Cells were selected randomly for each experimental condition, and fluorescence images were loaded into the program in their native format using Bio-Formats plug-in. To improve contrast between all mitochondrial structures and background, following preprocessing steps were performed: contrast limited adaptive histogram equalization (CLAHE), median filtering (a 2-pixel radius), and "unsharp mask." In the processed image, fluorescent mitochondrial signal was subjected to thresholding in order to eliminate background signal, which could generate an artifact. A binary image was generated by thresholding, the level of which was determined using Otsu's algorithm. From the binary, the area of the image occupied by signal is calculated as the mitochondrial footprint. For the purpose of estimating the lengths of mitochondrial structures and the degree of branching, the Ridge Detection plugin was applied (Steger, 1998; Wagner et al., 2017). Ridge detection uses florescence intensity to produce binary images, from the binary image morphological skeleton was generated using the Skeletonize3D plugin. The topology is then captured by the Analyze Skeleton plug in, the results of which are used by MiNA to generate quantitative parameters. The information extracted from the morphological skeleton is the mean of the branch lengths for each independent feature and the number of branches in each network. At least 30 cells per condition were selected randomly from at least three separate experiments.

Estimation of Mitochondrial Membrane Potential

Tetramethyl rhodamine methyl ester (TMRM) dye was used to semi- quantitatively assess mitochondrial membrane potential in intact live cells. C2C12 cells (1×10^3) were cultured on Matek 35 mm poly-D-lysine-coated glass bottom culture dishes for 48 h. Media and treatments were refreshed every 24 h. Immediately before imaging, cells were incubated for 45 min in complete media containing 20 nM TMRM. TMRM fluorescence was detected using a fluorescence channel with excitation and emission wavelength filter sets of 540–552 nm and 590–660 nm, respectively, with set excitation and emission wavelengths of 587 nm and 610 nm, respectively. To quantify changes in mitochondrial membrane potential, ImageJ/FIJI software was used to measure TMRM fluorescence intensities in each cell. To account for cytosolic background fluorescence, fluorescence intensities of two regions inside of each cell were measured and the average was subtracted from fluorescence intensity of mitochondrial TMRM in each cell using Microsoft Excel. TMRM fluorescence intensities were normalized against mitochondrial footprint.

STATISTICAL ANALYSES

All statistical analyses were performed using GraphPad Prism 5 software (San Diego) and Statistical Package for the Social Sciences (SPSS) (V.26). Since all data met ANOVA normality distributions assumptions (e.g., homogeneity of variance), two-way ANOVAs was performed for datasets. When statistical significance in datasets was observed from two-way ANOVAs, post hoc analysis was performed using Tukey's honestly significant difference (HSD) test. A P-value of <0.05 was considered significant for all statistical tests. All data are presented as means ± standard deviation (SD).

RESULTS

Balanced mitochondrial fission and fusion play an integral role in shaping and distributing mitochondria, as well as contributing to mitochondrial homeostasis and adaptation to stress. There is evidence indicating interactions between mitochondrial network, cytosolic redox state (Shut et al., 2012), and media constituents such as glucose levels (Rossignol et al., 2004; Elkalaf et al., 2013). Using the Mitochondrial Network Analysis tool (MiNA) that we recently developed and have described in detail elsewhere (Valente et al., 2017), we demonstrated that the effects of E_2, DPN, and PPT on C2C12 cells are highly dependent on culture conditions such as O_2 level and media composition (Figure 3.1; Supplemental Figure S3.1). MiNA was used to identify and quantify features like "mitochondrial footprint" (area of a 2-D cell image occupied by mitochondria), mean network size (number of branched mitochondrial networks), and mitochondrial branch mean length.

One of the more robust effects of E_2 on mitochondria that have been reported in many different contexts is the stimulation of PGC-1a-mediated biogenesis (Capllonch-Amer et al., 2014; Sbert-Roig et al., 2016; Galmes-Pascual et al., 2017; Bauzá-Thorbrugge et al., 2018). This effect was observed here, as increases in mitochondrial footprint, under most experimental conditions. Interestingly, independent of E_2, media and O_2 both significantly affected the mitochondrial footprint (Figure 3.1B). For example, mitochondrial footprint was more than 50% greater in cells growing in Plasmax/18% O_2 relative to Plasmax/5% O_2 and DMEM/18% O_2 ($F_{1,317} = 27$; $F_{1,317} = 29$; $P < 0.05$, respectively). Media and O_2 also exerted significant influence on E_2 effects. E_2 increased mitochondrial footprint (a proxy of mitochondrial abundance) in all experimental conditions except in 5% O_2/ DMEM ($F_{1, 317} = 25$; $P < 0.05$ (18% O_2/DMEM); $F_{1, 317} = 35$; $P < 0.05$ (5%O_2/Plasmax); $F_{1, 317} = 46$ (18%O_2/Plasmax); Figure 3.1). Interestingly, PPT significantly increased mitochondrial footprint only in cells growing in 5%O_2/Plasmax (the most physiologic condition) ($F_{1, 317} = 18$; $P < 0.05$; Supplemental Figure S3.1B). DPN increased mitochondrial footprint only in cells growing in 18%O_2/DMEM (the most common non physiological condition) ($F_{1, 317} = 24$; $P < 0.05$; Supplemental Figure S3.1B). As with mitochondrial footprint, E_2 increased mean network size (no. of branches) in all experimental conditions, except for 5% O_2/DMEM ($F_{1, 317} = 25$ (18% O_2/DMEM); $F_{1, 317} = 27$ (5% O_2/Plasmax); $F_{1, 317} = 29$ (18% O_2/Plasmax); $P < 0.05$; Figure 3.1C). Although no interaction between O_2/media/treatment was observed, cells grown in Plasmax had greater mean network size ($F_{1, 317} = 75$; $P < 0.05$; Figure 3.1C).

On the other hand, O_2 as a variable did not significantly modulate this mitochondrial characteristic. DPN significantly increased mean network size (no. of branches) only in 18% O_2/DMEM ($F_{1,317} = 32$; $P < 0.05$; Supplemental Figure S3.1C), but this was not phenocopied by PPT indicating that such condition might interfere with the ability of ERα (e.g., lower expression) in modulating mitochondrial morphology. Alternatively, culture condition imposed on the cells can modulate drug metabolism pathways leading to unexpected outcomes, which were not explored here. Under 5%O_2/Plasmax, mitochondrial network size (no. of branches) was significantly higher ($F_{1, 317} = 19$; $P < 0.05$; Figure 3.1C) compared with 18%O_2/DMEM condition. Under all experimental conditions, mean branch length remained unaffected by E_2 and DPN (Figure 3.1C; Supplemental Figure S1D). Although no interaction between O_2/media/treatment was detected, the main effect of O_2 and media was significant. Plasmax ($F_{1, 317} = 25$) and 18% O_2 ($F_{1, 317} = 27$) increased mean branch length ($P < 0.05$; Figure 3.1D). Similar to mitochondrial network size (no. of branches), in 5%O_2/Plasmax (the most physiologically relevant) mitochondrial branch mean length was significantly higher ($F_{1, 317} = 17$; $P < 0.05$; Figure 3.1D) when compared with the 18%O_2/DMEM (the least physiologically relevant). Taken together, these results indicate that O_2 and media formulation interact with E_2s and specific estrogen receptor modulators (SERMs) effects on C2C12 mitochondrial morphology.

In addition to the reported effects of E_2 on ROS metabolism, mitochondrial morphology, and biogenesis, there is evidence that E_2 and SERMs alter mitochondrial bioenergetic function, manifesting as increased membrane potential in various cell types (Wang et al., 2001; Moor et al., 2005; Ronda et al., 2013). However, as discussed already, almost all these experiments have been conducted in non physiological conditions (e.g., O_2 levels and media composition). Using tetramethyl rhodamine methyl (TMRM), a fluorescent lipophilic cationic probe and confocal microscopy, we determined mitochondrial membrane potential ($\Delta\Psi m$) semi quantitatively under all experimental conditions and normalized the TMRM signal to mitochondrial footprint to account for the E_2-induced increase in mitochondrial abundance. $\Delta\Psi m$ was not affected by E_2, DPN, or PPT under any experimental condition (Figure 3.1E; Supplemental Figure S3.1E).

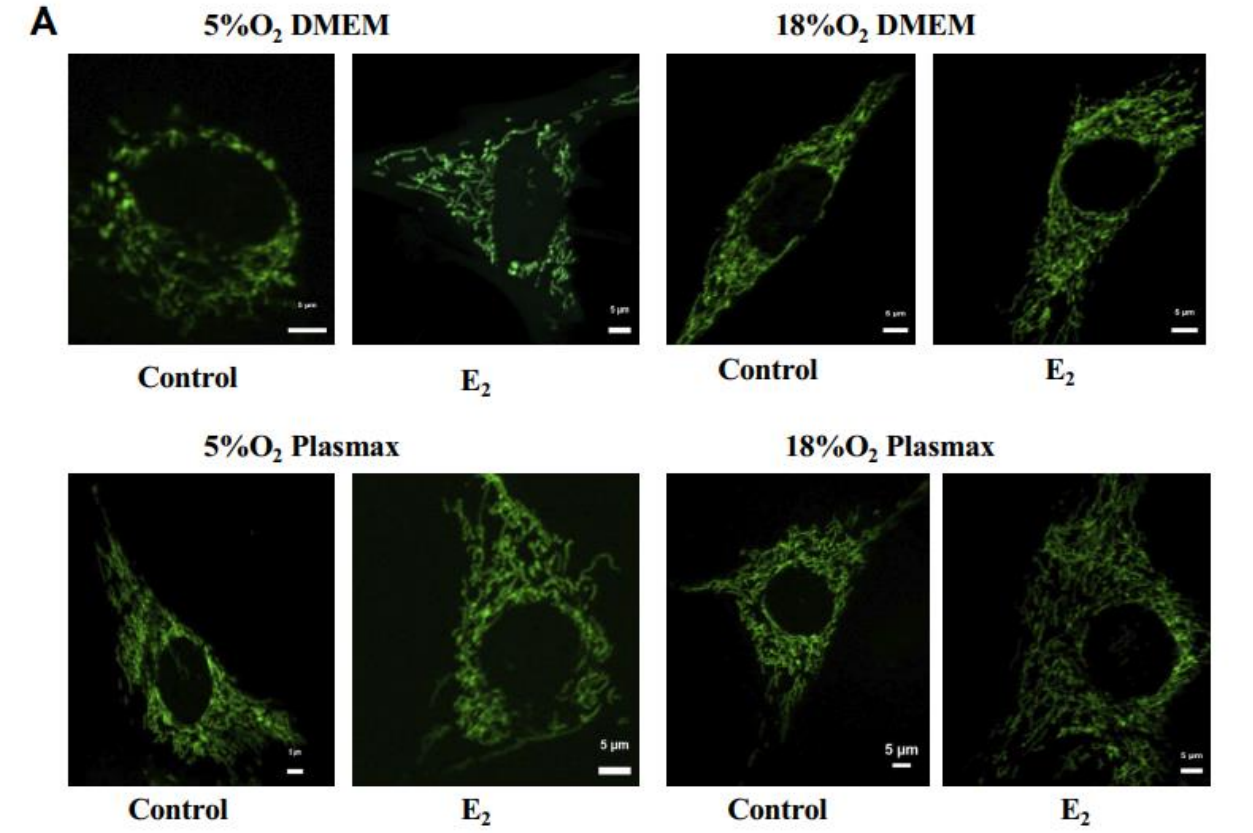
A
5%O2 DMEM
18%O2 DMEM
Control
E2
Control
E2
5%O2 Plasmax
18%O2 Plasmax
5 µm
5 µm
Control
E2
Control
E2

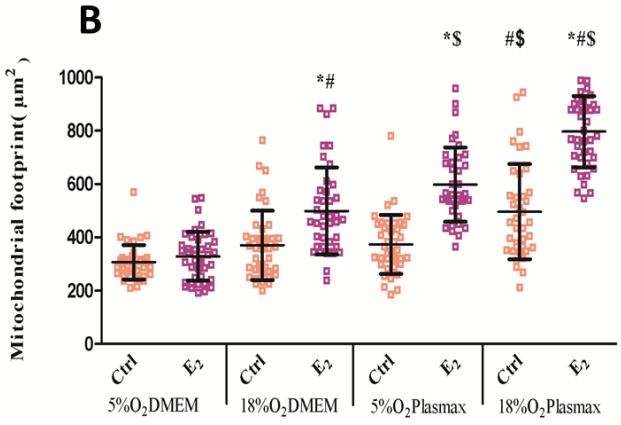
B
Mitochondrial footprint(µm2)
1000
800
600
400
200
0
*#
*$
#$
*#$
Ctrl
E2
5%O2DMEM
18%O2DMEM
5%O2Plasmax
18%O2Plasmax

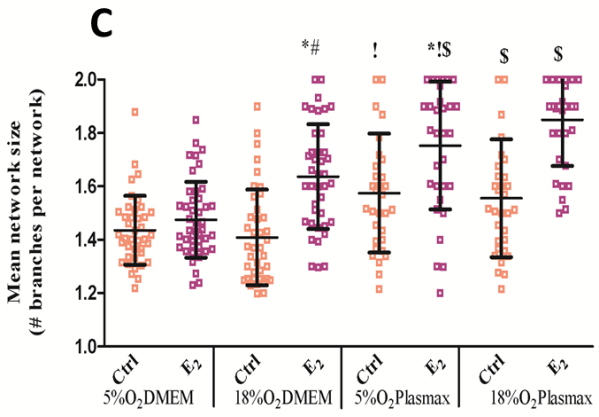
C
Mean network size
(# branches per network)
2.0
1.8
1.6
1.4
1.2
1.0
*#
!
*!$
$
$
Ctrl
E2
5%O2DMEM
18%O2DMEM
5%O2Plasmax
18%O2Plasmax

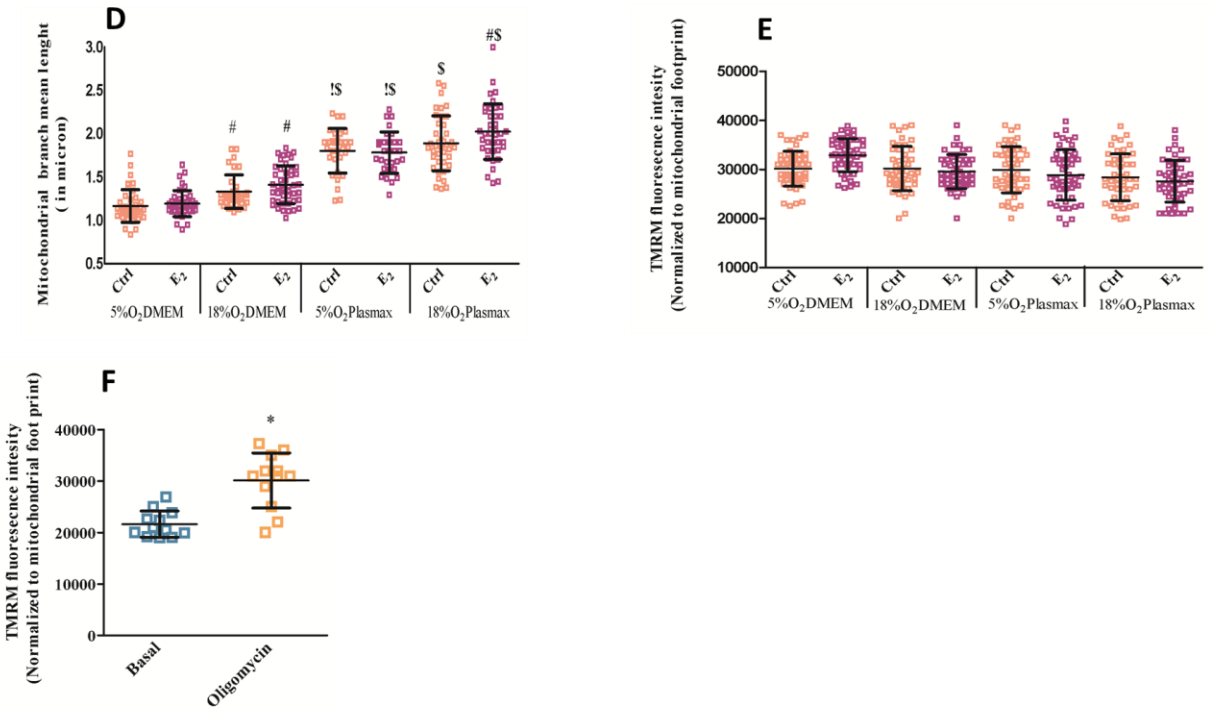

Figure 3.1. Estradiol (E_2) modulates mitochondrial morphology in a media type and O_2-dependent manner. **A:** representative images of mitochondrial networks in modified emerald fluorescent protein (mEFP)-C2C12 cells. **B:** mitochondrial footprint (area in μm^2). **C:** mean network size (number of branches per network). **D:** mean branch length (in micron). Features in A–D were measured in mEFP-C2C12 cells at either 5% O_2 or 18% O_2 in either Dulbecco's modified Eagle's medium (DMEM) or Plasmax. Data shown for mitochondria morphology are means ± SD from 40 cells from three independent experiments from six culture plates per treatment (n = 40 cells per treatment). **E:** tetramethyl rhodamine methyl ester (TMRM) fluorescent intensity as a proxy for mitochondrial membrane potential was measured in C2C12 cells, which were cultured at either 5% O_2 or 18% O_2 in either DMEM or Plasmax. Data from TMRM intensity are means ± SD from 50 cells from three independent experiments from six culture plates per condition (n = 50 cells per each condition which includes both cell culture condition and treatment). **F:** TMRM assay sensitivity test (n = 12 cells randomly selected from two plates of C2C12 cells). Under the same protocol, applying oligomycin (1 µg/mL) for around 10 min caused a 32% increase in TMRM fluorescence intensity. For F, statistical significance was determined by paired t test. In all experiments (A–E), cells were treated for 48 h with either 10 nM E_2, or an equal volume of vehicle control (dimethyl sufoxide, DMSO). '*'Differences in a given parameter between E_2-treated cells and their corresponding vehicle control. '#'Differences between 18% O_2 and 5% O_2 in the same media. '$' Differences between Plasmax and DMEM at the same O_2 level. '!' Differences between 5%O_2/Plasmax versus 18%O_2/ DMEM. Statistical significance was determined by two-way ANOVA followed by Tukey's post hoc analysis.

Since mitochondrial abundance and network characteristics were shown to be affected by cell culture conditions and estradiol, we set out to determine how this impacted cellular oxygen consumption rates (OCR) as a proxy of bioenergetic status of the cells under the same experimental conditions. In the most physiologically relevant 5% O_2/Plasmax/regimen, E_2 increased basal OCR ($F_{1, 316} = 24$; $P < 0.05$; Figure 3.2), maximal OCR ($F_{1, 316} = 32$; $P < 0.05$; Figure 3.2), and spare respiratory capacity ($F_{1, 316} = 19$; $P < 0.05$; Figure 3.2). However, these effects were entirely absent in18% O_2/Plasmax ($P > 0.05$; Figure 3.2). And in 18% O_2/DMEM (the least physiologic condition), E_2 had the opposite effect, reducing both basal ($F_{1, 316} = 17$; $P < 0.05$) and maximal ($F_{1,316} = 20$; $P < 0.05$; Figure 3.2) OCR. Broadly, similar trends were observed with DPN and PPT (Supplemental Figure S3.2). In 5% O_2/Plasmax, DPN increased basal OCR ($F_{1, 316} = 17$; $P < 0.05$) and maximal OCR ($F_{1, 316} = 18$; $P < 0.05$). Under the same culture condition, PPT increased basal OCR ($F_{1, 316} = 15$; $P < 0.05$; Supplemental Figure S3.2) and maximal OCR ($F_{1, 316} = 18$; $P < 0.05$; Supplemental Figure S3.2). The inability of E_2 to affect cellular OCR under certain culture conditions may have been secondary to the direct effects of those conditions. For example, basal OCR was significantly elevated in 5% O_2/DMEM compared with other conditions, and this may have limited the ability of E_2 to effect further change. Overall, O_2 level had a significant effect on basal OCR and spare respiratory capacity. In the 5% O_2 condition, basal OCR was significantly higher ($F_{1,316} = 35$; $P < 0.05$; Figure 3.2) than in 18% O_2, whereas spare respiratory capacity was higher in cells growing in 18% O_2 ($F_{1,316} = 22$; $P < 0.05$). We followed the Agilent Technologies protocol to seed fewer cells for Seahorse bioenergetics assays under lower than atmospheric O_2 levels. Although we normalized the data to total protein levels, still this might be a source of variability. Moreover, growth in DMEM significantly increased basal OCR ($F_{1, 316} = 18$; $P < 0.05$). Overall, it is perhaps surprising that conditions associated with reduced mitochondrial footprint, such as 5% O_2/DMEM, also had higher basal OCR. Similarly, though Plasmax increased mitochondrial footprint, it reduced respiratory rates.

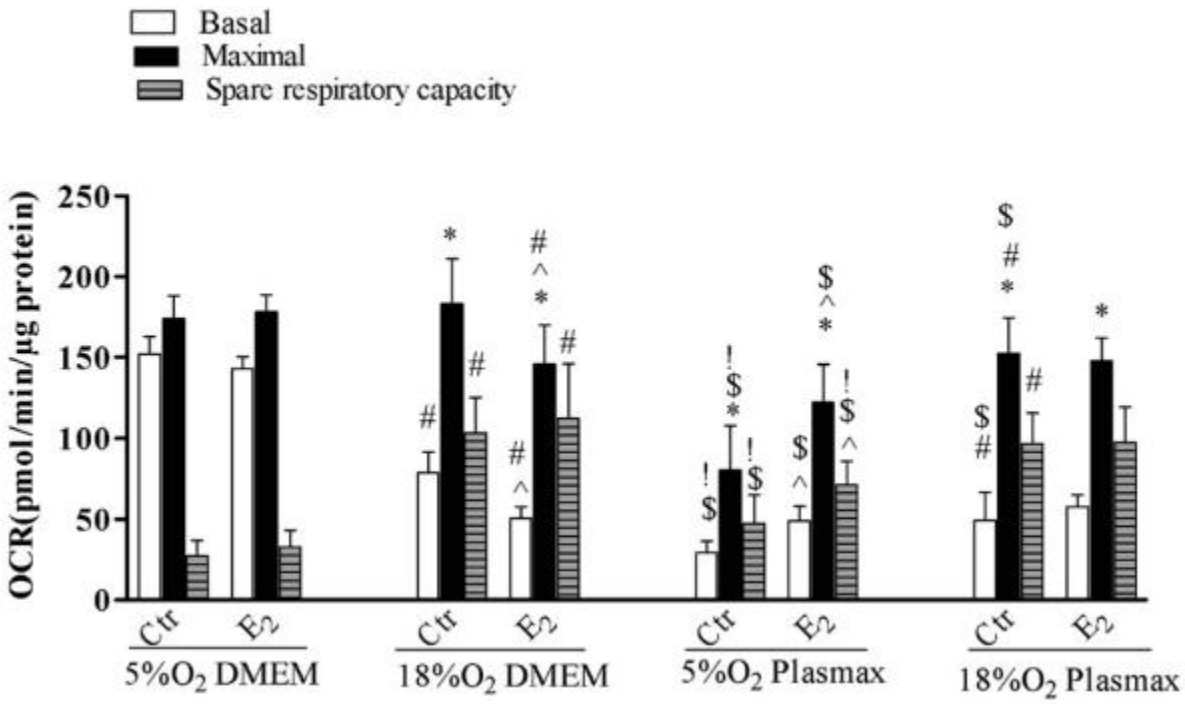

Figure 3.2. Effects of estradiol (E_2) on cellular respiration depend on O_2 concentration and media type. C2C12 cells were cultured at either 5% O_2 or 18% O_2 in either Dulbecco's modified Eagle's medium (DMEM) or Plasmax. In all experiments, cells were treated for 48 h with either 10 nM E_2, or an equal volume of vehicle control (dimethyl sufoxide, DMSO). Basal, maximal, and spare respiratory capacity oxygen consumption rates (OCRs) are shown for control and E_2-treated cells. Data shown are means ± SD from three independent experiments per condition (n = 23 wells per each condition which includes both cell culture condition and treatment). '* 'Differences between maximal and basal OCR for each condition. '^'Differences in a given parameter between E_2-treated cells and their corresponding vehicle control. '#'Differences between 18%O_2 and 5%O_2 in the same media. '$'Differences between Plasmax and DMEM when O_2 level is the same. '!' Differences between 5%O_2/Plasmax versus 18%O_2/DMEM. Statistical significance was determined by two-way ANOVA followed by Tukey's post hoc analysis.

Mitochondria are thought to be a major cellular source of ROS. E_2's effects on mitochondrial form and function may thus alter cellular ROS production under the different experimental conditions. In addition, E_2 modifies ROS metabolism via effects on other ROS producers as well as antioxidant enzymes (e.g., Robb and Stuart, 2014; Savoia et al., 2018; Xu et al., 2018). The effects of E_2, DPN, and PPT on H_2O_2 production under the different O_2 and media regimes were determined using the Amplex Red assay. Again, the effects of E_2 on C2C12 cells were dependent on culture conditions. Although E_2 significantly lowered H_2O_2 production from cells growing in 18% O_2/DMEM ($F_{1, 80} = 15$; $P < 0.05$; Figure 3.3), it had the opposite effect in 5% O_2/ DMEM ($F_{1, 80} = 22$; $P < 0.05$). Although PPT had no effect on H_2O_2 production in DMEM at any O_2 level, DPN lowered this readout in 18%O_2/DMEM ($F_{1, 80}= 17$; $P < 0.05$, Supplemental Figure S3.3). Consistent with Maddalena et al. (2017) and others (e.g., Halliwell, 2014), we found that in 18% O_2 cellular H_2O_2 production was greater in DMEM ($F_{1, 80}= 28$; $P < 0.05$; Figure 3.3), though surprisingly it had no effect in Plasmax. Also surprising was the absence of any effect of E_2, DPN, or PPT on cellular H_2O_2 production when cells were growing in Plasmax (Figure 3.3; Supplemental Figure S3.3). Notably, while media as a main effect did not significantly change the H_2O_2 production, the rates were lower in the most physiological 5% O_2/Plasmax condition compared with standard 18%O2/ DMEM ($F_{1,80} = 32$; $P < 0.05$; Figure 3.3). At 18%O_2, control and PPT treated cells produced less H_2O_2 in Plasmax condition compared with DMEM ($F_{1, 80}= 22$; $F_{1, 80} = 16$; respectively, $P < 0.05$; Figure 3.3 Supplemental Figure S3.3). However, at 5%O_2, cells in all experimental groups released more H_2O_2 in Plasmax versus DMEM ($F_{1, 80} = 29$; $F_{1, 80} = 24$; $F_{1, 80} = 27$; $F_{1, 80} = 27$; respectively, $P < 0.05$; Figure 3.3, Supplemental Figure S3.3).

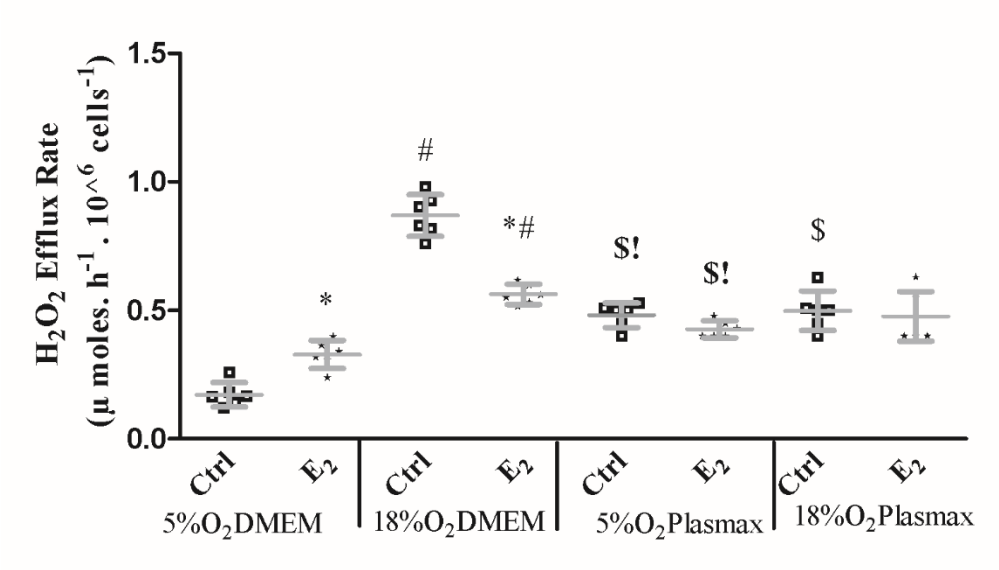

Figure 3.3. Media type and O_2 level modulate estradiol (E_2) effects on cellular hydrogen peroxide production. C2C12 cells were cultured at either 5% O_2 or 18% O_2 in either Dulbecco's modified Eagle's medium (DMEM) or Plasmax. Cells were treated for 48 h with either 10 nM E_2 or an equal volume of vehicle control (dimethyl sulfoxide, DMSO). Using Amplex red assay, H_2O_2 efflux rates (μmol/h) were measured and standardized to cell number. Data shown are means ± SD from three independent experiments per condition (n = 6 cell culture plates per each condition which includes both cell culture condition and treatment). '*'Differences between E_2-treated and DMSO-treated cells. '#'Differences between 18%O_2 and 5% O_2 in the same media. '$'Differences between Plasmax and DMEM when O_2 level is the same. '!'Differences between 5%O_2/Plasmax (the most physiologic condition) versus 18%O_2/DMEM (the least physiological condition). Statistical significance was determined by two-way ANOVA followed by Tukey's post hoc analysis.

DISCUSSION

E_2 has robust effects on mitochondrial biogenesis and function in multiple cell types *in vivo* (reviewed in Galmes-Pascual et al., 2017; Torres et al., 2018; Capllonch-Amer et al., 2014). In mouse skeletal muscle, loss of E_2 due to ovariectomy causes a significant reduction in mitochondrial respiratory capacity that can be reversed by E_2 treatment (Torres et al., 2018; Capllonch-Amer et al., 2014). The E_2 effect on mitochondrial abundance was measured here as "mitochondrial footprint," which is the area occupied by mitochondria in a 3-D confocal microscopy image compressed to 2-D. In most cell culture conditions, including the condition most representative of *in vivo* (5% O_2 and Plasmax), E_2 significantly increased mitochondrial footprint. Interestingly, however, in DMEM at physiological O_2 this effect was not significant. A similar observation was made for mean "network size," which is the number of branches in each independent mitochondrial structure. Although this parameter is not readily measurable *in vivo*, in culture it was increased by E_2 under the most physiological conditions, but notably not in other conditions such as 5% O_2 and DMEM.

This media-dependency of E_2's effects on mitochondrial abundance and network form was evident also on mitochondrial bioenergetic function. E_2 significantly increased all measured cellular respiratory parameters in 5% O_2 and Plasmax but failed to do so under some other cell culture conditions. The sensitivity of these mitochondrial effects of E_2 to the cell culture environment emphasizes the importance of using a more physiologically representative approach for *in vitro* studies of E_2. E_2 exerts multiple effects on cellular ROS metabolism *in vivo*, where it modifies both mitochondrial and nonmitochondrial sources of ROS, as well as the expression of antioxidant enzymes (Strehlow et al., 2003; Juan et al., 2004; Stirone et al., 2005; Miller et al., 2007). Chronic *in vivo* exposure to E_2 increased protein levels of mitochondrial antioxidant enzyme manganese superoxide dismutase (MnSOD) and reduced H_2O_2 production in cerebral vessels of ovariectomized rats (Stirone et al., 2005). In mouse skeletal muscle, mitochondrial H_2O_2 emission was increased following ovariectomy but restored to the level of intact mice by E_2 treatment (Torres et al., 2018). These findings can be reproduced in cell culture, where E_2 significantly reduced the rate of mitochondrial superoxide production in differentiated rat pheochromocytoma cells (Razmara et al., 2007). However, E_2 simultaneously affects a broad range of nonmitochondrial ROS-producing and neutralizing cellular activities. It reduces ROS production

from NADPH oxidases in vascular and neurovascular cells (Miller et al., 2007; reviewed in Brann et al., 2012), but exerts the opposite effect in an ovarian adenocarcinoma cell line (Maleki et al., 2015).

Given the myriad effects of E_2 on cellular ROS metabolism, we adopted the strategy of measuring total cellular H_2O_2 accumulation in the media. Dye-based detection systems are widely used to study ROS production in cell culture (reviewed in Vaneev et al., 2020) and the Amplex Red assay is a robust option to measure H_2O_2. Our measurements of E_2 effects on cellular H_2O_2 production demonstrate clear media dependence. In the least physiologic regimen (18% O_2 and DMEM), E_2 and DPN demonstrated inhibitory effects on H_2O_2 production, but had the opposite effect at physiologic O_2 levels. Notably, in the condition most representative of *in vivo* (5% O_2 and Plasmax), E_2, DPN, and PPT were all without effect on H_2O_2 production. We do not have a detailed molecular explanation for these differences, but it is important to note that the cells were acclimated for at least 2 weeks to each respective culture condition, which is long enough to adopt stable but different phenotypes that would interact with the E_2 treatment to produce different outcomes. Moreover, the absence of any modulatory effects on H_2O_2 production when cells were grown in more *in vivo* like environment can be related to the low steady state level of H_2O_2 in the cells. Another likely reason for such observations can be related to the impact of long-term culture conditions on expression level of ERs and their ratio which can significantly modify ER's downstream targets. Future research should focus on how the culture environment modulates E_2's transcriptional effects, ideally using proteomic approaches. Collectively, these findings highlight the impact of media conditions on E_2's modulatory functions on ROS production which indeed might be important for other hormones and other cell types.

As stated earlier, the different effects of E_2 under the four cell culture conditions studied here are likely explained by different baseline phenotypes of the C2C12 cells growing under different conditions. In the absence of E_2 treatment, O_2 level and media affected mitochondrial properties and H_2O_2 production. 18% O_2 tension (compared to 5%) and Plasmax (compared with DMEM) increased mitochondrial abundance with higher branch mean length, which indicate stimulated mitochondrial biogenesis and or inhibited mitophagy. Interestingly, mitochondria appeared more fused and longer when cultured under most representative of *in vivo* condition (5% O_2 and Plasmax). Similarly, both media and O_2 levels modified cellular OCR and H_2O_2 production.

Cells produced less H_2O_2 when grown in more physiological conditions, suggesting that less physiologically representative cell culture conditions can affect ROS metabolism. Consistent with others (e.g., Maddalena et al., 2017; Fonseca et al., 2018), our data show that cells produce more H_2O_2 at higher O_2 levels, however, growing in physiologic media abolished such an effect. The absence of O_2 stimulatory effect on H_2O_2 production in Plasmax might be related to higher expression/activity of antioxidant enzymes (e.g., catalase) which might be inhibited in DMEM. This higher ROS production at higher O_2 tension might not be an appropriate baseline from which to determine how E_2 and SERMs influence ROS metabolism, since the basal condition will not be experienced by most cells *in vivo*. Overall, our results demonstrate the importance of O_2 and media formulation as determinants of E_2's effects on ROS production, energy metabolism, and mitochondrial network characteristics. It is likely that many of E_2's diverse cellular effects are modulated by the cell culture environment. Similarly, the effects of other hormones studied *in vivo* may be substantially dependent on the cell culture regime. This highlights the need to consider the cell culture environment for all such studies.

CHAPTER 4: The effect of oxygen and micronutrient composition of cell growth media on cancer cell bioenergetics and mitochondrial networks

This chapter was published as: Moradi, F., Moffatt, C., & Stuart, J. A. (2021). The Effect of Oxygen and Micronutrient Composition of Cell Growth Media on Cancer Cell Bioenergetics and Mitochondrial Networks. *Biomolecules*, 11(8), 1177. https://doi.org/10.3390/biom11081177

Author Contributions: Study conceptualization: FM and JAS. Writing: original draft preparation by FM and editing by JAS. All experiments were performed by FM except Seahorse assays, which were performed by FM and CM

ABSTRACT

Cancer cell culture is routinely performed under superphysiologic O_2 levels and in media with nutrient composition dissimilar to extracellular fluid. However, recently developed cell culture media (e.g., Plasmax, Human Plasma-Like Medium (HPLM)), which are modeled on the metabolite composition of human blood plasma, have been shown to shift key cellular activities in several cancer cell lines. Similar effects have been reported with respect to O_2 levels in cell culture. Given these observations, we investigated how media composition and O_2 levels affect cellular energy metabolism and mitochondria network structure in MCF7 (breast cancer cells), SaOS2 (osteosarcoma cells), LNCaP (androgen-sensitive human prostate adenocarcinoma cells), and Huh7 (human hepatoma) cells. Cells were cultured in physiologic (5%) or standard (18%) O_2 levels, and in physiologic (Plasmax) or standard cell culture (Dulbecco's Modified Eagle's Medium (DMEM)) media. We show that both O_2 levels and media composition significantly affect mitochondrial abundance and network structure, concomitantly with changes in cellular bioenergetics. Physiologic cell culture was associated with a more oxidative energy metabolism, and this is an important consideration for the study of cancer drugs that target aspects of energy metabolism, including lactate dehydrogenase.

INTRODUCTION

Standard cell culture procedures originating in the mid-20th century remain widely used today for investigating cell biology, including toxicity testing, and drug development. However, it has become increasingly clear that media composition, including O_2, affects many aspects of cell biology, including metabolism and drug efficacy (Gui et al., 2016; Muir et al., 2017; Cantor et al., 2017). Cancer drugs are typically discovered and studied, at least initially, using cell culture models, and the media environment can affect the outcome of these studies (eg., Cantor et al., 2017: Vande Voorde et al., 2019). The most commonly used medium for culturing human cancer cells is Dulbecco's Modified Eagles' Medium (DMEM) (Abbas et al., 2021). DMEM has a base nutrient formulation substantially different from human plasma (Psychogios et al., 2011; Ackermann et al., 2019) but can also be formulated with a range of glucose, pyruvate, and L-glutamine concentrations that are often not reported. The recent formulation of more 'physiologic' media, like Human Plasma-Like Medium (HPLM) (Vande Voorde et al., 2019) and Plasmax (Cantor et al., 2017) which are based on the human plasma metabolome, has focused attention on this topic.

Similarly, under standard cell culture conditions, O_2 is unregulated and equilibrates in the CO_2 incubator at 18-19%. This is much higher than the 1-6% O_2 levels that tissue cells normally experience *in vivo* (reviewed in Keeley and Mann, 2019). Several regulatory systems within human cells directly sense O_2 ensions and consequently influence physiology. Despite that, almost all present knowledge (including the initial characterizations of HPLM and Plasmax) related to the action of various stimuli (e.g., cytokines, growth factors, drugs) on cancer cells (eg., Metcalf ,2008; Ivanovic, 2009) is based on experiments done under non-physiological, near-atmospheric O_2 levels.

Media nutrients and O_2 in culture have broad effects on cancer cell metabolism and these influence experimental outcomes (Cantor et al., 2017; Vande Voorde et al., 2019; Alvarez et al., 2017; Birsoy et al., 2014; Fonseca et al., 2018; Zhang et al., 2019). For example, culture in HPLM significantly changes the cellular redox state relative to culture of the same cells in RPMI (Cantor et al., 2017). Physiological levels of uric acid in HPLM influence pyrimidine synthesis and remarkably reduce the efficacy of 5-fluorouracil (common chemotherapeutic drug) (Cantor et al., 2017). Consistent with that, we have shown that the concentration of even one single constituent

(e.g., glucose concentration in DMEM) in culture medium significantly affected the effects of two well-characterized anti-cancer molecules: resveratrol and rapamycin on multiple human cancer cell lines (e.g., LNCaP, Huh7) (Abbas et al., 2021).

Interestingly, in triple negative breast cancer cells (TNBC), pyruvate triggers a pseudo hypoxic response even under atmospheric O_2 leading to stabilization of hypoxia-inducible factor 1α (HIF1α) at the concentrations found in some commercial media (0.5–1mM). Likewise, the high concentrations of arginine in RPMI reverse the direction of the reaction catalyzed by the urea cycle enzyme, arginosuccinate lyase. In addition, the metabolic profile of TNBC spheroids grown in Plasmax for only 4 days resembled the metabolic landscape of orthotopic xenografts more closely than those in RPMI (Vande Voorde et al., 2019). Collectively, these results demonstrate that physiologic media like HPLM and Plasmax alter cellular metabolism and the response to specific drugs. However, detailed information on the effects of media on cellular bioenergetics, including mitochondrial form and function, are presently lacking.

Here, we investigated the effects of the Plasmax formulation used by VandeVoorde et al. (2019) versus DMEM, on cellular energy metabolism and mitochondrial network characteristics. Four well-studied cancer cell lines, MCF7 breast cancer cells, SaOS2 osteosarcoma cells, LNCaP androgen-sensitive human prostate adenocarcinoma cells, and Huh7 human hepatoma cells, were included in the investigation. Cells were cultured for a minimum of two weeks to acclimatize them to one of four different cell culture conditions: (1) the most common condition used for cancer cell culture, i.e. high-glucose DMEM supplemented with 10% FBS and unregulated O_2 (thus ~18%); (2) this same medium but with O_2 regulated at 5%; (3) the Plasmax formulation of VandeVoorde et al, (2019); (4) this same medium but with O_2 regulated at 5%. Under these four conditions, we evaluated cellular bioenergetics, mitochondrial abundance, and mitochondrial network morphology in all four cell lines. We found that mitochondrial form and function were significantly influenced by cell culture conditions, with both medium formulation and O_2 levels driving different bioenergetic phenotypes. These results indicate the importance of considering culture conditions in studies of energy metabolism and mitochondrial function *in vitro*.

EXPERIMENTAL PROCEDURES

Materials

Dulbecco's Modified Eagle Medium with glucose (4500 mg/L), L-glutamine, and sodium pyruvate (Cat. #D6429), and supplement-free Dulbecco's Modified Eagle Medium powdered media (Cat. #5030), Dimethyl sufoxide (DMSO), L-glutamine, HEPES ((4-(2- hydroxyethyl)-1 piperazineethane-sulfonic acid), DL-dithiothreitol (DTT), Bradford reagent, and Trypan Blue were obtained from BioShop (Burlington, ON, Canada). FBS (Cat. #F1051), nonessential amino acids (100X) (Cat. #M7145), penicillin/streptomycin solution, 0.25% trypsin/EDTA solution were obtained from Sigma-Aldrich (St. Louis, MO, USA). Tissue culture dishes (100 × 20 mm & 60 × 15 mm) were obtained from Sarstedt, Inc (Newton, SC, USA). MatTek glass bottom dishes (35mm) were purchased from MatTek corporation (Ashland, MA, USA). All cell lines were purchased from American Type Culture Collection (Manassas, VA, USA). Plasmax media constituents are shown in Table1.1 [4] α-Aminobutyrate (L-2-Aminobutyric acid; Cat. #438371), L-carnosine (Cat. #535080) and DL-3-Hydroxybutyric acid sodium salt (Cat. # A 11613-06) were purchased from CEDARLANE (Burlington, ON, Canada). 2-Hydroxybutyrate (2-Hydroxybutyric acid sodium salt; Cat. # S509425) and Ammonium Metavanadate (Cat. # A634095) were purchased from Toronto Research Chemicals Inc (Toronto, ON, Canada). Agilent Seahorse Calibrant XF (Cat. #100840-000), XFe 96 Extracellular Flux assay kit (Cat. # W17619) and XFe 96 cell culture microplate (Cat. # 101085-004) were purchased from Agilent Technologies (Mississauga, ON, Canada). carbonyl cyanide-4-(trifluoromethoxy) phenylhydrazone (FCCP) (Cat. # C2920), Oligomycin (Cat. # 579-13-5), Rotenone (Cat. # 83-79-4), sulfite (Na_2SO_3 (Cat. #S0505), and Antimycin A (Cat. # 1397-94-0) were purchased from Sigma-Aldrich (St. Louis, MO, USA). Unless otherwise stated, all other chemicals, reagents, and solutions (mainly used to make Plasmax) were purchased from Sigma-Aldrich (St. Louis, MO, USA), BioSHOP (Burlington, ON, Canada), or Fisher Scientific (Mississauga, ON, Canada).

Cell culture

To acclimatize the cells to the experimental conditions, all cell lines were cultured in either DMEM supplemented with 10% fetal bovine serum (FBS), 2× MEM nonessential amino acid solution, and penicillin (50 I.U./mL)/streptomycin (50 μg/mL) solution or in Plasmax media supplemented with 2.5% FBS (Vande Voorde et al., 2019) and penicillin (50 I.U./mL) / streptomycin (50 μg/mL)

solution for two weeks prior to initiation of experiments (a minimum of 4 -6 passages). Cells were maintained within a humidified 5% CO_2 atmosphere at 37 °C inside one of two Forma 3110 water-jacketed incubators with O_2 control (Thermo Fisher, Waltham, MA, USA). In one incubator, O_2 was not regulated (standard cell culture approach) and thus equilibrated to ~18% O_2 (super physiologic). In the other incubator, O_2 was regulated at 5% (physiological). All media were conditioned in the corresponding incubator for 24hr prior to use to ensure equilibration with the ambient condition.

Sample preparation for measuring cellular respiration at 18% O_2

Cellular respiration parameters were measured using a Seahorse Extracellular Flux Analyzer XF96 Mito Stress test (Agilent, Santa Clara, CA). Cells were seeded at a concentration of 15×10^3/well (MCF7, SaOS2, and Huh7) and 20×10^3/well (LNCaP), in a XF96-well microplate 14hr prior to OCR measurements as in (Plitzko and Loesgen, 2018) with some modifications. This optimal cell density per cell line was selected following titration assay to determine the optimal cell number. Cells were seeded in an 80µl final volume of media. Wells on the four corners of the plate were medium-only to serve as background correction wells. When cells are seeded at room temperature and then transferred immediately into a tissue culture incubator (~37°C), the environmental condition of the edge wells changes more rapidly than the environmental conditions of the interior wells with respect to temperature, humidity and %CO_2. Thus, to avoid the effect of edge effect on cell growth, cells were left at room temperature for 60 min prior to transferring them to the incubator. Hydration of a flux analyzer sensor cartridge probe plate was done by adding 200µl milliQ water into each well of the utility plate and putting the cartridge back onto the utility microplate. The utility plate was then placed in a non-CO_2 incubator at 37ºC overnight. At least one hour prior to commencing the assay, 200 µl of the Seahorse Bioscience XF96 Calibrant pH 7.4 solution was added to each well of the utility plate (after removing the milliQ water from the wells). Prior to analysis, the culture media was replaced with either unbuffered (lacking sodium bicarbonate) DMEM pH 7.4 or Plasmax pH 7.4 and cells were then allowed to equilibrate in a non-CO_2, at 37º C incubator to allow for precise measurement (45 minutes). One hour prior to measurement, the following compounds were added to the hydrated sensor cartridges: Oligomycin (1.0 µM), FCCP (1.0 µM), and rotenone/antimycin A (0.5 µM). These concentrations are selected following titration experiments (according to Agilent Seahorse XF Cell Mito Stress guideline).

Then, the sensor cartridges were loaded into the Seahorse Analyzer. After calibration, the sensor cartridges were replaced with the XF96 microplates and the measurement program was resumed to obtain the following OCR parameters: Basal, maximal, spare respiratory capacity, proton leak, and ATP linked. Extracellular acidification rate (ECAR) as measure of glycolysis was also measured (Plitzko and Loesgen, 2018). Wave Desktop 2.6 Software (Agilent) was used for data acquisition and data analysis for assays. The OCR and ECAR values were normalized to the protein concentration per well and were presented as pmol/minute/µg protein.

Sample preparation for measuring cellular respiration measurements at 5% O_2

For experiments at non-atmospheric O_2 conditions, the XF Analyzer was placed within a gas flow controlled Hypoxic Glove chamber (Coy Laboratories, Grass Lake, MI, USA). The atmosphere was CO_2-free and O_2 levels were set to 5%. During the assay, temperature was controlled within the Seahorse analyser; and the air circulation within the chamber was maintained by a fan. Media and other reagents were pre-equilibrated to the 5% O_2 atmosphere 24hr prior to the assay. To avoid reoxygenation, cell culture plates were transported from their incubators to the Hypoxic Glove chamber, where all washes were carried out. In compliance with Agilent Seahorse XF guideline for experiments under lower than atmosphere O_2 levels seeding density was reduced to12×10^3/well (MCF7), 17×10^3/well (LNCaP), 17×10^3/well (SaOS2), 12×10^3/well (Huh7). Furthermore, the last column of wells (in addition to background wells) was refilled with XF calibrant solution without any cells to serve as "zero" O_2 reference as specified by the manufacturer. To scavenge the O_2 sodium sulfite (Na_2SO_3) was injected into "zero" and XF Hypoxia Rate Calculator Software was used to calculate OCR measurements. The OCR values were normalized to the protein concentration per well and were presented as pmol/minute/µg protein.

Fluorescence microscopy

Fluorescence micrographs of live cells were obtained using a Carl Zeiss Axio Observer. Z1 inverted light/epifluorescence microscope equipped with ApoTome.2 optical sectioning and a Hamamatsu ORCA-Flash 4.0 V2 digital camera. 1×10^3 cells were cultured on Matek 35mm poly-D-lysine-coated glass bottom culture dishes for 48hr. Cells were switched to phenol red free DMEM or Plasmax media containing 50nM Mito Tracker Red and maintained at 37°C in humidified 5% CO_2, 18% O_2 atmosphere or 5% O_2 for 30 minutes. Then, cells were washed three times with fresh medium to remove the free dye and kept in DMEM or Plasmax for imaging. Images were collected

with a Plan-Apochromat 63x/1.40 Oil DIC M27 microscope objective. The microscope stage and objective were maintained with temperature control achieved through Temp Module S-controlled stage heater and objective heater (PeCon, Erbach, Germany) at 37 °C, and a humidified 5% CO_2 environment with either 18% or 5% O_2 throughout the experiments. During experiments conducted at 5% O_2, a humidified 5% O_2/5% CO_2/90% N_2 gas mix was continuously delivered through the Temp Module on-stage heater. Mito Tracker Red CMXRos signal was imaged with set excitation and emission wavelengths of 587 nm and 610 nm, respectively. The intensity of fluorescence illumination by an X-Cite 120LED light source and camera exposure times were both held constant across experiments. Z-stack series were rendered into single 2D images using the "extended depth of focus" processing tool in the Zeiss Zen 2 software. Z-stacks consisted of 20 slices, each 0.25 µm apart. Maximum intensity projections were generated for each stack using the Fiji distribution of ImageJ.

Image analysis

Mitochondrial morphology was analyzed and quantified using the Mitochondrial Network Analysis tool (MiNA) a macro tool developed for use with the FIJI distribution of ImageJ (Valente et al., 2017). Cells were selected randomly for each experimental condition, and fluorescence images were loaded into the program in their native format using Bio-Formats plug-in. To improve contrast between all mitochondrial structures and background, following pre-processing steps were performed: contrast limited adaptive histogram equalization (CLAHE), median filtering (a 2-pixel radius) and 'unsharp mask'. In the processed image, fluorescent mitochondrial signal was subjected to thresholding to eliminate background signal, which could generate an artifact. A binary image was generated by thresholding, the level of which was determined using Otsu's algorithm. From the binary, mitochondrial footprint was calculated from the total area of mitochondrial-signal positive pixels. To estimating the lengths of mitochondrial structures and the degree of branching, the Ridge Detection plugin was applied (Steger, 1998; Wagner and Hiner, 2017). Ridge detection uses florescence intensity to produce binary images, from the binary image morphological skeleton was generated using the Skeletonize3D plugin. The topology is then captured by the Analyze Skeleton plug in, the results of which are used by MiNA to generate quantitative parameters. The information extracted from the morphological skeleton is the mean of the branch lengths for each independent feature and the number of branches in each network. Mean

branch length is calculated as the average length of a mitochondrial structure between two nodes. Mitochondria appear as interconnected, branching networks in which branches are connected at a node. Mean network size was calculated by computing the sum of all branch lengths within an independent network and dividing this by the total number of individual networks within a cell. 35 cells per condition were selected randomly from at least three separate experiments.

STATISTICAL ANALYSES

All statistical analyses were performed using GraphPad Prism 5 software (San Diego, USA). Two-way ANOVAs was performed for data sets. When statistical significance in data sets was observed from two-way ANOVAs, post-hoc analysis was performed using Tukey's honestly significant difference (HSD) test. A P-value of < 0.05 was considered significant for all statistical tests. All data are presented as means ± standard error of mean (SEM).

RESULTS

Here, we investigated how cell culture conditions affect cellular bioenergetics and mitochondrial form and function using four cancer cells that are routinely cultured in DMEM, or other non-physiologic commercial media, and with unregulated O_2 that therefore equilibrates to ~18%. Both media composition and O_2 had significant effects on these parameters, though many effects were cell line specific.

Media effects on OCR

At 18% O_2, MCF7 basal, maximal, and ATP-linked OCR were higher in Plasmax compared to DMEM ($F_{1, 176}$=32; F1, 176=36; $F_{1, 176}$; $F_{1, 176}$=124, respectively, P<0.05, Figure 1A). The same trend was observed at 5% O_2 ($F_{1, 176}$=18; $F_{1, 176}$=22; $F_{1, 176}$=24, respectively; P<0.05, Figure 4.1A), though in 5% O_2 proton leak-associated OCR was reduced in Plasmax ($F_{1, 176}$=24; P<0.05, Figure 4.1A). Broadly similar effects of media were seen in Huh7 cells. At 18% O_2, basal ($F_{1, 174}$=33), maximal ($F_{1, 174}$=42), spare respiratory capacity ($F_{1, 174}$=28), and ATP-linked OCR were higher in Plasmax versus DMEM ($F_{1, 174}$=19; P<0.05, Figure 4.1B). This trend was seen also at 5% O_2 except with no effect on spare respiratory capacity (basal ($F_{1, 174}$=27); maximal ($F_{1, 174}$=29); proton leak ($F_{1, 174}$=41); ATP-linked ($F_{1, 174}$=133); P<0.05, Figure 4.1B).

The media effects were notably cell-type specific. While Plasmax elevated basal and maximal OCR and spare respiratory capacity in LNCaP cells at 18% O_2 ($F_{1, 176}$=22; $F_{1, 176}$=46; $F_{1, 176}$ =110; respectively; P<0.05, Figure 4.1C), it had essentially the opposite effect at 5% O_2 (basal ($F_{1, 176}$=31), maximal ($F_{1, 176}$=78), proton leak ($F_{1, 176}$=31), and ATP-linked ($F_{1, 176}$=33)). SaOS2 cells, in contrast, had higher maximal ($F_{1, 175}$=23), spare respiratory capacity ($F_{1, 175}$=23), and proton leak ($F_{1, 175}$=23) in Plasmax versus DMEM (P<0.05, Figure 4.1D) when the experiments were conducted in 5% O_2, but these effects were largely absent at 18% O_2 where only maximal OCR was affected, and it was reduced in Plasmax ($F_{1, 175}$=23; P<0.05, Figure 4.1D)

O_2 effects on OCR

The incubator O_2 levels at which cells were grown and measurements performed significantly affected OCR in most of the cell lines. For example, all OCR parameters (basal ($F_{1, 176}$=43), maximal ($F_{1, 176}$=52), spare respiratory capacity ($F_{1, 176}$=47), proton leak ($F_{1, 176}$=40), ATP-linked ($F_{1, 176}$=49) ($P<0.05$, Figure 4.1A)) were elevated at 5% versus 18% O_2 in MCF7 cells grown in DMEM. Cells grown in Plasmax behaved essentially in a similar manner, with basal, maximal, and spare respirator capacity ($F_{1, 176}$=42; $F_{1, 176}$=55; $F_{1, 176}$=72, respectively, $P<0.05$, Figure 4.1A) being higher at 5% versus 18% O_2. Similar trends were seen with Huh7 cells. In DMEM, basal, maximal, proton leak-associated, and ATP-linked OCRs ($F_{1, 174}$=49; $F_{1, 174}$=42; $F_{1, 174}$=50; $F_{1, 174}$=72; $F_{1, 174}$=68, $P<0.05$, Figure 4.1B) were higher at 5% versus 18% O_2. Similarly, basal, maximal, proton leak, and ATP-linked OCRs ($F_{1, 174}$=49; $F_{1, 174}$=42; $F_{1, 174}$=50; $F_{1, 174}$=68, $P<0.05$, Figure 4.1B) were higher at 5% versus 18% O_2 in Plasmax. However, spare respiratory capacity decreased at 18% versus 5%O_2 when Huh7 cells were grown in Plasmax ($F_{1, 174}$=17, $P<0.05$, Figure 4.1B)

LNCaP cells also had higher basal, maximal, proton leak, and ATP-linked OCR ($F_{1, 176}$=122; $F_{1, 176}$=123; $F_{1, 176}$=98; $F_{1, 176}$=112 respectively, $P<0.05$, Figure 4.1C) at 5% versus 18% O_2 when grown in DMEM. However, in Plasmax only basal and proton leak associated ($F_{1, 176}$=102; $F_{1, 176}$=83; respectively, $P<0.05$, Figure 1C) were higher at 5% versus 18% O_2. At 18% versus 5% O_2, however, maximal, and spare respiratory capacity ($F_{1, 176}$=108; $F_{1, 176}$=130, respectively, $P<0.05$, Figure 4.1C) were elevated. Our data robustly indicate that LNCaP cells had greater basal and proton leak-associated OCRs at more physiologic O_2 tension. SaOS2 cells also showed different responses to O_2, with cells grown in DMEM having elevated basal, maximal OCRs ($F_{1, 175}$=19; $F_{1, 175}$=29, $P<0.05$, Figure 4.1D) at 18% versus 5% O_2. These cells in Plasmax exhibited lower maximal, spare respiratory capacity, and proton leak associated OCRs at 18% O_2 ($F_{1, 175}$=21; $F_{1, 175}$=25, $F_{1, 175}$=23, respectively, $P<0.05$, Figure 4.1D).

OCR in standard versus physiologic cell culture

An interesting comparison is that between a standard cell culture condition (18%O_2/DMEM) and more physiologic cell culture (5%O_2/Plasmax). In MCF7 cells, basal ($F_{1,}$

$_{176}$=64) and maximal ($F_{1, 176}$=68) OCR, spare respiratory capacity ($F_{1, 176}$=74), proton leak ($F_{1, 176}$=60), and ATP-linked OCR ($F_{1, 176}$=72; P<0.05, Figure 4.1A) were all higher in the physiologic cell culture condition. Essentially the same results were seen in the other three cell lines. In Huh7 cells basal, maximal, proton leak-associated, and ATP-linked OCRs ($F_{1, 174}$=31; $F_{1, 174}$=43; $F_{1, 174}$=34; $F_{1, 174}$=87, respectively, P<0.05, Figure 4.1B) were elevated in physiologic conditions. In LNCaP cells basal, maximal, proton leak, and ATP-linked OCRs ($F_{1, 176}$=178; $F_{1, 176}$=122; $F_{1, 176}$=103; $F_{1, 176}$=102, respectively, P<0.05, Figure 4.1C) were elevated in physiologic cell culture. SaOS2 cells had lower basal OCR ($F_{1, 176}$=22; P<0.05, Figure 4.1D) in physiologic conditions, but spare respiratory capacity, proton leak, and ATP-linked OCR ($F_{1, 174}$=31; $F_{1, 174}$=18; $F_{1, 174}$=20, respectively, P<0.05, Figure 4.1D) were elevated. Overall, these comparisons suggest that physiologic conditions increase mitochondria-dependent metabolism in cancer cells.

(A) MCF7

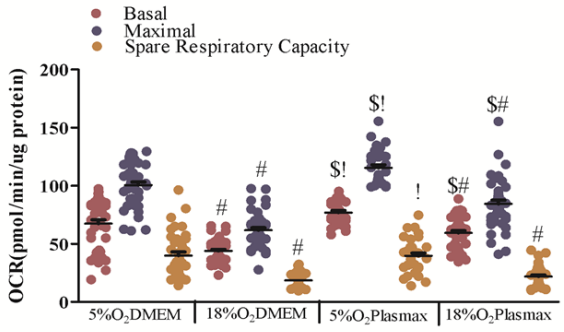

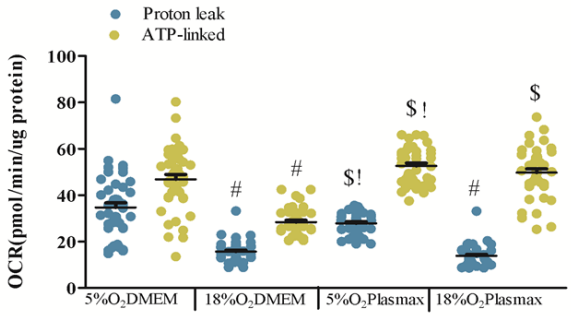

(B) Huh7

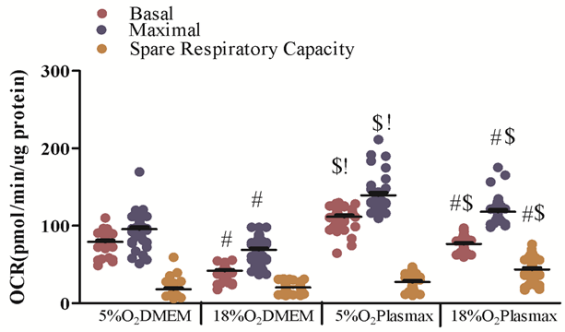

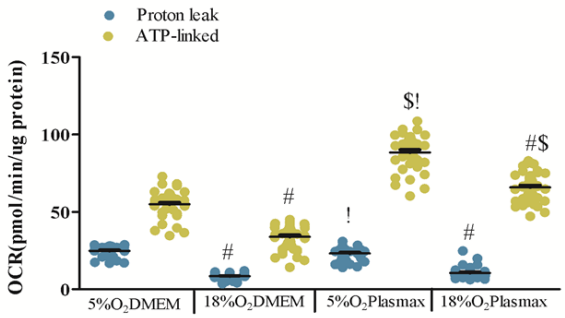

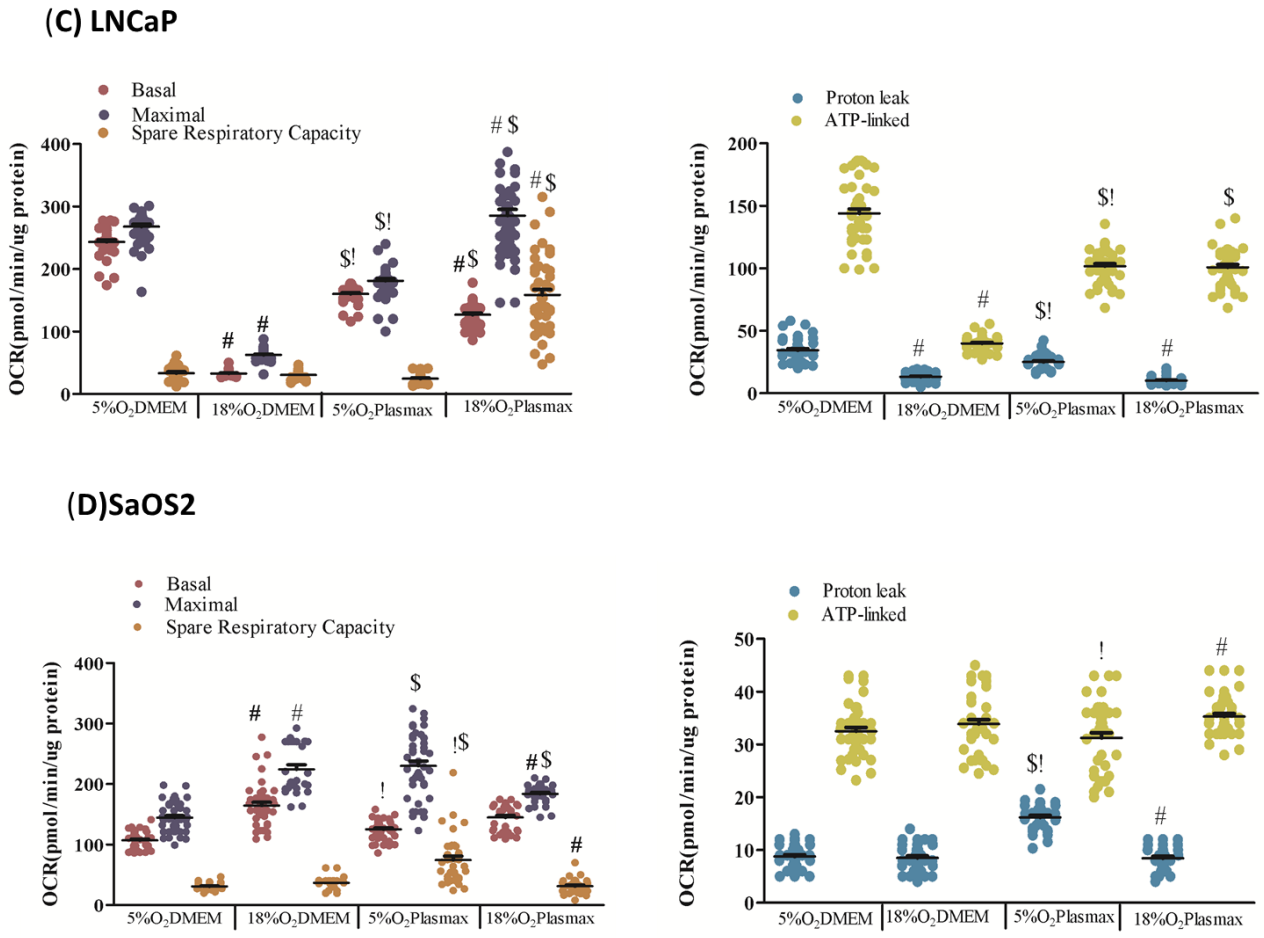

Figure 4.1. Bioenergetics profiles of cancer cell lines as a function of O_2 concentration and media composition. **(A)** MCF7, **(B)** Huh7, **(C)** LNCaP, and **(D)** SaOS2 cell lines were cultured at either 5% O_2 or 18% O_2 in either DMEM or Plasmax for at least two weeks prior to commencing the assay. Basal, maximal, spare respiratory capacity, proton leak, ATP-linked OCRs (normalized to protein content) were measured using a Seahorse XF96 Flux Analyzer. Data shown are means ± SEM from 3 independent experiments per condition (n=43 wells per each condition for each cell line). '#' represents differences between 18% O_2 and 5% O_2 in the same media. '$' represents differences between Plasmax and DMEM when O_2 level is the same. '!' represents differences between 5% O_2/ Plasmax versus 18% O_2 /DMEM. Statistical significance was determined by tow-way ANOVA followed by Tukey's post-hoc analysis.

O_2 and media effects on ECAR

Measurement of the medium extracellular acidification rate (ECAR) provides an indirect analysis of the cellular glycolytic rate. All four cell lines showed higher ECAR rates in DMEM versus Plasmax (Figure 4.2). In MCF7 cells at either 18% or 5% O_2 cells in DMEM demonstrated greater glycolytic activity as shown by higher ECAR ($F_{1, 176}$=117; $F_{1, 176}$=16, respectively, P<0.05, Figure 4.2A). Huh7 cells exhibited higher glycolysis in DMEM at both O_2 levels (18% O_2 ($F_{1, 174}$=40, P<0.05, Figure 4.2B), 5% O_2 ($F_{1, 174}$=38, P<0.05, Figure 4.2B)). Similarly, LNCaP cells at 18% and 5% O_2 had elevated ECAR in DMEM ($F_{1, 176}$=47; $F_{1, 176}$=33, respectively, P<0.05, Figure 4.2C). SaOS2 cells also had higher ECAR in DMEM versus Plasmax at both 18% and 5% O_2 ($F_{1, 174}$=36; $F_{1, 174}$=24, respectively, P<0.05, Figure 4.2D). Thus, in all four cancer cell lines tested here, glycolytic activity was higher in DMEM versus Plasmax.

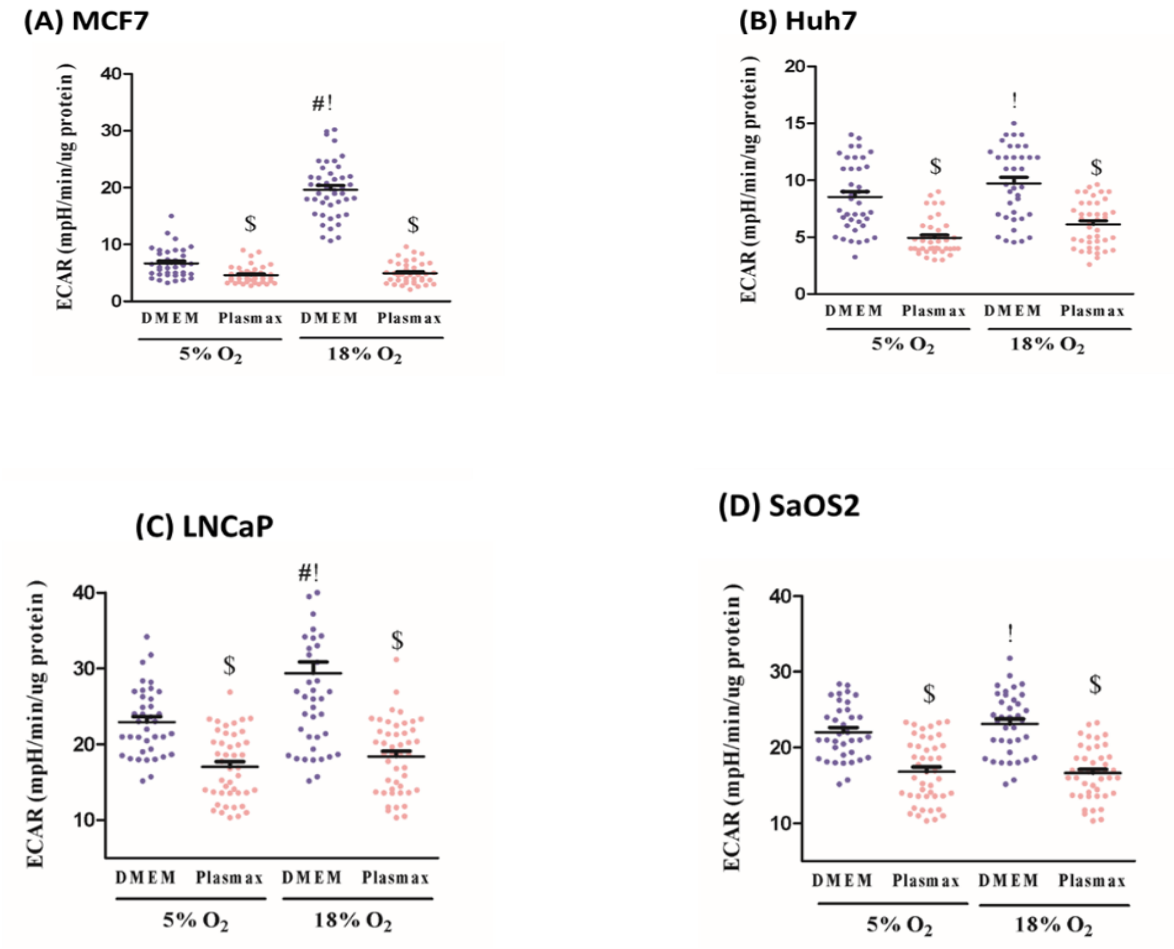

Figure 4.2. Glycolysis activity as a function of media composition and O_2. (A) MCF7, **(B)** Huh7, **(C)** LNCaP, and **(D)** SaOS2 cell lines were cultured at either 5% O_2 or 18% O_2 in either DMEM or Plasmax for at least two weeks prior to commencing the assay. Extra cellular acidification (ECAR, normalized to protein content) was measured using a Seahorse XF96 Flux Analyzer. Data shown are means ± SEM from 3 independent experiments per condition (n=43 wells per each condition for each cell line). '#' represents differences between 18%O_2 and 5%O_2 in the same media. '$' represents differences between Plasmax and DMEM when O_2 level is the same. '!' represents differences between 5% O_2/ Plasmax versus 18% O_2 /DMEM. Statistical significance was determined by two-way ANOVA followed by Tukey's post-hoc analysis.

Finally, we investigated the effect of O_2 on glycolysis within a given medium. MCF7 cells exhibited higher ECAR in 18% O_2 versus 5% O_2 in DMEM ($F_{1, 176}$=98, P<0.05, Figure 4.2A), but there was no O_2 effect in Plasmax. The same was seen in LNCaP cells with having higher ECAR at 18% versus 5% O_2 in DMEM ($F_{1, 176}$=21, P<0.05, Figure 4.2C) but not Plasmax. However, ECAR in Huh7 and SaOS2 cells was not affected by O_2 levels (Figure 4.2B, D). In the comparison between standard and physiologic cell culture, MCF7, Huh7, LNCaP, and SaOS2 cell lines had elevated ECAR in the standard condition ($F_{1, 176}$=129; $F_{1, 176}$=79; $F_{1, 176}$=62; $F_{1, 176}$=59, respectively, P<0.05, Figure 4.2A-D). Altogether, O_2 does not seem to affect glycolysis activity when cells are in a more physiologic media, though it was not an observation in all cell lines tested here.

O_2 and media effects on mitochondrial abundance

We used live cell imaging with Mito tracker labelling and the Mitochondrial Network Analysis Tool (MiNA) (Valente et al., 2017) to assess mitochondrial network characteristics including the 'mitochondrial footprint', which is an estimate of mitochondrial abundance in cells. At both O_2 levels, no effect of media on mitochondrial footprint was detected in MCF7; Huh7or SaOS2 cells (Figure 4.3). However, a moderate higher footprint in LNCaP cells when grown in Plasmax was observed at only 5% O_2 ($F_{1, 136}$=21; P<0.05; Figure 4.3C).

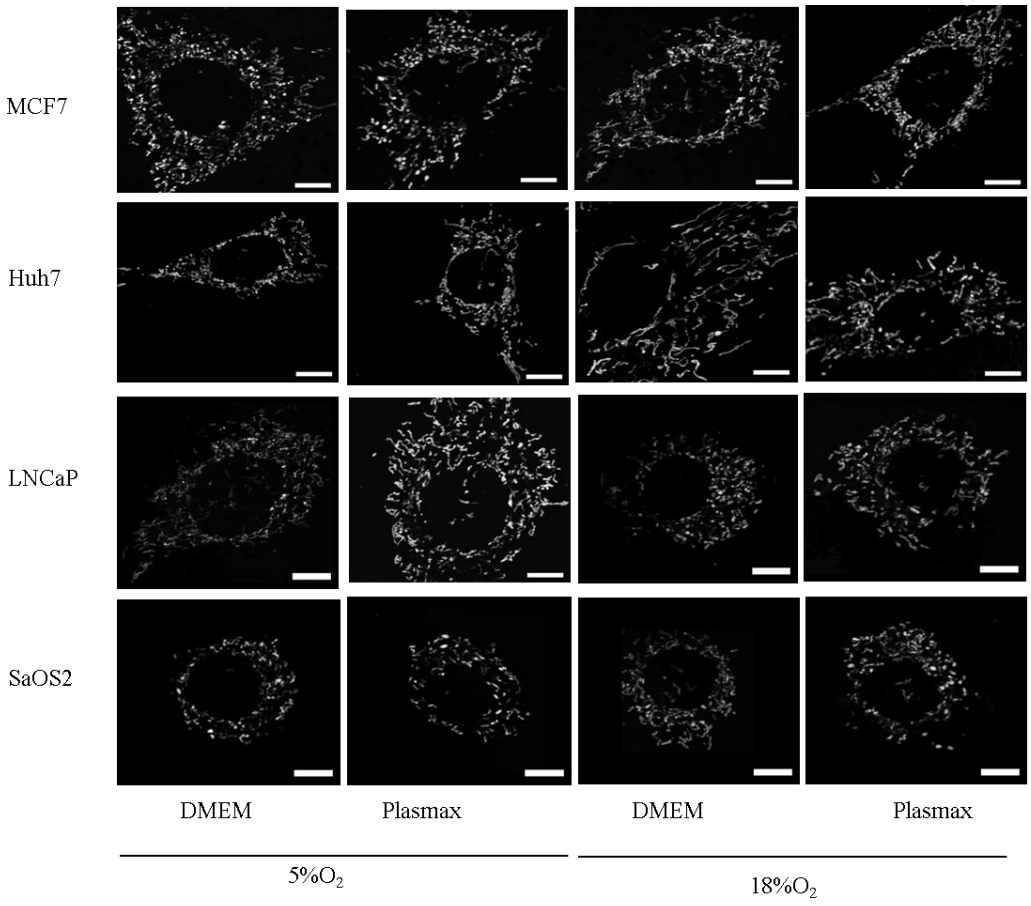
MCF7
Huh7
LNCaP
SaOS2
DMEM
Plasmax
DMEM
Plasmax
5%O2
18%O2

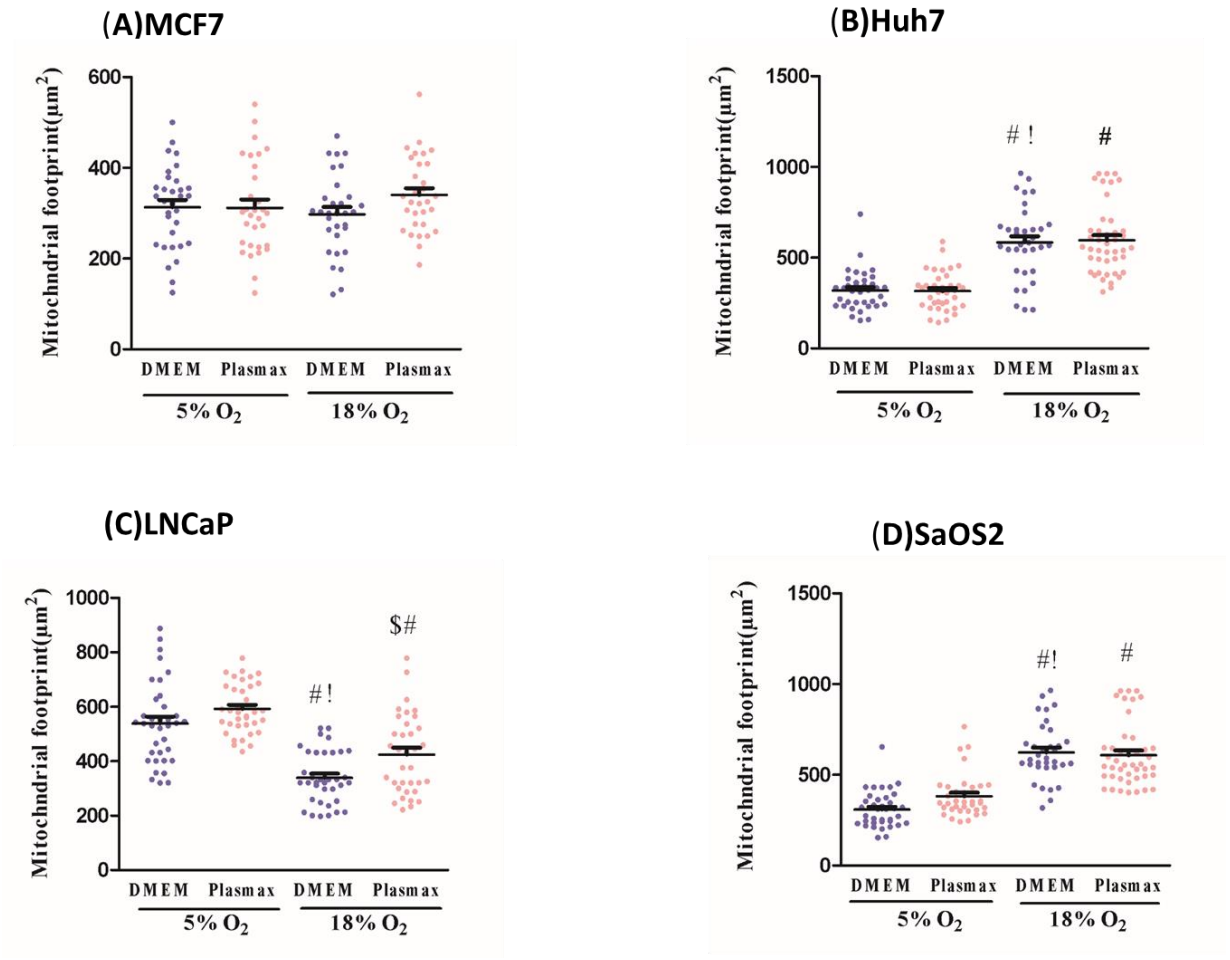

Figure 4.3. O_2 concentration and media type influence mitochondrial abundance. Representative images from mitochondrial network from cells stained by Mito tracker red (Scale bar is 5µm). Mitochondrial footprint (area in μm^2) as a proxy of abundance in the cells was measured applying MiNA tool (Valente et al., 2017). Feature was graphed from: **(A)** MCF7, **(B)** Huh7, **(C)** LNCaP, and **(D)** SaOS2. Cells were cultured at either 5% O_2 or 18% O_2 in either DMEM or Plasmax for at least two weeks prior to commencing the measurements. Data shown are means ± SEM from 3 independent experiments per condition (n=35) cells per each condition for each cell line). '#' represents differences between 18% O_2 and 5% O_2 in the same media. '$' represents differences between Plasmax and DMEM when O_2 level is the same. '!' represents differences between 5% O_2/ Plasmax versus 18% O_2 /DMEM. Statistical significance was determined by two-way ANOVA followed by Tukey's post-hoc analysis.

O_2 levels had no effect on mitochondrial footprint in MCF7 cells growing in either medium. In contrast, O_2 had significant effects in Huh7, LNCaP, and SaOS2 cell lines (Figure 4.3B-D). Higher O_2 level condition was associated with greater mitochondrial footprint in Huh7 cell line in either cell culture medium (DMEM ($F_{1, 136}$=24), Plasmax ($F_{1, 136}$=26; P<0.05; Figure 4.3B). In stark contrast, this feature in LNCaP cells was greater at 5% O_2 in either medium (DMEM ($F_{1, 136}$=20); Plasmax ($F_{1, 136}$=18); P<0.05; Figure 4.3C). SaOS2 behaved similarly to Huh7 cells where 18% O_2 was associated with increased mitochondrial footprints in either culture medium (DMEM ($F_{1, 136}$=23); Plasmax ($F_{1, 136}$=17); P<0.05; Figure 4.3D). Comparing more physiologic relevant regimen to the standard cell culture condition, Huh7 and SaOS2 cells had greater mitochondrial footprint in standard versus physiologic ($F_{1,136}$=27; $F_{1,136}$=32, respectively, P< 0.05; Figure 4.3C, D). However, this measurement was greater in physiologic culture condition than in standard conditions in LNCaP cell line ($F_{1, 136}$=32; P<0.05; Figure 4.3C). Overall, O_2 level appeared to be a more important driver of mitochondrial footprint than culture medium.

O_2 and media effects on mitochondrial network morphology

Changes in mitochondrial network morphology are associated with changes in energy metabolism. Notably, rich-nutrient environments can promote mitochondrial network fragmentation, while nutrient deprivation (lack of glucose, lipids and amino acids) are associated with more elongated and fused mitochondrial structures (Liesa and Shiriha, 2013). We measured mitochondrial mean network size (# of branches per network), and branch mean length (in micron) to assess the extent of fusion of mitochondrial structures into longer and more highly branched networks. Once again, effects of culture condition on mitochondrial network were highly cell line dependent.

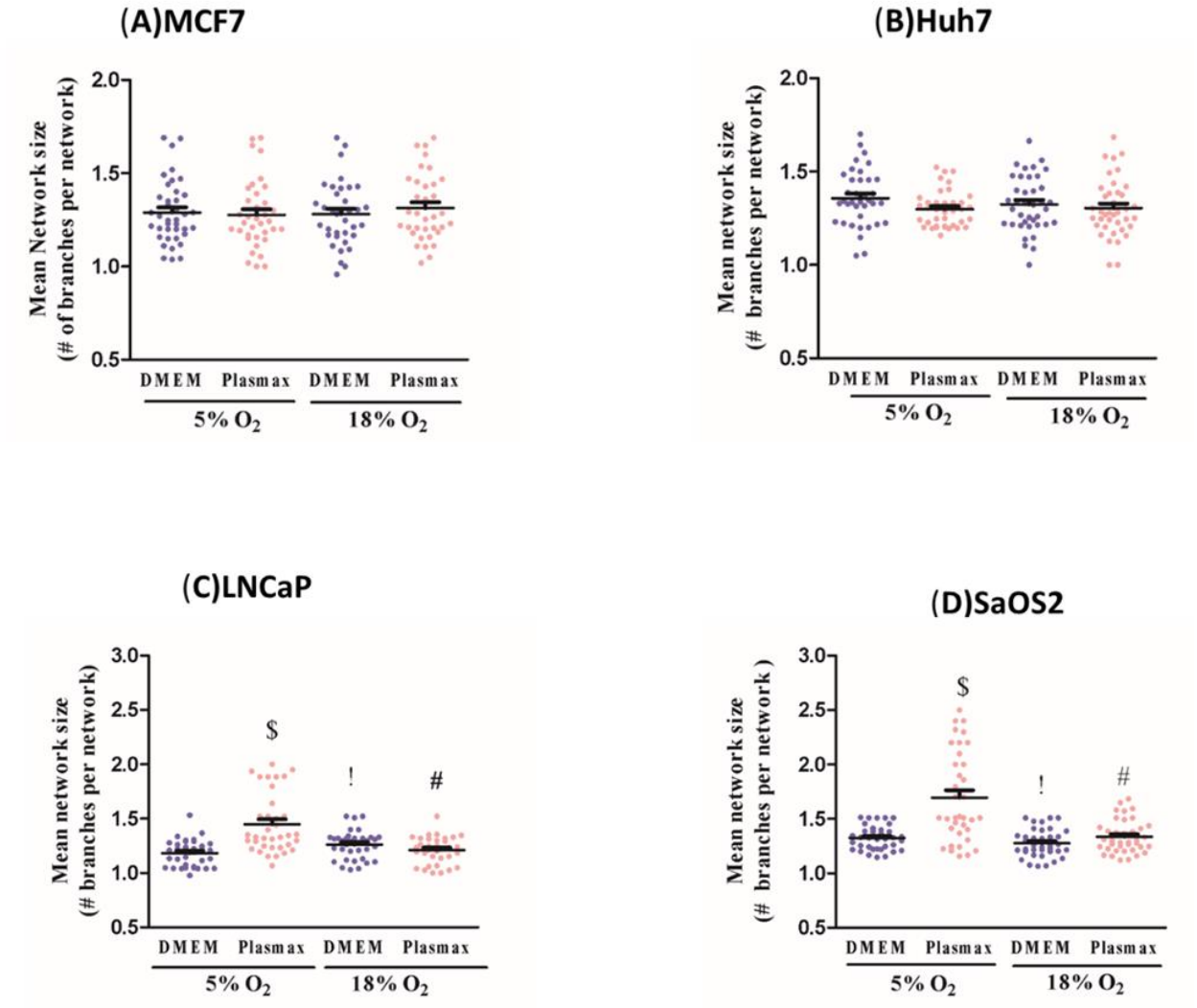

Figure 4.4. O_2 **concentration and media type influence mitochondrial network status.** Mitochondrial mean network size (# of branches per network) was measured using MiNA tool in **(A)** MCF7, **(B**) Huh7 **(C)** LNCaP, and **(D)** SaOS2 cell lines. Cells were cultured at either 5% O_2 or 18% O_2 in either DMEM or Plasmax for at least two weeks prior to commencing the measurements. Data shown are means ± SEM from 3 independent experiments per condition (n=35 cells per each condition for each cell line). '#' represents differences between 18% O_2 and 5% O_2 in the same media. '$' represents differences between Plasmax and DMEM when O_2level is the same. '!' represents differences between 5% O_2/ Plasmax versus 18% O_2 /DMEM. Statistical significance was determined by two-way ANOVA followed by Tukey's post-hoc analysis.

In MCF7 and Huh7 cells, neither media nor O_2 level affected mean network size (# of branches per network) (Figure4 A, B). In LNCaP and SaOS2 cells, however, this measurement was elevated in Plasmax versus DMEM at 5%O_2 with no significant difference at 18% O_2 ($F_{1, 136}$=31; $F_{1, 136}$=28, respectively, P<0.05; Figure 4.4C, D). More physiologic O_2 level (5%) was associated with greater mean network size in only Plasmax regimen ((LNCaP) $F_{1, 136}$=28; (SaOS2) $F_{1, 136}$=24; P<0.05; Figure 4.4C, D). Mean network size was also higher in more physiologic condition than in common cell culture in both LNCaP and SaOS2 cell lines ($F_{1,136}$=23; $F_{1,136}$=19, respectively, P<0.05; Figure 4.4C, D). Overall, mitochondrial seems to be affected by cell culture condition in a cell type specific manner with greater fused mitochondrial network in cells grown in Plasmax and 5%O_2.

Neither media nor O_2 level affected branch mean length (in micron), another proxy of mitochondrial fusion, in MCF7 or LNCaP cells (Figure 4.5A, C). However, at 5% O_2 this value was greater in Plasmax than DMEM in SaOS2 cells ($F_{1, 136}$=22, P<0.05; Figure 4.5 D), and at 18% O_2 Huh7 cells in DMEM had elevated branch mean length ($F_{1, 136}$=23; P<0.05; Figure 4.5 B). Collectively, our data indicate that the media does not affect the mitochondrial branch mean length. Similarly, O_2 effect on this measurement is not notable except to Huh7 and SaOS2 cell lines with having larger branch mean length at 18% O_2 when in DMEM ($F_{1,136}$=25; $F_{1,136}$=21, respectively, P<0.05; Figure 4.5B, D). When comparing standard condition against the most physiologic one, Huh7 and SaOS2 cell lines had higher branch mean length in the former ($F_{1,136}$=32; $F_{1,136}$=26, respectively, P<0.05; Figure 4.5B, D) while in other cell types no significant different was detected. Collectively, we observed differences in energy metabolism (eg., basal OCRs, ECAR) and mitochondrial morphology in response to media composition and O_2 levels. These differences were mostly cell type specific which we attribute to the heterogeneity of cancer cells in general (reviewed in (Meacham and Morrison, 2013).

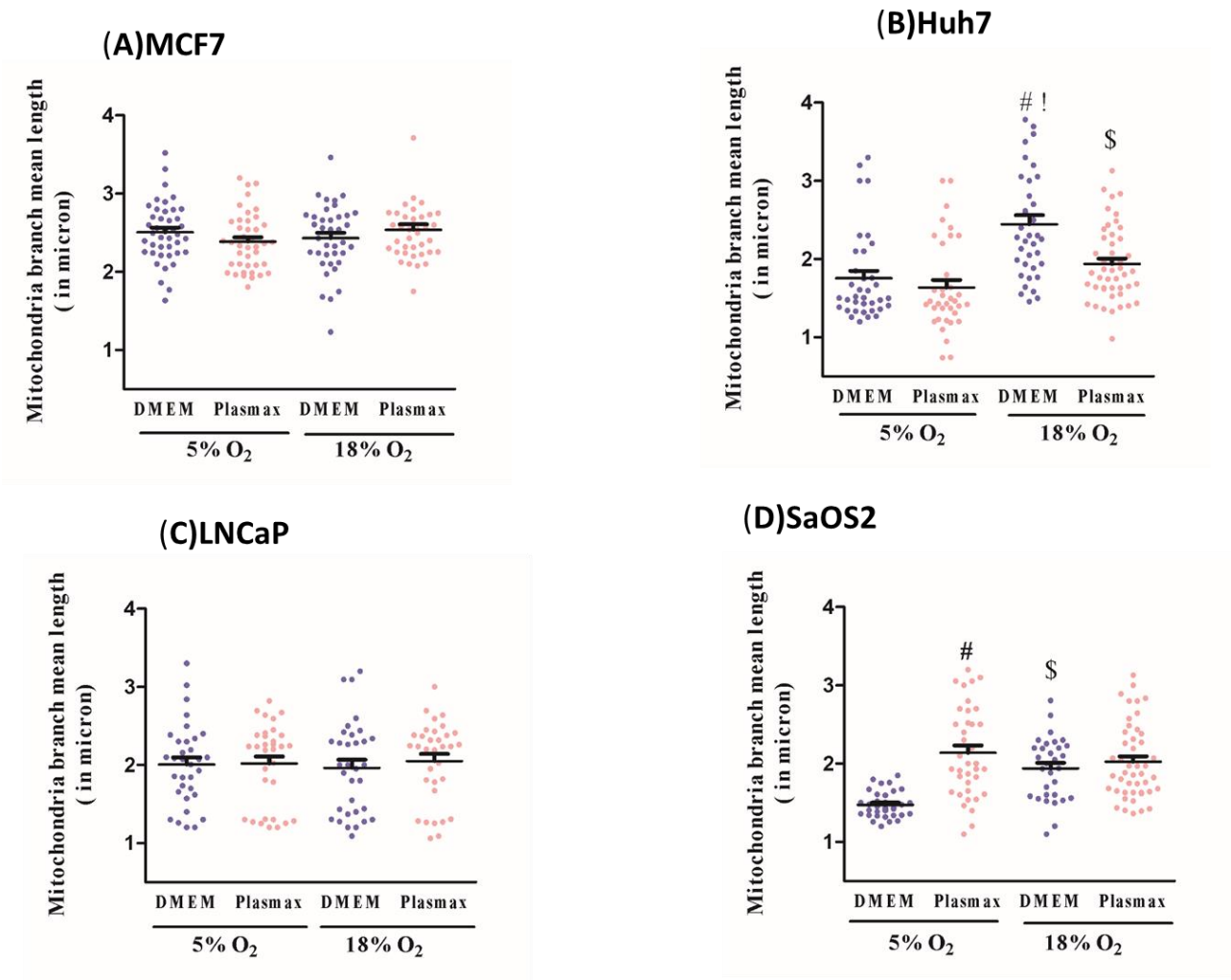

Figure 4.5. O_2 **concentration and media type influence mitochondrial branch size.** Mitochondrial branches mean length (in microns) was measured using MiNA tool in: **(A)** MCF7; **(B)** Huh7; **(C)** LNCaP; **(D)** SaOS2. Cells were cultured at either 5% O_2 or 18% O_2 in either DMEM or Plasmax for at least two weeks prior to commencing the measurements. Data shown are means ± SEM from 3 independent experiments per condition (n=35 cells per each condition for each cell line). '#' represents differences between 18% O_2 and 5% O_2 in the same media. '$' represents differences between Plasmax and DMEM when O_2 level is the same. '!' represents differences between 5% O_2/ Plasmax versus 18% O_2 /DMEM. Statistical significance was determined by two-way ANOVA followed by Tukey's post-hoc analysis.

DISCUSSION

Our results clearly indicate the extent to which the energy metabolism of cancer cell lines is affected by culture conditions. In all four cell lines investigated, ECAR was significantly elevated when cells were growing in standard cell culture conditions, compared to physiologic media and O_2 levels. This appeared to be driven by the culture media since, for any given O_2 concentration, ECAR tended to be greater in DMEM than in Plasmax. Concomitant with this effect, in three of the four cell lines (MCF7, Huh7, and LNCaP) basal and maximal OCR were lower in DMEM. Together, these results suggested that energy metabolism was shifted toward dependence on glucose fermentation to lactate in cells growing in DMEM, whereas cells growing in Plasmax had a more oxidative metabolism. Here we used a formulation of DMEM containing 25 mM glucose, whereas Plasmax contains 5.5 mM glucose. Although most published papers do not report the actual formulation of DMEM used (Abbas et al., 2021) and therefore not the concentration of glucose, it is likely that DMEM with 25 mM glucose is used commonly to avoid glucose depletion during multi-day cell culture. Although cancer cells are generally characterized by elevated rates of glucose consumption, this can be further promoted when they are grown in hyperglycemic media (Wang et al., 2017; Liu et al., 2013; Huang et al., 2018).

Increasing the reliance of cancer cells on glucose fermentation to lactic acid is problematic particularly for the experiment in which lactates dehydrogenase (LDH) is targeted. RNAi-mediated knockdown of the A-isoform of LDH, which favors pyruvate reduction to lactic acid, has toxic effects on several cancer cell lines (LDH knockdown inhibits *in vitro* and *in vivo* growth of various cancer cell lines (Le et al., 2010; Xie et al., 2014; Allison et al., 2014). Similar observations have been made in experiments targeting LDHA activity pharmacologically. For example, 1-(Phenylseleno)-4-(Trifuoromethyl) Benzene (PSTMB) inhibits LDHA activity while causing cell death in a range of cancer cell lines (Kim et al., 2019). NCI-006 potently inhibits LDH *in vitro* and *in vivo* (Oshima et al., 2020) and is considered a promising prospective drug for targeting tumor metabolism. Given the significant attention currently focused on metabolic inhibition strategies to combat cancers, it is particularly important to avoid non-physiological cancer cell culture approaches that alter energy metabolism in ways that may artifactually augment vulnerability to LDHA inhibiting drugs.

It is important to note that, although the use of media modeled after the human blood plasma metabolome represents a step forward in the development of a more *in vivo*-like cell culture environment; the extracellular environment of many cancer cells *in vivo* is depleted of many nutrients relative to plasma (reviewed in Lane et al., 2019). For example, in murine pancreatic cancer tumours, interstitial fluid glucose concentration can be ~50% lower than in plasma (Sullivan et al., 2019). Thus, arguably an even lower glucose concentration medium should be used in studies of LDH inhibitors, or indeed of any metabolic inhibitor.

It is surprising that, even in studies characterizing physiologic media like Plasmax and HPLM, experiments were performed at non-physiological O_2. Hypoxia-inducible factor-1 (HIF-1) is a well characterized mediator of aerobic glycolysis, via transcriptional stimulation of genes encoding glucose transporters and glycolytic enzymes (reviewed in Semenza, 2014). Although the vast majority of studies examining the O_2-regulated α-subunit (HIF-1α) have compared standard cell culture O_2 (18%) with hypoxia (typically 1%), a more physiologically relevant comparison might be between 5% (physioxia) and 1% (hypoxia). Notably, HIF-1α is present in relatively low amounts in the physiological range from 2-5% O_2 (reviewed in Stuart et al., 2019) where effects on transcription of glycolytic enzymes are likely significant. Alternatively, since cellular species ROS production can be influenced by environmental O_2 levels (Maddalena et al., 2017; reviewed in Stuart et al., 2018) and concomitantly affects cellular metabolism and other functions, it is important to consider this parameter. Our data indicate that, within a given medium, O_2 levels during cell culture can affect energy metabolism, apparent mitochondrial abundance and, to a lesser extent, mitochondrial network characteristics. Taken together, these effects of environmental O_2 levels on metabolic and mitochondrial characteristics of cancer cells emphasize the importance of this variable in experimental design. As noted for glucose above, although we used 5% O_2, which is typical of many normal human tissues (Mann and Keely. 2019), the O_2 levels in tumours are often lower. Certainly, unregulated O_2 that equilibrates to around 18% is inappropriate for cancer cell culture. Maintaining O_2 at 5% or lower will better mimic the *in vivo* environment.

In summary, here we have described metabolic effects of the cell culture environment on several well-studied cancer cell lines. These effects are substantial and may affect experiments

aiming to identify or characterize metabolic inhibitors for targeting cancer cell *in vivo*. Given these observations, it is important to consider maintaining physiologically relevant nutrient concentrations, including O_2, *in vitro*.

CHAPTER 5. The effect of media composition and O_2 level on the transcriptomic and proteomic signature of MCF7 cells

HYPOTHESIS

In vitro cancer cell culture is routinely performed under super physiologic O_2 levels and non-physiologic media composition that poorly recapitulate metabolite availability in human blood. This impacts cellular physiology, including energy metabolism, replicative cell growth, mitochondrial dynamics, and responses to drugs. These observations suggest that culture conditions broadly affect cell biology, but the nature of these effects is incompletely understood. Given that culture condition was shown to affect MCF7 cells metabolism and mitochondrial morphology (Chapter 4), I hypothesized that the signature of culture condition at the transcriptomic and proteomic level is substantial.

OBJECTIVES

The overall aim of this study was to better understand how O_2 level and culture medium affect gene expression and the proteome. I used RNA-seq and protein expression profiling via iTRAQ with the human breast cancer cell line (MCF7) for this investigation. Specific objective: (1) to identify genes, proteins, and biological processes, cellular components, and KEGG pathways affected by culture conditions.

CONTRIBUTIONS

Study conceptualization: FM and JAS. All cell culture and RNA- extraction was performed by FM. Ilona Hilson performed RNA –seq alignment and data analysis. Dr. Sarah L, Alderman performed following procedures: cell lysis; protein extraction & digestion; iTRAQ labelling; writing the R-script to do the raw data cleaning, and normalization. All proteomics pathway analysis was performed by FM.

INTRODUCTION

The use of cell lines as experimental models to investigate cellular and molecular pathways in cancer is a fundamental approach for biomedical discovery. It has played an indispensable role in the identification of BRAF (B-Raf Proto-Oncogene, Serine/Threonine Kinase)- mutations (Davies et al., 2002), drug development (Druker et al., 1996; Shoemaker 2006), identification of mechanisms of therapeutic resistance (Engelman et al., 2007), and many other critical insights (Boonstra et al., 2015; reviewed in Mirabelli et al., 2019).

Standard cancer *in vivo* environment. Rather, the focus has been on providing cells with excess nutrients to promote growth. Yet, the composition of standard cell culture media, including O_2 levels, has profound effects on many aspects of cancer cell biology, including metabolism (Moradi et al., 2021a, b), ROS production, cell growth, and drug efficacy (Gui et al., 2016; Muir et al., 2017; Cantor et al., 2017; Fonseca et al., 2018). Culture conditions that are more representative of the *in vivo* state should improve the translatability of cell culture findings cell culture procedures are well established but were not developed with the goal of mimicking the

The most frequently used medium for culturing human cancer cells is Dulbecco's Modified Eagles' Medium (DMEM) (Abbas et al., 2021). DMEM has a base nutrient formulation substantially different from that of human plasma (reviewed in Ackermann and Tardito, 2019) but can also be formulated with a range of glucose, pyruvate, and L-glutamine concentrations that are usually not reported (Abbas et al., 2021). The recent formulation of more 'physiologic' media, like Human Plasma-Like Medium (HPLM) (Cantor et al., 2017) and Plasmax (VandeVoorde et al., 2019), which are based on the human plasma metabolome, has focused attention on this topic.

Similarly, cell culture is traditionally performed in CO_2 incubators in which the O_2 level is not regulated and equilibrate to ~18%. This is much higher than the range of 1-6% O_2 that most tissue cells normally experience *in vivo* (reviewed in Keely and Mann, 2019). Despite that, almost all present knowledge (including the initial characterizations of HPLM and Plasmax) comes from experiments done under non-physiological, near-atmospheric O_2 levels (e.g., Metcalf, 2008; reviewed in Ivanovic, 2009).

Recent findings indicate that changes in media nutrients and O_2 in culture have broad effects on cancer cell behaviour and that these can influence experimental outcomes (Alvarez et al., 2017; Birsoy et al., 2014; Cantor et al., 2017; Vande Voorde et al., 2019; Rossiter et al., 2021). For example, physiological levels of uric acid in HPLM influence pyrimidine synthesis and markedly reduce the efficacy of the common chemotherapeutic drug 5-fluorouracil (Cantor et al., 2017). In triple negative breast cancer cells (TNBC), pyruvate concentrations found in some commercial media triggers a pseudo hypoxic response even under atmospheric O_2, leading to stabilizing of hypoxia-inducible factor 1α (HIF1α) with concomitant effects on metabolism. This is not observed in the same cells cultured in Plasmax or in mammary orthotopic xenografts (VandeVoorde et al., 2019). In addition, the metabolic profile of TNBC spheroids grown in Plasmax for only 4 days resembled the metabolic landscape of orthotopic xenografts more closely than those grown in RPMI (VandeVoorde et al., 2019). Consistent with this, gene essentiality of blood cancer cell lines was also revealed to depend on the culture media composition (Rossiter et al., 2021).

Collectively, these results demonstrate that physiologic media like HPLM and Plasmax alter cellular metabolism and response to specific drugs. The tumour microenvironment *in vivo* has profound effects on gene expression (Langley and Fidler, 2011) and protein expression profiles of cancer cells (Fernando et al., 2021). Similarly, whole-genome microarray analysis of MDA-MB-231 breast cancer cells have shown that one-quarter (25.6%) of all genes were differentially expressed when cells were grown in different commercial media formulations (Kim et al., 2015). This level of response is significantly higher than the 10% as the overall average ratio of differential response (Lee et al., 2006; Williams et al., 2016), and it highlights the extent of media composition effects on cancer cell gene expression.

Despite overwhelming evidence that cell culture conditions impact many aspects of cancer cell biology, there is little on the effects of O_2 and media composition at the transcriptomic and proteomic level on cancer cells. Here, I investigated the effects of the Plasmax formulation of VandeVoorde (2019), versus a common DMEM formulation, in either 18% (standard cell culture) or 5% (physioxia) O_2 on the transcriptomic and proteomic profiles of MCF7 cells. MCF7 is a well-

studied cancer cell line for which we have previously demonstrated significant effects of media composition and O_2 level on mitochondrial energy metabolism (Moradi et al., 2021b). To identify how gene expression and the proteome are affected by the cell culture environment, MCF7 cells were cultured for a minimum of two weeks in one of four cell culture conditions: (1) DMEM which appears to be the most common protocol used in the literature (Abbas et al., 2021); (2) this same medium but with O_2 regulated at 5%; (3) Plasmax with unregulated O_2 (thus 18%), as used by VandeVoorde et al. (2019) in their seminal Plasmax paper; (4) this same medium but with O_2 regulated at 5% (physioxia). The expression of hundreds of genes was influenced by culture conditions. GO terms involving biological processes of nucleotide metabolism and cell division were strongly affected by medium nutrient composition and O_2. The levels of many proteins were similarly affected. Functional analysis of proteins revealed that numerous metabolic pathways were affected by culture conditions.

EXPERIMENTAL PROCEDURES

Materials

The MCF7 cell line was purchased from American Type Culture Collection (Manassas, VA, USA). Dulbecco's Modified Eagle Medium with glucose (4500 mg/L), L-glutamine, and sodium pyruvate (Cat. #D6429), Dimethyl sufoxide (DMSO), L-glutamine, HEPES ((4-(2- hydroxyethyl)-1 piperazineethane-sulfonic acid), DL-dithiothreitol (DTT), Trypan Blue were obtained from BioShop (Burlington, ON, Canada). Fetal bovine serum (Cat. #F1051), nonessential amino acids (100X) (Cat. #M7145), penicillin/streptomycin solution, 0.25% trypsin/EDTA solution were obtained from Sigma-Aldrich (St. Louis, MO, USA). Tissue culture dishes (100 × 20 mm & 60 × 15 mm) were obtained from Sarstedt, Inc (Newton, SC, USA). Plasmax media constituents are shown in supplementaryTable1.1 in reference (Vande Voorde et al., 2019). α-Aminobutyrate (L-2-Aminobutyric acid; Cat. #438371), L-carnosine (Cat. #535080) and DL-3-Hydroxybutyric acid sodium salt (Cat. # A 11613-06) were purchased from CEDARLANE (Burlington, ON, Canada). 2-Hydroxybutyrate (2-Hydroxybutyric acid sodium salt; Cat. # S509425) and Ammonium Metavanadate (Cat. # A634095) were purchased from Toronto Research Chemicals Inc (Toronto, ON, Canada). RNeasy Mini Kit (Cat. # 74104) was purchased from QIAGEN (Toronto, ON, Canada), iTRAQ kits (8-PLEX) were purchased from SCIEX (Framingham, MA, USA). Trypsin Gold Mass Spectrometry Grade was purchased from Promega Corporation (Madison, WI, USA). Unless otherwise stated, all other chemicals, reagents, and solutions (mainly used to make Plasmax) were purchased from Sigma-Aldrich (St. Louis, MO, USA), BioSHOP (Burlington, ON, Canada), or Fisher Scientific (Mississauga, ON, Canada).

Cell culture

To acclimatize the cells to the experimental conditions, MCF7 cells were cultured in 10-cm plates in either high glucose DMEM (25mM) supplemented with 10% fetal bovine serum (FBS), 2× MEM nonessential amino acid solution, and penicillin (50 I.U./mL)/streptomycin (50 μg/mL) solution or in Plasmax media(5.5mM) supplemented with 2.5% FBS and penicillin (50 I.U./mL)/streptomycin (50 μg/mL) solution for two weeks prior to initiation of experiments. Cells were maintained within a humidified 5% CO_2 atmosphere at 37 °C inside one of two Forma 3110

water-jacketed incubators with O_2 control (Thermo Fisher, Waltham, MA, USA). In one incubator, O_2 was not regulated (standard cell culture approach) and thus equilibrated to ~18% O_2 (super physiologic). In the other incubator, O_2 was regulated at 5% (physiological). Media was refreshed every 24hr and was initially tested with DAPI DNA fluorescence staining to check for mycoplasma contamination.

RNA extraction

For RNA-seq, total RNA was extracted using the RNeasy Mini kit (Qiagen) according to manufacturer's protocol. RNA concentration and purity were evaluated as A260/280 ratio using a Thermo Fisher Scientific Nanodrop spectrometer. RNA degradation and integrity were assessed using 1.5% agarose gel electrophoresis. RNA samples from three biological replicates per experimental condition were then pooled together into one sample per experimental condition. Finally, pooled samples were snap frozen in liquid nitrogen and stored at -80ºC until being sent to Novogene (Sacramento, CA) for sequencing.

Library preparation and sequencing

Quality check (QC), library preparation, and sequencing were performed by Novogene. Preliminary quantitation of RNA samples was performed with Nanodrop, and electrophoresis, and Agilent 2100 were performed for RNA integrity and quantitation check. mRNA was enriched using oligo (dT) beads for selecting polyA carrying RNAs and the Ribo-Zero kit was used for removing rRNA. RNA was subject to fragmentation before cDNA synthesis using random hexamer primers. Sequencing adaptor ligation, size selection, and PCR enrichment were performed to generate cDNA sequencing. The cDNA library was subject to QC processes, consisting of library concentration preliminarily tests with Qubit v2.0, insert size tests using Agilent 2100, and Q-PCR for library effective concentration precisely quantification. mRNA sequencing was performed on the Illumina NovaSeq 6000 S4 platform via (paired - end) PE sequencing at 150 bp x 2.

Assessment of RNA-seq DATA

QC was performed using FastQC v0.11.8 (Andrews, 2010). Sequencing data was subject to QC for sequencing error rate, GC content, filtering by removing the adapters, and reads containing N >10%

and low-quality bases with Q score ≤ 5. The total number of reads in FASTQ format was processed to calculate the sequencing coverage depth for each sample using in-house shell scripts. The total exon length of the transcripts from *Homo sapiens* GRCh38 from Ensembl (release 97) in "gene finding format" (gff) was calculated as the length of human reference transcriptome.

The pre-processed reads in the FASTQ file format from all samples were mapped to the *Homo sapiens* reference genome, GRCh38 from Ensemble (release 97) using STAR v2.7.0a (Dobin et al., 2013). To improve alignment accuracy and identify potential spliced sequencing reads correctly, a dataset of known splices sites; *Homo sapiens* GRCh38 from Ensemble (release 97) in gff format was added to the inputs for the mapping runs. Raw sequencing results are shown in Table 1

Table 5.1. **RNA-seq data sequencing coverage statistic summary.** Total length is calculated by multiplying the total number of reads by the length of read (150 bps). Coverage value is the total length divided by total exon length of human reference transcriptome in Homo sapiens (354,866,726 bps)

Culture condition	**Number of read pairs**	**Number of reads**	**Total length**	**Coverage**
5%O_2/DMEM	39,750,784	79,501,568	11,925,235,200	34
5%O_2/Plasmax	53,307,181	106,614,362	15,992,154,300	45
18%O_2 /DMEM	45,768,533	89,537,270	13,430,590,500	38
18%O_2/Plasmax	61,205,716	91,537,066	13,730,559,900	39

Differentially gene expression (DGE) analysis

DGE analysis was performed to identify differentially expressed genes (DEGs) across conditions using the Cufflinks package with the recommended default setting (Trapnell et al., 2012). The cufflinks utility was used to assemble the transcripts from the aligned reads for each sample. The resulting assemblies were merged and integrated with the reference transcripts file using the cuffmerge, followed by using the cuffdiff utility to calculate and test the statistical significance of changes in expression between each pair of the experimental conditions. By using the ggplot function from the R statistical computing environment, the outputs of cuffdiff were visualized using a scatter boxplot and pairwise comparison across samples was performed using Pearson correlation

and paired T-test based on fragments per kilobase of transcript per million mapped reads (FPKM). DGE downstream analysis was performed first by filtering the individual DEG lists from the above step based on the p-value (0.05) and $\log_2(FC) \geq 1$ (equal to $FC \geq 2$) to determine the statistically significant change in gene expression. The lists were further filtered by requiring the FPKM value to be a minimum of 5 in at least one of the two samples in the comparison. Venn diagram was generated using a web tool from http://bioinformatics.psb.ugent.be/webtools/Venn/ to find the overlapped genes across different DEG lists.

Functional enrichment analysis

Functional enrichment analysis was performed using Database for Annotation, Visualization, and Integrated Discovery (DAVID) version 6.7 (Huang, et al., 2009) for the DEG list. *Homo sapiens* was used as the selected species. Enriched gene ontology (GO) terms and KEGG pathways were identified using the default setting of DAVID functional annotation. A Benjamini corrected p-value (≤ 0.05) was applied for identifying the most statistically significant enriched GO terms and KEGG Pathways.

Proteome quantitation and characterization

Proteome quantitation and characterization were carried out using isobaric tags for relative and absolute quantitation (iTRAQ), as described in (Alderman et al., 2019). Briefly, MCF7 cells were tested with DAPI DNA fluorescence staining to check for mycoplasma contamination. Cells from each culture conditions (n=3 per treatment) were lysed for 15 min in ice-cold RIPA buffer (150 mM NaCl, 1.0% Triton X-100, 0.5% sodium deoxycholate, 0.1% SDS (sodium dodecyl sulfate), 50mM Tris-HCl (pH 8), 1 mM EGTA, 1X Protease inhibitor (Roche, Mississauga, ON)). Lysates were precleared by centrifugation at 13000 g for 10 min and protein concentrations were determined by Bradford assay. Proteins were precipitated using the Calbiochem Protein Precipitation Kit (EMD Millipore, Billerica, MA) according to the manufacturer protocols. The protein pellet was dissolved in HEPES buffer (1 M HEPES, 8 M urea, 2 M thiourea, 4% CHAPS w/v; pH 8.5) and re-quantified. A reference sample was prepared by combining an equal quantity of each sample. 200 ug of total protein from each sample were reduced with 5 mM DTT to block disulfide bonds and cysteines were subsequently alkylated with 10 mM iodoacetamide (IAA, Sigma-Aldrich, Oakville,

ON) for 30 minutes in the dark prior to overnight digestion with Trypsin Gold Mass Spectrometry Grade. Following incubation with IAA, samples were washed 3 times with 0.5 M of triethylammonium bicarbonate (TEAB, Sigma-Aldrich). Trypsin was dissolved in 0.5 M TEAB and was added to each sample at a 1:50 enzyme: protein ratio. Samples were digested with trypsin overnight (approximately 18 h) at 37 °C. Digested peptides were labeled for 2 h at room temperature using two 8-plex iTRAQ kits (SCIEX, Framingham, MA) according to manufacturer's instructions, such that each treatment and the reference sample were represented on each kit. Labelled peptides were then pooled for each kit, purified through C18 columns, and analyzed by LC-MS/MS (SickKids Proteomics Analysis Robotics & Chemical Biology Centre, Toronto, ON) as in (Alderman et al., 2017). Identification and quantification of proteins were performed using Proteome Discoverer v2.2.0.388 (Thermo Fisher, Waltham, MA), and mass spectra were searched against the NCBI non-redundant protein database (March 8, 2018) using the following spectrum file search settings: 20 ppm precursor mass tolerance, 0.5 Da fragment mass tolerance, carbamido methylation and iTRAQ static modifications, at least two unique identifying peptides, and target false discovery rate (FDR) 5%. Protein abundances were normalized to total protein in each run and missing values were imputed by low abundance re-sampling. Data were scaled to the reference sample to normalize abundance values across both plexes, and only proteins identified on both plexes were used for bioinformatics analysis.

Bioinformatics analyses of proteomics data

The full list of retrieved protein identifications was collated to remove duplicated entries, entries do not present on both plexes, and proteins identified by single unique peptides. Abundance values for each plex were then normalized using a variance stabilization function (vsn) and missing values imputed using k-nearest neighbour classification (knn). Data from the two plexes were then combined and abundance values scaled to the reference sample measured on each plex. All data processing steps were performed in R Studio. Differentially abundant (DA) proteins were identified using the Differential Enrichment analysis of Proteomics data package in R (DEP 1.10.0). To maximize input for functional analyses, significant differences were considered for any protein with an absolute fold-change in abundance greater than 1.2 and a raw p-value less than 0.05 in one or more of the above comparisons. The commonality of DEGs identified based on the RNA-seq and

proteomic data was analyzed based on the associated gene symbol using an in-house computer script.

Functional enrichment analysis of proteomics data

The list of genes corresponding to differentially expressed proteins was subjected to DAVID's analytical modules. Using DAVID 6.7 analytical tools, we identified the gene enrichment in the biological process and functions in gene ontology, and the KEGG pathway database most relevant biological terms associated with the gene list. A Benjamini corrected p-value (≤ 0.05) was applied for identifying the most statistically significant enriched GO terms and KEGG Pathways.

RESULTS

RNA-seq was used to investigate differential gene expression at the transcription level in MCF7 cells cultured at either 5% or 18% O_2 and in DMEM or Plasmax media. The distribution of overall gene expression values showed a consistent pattern among all experimental conditions with the transcript abundance of the vast majority of the genes showing $\log_{10}$ (FPKM)) between -2.5 (FPKM =0.0032-0.0035) and 2.5 (FPKM = 280-310) (Figure S5.1). The list of differentially expressed genes (DEGs) was generated using a set of cut-offs including p-value ≤ 0.05, FC ≥ 2, and minimum FPKM value ≥ 5 in at least one of two samples in comparison. As shown in Figure 5.1**,** the total number of DEGs comparisons ranges from 588 for DMEM versus Plasmax under 18%O_2 level to 471 for Plasmax when comparing 5% versus 18%O_2.

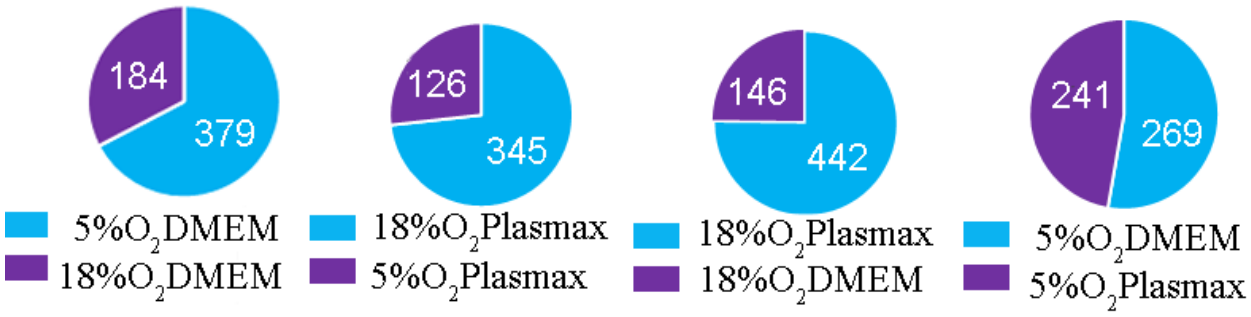

Figure 5.1. Differentially expressed genes (DEGs) for pairwise comparisons of different culture conditions. Pie charts show the number of DEGs between conditions based on P-value (<0.05), fold change (≥ 2), and FPKM (≥ 5 in at least in one of the two samples). Each number shows the number of genes with higher expression level in each condition.

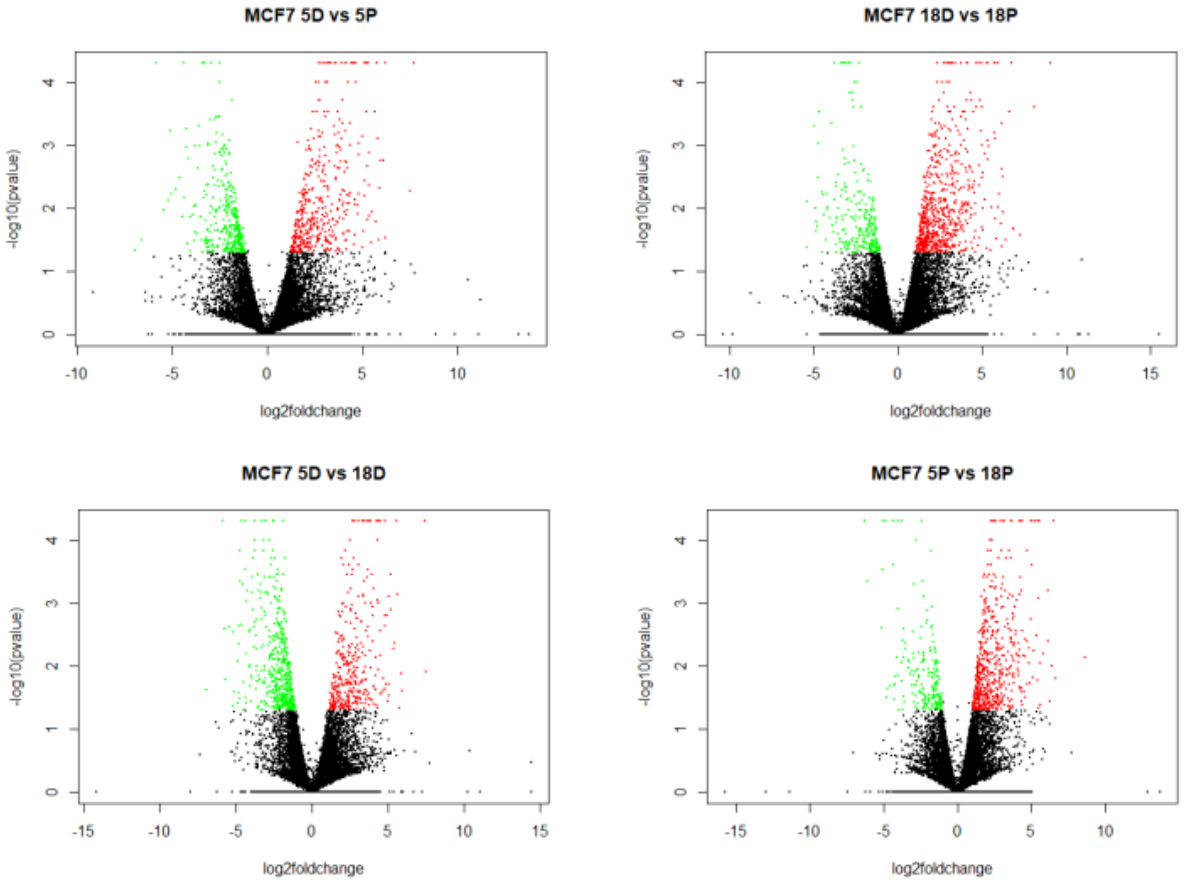

Figure 5.2. Volcano plots demonstrating the expression distribution of DEGs for each culture condition comparison. Red and green dots indicate significant DEGs (P-value < 0.05) showing up and down-regulated expression (FC ≥ 2.0), respectively. Genes are coloured black if they do not pass the Log2 (fold change) and Log10 (p-value). Upregulated genes in the first condition are coloured red and green if they are downregulated. **5P,** 5% O_2 in Plasmax; **5D,** 5% O_2 in DMEM; **18P,** 18% O_2 in Plasmax; **18D,** 18% O_2 in DMEM**.**

Effect of O_2 level on transcript abundance in MCF7 cells growing in DMEM

563 genes were identified as being differentially expressed in response to O_2 level. The list of all genes with higher expression levels at each O_2 level is shown in the appendix section (Table 5.1S; Table 5.2S). Among these DEGs, 184 genes showed higher expression at 18% O_2, while 379 showed higher expression at 5% O_2 (Figure 5.1). Enrichment analysis for GO terms and KEGG Pathways was performed using DAVIDs tool. Gene function enrichment analysis showed that the 379 DEGs with higher expression at 5% O_2 in DMEM are associated with 38 Biological Processes, 23 Cellular Components, 9 Molecular Functions, and 15 KEGG Pathways (Table 5.2). The vast majority of these enriched processes and pathways were related to cell division and associated DNA replication and quality surveillance, including specific terms such as: regulating cell cycle (e.g., G1/S and G2/M transition of cells and cell division), and DNA damage repair (e.g., base excision repair, mismatch repair, and homologous recombination) (Table 5.3). The 184 DEGs showing higher expression at 18% O_2 showed enrichment for 8 Biological Processes, 2 Cellular Components, 2 Molecular Functions, and 4 KEGG Pathways including FoxO signaling pathway (Table 5.3). Interestingly, the p53 signaling pathway was shown to be sensitive to O_2 levels as the related KEGG Pathway term was shown to be enriched under both O_2 conditions. The cellular response to hypoxia pathway was also affected by O_2, with 7 genes up-regulated at 5% and 5 genes up-regulated at 18% O_2 (Tables 5.2 and 5.3).

Table 5.2 Significantly enriched functional annotation clusters observed from up-regulated genes in cells grown in DMEM at 5% vs 18% O_2. All terms shown are significantly enriched based on Benjamini corrected *p*-value ≤ 0.05, except where indicated otherwise; * denotes significance based on *p*-value (≤0.05) but not Benjamini corrected P-value.

Biological Process	Gene count
GO:0000070~mitotic sister chromatid segregation	10
GO:0000079~regulation of cyclin-dependent protein serine/threonine kinase activity	7
GO:0000082~G1/S transition of mitotic cell cycle	27
GO:0000083~regulation of transcription involved in G1/S transition of mitotic cell cycle	9
GO:0000086~G2/M transition of mitotic cell cycle	21
GO:0000281~mitotic cytokinesis	7
GO:0000722~telomere maintenance via recombination	8
GO:0000731~DNA synthesis involved in DNA repair	8
GO:0000732~strand displacement	6
GO:0006096~glycolytic process	8
GO:0006260~DNA replication	38
GO:0006268~DNA unwinding involved in DNA replication	5
GO:0006270~DNA replication initiation	13
GO:0006271~DNA strand elongation involved in DNA replication	5
GO:0006281~DNA repair	27
GO:0006297~nucleotide-excision repair, DNA gap filling	6
GO:0006974~cellular response to DNA damage stimulus	13
GO:0006977~DNA damage response, signal transduction by p53 class mediator resulting in cell arrest	8
GO:0007049~cell cycle	17
GO:0007051~spindle organization	7
GO:0007052~mitotic spindle organization	7
GO:0007059~chromosome segregation	13
GO:0007062~sister chromatid cohesion	21
GO:0007067~mitotic nuclear division	44
GO:0007080~mitotic metaphase plate congression	8
GO:0007093~mitotic cell cycle checkpoint	7
GO:0015949~nucleobase-containing small molecule interconversion	5
GO:0031145~anaphase-promoting complex-dependent catabolic process	11
GO:0032508~DNA duplex unwinding	7
GO:0034501~protein localization to kinetochore	5
GO:0042493~response to drug	16
GO:0051301~cell division	56
GO:0051439~regulation of ubiquitin-protein ligase activity involved in mitotic cell cycle	7
GO:0051726~regulation of cell cycle	11
GO:0061621~canonical glycolysis	8
GO:0071456~cellular response to hypoxia	7*
GO:0090307~mitotic spindle assembly	7
GO:1901796~regulation of signal transduction by p53 class medium tor	13
Cellular Component	**Gene count**
GO:0000775~chromosome, centromeric region	12
GO:0000776~kinetochore	15
GO:0000777~condensed chromosome kinetochore	16
GO:0000784~nuclear chromosome, telomeric region	11
GO:0000790~nuclear chromatin	11*
GO:0000793~condensed chromosome	6

GO:0000922~spindle pole	17
GO:0000942~condensed nuclear chromosome outer kinetochore	4
GO:0005634~nucleus	184
GO:0005654~nucleoplasm	140
GO:0005657~replication fork	5
GO:0005737~cytoplasm	151
GO:0005813~centrosome	28
GO:0005819~spindle	16
GO:0005829~cytosol	126
GO:0005874~microtubule	21
GO:0005876~spindle microtubule	7
GO:0005971~ribonucleoside-diphosphate reductase complex	2
GO:0030496~midbody	16
GO:0032133~chromosome passenger complex	4
GO:0042555~MCM complex	7
GO:0051233~spindle midzone	7
GO:0072686~mitotic spindle	7
Molecular Function	**Gene count**
GO:0000405~bubble DNA binding	4
GO:0003677~DNA binding	51*
GO:0003678~DNA helicase activity	6*
GO:0003682~chromatin binding	23
GO:0003688~DNA replication origin binding	5
GO:0003697~single-stranded DNA binding	12
GO:0005515~protein binding	241
GO:0005524~ATP binding	72
GO:0042802~identical protein binding	26*
KEGG Pathway	**Gene count**
hsa00010: Glycolysis / Gluconeogenesis	9
hsa00240: Pyrimidine metabolism	10
hsa01230: Biosynthesis of amino acids	10
hsa03030: DNA replication	13
hsa03410: Base excision repair	10
hsa03430: Mismatch repair	6
hsa03440: Homologous recombination	6
hsa03460: Fanconi anemia pathway	10
hsa04068: FoxO signaling pathway	8*
hsa04110: Cell cycle	35
hsa04114: Oocyte meiosis	17
hsa04115: p53 signaling pathway	8
hsa04914: Progesterone-mediated oocyte maturation	12
hsa05166: HTLV-I infection	18
hsa05219: Bladder cancer	5*

Table 5.3 Significantly enriched functional annotation clusters observed from up-regulated genes in cells grown in DMEM at 18% vs 5% O_2. All terms shown are significantly enriched based on Benjamini corrected *p*-value ≤ 0.05, except where indicated otherwise; * denotes significance based on *p*-value (≤0.05) but not Benjamini corrected *p*-value.

Biological Process	**Gene count**
GO:0000079~regulation of cyclin-dependent protein serine/threonine kinase activity	3*
GO:0006974~cellular response to DNA damage stimulus	7*
GO:0006977~DNA damage response, signal transduction by p53 class mediator resulting in cell arrest	4*
GO:0009612~response to mechanical stimulus	7
GO:0009636~response to toxic substance	6*
GO:0051726~regulation of cell cycle	4*
GO:0071456~cellular response to hypoxia	5*
GO:0097193~intrinsic apoptotic signaling pathway	4*
Cellular Component	**Gene count**
GO:0005634~nucleus	61*
GO:0005737~cytoplasm	56*
Molecular Function	**Gene count**
GO:0005515~protein binding	98*
GO:0042802~identical protein binding	14*
KEGG Pathway	**Gene count**
hsa04068: FoxO signaling pathway	5*
hsa04115: p53 signaling pathway	14
hsa05161: Hepatitis B	8*
hsa05166: HTLV-I infection	7*

Effect of O_2 level on transcript abundance in MCF7 cells growing in Plasmax

In MCF7 cells grown in Plasmax, 471DEGs were identified in response to change of O_2 level, with 345 and 126 of these showed higher expression at 18% and 5% O_2, respectively (Figure 1; Tables 5.S3 and 5.S4). DEGs at 5% O_2 showed enrichment for 1 Biological Processes, 3 Cellular Components, and 3 Molecular Functions (Table 5.4). This represented a much more subtle effect of O_2 than that observed in the same cells growing in DMEM, and perhaps surprisingly, there was essentially no overlap in DEGs with the same experiment in DMEM. In stark contrast to DMEM, where most of the enrichment of GO terms and KEGG Pathways were associated with 5% O_2, in Plasmax these were either not affected by O_2 level or were primarily enriched at 18% O_2, highlighting the impact of the culture medium on cell's response to O_2 level. At 18% O_2, 8 Biological Processes, 15 Cellular Components, 10 Molecular Functions, and 3 KEGG Pathways were enriched in MCF7 cells grown in Plasmax (Table 5.5). These included cell cycle (e.g., negative regulation of cell proliferation and G1/S transition of mitotic cell cycle) and DNA replication initiation and biosynthesis of unsaturated fatty acids.

Table 5.4 Significantly enriched functional annotation clusters observed from up-regulated genes in cells grown in Plasmax at 5% vs 18% O_2. All terms shown are significantly enriched based on Benjamini corrected p-value ≤ 0.05, except where indicated otherwise; * denotes significance based on P-value (≤0.05) but not Benjamini corrected p-value.

Biological Process	**Gene count**
GO:0043524~negative regulation of neuron apoptotic process	5*
Cellular Component	**Gene count**
GO:0005737~cytoplasm	43*
GO:0005654~nucleoplasm	27*
GO:0005634~nucleus	44*
Molecular Function	**Gene count**
GO:0005515~protein binding	68*
GO:0005524~ATP binding	20*
GO:0001077~transcriptional activator activity, RNA polymerase II core promoter proximal region sequence-specific binding	6*

Table 5.5 Significantly enriched functional annotation clusters observed from up-regulated genes in cells grown in Plasmax at 18% vs 5% O_2. All terms shown are significantly enriched based on Benjamini corrected p-value ≤ 0.05, except where indicated otherwise; * denotes significance based on p-value (≤0.05) but not Benjamini corrected p-value.

Biological Process	**Gene count**
GO:0000082~G1/S transition of mitotic cell cycle	19
GO:0006260~DNA replication	22
GO:0006270~DNA replication initiation	11
GO:0000083~regulation of transcription involved in G1/S transition of mitotic cell cycle	8
GO:0045429~positive regulation of nitric oxide biosynthetic process	9
GO:0071353~cellular response to interleukin-4	8
GO:0008285~negative regulation of cell proliferation	21
GO:0043524~negative regulation of neuron apoptotic process	8*
Cellular Component	**Gene count**
GO:0005737~cytoplasm	131
GO:0070062~extracellular exosome	84
GO:0005654~nucleoplasm	78
GO:0005634~nucleus	126
GO:0005829~cytosol	91
GO:0005615~extracellular space	51
GO:0005925~focal adhesion	23
GO:0042555~MCM complex	5
GO:0015629~actin cytoskeleton	16
GO:0016020~membrane	62
GO:0001726~ruffle	8
GO:0031012~extracellular matrix	18
GO:0005884~actin filament	6*

GO:0000784~nuclear chromosome, telomeric region	8*
GO:0030141~secretory granule	6*
Molecular Function	**Gene count**
GO:0005515~protein binding	207
GO:0005524~ATP binding	44*
GO:0001786~phosphatidylserine binding	8
GO:0001077~transcriptional activator activity, RNA polymerase II core promoter proximal region sequence-specific binding	12*
GO:0042803~protein homodimerization activity	27*
GO:0003678~DNA helicase activity	5*
GO:0008134~transcription factor binding	14*
GO:0005200~structural constituent of cytoskeleton	9*
GO:0005544~calcium-dependent phospholipid binding	8
GO:0001135~transcription factor activity, RNA polymerase II transcription factor recruiting	4
KEGG Pathway	**Gene count**
hsa04110: Cell cycle	16
hsa03030: DNA replication	10
hsa01040: Biosynthesis of unsaturated fatty acids	6

Effect of culture medium on transcript abundance in MCF7 cells

In MCF7 cells grown at 5% O_2, 510 DEGs were identified in response to changes in medium, with 269 and 241 showing higher expression in DMEM and Plasmax, respectively (Figure 5.1; Tables 5.S5 and 5.S6). DEGs with higher expression in DMEM versus Plasmax showed enrichment for 19 Biological Processes, 12 Cellular Components, 8 Molecular Functions, and 5 KEGG Pathways with the main themes related to regulation of cell cycle and DNA replication (e.g., cell division and G1/S transition of mitotic cell cycle; Table 5.6). The majority of genes with higher expression in Plasmax at 5% O_2 showed enrichment of 16 Biological Processes, 9 Cellular Components, 6 Molecular Functions, and 4 KEGG Pathways in association with viral carcinogenesis and viral infections (e.g., Measles and Hepatitis B) (Table 5.). More specifically, defense response to the virus, type I interferon signaling pathway, interferon-gamma-mediated signaling pathway, and negative regulation of viral genome replication were also upregulated under Plasmax /5% O_2 regimen (Table 5.7). Genes related to cellular response to hypoxia were also shown to be affected by medium changes at 5% O_2 with 7 genes showing higher expression in DMEM and 5 genes showing higher expression in Plasmax (Tables 5.6 and 5.7). The p53 signaling pathway was also affected by medium as was seen by O_2 level.

For cells grown at 18% O_2, a total of 588 DEGs were identified in response medium change, of which 442 and 146 showed higher expression in Plasmax and DMEM, respectively (Figure5. 1; Tables 5.S7 and 5.S8). The 442 DEGs showed enrichment of just 2 Biological Processes, 2 Cellular Components, and 1 Molecular Function (Table5. 8), while the 146 DEGs showed enrichment of 13 Biological Processes, 6 Cellular Components, 2 Molecular Functions and 1 KEGG Pathway (Table 5.9). These enrichment terms in DMEM were associated with cell division and DNA replication as well as viral defense (Table 5.8). On the other hand, these enrichment terms in Plasmax were associated with lipoprotein metabolic process, ATP and protein bindings (Table 5.9).

A notable result of the above comparisons was that it was relatively uncommon for transcripts to be similarly affected by O_2 in both media, and to be similarly affected by media at both O_2 levels. The overall overlap was minimal (Table S9), with only 22 genes with higher expression at 18% O_2 in both media and 10 genes at 5% O_2. In DMEM, 11 genes had higher expression versus Plasmax regardless of O_2 level. However, in Plasmax versus DMEM, 73 genes had higher abundance levels across both O_2 levels.

Table 5.6 Significantly enriched functional annotation clusters observed from up-regulated genes in cells grown in DMEM vs Plasmax at 5% O_2. All terms shown are significantly enriched based on Benjamini corrected *p*-value ≤ 0.05, except where indicated otherwise; * denotes significance based on P-value (≤0.05) but not Benjamini corrected p-value.

Biological Process	Gene count
GO:0009615~response to virus	6*
GO:0000082~G1/S transition of mitotic cell cycle	19
GO:0006270~DNA replication initiation	12
GO:0006260~DNA replication	22
GO:0071353~cellular response to interleukin 4	7
GO:0042493~response to drug	13*
GO:0000083~regulation of transcription involved in G1/S transition of mitotic cell cycle	7
GO:0071456~cellular response to hypoxia	7*
GO:0043627~response to estrogen	7
GO:0006268~DNA unwinding involved in DNA replication	5
GO:0051290~protein heterotetramerization	4*
GO:0032508~DNA duplex unwinding	8
GO:0000722~telomere maintenance via recombination	7

GO:0071480~cellular response to gamma radiation	4*
GO:0031100~organ regeneration	4*
GO:0006139~nucleobase-containing compound metabolic process	6*
GO:0051301~cell division	22
GO:0061621~canonical glycolysis	6
GO:0000079~regulation of cyclin-dependent protein serine/threonine kinase activity	4*
Cellular Component	**Gene count**
GO:0005654~nucleoplasm	90
GO:0016020~membrane	74
GO:0005829~cytosol	92
GO:0005634~nucleus	99
GO:0005737~cytoplasm	104
GO:0042555~MCM complex	6
GO:0070062~extracellular exosome	71
GO:0000784~nuclear chromosome, telomeric region	10
GO:0005739~mitochondrion	9
GO:0043209~myelin sheath	13
GO:0005913~cell-cell adherens junction	13
GO:0000790~nuclear chromatin	8*
Molecular Function	**Gene count**
GO:0005515~protein binding	166
GO:0005524~ATP binding	56
GO:0003677~DNA binding	34*
GO:0003688~DNA replication origin binding	5
GO:0003682~chromatin binding	15*
GO:0098641~cadherin binding involved in cell-cell adhesion	13*
GO:0042802~identical protein binding	23*
GO:0042393~histone binding	6*
KEGG Pathway	**Gene count**
hsa04110: Cell cycle	17
hsa03030: DNA replication	11
hsa04115: p53 signaling pathway	5*
hsa01130: Biosynthesis of antibiotics	18
hsa01100: Metabolic pathways	41

Table 5.7 Significantly enriched functional ann1otation clusters observed from up-regulated genes in cells grown in Plasmax vs DMEM at 5% O_2. All terms shown are significantly enriched based on Benjamini corrected *p*-value ≤ 0.05, except where indicated otherwise; * denotes significance based on p-value (≤0.05) but not Benjamini corrected P-value.

Biological Process	**Gene count**
GO:0060337~type I interferon signaling pathway	18
GO:0009615~response to virus	15*
GO:0051607~defense response to virus	20
GO:0045071~negative regulation of viral genome replication	11
GO:0006334~nucleosome assembly	14
GO:0070059~intrinsic apoptotic signaling pathway in response to endoplasmic reticulum stress	8
GO:0042493~response to drug	12*
GO:0043065~positive regulation of apoptotic process	16
GO:0071456~cellular response to hypoxia	5*
GO:0051290~protein heterotetramerization	4*
GO:0098609~cell-cell adhesion	13*

GO:0051591~response to cAMP	6
GO:0031100~organ regeneration	4*
GO:0042542~response to hydrogen peroxide	5*
GO:0051726~regulation of cell cycle	7*
GO:0034340~response to type I interferon	4
Cellular Component	**Gene count**
GO:0005654~nucleoplasm	52
GO:0016020~membrane	38
GO:0005829~cytosol	54*
GO:0005634~nucleus	106
GO:0005737~cytoplasm	91
GO:0000786~nucleosome	13
GO:0005739~mitochondrion	24*
GO:0000788~nuclear nucleosome	8
GO:0042470~melanosome	7*
Molecular Function	**Gene count**
GO:0005515~protein binding	136
GO:0003725~double-stranded RNA binding	7
GO:0003677~DNA binding	39
GO:0046982~protein heterodimerization activity	22
GO:0000982~transcription factor activity, RNA polymerase II core promoter proximal region sequence-specific binding	6
GO:0042393~histone binding	6*
KEGG Pathway	**Gene count**
hsa04115: p53 signaling pathway	7
hsa05162: Measles	11
hsa05203: Viral carcinogenesis	13
hsa05161: Hepatitis B	9

Table 5.8 Significantly enriched functional ann1otation clusters observed from up-regulated genes in cells grown in DMEM vs Plasmax at 18% O_2. All terms shown are significantly enriched based on Benjamini corrected *p*-value ≤ 0.05, except where indicated otherwise; * denotes significance based on p-value (≤0.05) but not Benjamini corrected p-value.

Biological Process	**Gene count**
GO:0042157~lipoprotein metabolic process	6*
Cellular Component	**Gene count**
GO:0005737~cytoplasm	51*
GO:0005829~cytosol	36*
Molecular Function	**Gene count**
GO:0005515~protein binding	77*
GO:0005524~ATP binding	16*

Table 5.9 Significantly enriched functional ann1otation clusters observed from up-regulated genes in cells grown in Plasmax vs DMEM at 18% O_2. All terms shown are significantly enriched based on Benjamini corrected p-value ≤ 0.05, except where indicated otherwise; * denotes significance based on p-value (≤0.05) but not Benjamini corrected p-value.

Biological Process	**Gene count**
GO:0006260~DNA replication	27
GO:0060337~type I interferon signaling pathway	17
GO:0000082~G1/S transition of mitotic cell cycle	18
GO:0071222~cellular response to lipopolysaccharide	13
GO:0006270~DNA replication initiation	9
GO:0009615~response to virus	13
GO:0045071~negative regulation of viral genome replication	9
GO:0051301~cell division	24
GO:0000122~negative regulation of transcription from RNA polymerase II promoter	36*
GO:0060333~interferon-gamma-mediated signaling pathway	11
GO:0000731~DNA synthesis involved in DNA repair	8
GO:0000732~strand displacement	7
GO:0051607~defense response to virus	15
Cellular Component	**Gene count**
GO:0005654~nucleoplasm	111
GO:0005634~nucleus	175
GO:0005737~cytoplasm	156
GO:0042555~MCM complex	6
GO:0005615~extracellular space	54
GO:0005829~cytosol	96*
Molecular Function	**Gene count**
GO:0005515~protein binding	255
GO:0005524~ATP binding	59
KEGG Pathway	**Gene count**
hsa03030: DNA replication	10

The effects of culture conditions on proteomics of MCF7 cells

Using iTRAQ 8-plex reagents and LC-MS/MS analysis, 2332 unique proteins were identified for meeting our validation threshold (see Materials and Methods; Figure 5.2) from which a total of 474 proteins (~21%) were found to be differentially expressed proteins (DEPs)across our experimental comparisons. Notably, medium change at 18%O_2 is associated with more substantial response such that 225 proteins (~48% of total differentially abundant ones) demonstrated significantly different levels (Table 5.S16, Table 5.S17). DEPs were subject to enrichment analysis to identify the key functions and pathways under specific culture.

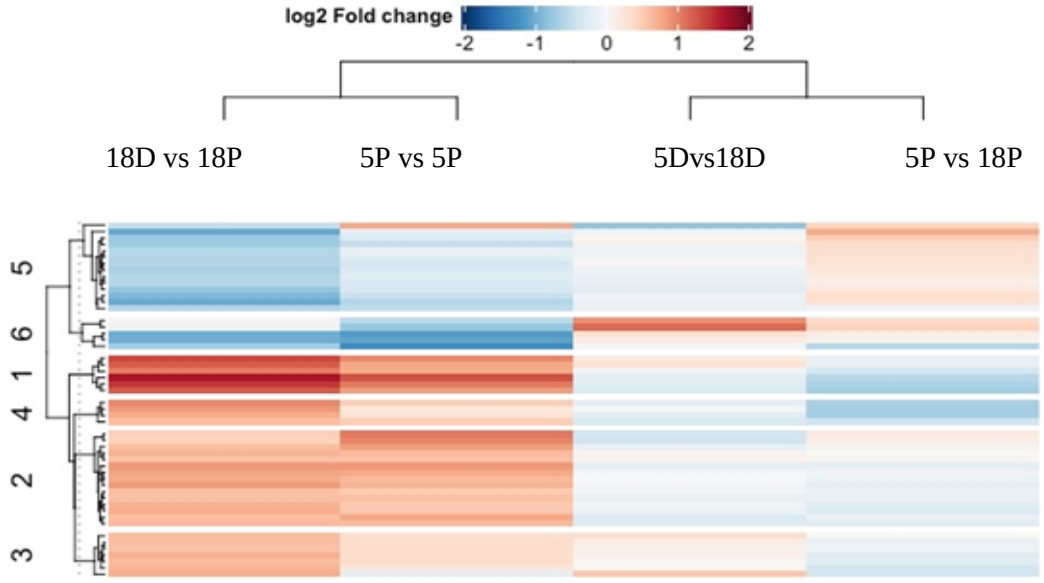

Figure 5.3 Heatmap of pairwise comparisons of different culture conditions. 5P, 5% O_2 in Plasmax; 5D, 5% O_2 in DMEM; 18P, 18% O_2 in Plasmax; 18D, 18% O_2 in DMEM.

Effects O_2 level on the MCF7 cell proteome

When grown in DMEM, 31 proteins were significantly more abundant at 5% versus 18% O_2 (Table 5.S10). From the list, isoform 2 of tumor susceptibility protein101 (a tumor suppressor gene) has the highest fold change ratio (FC=2), this protein is mainly involved in

adhesion signals and Bcl2 expression. Peptidyl-tRNA hydrolase 2 (PTRH2) and CCAAT/enhancer-binding protein zeta (a transcription factor involved in cell growth and differentiation) also showed high fold change ratio (Table S10). PTRH2 is a potential oncogene that promotes malignancy and metastasis (Corpuz et al., 2020**).** Functional analysis revealed enrichment of 4 Biological Processes, 3 Cellular Components, 3 Molecular Functions, and 3 KEGG Pathways (Table 5.10). However, only 16 proteins were significantly more abundant at 18% O_2 (Table 5.S11) which did not result in any GO or KEGG Pathway enrichments. Pathways enriched in 5% O_2 were related primarily to energy metabolism including glycolysis, amino acid metabolism, and central carbon metabolism.

When MCF7 cells were grown in Plasmax, the effects of O_2 level on protein expression were quite different While the number of ptoteins with higher abundance were almost doubled at 5% versus 18%O_2 in DMEM, in Plasmax cells appeared to be affected more similarly such that 34 proteins were significantly more abundant at 5% and 30 were more abundant at 18% O_2 (Tables 5.S12 and 5.S13). Importin subunit alpha-1(superfamily comprises nuclear transport proteins, involved in the shuttling of certain cargo proteins into and out of the nucleus) (Van Der Watt et al., 2011), and BolA-like protein 1 (a mitochondrial protein that prevents mitochondrial fragmentation induced by GSH depletion and reduces the associated oxidative shift of the mitochondrial thiol redox potential) (Willems et al., 2013) showed the highest fold change ratio (Table 5.S12).

As seen with DMEM no GO or KEGG terms were significantly enriched at 18% versus 5% O_2. In contrast, 2 Biological Processes, 2 Molecular Functions, and 4 KEGG Pathways were enriched at 5% O_2 (Table 5.11). Again, energy metabolism, including glycolysis and amino acid metabolism, were enriched. Indeed, the data indicate that the effect of O_2 level on the MCF7 proteome is largely focused on energy metabolism. However, several key proteins associated with cancer progression and aggressiveness were affected by O_2 level. In DMEM, Isoform 2 of Tumor susceptibility gene 101 (a tumor suppressor gene) and peptidyl-tRNA hydrolase 2 (PTRH2) were significantly higher at 5% versus 18% O_2. The former protein is involved in adhesion signaling and Bcl2 expression, while PTRH2 is a potential oncogene that promotes malignancy and metastasis (Table 5.S10) (Corpuz et al., 2020). FAM3C was shown to be more abundant at 18% O_2. This protein is associated with

epithelial-to-mesenchymal, which is critical for tumor invasion, metastasis, and recurrence (Table 5.S11) (Waerner et al., 2006).

Table 5. 10 Significantly enriched functional annotation clusters observed from up-regulated proteins in DMEM at 5%O_2 vs 18%O_2. All terms shown are significantly enriched based on Benjamini-corrected p-value ≤ 0.05, except where indicated otherwise; * denotes significance based on p-value (≤0.05) but not Benjamini-corrected p-value

Biological Process	**Gene count**
GO:0061621~canonical glycolysis	8
GO:0006096~glycolytic process	6
GO:0006094~gluconeogenesis	9
GO:0098609~cell-cell adhesion	4*
Cellular Component	**Gene count**
GO:0016020~membrane	11
GO:0005913~cell-cell adherens junction	10
GO:0070062~extracellular exosome	10
Molecular Function	**Gene count**
GO:0000287~magnesium ion binding	3*
GO:0044822~poly(A) RNA binding	5
GO:0098641~cadherin binding involved in cell-cell adhesion	4
KEGG Pathway	**Gene count**
hsa00010: Glycolysis	8
hsa05230: Central carbon metabolism in cancer	4
hsa01230: Biosynthesis of amino acids	8

Table 5.11 Significantly enriched functional annotation clusters observed from up-regulated proteins at 5% O_2 vs 18% O_2 in MCF7 cells growing in Plasmax. All terms shown are significantly enriched based on Benjamini-corrected p-value ≤ 0.05, except where indicated otherwise; * denotes significance based on p-value (≤0.05) but not Benjamini-corrected p-value

Biological Process	**Gene count**
GO:0061621~canonical glycolysis	3
GO:0006096~glycolytic process	3
GO:0006094~gluconeogenesis	3
Molecular Function	**Gene count**
GO:0044822~poly(A) RNA binding	7
KEGG Pathway	**Gene count**
hsa00010: Glycolysis / Gluconeogenesis	3
hsa01230: Biosynthesis of amino acids	3
hsa01200: Carbon metabolism	3
hsa01130: Biosynthesis of antibiotics	4

Effects of culture medium on the MCF7 cell proteome

In MCF7 cells grown at 5% O_2, 58 DEPs showed higher expression in DMEM versus Plasmax (Table 5.S14). Among which, heat shock factor-binding protein 1, isoform 2 of Zinc finger MYM-type protein 3, ornithine aminotransferase mitochondrial, and Acyl-CoA desaturase had the fold change ratio greater than 2. In addition, Functional analysis showed 12 Biological Processes, 4 Cellular Components, 6 Molecular Functions, and 8 KEGG Pathways were significantly enriched in DMEM (Table 5.12). These included metabolic pathways such as glycolysis, the pentose phosphate pathway, amino acid metabolism and fructose/mannose metabolism (Table 5.12). At 5% O_2, 80 DEPs showed higher expression in Plasmax versus DMEM from which E3 ubiquitin-protein ligase TRIM21, Dehydrogenase/reductase SDR family member 2 mitochondrial, and E3 ubiquitin-protein ligase DTX3L showed the fold change ratio greater than 2(Table S15).

These proteins are associated with 8 Biological Processes, 2 Cellular Components, 4 Molecular Functions and 6 KEG Pathways (Table 5.13). As has been observed in the transcriptional analysis, most of these pathways are related to viral defense, such as type I interferon signaling.

At 18% O_2, 94 DEPs had higher abundance in MCF7 cells grown in DMEM (Table 5.S16), showing enrichment of 21 Biological Processes, 9 Cellular Components, 11 Molecular Functions, and 5 KEGG Pathways (Table 5.14). Translational initiation**,** DNA replication initiation, and G1/S transition of mitotic cell cycle were among the most highly enriched GO terms (Table 5.14). MCF7 cells grown at 18%O_2 in Plasmax had 131 DEPs with higher abundance than in DMEM (Table 5.S17), showing enrichment for 8 Biological Processes, 4 Cellular Components, 5 Molecular Functions and 5 KEGG Pathways (Table 5.15). Interestingly, the strong enrichment of viral defense pathways observed in Plasmax at 5% O_2 was not as evident at 18% O_2. Instead, metabolic pathways such as valine, leucine and isoleucine degradation, the TCA cycle, and fatty acid beta-oxidation were among the enriched pathways **(**Table 5.15). These data indicate that medium as a variable substantially affects the proteome of MCF7 cells, but it is interesting that the medium effects differ rather markedly with O_2 level.

Translational initiation**,** DNA replication initiation, and G1/S transition of mitotic cell cycle were some examples of enriched Biological Processes (Table 5.14). MCF7 cells grown at 18%O_2 in Plasmax versus DMEM had 131 proteins with significantly higher abundance (Table 5.S17). These proteins are associated with 8 biological processes, 4 cellular components, 5 molecular functions and 5 KEGG pathways (Table 5.15). Interestingly, the strong enrichment of viral defense pathways observed in Plasmax at 5% O_2 was not as evident at 18% O_2. Instead, metabolic pathways such as valine, leucine and isoleucine degradation, the TCA cycle, and fatty acid beta-oxidation were among the enriched pathways **(**Table 5.15). These data indicate that medium as a variable substantially affects the proteome of MCF7 cells, but it is interesting that the medium effects differ rather markedly with O_2 level.

Table 5.12 Significantly enriched functional annotation clusters observed from up-regulated proteins in DMEM vs Plasmax at 5%O_2. All terms shown are significantly enriched based on Benjamini-corrected p-value ≤ 0.05, except where indicated otherwise; * denotes significance based on p-value (≤0.05) but not Benjamini-corrected p-value

Biological Process	**Gene count**
GO:0006614~SRP-dependent co-translational protein targeting to membrane	8
GO:0019083~viral transcription	8
GO:0000184~nuclear-transcribed mRNA catabolic process, nonsense-mediated decay	8
GO:0006413~translational initiation	8
GO:0006364~rRNA processing	8
GO:0050821~protein stabilization	4
GO:0006457~protein folding	4*
GO:0098609~cell-cell adhesion	5
GO:0006094~gluconeogenesis	5
GO:0050821~protein stabilization	5
GO:0061621~canonical glycolysis	6
GO:0006412~translation	8
Cellular Component	**Gene count**
GO:0005925~focal adhesion	4*
GO:0005840~ribosome	8
GO:0022625~cytosolic large ribosomal subunit	7
GO:0005913~cell-cell adherens junction	5
Molecular Function	**Gene count**
GO:0003723~RNA binding	7*
GO:0005524~ATP binding	8
GO:0098641~cadherin binding involved in cell-cell adhesion	5
GO:0051082~unfolded protein binding	4
GO:0044822~poly(A) RNA binding	14
GO:0003735~structural constituent of ribosome	8
KEGG Pathway	**Gene count**
hsa03010: Ribosome	8

hsa00010: Glycolysis	8
hsa01200: Carbon metabolism	8
hsa01230: Biosynthesis of amino acids	6
hsa00051: Fructose and mannose metabolism	4
hsa01100: Metabolic pathways	12
hsa01130: Biosynthesis of antibiotics	10
hsa00030: Pentose phosphate pathway	3
hsa05230: Central carbon metabolism in cancer	3*

Table 5.13 Significantly enriched functional annotation clusters observed from up-regulated proteins in Plasmax vs DMEM at 5% O_2. All terms shown are significantly enriched based on Benjamini-corrected p-value ≤ 0.05, except where indicated otherwise; * denotes significance based on p-value (≤0.05) but not Benjamini-corrected p-value

Biological Process	**Gene count**
GO:0060337~type I interferon signaling pathway	7
GO:0051607~defense response to virus	8
GO:0060333~interferon-gamma-mediated signaling pathway	5
GO:0045071~negative regulation of viral genome replication	4
GO:0009615~response to virus	5
GO:0032480~negative regulation of type I interferon production	4
GO:0019985~translesion synthesis	4
GO:0098609~cell-cell adhesion	5
Cellular Component	**Gene count**
GO:0005913~cell-cell adheren junction	4*
GO:0030529~intracellular ribonucleoprotein complex	4
Molecular Function	**Gene count**
GO:0005524~ATP binding	3*
GO:0003723~RNA binding	8
GO:0098641~cadherin binding involved in cell-cell adhesion	3*
GO:0030170~pyridoxal phosphate binding	4
KEGG Pathway	**Gene count**
hsa05168: Herpes simplex infection	5*
hsa05160: Hepatitis C	4*
hsa05162: Measles	4*
hsa01230: Biosynthesis of amino acids	4*
hsa01130: Biosynthesis of antibiotics	3*
hsa00970: Aminoacyl-tRNA biosynthesis	3*

Table 5.14 Significantly enriched functional annotation clusters observed from up-regulated proteins in DMEM vs Plasmax at 18%O_2. All terms shown are significantly enriched based on Benjamini-corrected p-value ≤ 0.05, except where indicated otherwise; * denotes significance based on p-value (≤0.05) but not Benjamini-corrected p-value

Biological Process	**Gene count**
GO:0006413~translational initiation	16
GO:0006614~SRP-dependent cotranslational protein targeting to membrane	12
GO:0019083~viral transcription	12
GO:0000184~nuclear-transcribed mRNA catabolic process, nonsense-mediated decay	12
GO:0006412~translation	14
GO:0002181~cytoplasmic translation	7
GO:0098609~cell-cell adhesion	13
GO:0006364~rRNA processing	12
GO:0006268~DNA unwinding involved in DNA replication	4
GO:0006270~DNA replication initiation	5
GO:0006260~DNA replication	7
GO:0000082~G1/S transition of mitotic cell cycle	6
GO:0006446~regulation of translational initiation	4
GO:0006986~response to unfolded protein	4
GO:0006457~protein folding	6
GO:0007076~mitotic chromosome condensation	3
GO:0050821~protein stabilization	5*
GO:0001731~formation of translation preinitiation complex	3*
GO:1901998~toxin transport	3
GO:0006950~response to stress	3
GO:1900034~regulation of cellular response to heat	3*
Cellular Component	**Gene count**
GO:0042555~MCM complex	4
GO:0005913~cell-cell adherens junction	13
GO:0000784~nuclear chromosome, telomeric region	5
GO:0005925~focal adhesion	8
GO:0005840~ribosome	13
GO:0022625~cytosolic large ribosomal subunit	13
GO:0043209~myelin sheath	6
GO:0000796~condensin complex	3
GO:0042470~melanosome	6
Molecular Function	**Gene count**
GO:0003678~DNA helicase activity	4*
GO:0005524~ATP binding	19
GO:0098641~cadherin binding involved in cell-cell adhesion	13
GO:0004003~ATP-dependent DNA helicase activity	3*
GO:0001948~glycoprotein binding	4
GO:0005525~GTP binding	8
GO:0023026~MHC class II protein complex binding	3
GO:0051082~unfolded protein binding	6
GO:0003735~structural constituent of ribosome	13
GO:0003743~translation initiation factor activity	4
GO:0003723~RNA binding	11
KEGG Pathway	**Gene count**
hsa04612: Antigen processing and presentation	3
hsa04141: Protein processing in endoplasmic reticulum	6
hsa03013: RNA transport	5

hsa03010: Ribosome	13
hsa04110: Cell cycle	5*
hsa03030: DNA replication	5*

Table 5.15 Significantly enriched functional annotation clusters observed from up-regulated proteins in Plasmax vs DMEM at 18%O_2. All terms shown are significantly enriched based on Benjamini-corrected p-value ≤ 0.05, except where indicated otherwise; * denotes significance based on p-value (≤0.05) but not Benjamini-corrected p-value

Biological Process	**Gene count**
GO:0008152~metabolic process	5
GO:0006635~fatty acid beta-oxidation	3
GO:0006821~chloride transport	3*
GO:0006099~tricarboxylic acid cycle	3*
GO:0006749~glutathione metabolic process	3*
GO:0060337~type I interferon signaling pathway	6
GO:0051607~defense response to virus	8
GO:0045071~negative regulation of viral genome replication	3*
Cellular Component	**Gene count**
GO:0034707~chloride channel complex	3*
GO:0005913~cell-cell adherens junction	6*
GO:0005739~mitochondrion	26
GO:0005759~mitochondrial matrix	13
Molecular Function	**Gene count**
GO:0005244~voltage-gated ion channel activity	3*
GO:0004364~glutathione transferase activity	3
GO:0005254~chloride channel activity	3
GO:0098641~cadherin binding involved in cell-cell adhesion	6*
GO:0030170~pyridoxal phosphate binding	5
KEGG Pathway	**Gene count**
hsa00280: Valine, leucine and isoleucine degradation	4*
hsa00071: Fatty acid degradation	3*
hsa00020: Citrate cycle (TCA cycle)	3
hsa01200: Carbon metabolism	5*
hsa00630: Glyoxylate and dicarboxylate metabolism	3*

DISCUSSION

In this study, we showed that gene expression at both the transcript and protein level was significantly affected by culture conditions, which included the O_2 level and culture medium composition. In MCF7 cells growing in DMEM, lower O_2 levels were associated with a marked enrichment of genes involved in cell replication processes (Table 2). This is consistent with many previous observations that lower O_2 levels (i.e. physioxia) promote replication, reduce DNA damage, and delay replicative senescence in primary cell lines (e.g. Saito et al., 1995; Parinello et al., 2003). However, this pattern was seen only in DMEM at the transcription level and not evident in the proteome levels, so it does not appear to be a robust response to O_2 in these cells that might occur *in vivo*. Consistently, our MTT (3-[4,5-dimethylthiazol-2-yl]-2,5 diphenyl tetrazolium bromide)-based cell growth data (not shown) indicated that MCF7 cells in DMEM grow faster at 5% vs 18% O_2 while, when growing in Plasmax, the opposite occurs, and growth is faster at 18% O_2. These observations, taken together, indicate that O_2 is interacting with media nutrient compositions to produce specific outcomes such as affecting various biological pathways (eg., glycolysis and cell replication, amino acid metabolism).

At both the transcript and protein levels, O_2 level and culture medium affected key pathways of energy metabolism in MCF7 cells. These included central carbon metabolism, glycolysis, the pentose phosphate pathway, fatty acid beta-oxidation, the TCA cycle, and amino acid biosynthesis. These wide-ranging effects illustrate a pervasive influence of the cell culture environment on energy metabolism. This supports and extends the observations of Vande Voorde et al. (2019), who noted the 'metabolic re-wiring' of BT549, CAL-120, and MDA-MB-468 cell lines grown in Plasmax. Specifically, they showed that exposing cells in more physiological culture medium significantly influences the colony-forming capacity by ferroptosis inhibition. Moreover, the transcriptional and metabolic profiles of those cells cultured in more physiological culture medium were rewired in a manner that is substantially independent of the cell proliferation rate. The ability of the culture environment to drive a different basal metabolic phenotype such as maximal and basal O_2 consumption rate (Moradi et al., 2021) will affect experiments aimed at identifying metabolic inhibitors capable of affecting tumour growth *in vivo* (e.g., Cantor et al., 2017; Vande Voorde et al., 2019).

At both the transcript and protein levels, glycolysis and glycolytic processes were affected by O_2 level and media composition. The expression of glycolytic genes can be enhanced by the elevated pyruvate concentrations found in DMEM formulations like that used here (Vande Voorde et al., 2019). Hypoxia-inducible factor-1 also drives the transcription of glycolytic genes. We are confident that MCF7 cells in our experiments did not experience hypoxia. We used continuous pericellular O_2 monitoring with the Presens Oxydish system in parallel metabolomic assays and found no evidence that hypoxia develops over the course of the experiment (unpublished data). Physioxia for most mammalian cells is between 2% and 8% O_2 (Keeley and Mann., 2019). In our experiments, the incubator gas phase O_2 level was maintained at 5% and pericellular O_2 measured in the medium remained above 4% throughout our experiments. Nonetheless, increased expression of glycolytic enzymes is expected given that stabilization of hypoxia-inducible factor-1α is evident in various cell lines at O_2 levels within the physioxic range (eg. near 5%; reviewed in Stuart et al., 2019).

One striking result here, which was observed at transcript and protein levels, was the enrichment of viral defense pathways in cells grown in Plasmax. This effect was more prominent at 5% O_2 (Tables 7 and 12) than at 18% O_2 (Tables 9 and 14). It is worth noting that the RNAseq and iTRAQ experiments took place several months apart and used different batches of Plasmax. Thus, while it is possible that there may indeed have been a viral contaminant in Plasmax (it was sterile-filtered using a 0.22 µm pore size that would not have excluded viruses), this would have had to happen on at least two separate occasions. Common viruses like Epstein-Barr and cytomegalovirus are thought to be present but latent in the majority of the human population (reviewed in Cannon et al., 2010; Al Hamed et al., 2020; Farrell and Stevens Stevenson, 2019), thus it is likely that growing cells in Plasmax might re-activate latent viruses in the present study. Consistently, replication of various RNA viruses, such as hepatitis C virus (HCV) influenza A virus (IAV), severe acute respiratory syndrome-related coronavirus 2 (SARS-CoV-2) and several other viruses in multiple cancerous and noncancerous cell lines were at lower levels and with delayed kinetics when grown in Plasmax than DMEM (Golikov et al., 2022). These observations strongly indicate that *in vivo* like medium condition promotes immune system activation more robustly compared to non-physiologic medium. In any case, this outcome of our study warrants future investigation.

At the transcriptional level, expression of components of the p53 signaling pathway were both O_2 and media sensitive. P53 signaling plays key roles in cell growth, cell cycle arrest, and cancer (reviewed in Chen, 2016), so its differential expression in response to changes in culture conditions is potentially important. However, it is interesting that no effect of either O_2 or medium composition on p53 signaling pathways emerged at the protein level. The reason for this discrepancy is unclear. In addition to p53 signaling, a number of other differentially expressed genes and/or proteins including dehydrogenase/reductase member 2 (DHRS2), isoform 2 of tumor susceptibility protein101 and peptidyl-tRNA hydrolase 2 (PTRH2) PTRH2 were identified here that are studied for their roles in cancer. This is a significant finding, since characterizing specific proteins in cell culture will fail to resemble to *in vivo* if those proteins play important roles only under non-physiological culture conditions.

For each experimental condition, we compared DEPs with DEGs to determine the extent of overlap. Overall, correlations between transcriptome enrichment and proteome enrichment for any given comparison were very low (see supplemental tables 5.S10-S17 where proteins for which enriched transcript was also detected are indicated by '*'). For example, in MCF7 cells grown in DMEM, at 5% O_2 several hundred transcripts were enriched relative to 18% O_2. Of these, only five were identified at the protein level (alpha-enolase, phosphoglycerate mutase 1, ATP-dependent 6-phosphofructokinase, pyruvate kinase, and high mobility group protein B2). Perhaps this is related in part to the distinct regulatory mechanisms of gene transcription and mRNA translation by O_2 (Ho et al., 2021). Correlations between transcript and protein abundances were also low in comparisons between media. In many comparisons where hundreds of transcripts are enriched, the overlap is less than 10% (see Tables S10-S17). Indeed, low correlations between mRNA and protein abundance appear to be common in many studies (eg., Bathke et al., 2019; Edfors et al., 2016; Foster et al., 2016). This discordance can be related in part to the post-transcriptional and post-translational regulatory phenomena, including alternative splicing, non-coding RNAs, RNA-binding proteins (RBPs), protein modification and degradation that influence nature of the proteome (eg., Prabakaran et al., 2012; Vogel and Marcotte., 2012).

In conclusion, we have shown how O_2 level and media composition exert significant influence over expression of genes at both transcription and translation levels in cultured MCF7 cells. In addition to metabolic pathways, the culture environment had effects on processes related to

cell growth and viral defense. These results should focus attention on the importance of culture conditions in experimental design. Experimental outcomes will certainly be influenced by the basal state of gene expression in these cells. We have performed similar transcriptomic analyses (unpublished) of culture conditions on PC3 human prostate cancer cells and observed similar wide-ranging effects. Together, this suggests that the results presented here will apply to many if not all cell in culture.

CHAPTER 6: Conclusions and perspectives

GENERAL DISCUSSION AND CONCLUSIONS

E_2, and the phytoestrogen RES, modulate many aspects of mitochondrial function, including biogenesis, fusion/ fission balance, oxidative phosphorylation and ROS production (eg., Anderson and Neufer, 2006; Robb and Stuart, 2014; Capllonch-Amer et al., 2014; Liu et al., 2017; Torres et al., 2018; Cipolletti et al., 2018; Galmes-Pascual et al., 2020). In Chapter 2, I showed that RES modulates mitochondrial dynamics via an Mfn2-dependent mechanism. Mitochondria are an important downstream target of RES in many cell types while the mechanisms underlying the effect are not always well characterized. The results presented in Chapter 2 showed that RES stimulated mitochondrial network morphology under basal, non-stressed conditions consistently in all three investigated cells (C2C12, PC3, and MEFs). In addition, the mitochondrial fusion and oxidative phosphorylation promoting effects elicited by RES were absent when Mfn2 was not expressed. Mfn2 is shown to have lower expression level in type 2 diabetes, which is associated with depressed oxidative phosphorylation and impaired mitochondrial fusion in skeletal muscle (Cassidy-Stone et al., 2008; Kelley et al., 2002). Consistent with that, liver and skeletal muscle deletion of Mfn2 in mice caused fragmented mitochondrial networks and numerous metabolic pathologies including glucose intolerance and elevated hepatic gluconeogenesis (Bach et al., 2005; Kulkarni et al., 2016). These results indicate the important regulatory role of Mfn2 in insulin signaling and glucose homeostasis associated with obesity and type 2 diabetes. Thus, the pro-mitochondrial fusion and concomitant promoting oxidative phosphorylation effects of RES may contribute to its ability to ameliorate the effects of various diseases associated with metabolic stress.

In parallel with this work, I collaborated with fellow PhD student Joao Fonseca, who demonstrated that RES's effects on cellular metabolism and mitochondrial dynamics were dependent upon glucose and O_2 concentrations in the culture condition (Fonseca et al., 2018). Our understanding of how E_2 affects mitochondrial form and function is mainly derived from experiments on cells cultured in traditional media. I hypothesized that, as we observed for RES in Fonseca et al. (2018), the effects of E_2 on mitochondria might be influenced by the cell culture environment. This hypothesis was tested and confirmed in Chapter 3, where I demonstrated that many of the effects of E_2 on mitochondria are different in standard versus physiologic media, and in standard O_2 levels versus physioxia. Consistent with previous reports, E_2 elicited significant effects on multiple aspects of mitochondrial function including mitochondrial morphology, metabolism,

and ROS production. However, such effects were in many cases either absent or opposite depending on the type of medium and O_2 levels in which cells were grown. Importantly, in the most physiologically relevant condition (Plasmax/5% O_2), E_2 increased basal, maximal OCR, and spare respiratory capacity of C2C12 cells, while the opposite effect on basal and maximal OCR was detected when cells were grown using a standard cell culture approach (DMEM/18% O_2). Furthermore, while the effect of E_2 under standard cell culture condition on mitochondrial footprint was stimulatory, cells had lower OCRs. I speculate that it might be partially related to the respiratory chain supercomplexes in the inner membrane of mitochondria which are known as 'respirasome' structures. Supercomplex assembly has been shown to enhance respiratory chain activity leading to elevated mitochondrial metabolism (Ikeda et al., 2013). Likewise, E_2 decreased H_2O_2 production in cells grown in standard cell culture condition while the opposite effect was observed in physiologic cell culture. The underlying reason for this observation is not clear; however, it can be due to low steady state production of ROS under physiologic condition such that E_2 did not play any modulatory functions. It is difficult to overstate the importance of this overall result: C2C12 cells are sufficiently sensitive to the cell culture environment that it profoundly affects experimental outcomes in a study of hormone effects.

The impacts of cell culture condition on the responsiveness of cells to hormones noted in Chapter 3 may extend to other aspects of cell physiology. To develop a better understanding of the pervasiveness of the culture media-cellular metabolism interaction, I studied how cellular metabolism and mitochondrial network morphology of cancer cells would be affected by cell culture condition in Chapter 4. Energy metabolism has become a focus for pharmacologically targeting cancer cell growth, so a clear understanding of how the culture environment affects this is important.

I had already shown that the anti-proliferative of effects of RES and Rapamycin on cancer cells can be altered in a cell culture condition manner (data included in my co-authored review by Abbas et al., 2021). In Chapter 4, I hypothesized that cancer cell metabolism and mitochondrial functions would be sensitive to culture conditions. Indeed, my data confirm this. More physiologic culture conditions increased mitochondria-dependent metabolism in several cancer cell lines. In all four cell lines investigated, glycolysis was significantly higher when cells were grown in standard

(DMEM) compared to physiologic cell culture (Plasmax). Consistent with this, three of the four cancer cell lines (MCF7, Huh7, LNCaP) had elevated basal and maximal OCR in physiologic conditions. All cell types exhibited elevated glycolysis rate in DMEM versus Plasmax which clearly indicated a shift in energy metabolism from oxidative phosphorylation toward glucose fermentation to lactate in cells growing in DMEM. This observation is particularly significant in the context of potential therapeutic molecules aimed at inhibiting glycolysis (e.g., LDH inhibitors). In general, it is critical to adopt a more *in vivo*-like cell culture medium to minimize artefactual behaviour of the cancer cells. My data broadly highlight the idea that commonly used culture conditions used may not be ideal for metabolic studies, mitochondrial function and response to drugs, and I also specifically identified a cell line dependency trend in all my experiments.

My findings from cancer cell lines in Chapter 4 robustly confirm that cell culture conditions impact many aspects of cancer cell biology, however; there are little data on the combined effects of O_2 and media composition at the transcriptomic and proteomic level on cancer cells. Given that metabolism of MCF7 cells was significantly affected by cell culture conditions, and the time and resource constraints of limiting an omics analysis to a single cell line, the MCF7 cell line was selected for the transcriptomic and proteomic investigation in Chapter 5. I identified a number of genes and proteins that are differentially expressed in response to O_2 level and media type. Notably, in traditional medium change of O_2 resulted in remarkable effects on expression of hundreds of genes. Interestingly, physioxia (versus standard 18% O_2) was associated with a broad enrichment of genes involved in cell replication and cell cycle progression in MCF7 cells growing in DMEM (though the opposite trend in Plasmax). It is possible that the utility of these pathways as a target for drug development will be limited by their sensitivity to culture conditions that may not closely resemble *in vivo*. The overall protein expression profile of MCF7 cells was also significantly affected by culture conditions. Interestingly, glycolysis and amino acid metabolism were enriched in physioxia regardless of media type, indicating the sensitivity of energy metabolism to ambient O_2 levels. Growth in traditional medium was associated with enrichment of multiple key metabolic pathways including TCA cycle, Fructose and mannose, pentose phosphate. Interestingly, most of the pathways having higher expression profile in plasma-like medium were related to viral defense such as type I interferon signaling.

LIMITATIONS & FUTURE CONSIDERATIONS

Physiologic media development can also extend beyond recapitulating conditions in human plasma. The plasma concentrations of glucose and several amino acids in mice are similar to those in humans, but the relative levels of several other metabolites (eg., uric acid) can be quite different (Adelman et al., 1988; Chandrasekera and Pippin, 2014; Demetrius, 2005; Elsea and Lucas, 2002; Martignoni et al., 2006). Thus, formulating a physiologic medium based on the mouse plasma metabolome is important for use with cultured murine cells. Similarly, metabolic characterization of interstitial fluid from different murine tumors showed that such composition can differ from that of matched plasma (Sullivan et al., 2019). Thus, while Plasmax is a 'physiologic medium', it is representative of blood plasma of a healthy human. It may not be representative of the environment in which cancer cells grow within a solid tumour. Such cells can be exposed to up to 10-fold lower glucose concentrations than normal tissue due to the high rate of glucose consumption by cancer cells and/or poor tumour vasculature (Hirayama et al., 2009; Kulkarni et al., 2016). Thus, refining plasma-like media to be more representative of tumour interstitial fluid will be important to further improving the fidelity of cancer cell culture. In addition, it will be interesting to test how more physiologic relevant media such as Plasmax and HPLM can be used to improve survival and growth rate of primary cells that have not been otherwise exposed to non-physiologic conventional media such as DMEM.

While acknowledging the tremendous pioneering efforts of Eagle and others to provide decades of productive cell culture and, in turn, advances in biological research and drug development, the next generation of scientists should embrace the arrival and rise of physiologic media. Without any doubt, endorsing more physiologic media and going forward to expand and manipulate the repertoire of physiologic media, will greatly improve the modeling capacity of cell culture and may support insights that would be difficult or even impossible to identify using existing cell culture methods. Further to medium composition, it is clear from our study that O_2 must be included in the list of medium constituents to maintain within a physiologically relevant range of O_2 levels had broad effects that were different between cell lines and influenced by medium. This indicates interactions between cell lines, media composition, and O_2 levels that result in unpredictable effects on cell biology. Since this has the potential to compromise a wide

range of observations made in cell cultures, it is important to move toward the use of physiologic media in physioxia.

APPENDIX

SUPPLEMENTARY TO CHAPTER 3

(A)

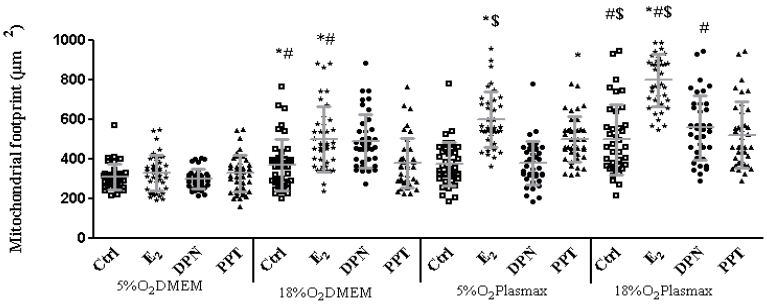

(B)

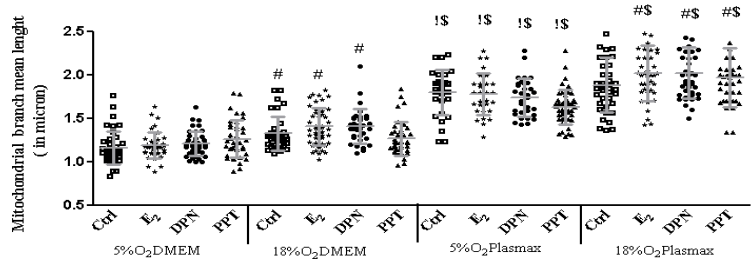

(C)

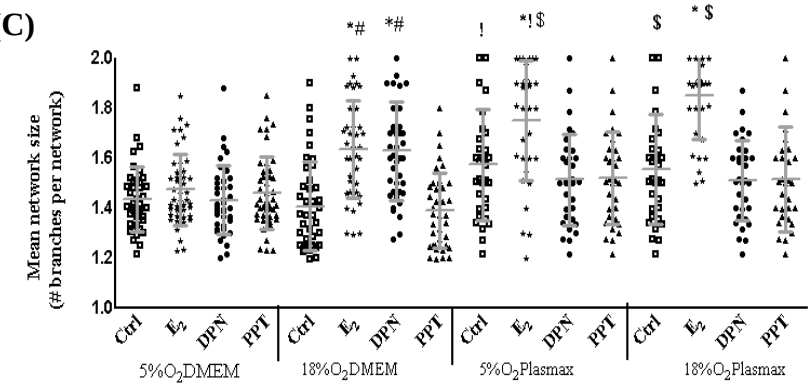

(D)

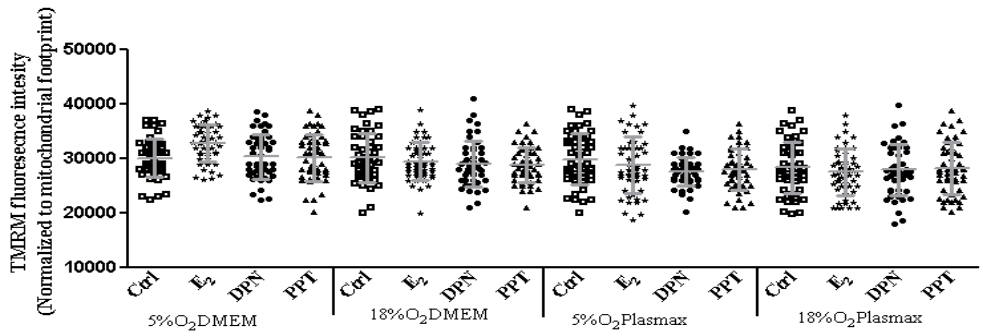

Figure 3.1S. E_2 and SERMs modulate mitochondrial morphology in a media-type and O_2-dependent manner. (A) mitochondrial footprint (area in μm^2); (B) mean network size (number of branches per network); (C) branch mean length (counts in micron). Features in A-C were measured in mEF-C2C12 cells at either 5% O_2 or 18% O_2 in either DMEM or Plasmax. Data shown for mitochondria morphology are means ± SEM from measurements performed on 40-45 cells from 3 independent experiments. mEFP-C2C12 cells were treated for 48 hr with one of the following molecules: 10 nM E_2, 10 nM DPN, 10 nM PPT or an equal volume of vehicle control (DMSO). (D) TMRM fluorescent intensity was detected and measured as a proxy for $\Delta\psi m$. Data shown are means ± SEM from 50 cells from 3 independent experiments. '*'represents differences in a given parameter between treated cells and their corresponding vehicle control. '#' represents differences between 18% O_2 and 5% O_2 in the same media. '$' represents differences between Plasmax and DMEM at the same O_2 level. '!' represents differences between 5% O_2 / Plasmax versus 18% O_2 /DMEM. Statistical significance was determined by two- wayANOVA followed by Tukey's post-hoc analysis.

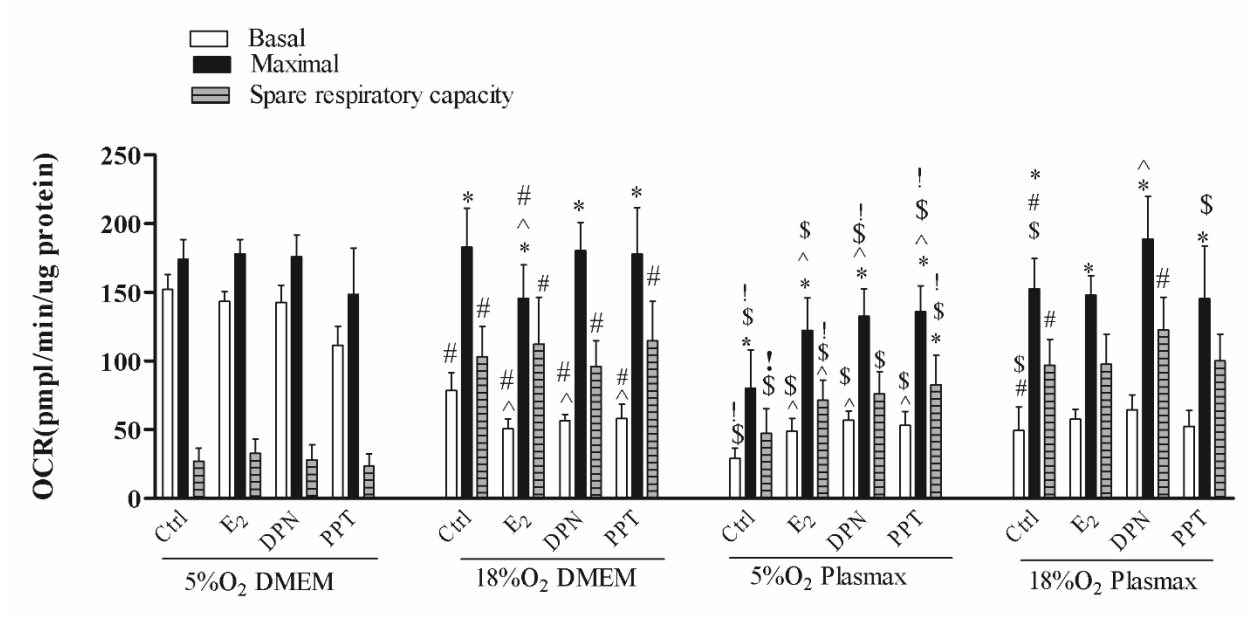

Figure 3.2S. **Effects of E_2 and SERMs on cellular respiration depends on O_2 concentration and media type.** C2C12 cells were cultured at either 5% O_2 or 18% O_2 in either DMEM or Plasmax. In all experiments, cells were treated for 48 hr with one of the following molecules: 10 nM E_2, 10 nM DPN, 10 nM PPT or an equal volume of vehicle control (DMSO). Cells were seeded at a XF96-well microplate 14hr prior to OCR measurements. Basal, maximal and spare reserve capacity OCRs are shown for control and treated cells. Data shown are means ± SEM from 3 independent experiments. '*' represents differences between maximal and basal OCR for each condition. '^'represents differences in a given parameter between treated cells and their corresponding vehicle control. '#' represents differences between 18%O_2 and 5%O_2 in the same media. '$' represents differences between Plasmax and DMEM when O_2 level is the same. '!' represents differences between 5%O_2 Plasmax versus 18%O_2 DMEM. Statistical significance was determined by two-way ANOVA followed by Tukey's post-hoc analysis.

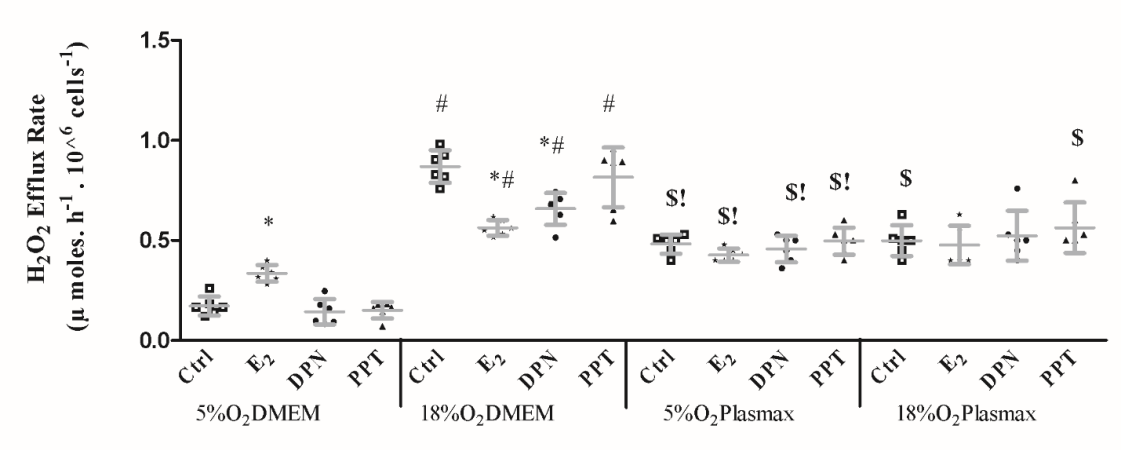
H_2O_2 Efflux Rate
(μ moles. h^{-1} . $10^{\wedge 6}$ cells^{-1})
1.5
1.0
0.5
0.0
Ctrl
E_2
DPN
PPT
5%O_2DMEM
18%O_2DMEM
5%O_2Plasmax
18%O_2Plasmax

Figure 3.3S. Media type and O_2 level modulate E_2 and SERM effects on cellular hydrogen peroxide production. C2C12 cells were cultured at either 5% O_2 or 18% O_2 in either DMEM or Plasmax and treated for 48 hr with 10 nM E_2, 10 nM DPN, 10 nM PPT, or an equal volume of vehicle control (DMSO). Immediately prior to H_2O_2 measurements, cells were washed and then incubated in the prepared KRB (1ml, 2hr) containing freshly added Amplex Red reagent (50 μM) and horseradish peroxidase (0.1 units/mL). A standard curve for H_2O_2 (0 to 3 μM) was created with each experiment. KRB buffer was collected and resorufin fluorescence was measured using Cary Eclipse fluorescence spectrophotometer. H_2O_2 efflux rates ($\mu mol \cdot h^{-1}$) were standardized to cell number. Data shown are means ± SEM from 3 independent experiments. '*'represents differences in a given parameter between treated cells and their corresponding vehicle control. '#' represents differences between 18%O_2 and 5%O_2 in the same media. '$' represents differences between Plasmax and DMEM at the same O_2. '!' represents differences between 5%O_2 /Plasmax and 18%O_2 /DMEM. Statistical significance was determined by two-way ANOVA followed by Tukey's post-hoc analysis.

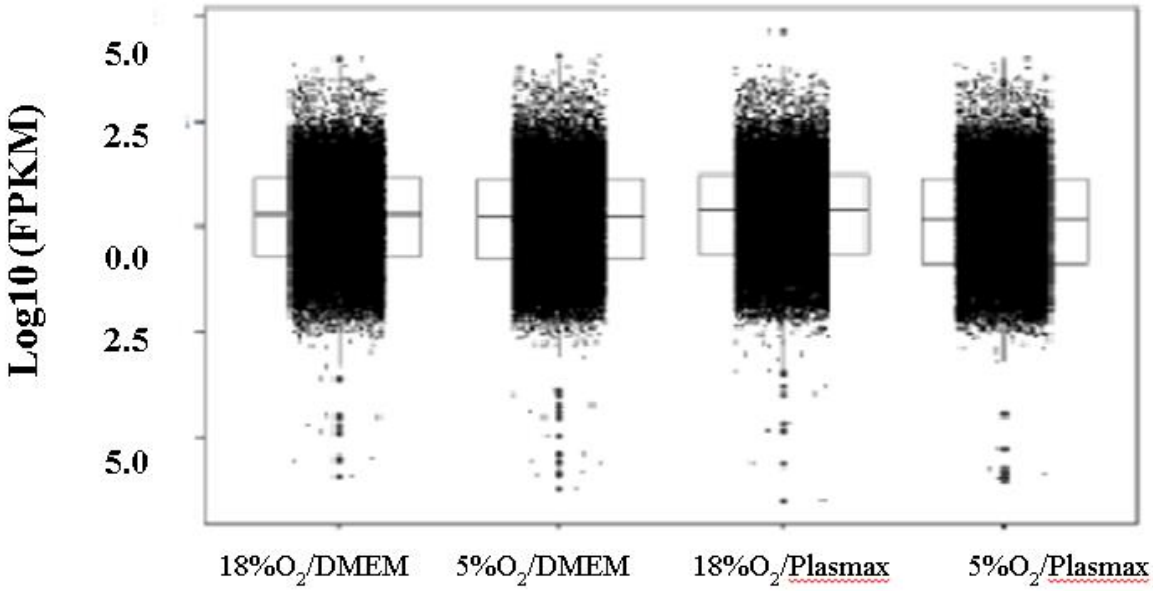

Figure 5S. Scatter box plot demonstrating the distribution of gene expression values in Log10(FPKM). The distribution of gene expression across all conditions is plotted.

Table 5.1S. List of significantly up-regulated genes in DMEM at 5% O_2 vs18% O_2, passing a P - value< 0.05 and with greater than 2-fold change in expression (Log2FC≥1). 'Infin' indicates infinity-fold based on an undetectable level at 18% O_2

Gene	Log2(FC)	P-value
TFRC	infin	0.04
AC005726.4	5.8	0.0271
PRELID2	5.2	0.0026
MT1X	4.9	0.0029
DLX3	4.8	0.0084
CLEC3A	4.8	0.0264
DHRS2	4.7	0.0005
HAPLN1	4.4	0.0002
PADI2	4.4	0.0003
CORO1A	4.3	0.0001
SP6	4.3	0.0010
BCYRN1	4.2	0.0386
TMPRSS4	4.1	0.0007
INSYN1	4.0	0.0029
FCGRT	3.9	0.0004
UHRF1	3.8	0.0002
CDCA7	3.8	0.0025
ITPKA	3.8	0.0051
MCM10	3.7	0.0001
TK1	3.7	0.0001
NXPH4	3.6	0.0033
PIMREG	3.5	0.0099
BOLA3	3.4	0.0145
CDC6	3.3	0.0009
NES	3.3	0.0012
RRM2	3.3	0.0001
E2F2	3.3	0.0007
PTN	3.2	0.0052
CENPM	3.2	0.0048
MCM5	3.1	0.0002
COQ3	3.1	0.0183
DNMT3B	3.1	0.0014
CDC45	3.1	0.0004
SCNN1A	3.1	0.0116
BIRC5	3.1	0.0001
FLT4	3.1	0.0156
POLE2	3.1	0.0016
KCNN4	3.0	0.0007
MYBL2	3.0	0.0001
E2F8	3.0	0.0025
WDR54	2.9	0.0007
FAM111B	2.9	0.0007
IGFBP6	2.9	0.0218
PCDH1	2.9	0.0047
SHCBP1	2.8	0.0008
PRRT3	2.8	0.0035
PLK1	2.8	0.0001
EXO1	2.8	0.0028

TRIP13	2.8	0.0004
E2F1	2.7	0.0004
CCNA2	2.7	0.0042
ZWINT	2.7	0.0010
AURKB	2.7	0.0002
PKMYT1	2.7	0.0065
MCM2	2.7	0.0003
GAL	2.6	0.0146
BLM	2.6	0.0134
GINS3	2.6	0.0035
KIF15	2.6	0.0080
NRM	2.6	0.0059
PLBD1	2.6	0.0265
CDC25A	2.5	0.0066
ACTL8	2.5	0.0177
ESPL1	2.5	0.0004
SKA3	2.5	0.0038
ODC1	2.5	0.0001
RMI2	2.5	0.0041
RFC2	2.5	0.0006
HJURP	2.5	0.0033
DHRS11	2.5	0.0314
TICRR	2.5	0.0111
RELT	2.5	0.0279
CDCA8	2.4	0.0053
CSRP2	2.4	0.0173
CHTF18	2.4	0.0079
FGFR3	2.4	0.0022
CDCA5	2.4	0.0008
RAD54L	2.4	0.0343
PDK1	2.4	0.0212
RBBP8NL	2.4	0.0121
TTC26	2.4	0.0435
CRABP2	2.4	0.0002
TUBA1B	2.4	0.0035
MELK	2.4	0.0131
BACE2	2.4	0.0052
AGK	2.4	0.0254
ASRGL1	2.4	0.0312
KIFC1	2.3	0.0006
FAH	2.3	0.0327
CDCA3	2.3	0.0159
CENPF	2.3	0.0005
CMSS1	2.3	0.0165
NPR3	2.3	0.0198
NEIL3	2.3	0.0242
NCAPG	2.3	0.0099
CEP55	2.3	0.0019
MATK	2.3	0.0031
KIF20A	2.3	0.0370
AP002761.4	2.3	0.0186
TACC3	2.3	0.0031
SSRP1	2.3	0.0004
NRGN	2.3	0.0311
NEURL1B	2.3	0.0059
ZNF367	2.3	0.0032

KIF18B	2.3	0.0036
IQGAP3	2.3	0.0013
RBL1	2.3	0.0064
SLC29A1	2.3	0.0021
MT2A	2.3	0.0009
CTSH	2.3	0.0247
DDIAS	2.3	0.0453
NDC80	2.3	0.0015
NUP205	2.3	0.0015
TUBB	2.2	0.0004
MCM4	2.2	0.0010
FANCE	2.2	0.0305
MKI67	2.2	0.0003
PHF19	2.2	0.0124
CIT	2.2	0.0021
C2CD4C	2.2	0.0212
ORC1	2.2	0.0085
ARHGEF19	2.2	0.0083
TCF19	2.2	0.0023
GTSE1	2.2	0.0037
CLSPN	2.2	0.0129
WDR76	2.2	0.0111
DTL	2.1	0.0464
R3HCC1	2.1	0.0079
NCAPH	2.1	0.0223
UBE2T	2.1	0.0022
TSEN15	2.1	0.0050
POLD2	2.1	0.0012
P2RY2	2.1	0.0239
DCLRE1A	2.1	0.0123
PGM1	2.1	0.0440
AARS2	2.1	0.0030
ASF1B	2.1	0.0025
NUDT1	2.1	0.0064
RHOV	2.1	0.0290
KIF4A	2.1	0.0267
CDKN2AIPNL	2.1	0.0038
DAPK2	2.1	0.0365
BRIP1	2.1	0.0013
MAD2L1	2.1	0.0170
SLC25A23	2.1	0.0341
KIF11	2.1	0.0044
BNIP3	2.0	0.0024
KCTD6	2.0	0.0477
NCAPG2	2.0	0.0010
ORC6	2.0	0.0113
COTL1	2.0	0.0128
PTGES2	2.0	0.0029
TEDC2	2.0	0.0055
TPX2	2.0	0.0007
H2AFX	2.0	0.0006
SUV39H1	2.0	0.0091
TROAP	2.0	0.0307
RND3	2.0	0.0367
C5	2.0	0.0206
BCAT2	2.0	0.0090

KIF22	2.0	0.0020
TOMM40	2.0	0.0445
GLB1L2	2.0	0.0369
MCM3	2.0	0.0026
GGH	2.0	0.0114
ANP32E	2.0	0.0037
GINS1	2.0	0.0043
HAUS5	2.0	0.0078
PPFIA4	2.0	0.0322
CHAF1A	1.9	0.0338
MPZL2	1.9	0.0413
ENDOD1	1.9	0.0365
WDHD1	1.9	0.0082
YBX2	1.9	0.0039
POGLUT3	1.9	0.0210
IGFBP2	1.9	0.0150
NUF2	1.9	0.0169
MCM7	1.9	0.0063
UBE2C	1.9	0.0031
WNT7B	1.9	0.0121
BUB1	1.9	0.0033
KIF14	1.9	0.0070
FOXO6	1.9	0.0446
PHGDH	1.9	0.0004
PFKP	1.9	0.0087
CDKN2C	1.9	0.0234
SAAL1	1.9	0.0285
RIOK2	1.9	0.0119
TTK	1.9	0.0081
SH2B2	1.9	0.0235
NUDT8	1.9	0.0353
FANCG	1.9	0.0408
CA12	1.9	0.0037
CCNF	1.8	0.0027
TUBB4B	1.8	0.0015
ENO1	1.8	0.0016
GAMT	1.8	0.0075
BRCA2	1.8	0.0329
ANLN	1.8	0.0059
CKS1B	1.8	0.0044
WDR34	1.8	0.0281
CDT1	1.8	0.0048
TPI1	1.8	0.0032
AC006538.1	1.8	0.0322
NCAPH2	1.8	0.0424
SGO1	1.8	0.0295
P3H4	1.8	0.0138
DTYMK	1.8	0.0088
LY6E	1.8	0.0019
PLEKHO1	1.8	0.0279
PGAM1	1.8	0.0018
MRPL54	1.8	0.0315
TTC5	1.8	0.0395
ASPM	1.8	0.0055
TMEM191A	1.8	0.0192
AURKA	1.8	0.0164

PTTG1	1.8	0.0149
XRCC2	1.8	0.0326
RANBP1	1.8	0.0313
CENPU	1.8	0.0368
TMPRSS13	1.8	0.0237
SGF29	1.8	0.0370
POFUT1	1.8	0.0092
FAM222A	1.8	0.0383
FAM83D	1.8	0.0081
LDHA	1.8	0.0018
CDC20	1.8	0.0051
SPDL1	1.8	0.0213
GAPDH	1.8	0.0059
FANCD2	1.7	0.0040
SNRNP25	1.7	0.0411
LMNB1	1.7	0.0044
HPDL	1.7	0.0163
FN3KRP	1.7	0.0127
HMGB1	1.7	0.0070
HNRNPD	1.7	0.0038
RACGAP1	1.7	0.0020
NEK2	1.7	0.0294
CDCA2	1.7	0.0243
PFKFB3	1.7	0.0060
C9orf40	1.7	0.0435
HMGB2	1.7	0.0062
PLK4	1.7	0.0381
CDCA4	1.7	0.0190
MELTF	1.7	0.0364
ARHGAP11A	1.7	0.0078
ATAD2	1.7	0.0037
AK4	1.7	0.0185
DLGAP5	1.7	0.0080
METRN	1.7	0.0354
PRMT5	1.7	0.0294
FNDC10	1.7	0.0255
E2F7	1.7	0.0224
ASCL2	1.7	0.0246
PCNA	1.7	0.0102
CIP2A	1.7	0.0500
SMAD6	1.7	0.0188
BRI3BP	1.7	0.0094
CDKN3	1.6	0.0375
GALE	1.6	0.0203
DHFR	1.6	0.0289
KNL1	1.6	0.0139
DEPDC1	1.6	0.0288
TONSL	1.6	0.0135
ACOT7	1.6	0.0165
TAGLN2	1.6	0.0052
FANCA	1.6	0.0255
MRPL48	1.6	0.0287
MIS18A	1.6	0.0334
TUBGCP3	1.6	0.0480
PPIF	1.6	0.0110
RPS26	1.6	0.0097

DCXR	1.6	0.0064
SART1	1.6	0.0187
DUSP12	1.6	0.0494
AC027237.1	1.6	0.0181
GMNN	1.6	0.0290
MCM6	1.6	0.0089
CDK1	1.6	0.0110
RAC3	1.6	0.0387
CALM1	1.6	0.0190
KNTC1	1.6	0.0325
DEF8	1.6	0.0420
CDH24	1.5	0.0438
LRRC59	1.5	0.0095
CDCA7L	1.5	0.0398
CCNB1	1.5	0.0106
ELOVL6	1.5	0.0384
CENPH	1.5	0.0366
H2AFZ	1.5	0.0091
RRM1	1.5	0.0098
CDK2	1.5	0.0168
CARD10	1.5	0.0474
CHEK1	1.5	0.0473
REEP4	1.5	0.0212
TYMS	1.5	0.0449
FSCN1	1.5	0.0486
METTL26	1.5	0.0244
TNNT1	1.5	0.0390
PSMC3	1.5	0.0089
BSPRY	1.5	0.0334
LIG1	1.5	0.0129
MRPS2	1.5	0.0200
INCENP	1.5	0.0169
HMMR	1.5	0.0468
KRT80	1.4	0.0148
POLE	1.4	0.0093
EZH2	1.4	0.0398
ITGB4	1.4	0.0483
EIF5A	1.4	0.0346
STMN1	1.4	0.0161
PKM	1.4	0.0121
ADI1	1.4	0.0225
CCNB2	1.4	0.0455
OXCT1	1.4	0.0351
HMGB3	1.4	0.0269
RNF26	1.4	0.0296
LDLRAP1	1.4	0.0445
TOP2A	1.4	0.0153
SAPCD2	1.4	0.0179
SIVA1	1.4	0.0425
ACSF3	1.4	0.0398
GPT2	1.4	0.0339
POLD3	1.4	0.0497
SDF2L1	1.4	0.0391
DHTKD1	1.4	0.0127
WDR62	1.4	0.0349
H1F0	1.4	0.0227

TMPO	1.4	0.0158
TRIM28	1.4	0.0236
SYT12	1.4	0.0197
TCOF1	1.4	0.0165
KNSTRN	1.4	0.0301
H1FX	1.4	0.0186
TFAP4	1.4	0.0423
PARP2	1.4	0.0365
MRTO4	1.4	0.0351
SMC4	1.4	0.0240
NDUFB10	1.3	0.0204
HK2	1.3	0.0360
IDH2	1.3	0.0353
NUP210	1.3	0.0251
USP1	1.3	0.0352
LYAR	1.3	0.0384
POP7	1.3	0.0342
UNC93B1	1.3	0.0414
TIMELESS	1.3	0.0349
TSKU	1.3	0.0239
PRXL2B	1.3	0.0416
ZMIZ1	1.3	0.0307
H2AFV	1.3	0.0466
FAM189B	1.3	0.0396
RECQL4	1.3	0.0406
RPS6KA4	1.3	0.0311
ANKRD40	1.3	0.0402
CCND3	1.3	0.0328
HRAS	1.3	0.0410
PACSIN3	1.3	0.0310
NOP56	1.3	0.0244
TRAP1	1.3	0.0471
MTHFD1	1.3	0.0417
NACC1	1.3	0.0386
FH	1.3	0.0459
WARS	1.3	0.0296
SRM	1.2	0.0339
CTPS1	1.2	0.0490
LMNB2	1.2	0.0334
NET1	1.2	0.0487
SELENOW	1.2	0.0466
BCKDK	1.2	0.0444
S100A14	1.2	0.0425
CNBP	1.2	0.0307
CCHCR1	1.2	0.0354
ANAPC5	1.2	0.0431
UNG	1.1	0.0351
NOLC1	1.1	0.0406
DDX39A	1.1	0.0431
KPNA2	1.1	0.0403
SLC25A39	1.1	0.0496

Table 5.2S. List of significantly up-regulated genes in DMEM at 18% O_2 vs 5% O_2, passing a P-value< 0.05 and with greater than 2-fold change in expression (Log2FC≥1).

Gene	Log2(FC)	P -value
AC093866.1	7.5	0.0125
LTB	5.9	0.0133
TCIM	5.7	0.0457
MRPS30-DT	5.4	0.0043
RASD1	5.2	0.0004
FOSB	5.0	0.0359
HGD	4.8	0.0024
SERPINE1	4.4	0.0010
FOS	4.3	0.0001
CCN2	4.3	0.0009
EDN1	4.0	0.0016
FAXDC2	3.9	0.0107
SPATA18	3.8	0.0010
YPEL2	3.8	0.0001
AL139383.1	3.8	0.0058
AC073114.1	3.7	0.0333
TEX19	3.6	0.0034
APOBEC3H	3.5	0.0243
ACTA2	3.5	0.0103
GDF15	3.4	0.0001
RND1	3.4	0.0008
KCNJ15	3.3	0.0050
COL12A1	3.3	0.0001
KLHL24	3.3	0.0001
LDLRAD4	3.2	0.0020
GULP1	3.2	0.0020
MSMB	3.2	0.0345
LMCD1	3.1	0.0008
EGR1	3.1	0.0001
AC108488.3	3.1	0.0056
NRCAM	3.0	0.0003
HIST2H2BF	3.0	0.0075
TIMP3	2.9	0.0018
CABYR	2.9	0.0485
LINC00894	2.9	0.0482
LIF	2.9	0.0085
ITPR1	2.8	0.0001
SLC39A10	2.7	0.0001
SERPINF1	2.7	0.0223
ZMAT3	2.7	0.0003
TCN1	2.7	0.0071
CDKN1A	2.7	0.0001
IDUA	2.7	0.0131
DRAM1	2.6	0.0011
NR4A1	2.6	0.0004
EGR3	2.6	0.0253

MALAT1	2.6	0.0014
GABARAPL1	2.6	0.0013
ABCA12	2.5	0.0006
AC142472.1	2.5	0.0235
CPE	2.5	0.0051
CNTD2	2.5	0.0117
CITED2	2.4	0.0003
FAS	2.4	0.0172
RLN2	2.4	0.0344
AMN1	2.3	0.0412
PDE5A	2.3	0.0186
MGP	2.3	0.0447
DUSP1	2.3	0.0091
AL158206.1	2.3	0.0306
SLC12A2	2.3	0.0004
PLEKHF1	2.3	0.0197
MYO15B	2.3	0.0021
CASP4	2.3	0.0167
SYP	2.2	0.0381
ZFP36	2.2	0.0012
CCDC159	2.2	0.0075
ATP8B2	2.2	0.0002
HIST1H2AI	2.2	0.0399
TFF3	2.2	0.0269
ST8SIA4	2.1	0.0093
CCN1	2.1	0.0039
BMF	2.1	0.0081
LINC00494	2.1	0.0354
CALCOCO1	2.1	0.0074
GADD45A	2.1	0.0200
YPEL3	2.1	0.0066
ARRDC4	2.1	0.0051
CCNG2	2.1	0.0074
ZFP36L1	2.1	0.0003
IGFBP5	2.1	0.0010
SLC41A3	2.1	0.0037
NPNT	2.1	0.0462
PHLDA3	2.0	0.0011
FRK	2.0	0.0033
BTG2	2.0	0.0040
SAT1	2.0	0.0179
AFF3	2.0	0.0014
B4GALNT3	2.0	0.0409
LURAP1L	1.9	0.0447
SWT1	1.9	0.0345
SLC38A2	1.9	0.0002
HIST2H2BE	1.9	0.0065
DDX60	1.9	0.0072
TMEM45B	1.9	0.0395
LPP	1.9	0.0108
SMAD3	1.9	0.0066
SLC6A14	1.9	0.0425

MST1	1.9	0.0273
RRM2B	1.9	0.0017
MAGI2	1.9	0.0150
BBC3	1.8	0.0279
HLA-DQB1	1.8	0.0316
JUN	1.8	0.0038
SYBU	1.8	0.0159
AL133367.1	1.8	0.0193
CLCN7	1.8	0.0016
RPS27L	1.8	0.0163
FAM107B	1.8	0.0150
SESN3	1.8	0.0257
PROB1	1.8	0.0204
ENPP1	1.8	0.0204
SDCBP	1.8	0.0105
ACCS	1.8	0.0303
PCNX2	1.7	0.0348
FAM214A	1.7	0.0129
ITGB5	1.7	0.0043
KDM5B	1.7	0.0014
OPTN	1.7	0.0216
YPEL5	1.7	0.0127
TFPI	1.7	0.0376
TSPYL2	1.7	0.0062
GOLGA8A	1.7	0.0274
SESN1	1.7	0.0262
TXNIP	1.7	0.0031
CRELD1	1.7	0.0376
ALCAM	1.6	0.0092
NAT1	1.6	0.0323
PPP1R3B	1.6	0.0208
SAMD4A	1.6	0.0256
MXD4	1.6	0.0065
NEU1	1.6	0.0148
LRIG1	1.6	0.0385
PBXIP1	1.6	0.0230
SVIL	1.6	0.0479
BASP1	1.6	0.0149
NIPAL2	1.6	0.0148
C1QTNF6	1.5	0.0207
THBS1	1.5	0.0030
CCDC170	1.5	0.0180
MCRIP1	1.5	0.0403
PNRC1	1.5	0.0406
RCBTB1	1.5	0.0455
ZSWIM6	1.5	0.0404
BAZ2B	1.5	0.0365
LGR4	1.5	0.0427
BAX	1.5	0.0152
TMC4	1.5	0.0241
WDR81	1.4	0.0151
IER3	1.4	0.0139

SESN2	1.4	0.0484
PGPEP1	1.4	0.0316
RFX5	1.4	0.0138
MFSD8	1.4	0.0356
ABHD4	1.4	0.0469
NR3C1	1.4	0.0408
PGR	1.4	0.0317
BCL2	1.4	0.0235
DZIP3	1.4	0.0435
ABCC10	1.4	0.0315
ANTXR1	1.4	0.0299
RHOQ	1.4	0.0325
NPY1R	1.4	0.0185
IER2	1.3	0.0216
BTG1	1.3	0.0380
ATRX	1.3	0.0272
ATP9A	1.3	0.0293
AHCYL2	1.3	0.0420
DDX58	1.3	0.0416
VPS13A	1.3	0.0445
ZNF76	1.3	0.0431
CCNG1	1.3	0.0192
TRIQK	1.3	0.0307
COL5A1	1.3	0.0408
ARMCX3	1.3	0.0433
TACC1	1.2	0.0405
CXCL12	1.2	0.0483
IER5	1.2	0.0443
N4BP3	1.2	0.0471
LETMD1	1.2	0.0391
AFF4	1.2	0.0268
NOP53	1.2	0.0355
TBC1D9	1.2	0.0495
NAT9	1.2	0.0478

Table 5.3S. List of significantly up-regulated genes in Plasmax at 5% O_2 vs18% O_2, passing a P -value< 0.05 and with greater than 2-fold change in expression (Log2FC≥1). 'Infin' indicates infinity-fold based on an undetectable level at 18%O_2

Gene	Log2(FC)	P-value
IARS	infin	0.0346
ASPRV1	infin	0.0272
LINC02485	5.1	0.0001
AC008834.1	5.1	0.0479
CLGN	4.4	0.0003
CYP1A1	4.4	0.0001
F7	3.8	0.0003
FAM129A	3.5	0.0001
TGM1	3.0	0.0001
AC016044.1	2.9	0.0054
CRYBG2	2.8	0.0029
UNC5B	2.7	0.0005
PKP1	2.6	0.0001
AC127526.5	2.5	0.0177
KCNG1	2.5	0.0062
SYNE3	2.4	0.0036
ABCG1	2.4	0.0001
SLFN5	2.4	0.0024
DHRS2	2.3	0.0005
CHRM1	2.3	0.0235
NUPR1	2.2	0.0118
TMPRSS13	2.1	0.0008
ANKRD20A19P	2.1	0.0385
GGACT	2.0	0.0399
C9orf152	2.0	0.0019
TRIL	2.0	0.0014
BEX2	1.9	0.0113
RFX2	1.9	0.0335
AL355338.1	1.9	0.0290
LINC00494	1.9	0.0317
ARHGEF2	1.9	0.0373
ST3GAL5	1.8	0.0052
FYN	1.8	0.0058
LONP1	1.8	0.0494
CLPB	1.7	0.0060
DDIT4	1.7	0.0025
SARS	1.7	0.0012
PROB1	1.7	0.0149
PIF1	1.7	0.0218
SNHG9	1.7	0.0408
CEBPB	1.7	0.0024
GPNMB	1.7	0.0129
GADD45A	1.7	0.0157
GTPBP2	1.7	0.0082
LAMP3	1.7	0.0245
RNF145	1.6	0.0042
DLX3	1.6	0.0297

C1orf115	1.6	0.0299
ID4	1.6	0.0333
EPHB3	1.6	0.0408
HIST1H2BD	1.6	0.0110
GAS5	1.6	0.0286
PCDH1	1.6	0.0239
RAB27B	1.6	0.0135
KRT10	1.6	0.0221
INPP5J	1.6	0.0311
ATP2C2	1.5	0.0053
CIART	1.5	0.0245
KLHDC7B	1.5	0.0205
TRIM3	1.5	0.0188
PPFIBP2	1.5	0.0209
TUBE1	1.5	0.0316
NOP10	1.5	0.0057
VEGFA	1.5	0.0055
LSM10	1.5	0.0189
ANK3	1.5	0.0094
TTC39B	1.5	0.0468
EIF4EBP1	1.5	0.0094
SEPHS2	1.5	0.0088
LINC00623	1.5	0.0383
CHCHD1	1.5	0.0126
TMEM168	1.5	0.0387
H1F0	1.5	0.0364
ERN1	1.5	0.0408
CYP1B1	1.5	0.0145
CEBPG	1.4	0.0085
PABPC1L	1.4	0.0467
ZNF593	1.4	0.0176
RIT1	1.4	0.0404
SCYL2	1.4	0.0081
ABCA12	1.4	0.0196
RNF187	1.4	0.0092
GADD45G	1.4	0.0454
S100P	1.4	0.0290
TCEA1	1.4	0.0090
IDH1	1.4	0.0110
NRF1	1.4	0.0197
TRIM68	1.4	0.0435
ALDH3B2	1.4	0.0376
SNHG19	1.3	0.0233
RAB3IL1	1.3	0.0468
GFPT1	1.3	0.0088
AARS	1.3	0.0121
NEU1	1.3	0.0198
HIST1H3H	1.3	0.0190
SLC9A1	1.3	0.0184
ID1	1.3	0.0149
CRYBG1	1.3	0.0465
DYRK2	1.3	0.0192

EIF1	1.3	0.0385
KLF4	1.3	0.0304
MOCOS	1.3	0.0310
HOXC13	1.3	0.0499
TRIB3	1.3	0.0145
RHOQ	1.3	0.0295
HIST1H3E	1.2	0.0468
NXPH4	1.2	0.0412
HMOX1	1.2	0.0333
SAPCD2	1.2	0.0274
CLIP1	1.2	0.0163
FTL	1.2	0.0399
ID3	1.2	0.0339
SERTAD1	1.2	0.0354
HIST1H1C	1.2	0.0369
FAM83D	1.2	0.0389
SNHG5	1.2	0.0449
GPT2	1.1	0.0320
TRIM21	1.1	0.0345
MKNK2	1.1	0.0439
KIF3B	1.1	0.0449
PLK1	1.1	0.0397
XPOT	1.1	0.0309
JRK	1.1	0.0420
CBX4	1.1	0.0385
UQCRFS1	1.1	0.0489
SEL1L	1.0	0.0347

Table 5.4S. List of significantly up-regulated genes in Plasmax at 18% O_2 vs 5% O_2, passing a P-value< 0.05 and with greater than 2-fold change in expression (Log2FC≥1). 'Infin' indicates infinity-fold based on an undetectable level at 5%O_2

Gene	Log2(FC)	P-value
AC126175.1	infin	0.0001
MYL7	8.6	0.0073
COL1A2	6.5	0.0001
TNFRSF11B	6.1	0.0007
CALB2	5.8	0.0065
FOXI1	5.6	0.0091
ACTG2	5.4	0.0001
FHL2	5.0	0.0001
CD36	5.0	0.0001
TCIM	5.0	0.0018
AGR3	4.7	0.0195
IL24	4.6	0.0038
CCNE2	4.4	0.0069
RASGRP1	4.4	0.0001
ACKR3	4.3	0.0001
PLAT	4.3	0.0004
TAGLN	4.2	0.0055
TNF	4.0	0.0032
PAPSS2	3.9	0.0012
SCNN1B	3.8	0.0084
NECAB1	3.8	0.0015
TMEM64	3.7	0.0001
RAPGEFL1	3.6	0.0001
ADRA2A	3.6	0.0043
CDCA7	3.5	0.0008
PHLDA1	3.5	0.0026
DUSP4	3.4	0.0009
IL32	3.3	0.0002
PTGES	3.2	0.0007
FADS1	3.2	0.0024
SFXN2	3.2	0.0001
NRP1	3.1	0.0001
AQP3	3.1	0.0012
E2F2	3.1	0.0004
RRM2	3.1	0.0001
LTB	3.0	0.0381
KRT81	3.0	0.0002
MMP13	3.0	0.0008
PDZK1	3.0	0.0006
ZNF385B	2.9	0.0150
DOK3	2.9	0.0396
GPRC5A	2.9	0.0224
KRT16	2.9	0.0226
RET	2.9	0.0001
TNFAIP2	2.8	0.0056

CXCL8	2.8	0.0119
KCNK5	2.8	0.0045
AC103770.1	2.8	0.0051
KIF1A	2.8	0.0002
KCNJ3	2.8	0.0027
SVIL	2.7	0.0055
SCD5	2.7	0.0030
MALRD1	2.7	0.0069
SDK2	2.7	0.0011
IL20	2.6	0.0009
INSR	2.6	0.0009
MSMB	2.6	0.0309
TCN1	2.6	0.0361
SOCS3	2.6	0.0006
DKK1	2.6	0.0004
KRT17	2.6	0.0001
TSPAN5	2.6	0.0020
IL17RB	2.6	0.0176
FABP5	2.6	0.0006
CSRP2	2.6	0.0113
SMAD3	2.5	0.0001
KISS1R	2.5	0.0165
MAST4	2.5	0.0017
CDC45	2.5	0.0006
ADORA1	2.5	0.0093
BAG3	2.5	0.0001
DUSP9	2.5	0.0138
SYTL5	2.5	0.0180
IGFBP6	2.5	0.0318
E2F1	2.5	0.0004
TUBB2B	2.4	0.0251
RELB	2.4	0.0030
AC044784.1	2.4	0.0128
MTCL1	2.4	0.0017
STC1	2.4	0.0028
HNRNPD	2.4	0.0001
PDZD4	2.4	0.0034
CAMK2B	2.4	0.0018
WIPF1	2.4	0.0063
ZNF367	2.4	0.0017
KRT19	2.3	0.0005
FOS	2.3	0.0006
NPNT	2.3	0.0080
BCL2	2.3	0.0001
GAL	2.3	0.0079
UHRF1	2.3	0.0003
SULT2B1	2.3	0.0037
CORO1A	2.2	0.0127
PGR	2.2	0.0002
SCN1B	2.2	0.0264
COL4A5	2.2	0.0090
ZBP1	2.2	0.0250

AFAP1L2	2.2	0.0024
SYTL2	2.2	0.0001
MCM6	2.2	0.0006
TK1	2.2	0.0001
FSCN1	2.2	0.0014
PDLIM3	2.2	0.0063
EVL	2.2	0.0012
LIF	2.2	0.0138
SYT12	2.1	0.0004
PALLD	2.1	0.0172
TNFAIP3	2.1	0.0086
AL161772.1	2.1	0.0199
RBPMS2	2.1	0.0380
PIM1	2.1	0.0127
HPRT1	2.1	0.0012
VASH1	2.1	0.0384
CENPH	2.1	0.0085
AL133367.1	2.1	0.0080
CHGA	2.1	0.0002
AC093001.1	2.1	0.0029
PMP22	2.1	0.0307
FRK	2.1	0.0003
EGR3	2.1	0.0220
FSTL3	2.0	0.0013
ENTPD8	2.0	0.0344
NAT8L	2.0	0.0021
FAM111B	2.0	0.0027
CDC6	2.0	0.0065
ABLIM2	2.0	0.0276
TYMS	2.0	0.0146
CA12	2.0	0.0004
AP000439.2	2.0	0.0316
ORC1	2.0	0.0205
KRT8P3	2.0	0.0290
PCNA	2.0	0.0009
KITLG	2.0	0.0042
PLXND1	1.9	0.0019
FNDC10	1.9	0.0059
CDC25A	1.9	0.0458
FJX1	1.9	0.0146
SCCPDH	1.9	0.0231
UNG	1.9	0.0015
COL12A1	1.9	0.0019
GATA3	1.9	0.0010
LFNG	1.9	0.0020
CALML5	1.9	0.0426
ASCL1	1.9	0.0012
CLDN1	1.9	0.0077
PKIB	1.9	0.0011
RIMS4	1.9	0.0228
ANXA6	1.9	0.0010
PMEPA1	1.9	0.0043

P2RX4	1.9	0.0117
MAN1B1-DT	1.9	0.0485
FAM222A	1.8	0.0288
LIG1	1.8	0.0059
HLA-A	1.8	0.0014
NRGN	1.8	0.0394
BRIP1	1.8	0.0004
AREG	1.8	0.0007
FSD1	1.8	0.0226
MEGF9	1.8	0.0028
KRT8P10	1.8	0.0251
HPGD	1.8	0.0140
KRT8P45	1.8	0.0432
NFATC2	1.8	0.0118
MSI1	1.8	0.0157
COL18A1	1.8	0.0024
DSCC1	1.8	0.0112
PCYOX1L	1.8	0.0221
COX6C	1.8	0.0065
TUBB	1.8	0.0030
ESR1	1.8	0.0009
MCM2	1.8	0.0014
MYEOV	1.8	0.0345
HSPA8	1.8	0.0004
MYB	1.8	0.0022
RBBP8	1.8	0.0109
E2F7	1.7	0.0125
HSPG2	1.7	0.0411
CALCR	1.7	0.0260
HNRNPA3	1.7	0.0016
CDK2	1.7	0.0036
IRX3	1.7	0.0031
ST8SIA4	1.7	0.0029
ACOT7	1.7	0.0078
MTHFD1	1.7	0.0079
ABCC3	1.7	0.0199
NRM	1.7	0.0296
CCM2L	1.7	0.0440
EHBP1L1	1.7	0.0032
NES	1.7	0.0117
PRPS2	1.7	0.0156
FREM2	1.7	0.0025
HELLS	1.7	0.0345
SBK1	1.7	0.0118
CLU	1.7	0.0100
C2CD4C	1.7	0.0192
CDYL2	1.7	0.0053
SRGAP1	1.7	0.0068
OPTN	1.7	0.0117
CRMP1	1.7	0.0271
NUAK2	1.7	0.0164
SPIRE2	1.7	0.0278

PRSS23	1.6	0.0043
PODXL	1.6	0.0051
MELTF	1.6	0.0221
CKB	1.6	0.0140
SEMA3B	1.6	0.0048
ELOVL5	1.6	0.0053
SLC25A1	1.6	0.0027
PQLC3	1.6	0.0100
OSTF1	1.6	0.0095
STARD13	1.6	0.0476
PBX1	1.6	0.0169
NRIP1	1.6	0.0043
MCM10	1.6	0.0164
C6orf141	1.6	0.0127
INPP5F	1.6	0.0170
SMS	1.6	0.0094
MOCS2	1.6	0.0055
MYBL1	1.6	0.0294
MCM5	1.6	0.0051
HPDL	1.6	0.0258
DHFR	1.6	0.0259
GSN	1.6	0.0469
TUBA1B	1.6	0.0444
HMGA1	1.6	0.0064
GAS6	1.5	0.0412
IDH2	1.5	0.0128
TLN2	1.5	0.0454
DSCAM-AS1	1.5	0.0292
CYBA	1.5	0.0028
OXCT1	1.5	0.0220
GFRA1	1.5	0.0157
CENPU	1.5	0.0366
DLC1	1.5	0.0214
CXCL12	1.5	0.0153
KCTD11	1.5	0.0404
SDC1	1.5	0.0043
ADAMTS19	1.5	0.0330
XBP1	1.5	0.0078
HAUS1	1.5	0.0340
HSP90AB1	1.5	0.0187
TNFRSF21	1.5	0.0478
FLNB	1.5	0.0337
PSMB3	1.5	0.0129
MARVELD1	1.5	0.0129
RBM24	1.5	0.0314
GREB1	1.5	0.0141
RAB31	1.5	0.0125
THBS1	1.5	0.0030
KCNK6	1.4	0.0092
CDT1	1.4	0.0085
MCM3	1.4	0.0101
THSD4	1.4	0.0246

SHANK3	1.4	0.0386
CD63	1.4	0.0164
EFR3B	1.4	0.0325
CAMK2N1	1.4	0.0299
SH3BP5	1.4	0.0085
EHF	1.4	0.0480
ASF1B	1.4	0.0129
IFI6	1.4	0.0145
UBE2T	1.4	0.0180
HIP1	1.4	0.0095
MYBL2	1.4	0.0075
CX3CL1	1.4	0.0294
IRX5	1.4	0.0108
REEP6	1.4	0.0423
MT2A	1.4	0.0070
INSIG1	1.4	0.0222
IMPDH2	1.4	0.0114
LGR4	1.4	0.0300
CELSR2	1.4	0.0177
KAT6B	1.4	0.0130
FH	1.4	0.0268
SLC39A6	1.4	0.0137
ZNF703	1.4	0.0138
TRIP13	1.4	0.0394
MX2	1.4	0.0119
PITPNC1	1.4	0.0484
TPM1	1.4	0.0148
FHDC1	1.4	0.0475
COL5A1	1.4	0.0090
SLC9A3R1	1.3	0.0153
SLC29A1	1.3	0.0191
JAK2	1.3	0.0289
SCD	1.3	0.0323
RFC2	1.3	0.0244
PARD6B	1.3	0.0100
GALE	1.3	0.0346
RMDN3	1.3	0.0225
GDI2	1.3	0.0109
MCF2L	1.3	0.0390
AC093323.1	1.3	0.0205
NDRG4	1.3	0.0273
SCIN	1.3	0.0387
SLC7A2	1.3	0.0199
HSP90AA1	1.3	0.0321
TFAP4	1.3	0.0291
SYT1	1.3	0.0356
OSBPL10	1.3	0.0460
TRAPPC9	1.3	0.0492
ANXA5	1.3	0.0146
MCM4	1.3	0.0487
SQLE	1.3	0.0166
PKM	1.3	0.0143

SLC6A6	1.3	0.0266
CHPT1	1.2	0.0447
GSTO1	1.2	0.0471
AMFR	1.2	0.0265
RRM1	1.2	0.0213
IL4R	1.2	0.0443
CCND3	1.2	0.0459
PSMB7	1.2	0.0222
TBC1D9	1.2	0.0231
FANCD2	1.2	0.0336
MSH2	1.2	0.0387
UQCRC1	1.2	0.0229
PRIM2	1.2	0.0441
TCF19	1.2	0.0280
LMF2	1.2	0.0358
FDFT1	1.2	0.0258
LIMK1	1.2	0.0420
ANXA2	1.2	0.0252
IVNS1ABP	1.2	0.0395
ABCA3	1.2	0.0348
RERG	1.2	0.0464
PACS1	1.2	0.0284
MYO1B	1.2	0.0426
SAMD1	1.2	0.0395
COTL1	1.2	0.0355
GYG1	1.1	0.0500
DDX60	1.1	0.0326
SREBF2	1.1	0.0291
CRABP2	1.1	0.0316
SOD1	1.1	0.0405
HSPB8	1.1	0.0410
CDC37	1.1	0.0476
CD9	1.1	0.0469
TIMELESS	1.1	0.0409
HACD3	1.1	0.0430
RHOBTB3	1.1	0.0434
TALDO1	1.1	0.0405
ACTN1	1.1	0.0380
POLD2	1.0	0.0473
SEPT9	1.0	0.0419

Table 5. 5S. List of significantly up-regulated genes in DMEM vs Plasmax at 5%O_2, passing a P-value< 0.05 and with greater than 2-fold change in expression (Log2FC≥1). 'Infin' indicates infinity-fold based on an undetectable level in Plasmax.

Gene	Log2(FC)	P-value
CLEC3A	infin	0.0001
HAPLN1	5.1	0.0006
CCNE2	4.8	0.0050
KCNN4	4.2	0.0011
TMPRSS4	3.8	0.0011
PADI2	3.6	0.0005
CDCA7	3.5	0.0011
RRM2	3.4	0.0001
DPYSL5	3.4	0.0069
TMEM64	3.3	0.0001
KCNK5	3.3	0.0054
INSYN1	3.3	0.0159
GRIN1	3.2	0.0044
DOK3	3.2	0.0360
E2F2	3.1	0.0010
DARS-AS1	3.1	0.0043
REEP1	3.0	0.0004
HSPA8	3.0	0.0001
CSRP2	3.0	0.0186
LYPD6	2.8	0.0069
EHF	2.8	0.0022
KRT19P1	2.8	0.0490
PDK1	2.8	0.0136
MCM6	2.7	0.0004
ORC1	2.7	0.0044
FAM111B	2.7	0.0014
RGS16	2.7	0.0025
FADS1	2.7	0.0416
CDC45	2.7	0.0004
TRGC1	2.7	0.0009
CDC6	2.7	0.0007
CDC25A	2.7	0.0109
JPH1	2.6	0.0228
CENPH	2.6	0.0101
ZNF367	2.6	0.0045
CA12	2.5	0.0004
HPGD	2.5	0.0014
DOCK8	2.5	0.0305
HNRNPD	2.5	0.0004
MCM2	2.5	0.0001
TK1	2.5	0.0001
PLK2	2.5	0.0013
E2F1	2.4	0.0012
LDHA	2.4	0.0015
HSP90AA1	2.4	0.0038
ACTL8	2.4	0.0228
PKM	2.4	0.0007
PCNA	2.3	0.0024
KRT19	2.3	0.0045
AK4	2.3	0.0043
ANXA6	2.3	0.0011

FAH	2.3	0.0481
TUBB	2.3	0.0090
SYT12	2.2	0.0010
ADAMTS19	2.2	0.0109
KIF1A	2.2	0.0051
MCM10	2.2	0.0031
HPDL	2.2	0.0104
P2RY2	2.2	0.0205
MTHFD1	2.2	0.0019
TUBA1B	2.2	0.0444
FAM222A	2.2	0.0206
FSD1	2.2	0.0094
UNG	2.2	0.0021
CDK2	2.1	0.0012
CLSPN	2.1	0.0063
FABP5	2.1	0.0121
SLCO4A1	2.1	0.0247
PHF10	2.1	0.0441
FJX1	2.1	0.0135
IDH2	2.1	0.0073
E2F7	2.1	0.0073
CCNA2	2.1	0.0083
TAFA5	2.1	0.0400
DSCC1	2.1	0.0117
PDZK1	2.1	0.0226
HPRT1	2.1	0.0051
HK2	2.1	0.0029
FREM2	2.1	0.0040
PFKP	2.1	0.0104
CTNNAL1	2.1	0.0444
UHRF1	2.1	0.0105
SPC24	2.1	0.0499
TYRO3	2.0	0.0091
OXCT1	2.0	0.0046
KIF12	2.0	0.0039
IL20	2.0	0.0255
TRIP13	2.0	0.0087
PDCD4	2.0	0.0067
BNIP3L	2.0	0.0442
GDI2	2.0	0.0009
RRM1	2.0	0.0014
TYMS	2.0	0.0290
IMPDH2	2.0	0.0015
FH	2.0	0.0096
SFXN2	2.0	0.0157
FANCI	2.0	0.0244
FAM102B	1.9	0.0043
HELLS	1.9	0.0264
GAL	1.9	0.0369
BRIP1	1.9	0.0028
HNRNPA3	1.9	0.0054
IVNS1ABP	1.9	0.0066
FAM162A	1.9	0.0464
NCAPH	1.9	0.0453
FNDC10	1.9	0.0187
PHF19	1.9	0.0495

EHBP1L1	1.9	0.0044
QPCTL	1.9	0.0460
ASF1B	1.9	0.0066
RAD51	1.9	0.0259
HSP90AB1	1.9	0.0219
B4GALNT1	1.9	0.0080
ZGRF1	1.9	0.0432
LPCAT4	1.8	0.0125
HMGA1	1.8	0.0085
OAT	1.8	0.0109
SCD	1.8	0.0425
MPPED2	1.8	0.0354
B4GAT1	1.8	0.0189
NRM	1.8	0.0413
CENPI	1.8	0.0479
PAICS	1.8	0.0047
PPFIA4	1.8	0.0416
FAM57A	1.8	0.0281
RFC2	1.8	0.0057
CSE1L	1.8	0.0051
IRX3	1.8	0.0135
UBE2T	1.8	0.0125
CXCL12	1.8	0.0100
INSIG1	1.8	0.0103
FASN	1.8	0.0135
FAM20C	1.8	0.0396
MCM5	1.7	0.0136
LNPK	1.7	0.0422
ZNF324B	1.7	0.0350
MSI1	1.7	0.0361
MCM3	1.7	0.0058
SLC2A6	1.7	0.0391
HNRNPLL	1.7	0.0316
STC1	1.7	0.0368
CIP2A	1.7	0.0367
IGFBP5	1.7	0.0120
RET	1.7	0.0356
WDHD1	1.7	0.0191
SLC29A1	1.7	0.0214
PACSIN3	1.7	0.0080
ENO1	1.7	0.0233
MGAT4A	1.7	0.0316
AUTS2	1.7	0.0128
ISOC1	1.7	0.0136
CCND3	1.7	0.0134
GINS1	1.7	0.0111
RAD51AP1	1.7	0.0439
BRI3BP	1.7	0.0100
PFKFB3	1.7	0.0108
LRP8	1.7	0.0148
BNIP3	1.7	0.0205
ANP32E	1.6	0.0126
KNSTRN	1.6	0.0140
FSCN1	1.6	0.0272
PRPS2	1.6	0.0447
BACE2	1.6	0.0339

MVD	1.6	0.0145
GPN3	1.6	0.0463
ATP2A3	1.6	0.0108
SFXN1	1.6	0.0099
DIAPH3	1.6	0.0343
HMCES	1.6	0.0214
BID	1.6	0.0296
CHPT1	1.6	0.0196
SPIRE2	1.6	0.0431
LIG1	1.6	0.0174
NCAPG	1.6	0.0295
GMNN	1.6	0.0275
FGFR4	1.6	0.0164
NLGN2	1.6	0.0215
DHTKD1	1.6	0.0112
PACSIN1	1.6	0.0500
PSMB7	1.6	0.0142
EEA1	1.6	0.0431
PSMB3	1.6	0.0261
ACOT7	1.6	0.0224
HMMR	1.6	0.0334
CAMK2N1	1.6	0.0347
DHCR24	1.6	0.0113
FAM189B	1.6	0.0183
DHFR	1.6	0.0371
ZWINT	1.6	0.0263
TSPAN13	1.6	0.0163
ANXA5	1.6	0.0133
RFC3	1.6	0.0296
ADCY9	1.5	0.0143
ELOVL1	1.5	0.0225
MYBL2	1.5	0.0209
DLGAP5	1.5	0.0207
LDLR	1.5	0.0440
FBP1	1.5	0.0260
PSMC1	1.5	0.0457
HSPH1	1.5	0.0363
GOLM1	1.5	0.0280
ATAD3A	1.5	0.0274
CDYL2	1.5	0.0382
KIF11	1.5	0.0234
KANK2	1.5	0.0353
TIMELESS	1.5	0.0322
LIMK1	1.5	0.0279
STMN1	1.5	0.0198
TPM3	1.5	0.0223
SLC2A1	1.5	0.0301
SQLE	1.5	0.0189
VRK1	1.5	0.0365
ESR1	1.5	0.0187
USP5	1.5	0.0247
SHCBP1	1.5	0.0221
SLC6A6	1.5	0.0214
PGAM1	1.5	0.0262
HSPD1	1.5	0.0380
RBMX	1.5	0.0326

XBP1	1.4	0.0387
CYBA	1.4	0.0233
IDH3A	1.4	0.0390
AHSA1	1.4	0.0365
SMS	1.4	0.0300
ACLY	1.4	0.0286
SLC9A3R1	1.4	0.0453
PSMB6	1.4	0.0207
PSMD1	1.4	0.0279
SUSD3	1.4	0.0474
TTC12	1.4	0.0433
LTA4H	1.4	0.0397
POP1	1.4	0.0499
NUP155	1.4	0.0290
CD63	1.4	0.0468
CBWD1	1.4	0.0393
KPNA2	1.4	0.0354
HNRNPM	1.4	0.0470
SNRPA1	1.4	0.0489
SLC25A1	1.4	0.0282
PRIM2	1.4	0.0421
ATAD2	1.4	0.0304
MTMR4	1.4	0.0365
GUCD1	1.4	0.0272
DHX9	1.3	0.0431
BUB1	1.3	0.0280
GLE1	1.3	0.0358
GATA3	1.3	0.0433
SDC1	1.3	0.0305
STIP1	1.3	0.0255
UQCRC1	1.3	0.0301
SLC39A6	1.3	0.0455
SPINDOC	1.3	0.0489
MCM4	1.3	0.0448
PHTF2	1.3	0.0498
FDFT1	1.3	0.0384
TONSL	1.3	0.0492
PSMD3	1.3	0.0402
GYS1	1.3	0.0279
BAG3	1.3	0.0490
POLE	1.3	0.0208
CCT2	1.3	0.0330
XRCC6	1.3	0.0442
BDH1	1.3	0.0476
DBI	1.3	0.0434
CRABP2	1.3	0.0490
FARSA	1.2	0.0463
PABPC4	1.2	0.0492
XRCC5	1.1	0.0476
VARS	1.1	0.0360

Table 5. 6S. List of significantly up-regulated genes in Plasmax vs DMEM at 5% O_2, passing a P-value< 0.05 and with greater than 2-fold change in expression (Log2FC≥1). 'Infin' indicates infinity-fold based on an undetectable level in DMEM.

Gene	Log2(FC)	P-value
LINC02485	infin	0.0002
SERPINE1	6.1	0.0018
CLGN	6.0	0.0018
LAMP3	5.8	0.0008
DHRS2	5.7	0.0001
AL109615.3	5.5	0.0114
BATF2	5.3	0.0043
GPNMB	5.3	0.0001
SLC15A3	5.3	0.0150
RSAD2	5.2	0.0022
MX2	5.2	0.0003
FOLR1	5.1	0.0064
TRANK1	4.6	0.0001
RENBP	4.6	0.0086
AC016044.1	4.6	0.0073
FAM129A	4.5	0.0001
SAMD9	4.5	0.0001
NRCAM	4.4	0.0001
IFI44L	4.4	0.0010
IFIT1	4.3	0.0005
KRT17	4.2	0.0001
ANKRD20A19P	4.2	0.0233
DNAJC27-AS1	4.2	0.0441
FAM83E	4.1	0.0316
APOL3	4.1	0.0001
CLDN9	4.1	0.0129
F7	4.1	0.0018
ACP5	4.0	0.0054
LGALS3	3.9	0.0001
AL137001.2	3.9	0.0012
CMPK2	3.8	0.0074
APOL6	3.8	0.0004
OASL	3.8	0.0011
CAPN2	3.7	0.0007
S100P	3.7	0.0003
UBA7	3.7	0.0010
CYP1A1	3.6	0.0011
CEBPB	3.6	0.0001
MSLN	3.5	0.0022
GDF15	3.5	0.0001
LINC00494	3.5	0.0007
HIST2H3D	3.5	0.0268
KLF4	3.5	0.0005
SYNPO	3.4	0.0086
XAF1	3.3	0.0001
ISG15	3.3	0.0001
IFI44	3.2	0.0001
UNC5B	3.2	0.0019
TENT5B	3.2	0.0067

HIST2H2BF	3.2	0.0047
TGM1	3.2	0.0003
CHAC1	3.2	0.0045
AL606500.1	3.2	0.0326
IRF7	3.1	0.0001
PPP1R15A	3.1	0.0001
OAS2	3.1	0.0302
GADD45A	3.1	0.0015
NUPR1	3.0	0.0046
HIST1H2BO	3.0	0.0463
NLRC5	3.0	0.0003
FYN	3.0	0.0001
TRIM21	3.0	0.0001
ATF3	3.0	0.0011
GSTP1	2.9	0.0025
CHRM1	2.9	0.0214
TRIL	2.9	0.0007
ASCL1	2.9	0.0027
KCNG1	2.9	0.0129
BEX2	2.9	0.0069
TRIM38	2.8	0.0038
DNMBP	2.8	0.0076
ASPRV1	2.8	0.0001
HMOX1	2.8	0.0008
ERRFI1	2.8	0.0012
HERC6	2.8	0.0002
SLC43A1	2.7	0.0072
LURAP1L	2.7	0.0077
SERTAD1	2.7	0.0019
KLHL24	2.7	0.0001
CEBPG	2.7	0.0001
MCRIP1	2.7	0.0008
RAB32	2.7	0.0200
FTL	2.7	0.0006
DDX58	2.7	0.0002
FABP6	2.7	0.0330
BMF	2.6	0.0019
HIST3H2BB	2.6	0.0171
HIST1H3H	2.6	0.0003
ULBP1	2.6	0.0068
HIST1H1C	2.6	0.0025
TFF3	2.5	0.0117
PKP1	2.5	0.0020
HELZ2	2.5	0.0001
MX1	2.5	0.0021
HIST1H4H	2.5	0.0171
ADM2	2.5	0.0008
H1F0	2.4	0.0140
PARP14	2.4	0.0003
AC005914.1	2.4	0.0277
AKNA	2.4	0.0049
SLC7A11	2.4	0.0023
SP110	2.3	0.0018
HIST1H2AC	2.3	0.0017
LHFPL2	2.3	0.0213
PARP12	2.3	0.0028

IFIT5	2.3	0.0012
TRIB3	2.3	0.0006
KNDC1	2.3	0.0151
CHST3	2.3	0.0075
PKIG	2.3	0.0161
CASP4	2.2	0.0160
IFI6	2.2	0.0012
YPEL2	2.2	0.0078
IER5L	2.2	0.0011
APOL2	2.2	0.0031
FOS	2.2	0.0242
BBC3	2.1	0.0153
CHST7	2.1	0.0487
ERN1	2.1	0.0073
VEGFA	2.1	0.0009
STAT1	2.1	0.0030
RAB3IL1	2.1	0.0168
ZNHIT2	2.1	0.0058
FADS3	2.1	0.0058
FAM167A	2.1	0.0307
HIST2H4A	2.1	0.0356
PPFIBP2	2.1	0.0044
PARP9	2.1	0.0389
CBX4	2.0	0.0012
ISG20	2.0	0.0412
SP100	2.0	0.0121
IFI35	2.0	0.0080
GADD45G	2.0	0.0181
PLSCR1	2.0	0.0029
COL12A1	2.0	0.0089
INHBB	2.0	0.0051
JMY	2.0	0.0073
MSX2	2.0	0.0057
EGR1	2.0	0.0036
HIST1H2BD	2.0	0.0064
TRIM68	2.0	0.0196
IFIH1	1.9	0.0035
SLC3A2	1.9	0.0099
DDX60	1.9	0.0060
SPSB1	1.9	0.0325
SLC6A9	1.9	0.0264
CALHM2	1.9	0.0107
DUSP8	1.9	0.0186
TTC39B	1.9	0.0383
PLEKHA4	1.9	0.0111
PABPC1L	1.9	0.0113
AMOTL2	1.9	0.0050
SIPA1L2	1.9	0.0330
PIP5KL1	1.9	0.0198
FOSL2	1.9	0.0068
GADD45B	1.9	0.0063
AC245297.3	1.8	0.0369
SARS	1.8	0.0055
NEU1	1.8	0.0089
NFIL3	1.8	0.0318
CCDC159	1.8	0.0143

C16orf91	1.8	0.0120
TIGD2	1.8	0.0319
ZBTB38	1.8	0.0247
MST1	1.8	0.0307
GTPBP2	1.8	0.0127
SYBU	1.8	0.0195
TGIF1	1.8	0.0229
HIST1H2BK	1.8	0.0107
H1FX	1.8	0.0153
VGF	1.8	0.0080
DDIT4	1.8	0.0097
TENT5C	1.8	0.0354
VAV3	1.8	0.0388
PROB1	1.8	0.0427
PHYKPL	1.7	0.0242
C19orf66	1.7	0.0336
OAS3	1.7	0.0451
HIST2H2BE	1.7	0.0108
DUSP1	1.7	0.0460
SAT1	1.7	0.0462
PARP8	1.7	0.0281
HES1	1.7	0.0158
HIST1H3E	1.7	0.0441
CDKN1A	1.7	0.0058
CA11	1.7	0.0460
RAB39B	1.7	0.0438
ARC	1.7	0.0209
ZMYND8	1.7	0.0117
ZSCAN18	1.7	0.0492
PARP10	1.7	0.0310
CAPG	1.7	0.0388
CACNA1H	1.6	0.0165
DYRK1B	1.6	0.0292
STAT2	1.6	0.0193
PHLDA3	1.6	0.0155
ARSA	1.6	0.0391
SESN2	1.6	0.0423
DAPK3	1.6	0.0111
MEIS3	1.6	0.0500
TNFRSF12A	1.5	0.0285
NOTCH1	1.5	0.0118
VPS28	1.5	0.0258
ACSL1	1.5	0.0494
MTMR11	1.5	0.0343
MFAP3L	1.5	0.0304
TAP1	1.5	0.0303
MID1IP1	1.5	0.0287
SERINC5	1.5	0.0356
RNF187	1.5	0.0158
JUND	1.5	0.0197
USP18	1.5	0.0278
SLC9A1	1.5	0.0250
SLC2A10	1.5	0.0479
TRIM16L	1.5	0.0283
TACC2	1.5	0.0176
HDHD3	1.5	0.0460

MOCOS	1.5	0.0414
LENG8	1.4	0.0366
CLCN7	1.4	0.0188
RNF146	1.4	0.0340
SH3BP2	1.4	0.0305
DOK7	1.4	0.0290
MNX1	1.4	0.0399
FANCF	1.4	0.0454
MARF1	1.4	0.0323
ATP2C2	1.4	0.0362
RHBDD1	1.4	0.0466
ABCG1	1.4	0.0336
IER2	1.4	0.0275
ADAR	1.4	0.0426
PIM3	1.3	0.0407
JUN	1.3	0.0398
SIN3B	1.3	0.0448
S1PR3	1.3	0.0429
JRK	1.3	0.0395
TSC22D1	1.3	0.0296
KLF10	1.3	0.0458
ATF4	1.3	0.0500
TXNIP	1.3	0.0416
SEPHS2	1.3	0.0463

Table 5. 7S List of significantly up-regulated genes in DMEM vs Plasmax at 18% O_2 , passing a P- value< 0.05 and with greater than 2-fold change in expression (Log2FC≥1). 'Infin' indicates infinity-fold based on an undetectable level at 18%O_2.

Gene	Log2(FC)	P-value
AC005726.4	infin	0.0271
PRELID2	5.8	0.0026
MT1X	5.2	0.0029
DLX3	4.9	0.0084
CLEC3A	4.8	0.0264
DHRS2	4.8	0.0005
HAPLN1	4.7	0.0002
PADI2	4.4	0.0003
CORO1A	4.4	0.0001
SP6	4.3	0.0010
BCYRN1	4.3	0.0386
TMPRSS4	4.2	0.0007
INSYN1	4.1	0.0029
FCGRT	4.0	0.0004
UHRF1	3.9	0.0002
CDCA7	3.8	0.0025
ITPKA	3.8	0.0051
MCM10	3.8	0.0001
TK1	3.7	0.0001
NXPH4	3.7	0.0033
PIMREG	3.6	0.0099
BOLA3	3.5	0.0145
CDC6	3.4	0.0009
NES	3.3	0.0012
RRM2	3.3	0.0001
E2F2	3.3	0.0007
PTN	3.3	0.0052
CENPM	3.2	0.0048
MCM5	3.2	0.0002
COQ3	3.1	0.0183
DNMT3B	3.1	0.0014
CDC45	3.1	0.0004
SCNN1A	3.1	0.0116
BIRC5	3.1	0.0001
FLT4	3.1	0.0156
POLE2	3.1	0.0016
KCNN4	3.1	0.0007
MYBL2	3.0	0.0001
E2F8	3.0	0.0025
WDR54	3.0	0.0007
FAM111B	2.9	0.0007
IGFBP6	2.9	0.0218
PCDH1	2.9	0.0047
SHCBP1	2.9	0.0008
PRRT3	2.8	0.0035
PLK1	2.8	0.0001
EXO1	2.8	0.0028
TRIP13	2.8	0.0004
E2F1	2.8	0.0004

CCNA2	2.7	0.0042
ZWINT	2.7	0.0010
AURKB	2.7	0.0002
PKMYT1	2.7	0.0065
MCM2	2.7	0.0003
GAL	2.7	0.0146
BLM	2.6	0.0134
GINS3	2.6	0.0035
KIF15	2.6	0.0080
NRM	2.6	0.0059
PLBD1	2.6	0.0265
CDC25A	2.6	0.0066
ACTL8	2.5	0.0177
ESPL1	2.5	0.0004
SKA3	2.5	0.0038
ODC1	2.5	0.0001
RMI2	2.5	0.0041
RFC2	2.5	0.0006
HJURP	2.5	0.0033
DHRS11	2.5	0.0314
TICRR	2.5	0.0111
RELT	2.5	0.0279
CDCA8	2.5	0.0053
CSRP2	2.4	0.0173
CHTF18	2.4	0.0079
FGFR3	2.4	0.0022
CDCA5	2.4	0.0008
RAD54L	2.4	0.0343
PDK1	2.4	0.0212
RBBP8NL	2.4	0.0121
TTC26	2.4	0.0435
CRABP2	2.4	0.0002
TUBA1B	2.4	0.0035
MELK	2.4	0.0131
BACE2	2.4	0.0052
AGK	2.4	0.0254
ASRGL1	2.4	0.0312
KIFC1	2.4	0.0006
FAH	2.3	0.0327
CDCA3	2.3	0.0159
CENPF	2.3	0.0005
CMSS1	2.3	0.0165
NPR3	2.3	0.0198
NEIL3	2.3	0.0242
NCAPG	2.3	0.0099
CEP55	2.3	0.0019
MATK	2.3	0.0031
KIF20A	2.3	0.0370
AP002761.4	2.3	0.0186
TACC3	2.3	0.0031
SSRP1	2.3	0.0004
NRGN	2.3	0.0311
NEURL1B	2.3	0.0059
ZNF367	2.3	0.0032
KIF18B	2.3	0.0036
IQGAP3	2.3	0.0013

RBL1	2.3	0.0064
SLC29A1	2.3	0.0021
MT2A	2.3	0.0009
CTSH	2.3	0.0247
DDIAS	2.3	0.0453
NDC80	2.3	0.0015
NUP205	2.3	0.0015
TUBB	2.3	0.0004
MCM4	2.2	0.0010
FANCE	2.2	0.0305
MKI67	2.2	0.0003
PHF19	2.2	0.0124
CIT	2.2	0.0021
C2CD4C	2.2	0.0212
ORC1	2.2	0.0085
ARHGEF19	2.2	0.0083
TCF19	2.2	0.0023
GTSE1	2.2	0.0037
CLSPN	2.2	0.0129
WDR76	2.2	0.0111
DTL	2.2	0.0464
R3HCC1	2.1	0.0079
NCAPH	2.1	0.0223
UBE2T	2.1	0.0022
TSEN15	2.1	0.0050
POLD2	2.1	0.0012
P2RY2	2.1	0.0239
DCLRE1A	2.1	0.0123
PGM1	2.1	0.0440
AARS2	2.1	0.0030
ASF1B	2.1	0.0025
NUDT1	2.1	0.0064
RHOV	2.1	0.0290
KIF4A	2.1	0.0267
CDKN2AIPNL	2.1	0.0038
DAPK2	2.1	0.0365
BRIP1	2.1	0.0013
MAD2L1	2.1	0.0170
SLC25A23	2.1	0.0341
KIF11	2.1	0.0044
BNIP3	2.1	0.0024
KCTD6	2.0	0.0477
NCAPG2	2.0	0.0010
ORC6	2.0	0.0113
COTL1	2.0	0.0128
PTGES2	2.0	0.0029
TEDC2	2.0	0.0055
TPX2	2.0	0.0007
H2AFX	2.0	0.0006
SUV39H1	2.0	0.0091
TROAP	2.0	0.0307
RND3	2.0	0.0367
C5	2.0	0.0206
BCAT2	2.0	0.0090
KIF22	2.0	0.0020
TOMM40	2.0	0.0445

GLB1L2	2.0	0.0369
MCM3	2.0	0.0026
GGH	2.0	0.0114
ANP32E	2.0	0.0037
GINS1	2.0	0.0043
HAUS5	2.0	0.0078
PPFIA4	2.0	0.0322
CHAF1A	2.0	0.0338
MPZL2	1.9	0.0413
ENDOD1	1.9	0.0365
WDHD1	1.9	0.0082
YBX2	1.9	0.0039
POGLUT3	1.9	0.0210
IGFBP2	1.9	0.0150
NUF2	1.9	0.0169
MCM7	1.9	0.0063
UBE2C	1.9	0.0031
WNT7B	1.9	0.0121
BUB1	1.9	0.0033
KIF14	1.9	0.0070
FOXO6	1.9	0.0446
PHGDH	1.9	0.0004
PFKP	1.9	0.0087
CDKN2C	1.9	0.0234
SAAL1	1.9	0.0285
RIOK2	1.9	0.0119
TTK	1.9	0.0081
SH2B2	1.9	0.0235
NUDT8	1.9	0.0353
FANCG	1.9	0.0408
CA12	1.9	0.0037
CCNF	1.9	0.0027
TUBB4B	1.8	0.0015
ENO1	1.8	0.0016
GAMT	1.8	0.0075
BRCA2	1.8	0.0329
ANLN	1.8	0.0059
CKS1B	1.8	0.0044
WDR34	1.8	0.0281
CDT1	1.8	0.0048
TPI1	1.8	0.0032
AC006538.1	1.8	0.0322
NCAPH2	1.8	0.0424
SGO1	1.8	0.0295
P3H4	1.8	0.0138
DTYMK	1.8	0.0088
LY6E	1.8	0.0019
PLEKHO1	1.8	0.0279
PGAM1	1.8	0.0018
MRPL54	1.8	0.0315
TTC5	1.8	0.0395
ASPM	1.8	0.0055
TMEM191A	1.8	0.0192
AURKA	1.8	0.0164
PTTG1	1.8	0.0149
XRCC2	1.8	0.0326

RANBP1	1.8	0.0313
CENPU	1.8	0.0368
TMPRSS13	1.8	0.0237
SGF29	1.8	0.0370
POFUT1	1.8	0.0092
FAM222A	1.8	0.0383
FAM83D	1.8	0.0081
LDHA	1.8	0.0018
CDC20	1.8	0.0051
SPDL1	1.8	0.0213
GAPDH	1.8	0.0059
FANCD2	1.8	0.0040
SNRNP25	1.7	0.0411
LMNB1	1.7	0.0044
HPDL	1.7	0.0163
FN3KRP	1.7	0.0127
HMGB1	1.7	0.0070
HNRNPD	1.7	0.0038
RACGAP1	1.7	0.0020
NEK2	1.7	0.0294
CDCA2	1.7	0.0243
PFKFB3	1.7	0.0060
C9orf40	1.7	0.0435
HMGB2	1.7	0.0062
PLK4	1.7	0.0381
CDCA4	1.7	0.0190
MELTF	1.7	0.0364
ARHGAP11A	1.7	0.0078
ATAD2	1.7	0.0037
AK4	1.7	0.0185
DLGAP5	1.7	0.0080
METRN	1.7	0.0354
PRMT5	1.7	0.0294
FNDC10	1.7	0.0255
E2F7	1.7	0.0224
ASCL2	1.7	0.0246
PCNA	1.7	0.0102
CIP2A	1.7	0.0500
SMAD6	1.7	0.0188
BRI3BP	1.7	0.0094
CDKN3	1.7	0.0375
GALE	1.6	0.0203
DHFR	1.6	0.0289
KNL1	1.6	0.0139
DEPDC1	1.6	0.0288
TONSL	1.6	0.0135
ACOT7	1.6	0.0165
TAGLN2	1.6	0.0052
FANCA	1.6	0.0255
MRPL48	1.6	0.0287
MIS18A	1.6	0.0334
TUBGCP3	1.6	0.0480
PPIF	1.6	0.0110
RPS26	1.6	0.0097
DCXR	1.6	0.0064
SART1	1.6	0.0187

DUSP12	1.6	0.0494
AC027237.1	1.6	0.0181
GMNN	1.6	0.0290
MCM6	1.6	0.0089
CDK1	1.6	0.0110
RAC3	1.6	0.0387
CALM1	1.6	0.0190
KNTC1	1.6	0.0325
DEF8	1.6	0.0420
CDH24	1.6	0.0438
LRRC59	1.5	0.0095
CDCA7L	1.5	0.0398
CCNB1	1.5	0.0106
ELOVL6	1.5	0.0384
CENPH	1.5	0.0366
H2AFZ	1.5	0.0091
RRM1	1.5	0.0098
CDK2	1.5	0.0168
CARD10	1.5	0.0474
CHEK1	1.5	0.0473
REEP4	1.5	0.0212
TYMS	1.5	0.0449
FSCN1	1.5	0.0486
METTL26	1.5	0.0244
TNNT1	1.5	0.0390
PSMC3	1.5	0.0089
BSPRY	1.5	0.0334
LIG1	1.5	0.0129
MRPS2	1.5	0.0200
INCENP	1.5	0.0169
HMMR	1.5	0.0468
KRT80	1.5	0.0148
POLE	1.4	0.0093
EZH2	1.4	0.0398
ITGB4	1.4	0.0483
EIF5A	1.4	0.0346
STMN1	1.4	0.0161
PKM	1.4	0.0121
ADI1	1.4	0.0225
CCNB2	1.4	0.0455
OXCT1	1.4	0.0351
HMGB3	1.4	0.0269
RNF26	1.4	0.0296
LDLRAP1	1.4	0.0445
TOP2A	1.4	0.0153
SAPCD2	1.4	0.0179
SIVA1	1.4	0.0425
ACSF3	1.4	0.0398
GPT2	1.4	0.0339
POLD3	1.4	0.0497
SDF2L1	1.4	0.0391
DHTKD1	1.4	0.0127
WDR62	1.4	0.0349
H1F0	1.4	0.0227
TMPO	1.4	0.0158
TRIM28	1.4	0.0236

SYT12	1.4	0.0197
TCOF1	1.4	0.0165
KNSTRN	1.4	0.0301
H1FX	1.4	0.0186
TFAP4	1.4	0.0423
PARP2	1.4	0.0365
MRTO4	1.4	0.0351
SMC4	1.4	0.0240
NDUFB10	1.4	0.0204
HK2	1.3	0.0360
IDH2	1.3	0.0353
NUP210	1.3	0.0251
USP1	1.3	0.0352
LYAR	1.3	0.0384
POP7	1.3	0.0342
UNC93B1	1.3	0.0414
TIMELESS	1.3	0.0349
TSKU	1.3	0.0239
PRXL2B	1.3	0.0416
ZMIZ1	1.3	0.0307
H2AFV	1.3	0.0466
FAM189B	1.3	0.0396
RECQL4	1.3	0.0406
RPS6KA4	1.3	0.0311
ANKRD40	1.3	0.0402
CCND3	1.3	0.0328
HRAS	1.3	0.0410
PACSIN3	1.3	0.0310
NOP56	1.3	0.0244
TRAP1	1.3	0.0471
MTHFD1	1.3	0.0417
NACC1	1.3	0.0386
FH	1.3	0.0459
WARS	1.3	0.0296
SRM	1.3	0.0339
CTPS1	1.2	0.0490
LMNB2	1.2	0.0334
NET1	1.2	0.0487
SELENOW	1.2	0.0466
BCKDK	1.2	0.0444
S100A14	1.2	0.0425
CNBP	1.2	0.0307
CCHCR1	1.2	0.0354
ANAPC5	1.2	0.0431
UNG	1.2	0.0351
NOLC1	1.1	0.0406
DDX39A	1.1	0.0431
KPNA2	1.1	0.0403
SLC25A39	1.1	0.0496
TFRC	1.1	0.0450

Table 5. 8S. List of significantly up-regulated genes in Plasmax vs DMEM at 18% O_2, passing a P-value< 0.05 and with greater than 2-fold change in expression (Log2FC≥1). 'Infin' indicates infinity-fold based on an undetectable level in DMEM.

Gene	Log2(FC)	P-value
MYL7	infini	0.00005
DHRS2	8.1	0.00025
MX2	6.7	0.00005
MSLN	6.2	0.00315
DUSP9	6.1	0.04030
KRT16	6.1	0.01760
ZBP1	6.0	0.00600
KRT17	6.0	0.00005
APOA1	5.8	0.03065
MT1X	5.8	0.00080
ACTG2	5.8	0.00005
GSTP1	5.7	0.00065
ASCL1	5.3	0.00170
CALB2	5.3	0.00085
SLC15A3	5.0	0.00280
CX3CL1	5.0	0.00100
TNF	5.0	0.00325
FHL2	4.9	0.00060
CD36	4.9	0.00020
S100P	4.8	0.00435
MMP13	4.8	0.00210
DNALI1	4.7	0.03945
CORO1A	4.6	0.00025
IL32	4.6	0.00005
CD74	4.5	0.02975
APOL1	4.5	0.00030
IL24	4.4	0.00265
AHNAK2	4.3	0.00230
MYEOV	4.3	0.00215
RTP4	4.2	0.00825
SCNN1B	4.2	0.00525
ADRA2A	4.2	0.00915
UHRF1	4.1	0.00020
PLAT	4.1	0.00115
ULBP1	4.0	0.00845
TMEM255B	3.9	0.02340
CHAC1	3.9	0.00085
ZNF385B	3.8	0.00030
CDCA7	3.8	0.00810
NES	3.8	0.00205
TNFRSF11B	3.8	0.01045
IFI6	3.8	0.00005
CSF1	3.7	0.00035
PAPSS2	3.7	0.00070
IFIT3	3.7	0.03920
AQP3	3.6	0.00515
PTGES	3.6	0.00140
SGPP2	3.5	0.01790

OASL	3.5	0.00375
IFI44L	3.5	0.00130
KCNH2	3.5	0.01725
AC126175.1	3.5	0.02680
TK1	3.4	0.00005
TENT5B	3.4	0.01935
SOX3	3.4	0.01875
APOL3	3.4	0.00275
BGN	3.4	0.00140
COL1A2	3.4	0.00180
LGALS3	3.4	0.00465
LY6E	3.4	0.00005
UBA7	3.3	0.00025
ITPKA	3.3	0.00805
KCNF1	3.3	0.02200
ST6GALNAC4	3.3	0.02475
BOLA3	3.3	0.01065
E2F2	3.3	0.00285
MT2A	3.3	0.00005
CENPM	3.3	0.00255
NXPH4	3.3	0.00345
HSPG2	3.2	0.00040
IGFBP6	3.2	0.03870
AC087289.1	3.2	0.00235
FSTL4	3.2	0.01060
PXYLP1	3.2	0.00210
PDLIM3	3.2	0.00580
CAPG	3.2	0.00150
MCM10	3.1	0.00290
LMO2	3.1	0.02575
SDK2	3.1	0.00060
XAF1	3.1	0.00030
HIST1H2BO	3.1	0.02750
PSMB9	3.1	0.04310
AL021807.1	3.1	0.04175
AC103770.1	3.1	0.01825
COTL1	3.1	0.00100
ACKR3	3.1	0.00010
FLT4	3.0	0.01220
SOCS2	3.0	0.02465
PRRT3	3.0	0.00130
USP2	3.0	0.01170
COL18A1	3.0	0.00005
MCM5	3.0	0.00030
GAL	3.0	0.01535
RRM2	3.0	0.00005
NUAK2	3.0	0.00895
CAMK2B	2.9	0.00025
SPATS2L	2.9	0.00125
THEMIS2	2.9	0.00990
SYNPO	2.9	0.00315
CDC45	2.9	0.00290
TAGLN	2.9	0.04125
PEG10	2.9	0.04875
CRMP1	2.9	0.02390
MYBL2	2.9	0.00010

SPSB1	2.9	0.02685
HIST3H2BB	2.9	0.00725
E2F8	2.8	0.00755
LRRC10B	2.8	0.04245
MTCL1	2.8	0.00080
NRP1	2.8	0.00050
CCL5	2.8	0.03490
E2F1	2.8	0.00115
ISG15	2.8	0.00005
CCN3	2.8	0.03795
EXO1	2.8	0.00710
NEK3	2.8	0.03610
TNFAIP3	2.8	0.01930
ARID5A	2.8	0.02125
SUSD4	2.7	0.01225
PKMYT1	2.7	0.00745
CMPK2	2.7	0.01000
CEBPB	2.7	0.00005
SCARA3	2.7	0.02055
GINS3	2.7	0.01155
CDC6	2.7	0.00515
GNAZ	2.7	0.02960
ACP5	2.7	0.03300
HMOX1	2.6	0.01090
DCLRE1A	2.6	0.01080
HLA-A	2.6	0.00055
VGF	2.6	0.00010
FIBCD1	2.6	0.02025
CLIC3	2.6	0.00405
DTL	2.6	0.01955
RMI2	2.6	0.00160
WNT7B	2.6	0.00295
PIM1	2.6	0.00545
OAS3	2.6	0.00160
NECAB1	2.6	0.00785
ODC1	2.6	0.00050
MTMR11	2.6	0.01020
PIMREG	2.6	0.04665
NEURL1B	2.5	0.00125
RPS6KL1	2.5	0.00720
RSAD2	2.5	0.03275
CCM2L	2.5	0.04825
KLF11	2.5	0.00385
CXCL8	2.5	0.04140
IKBKE	2.5	0.02055
CTSH	2.5	0.01585
UBALD2	2.5	0.00150
ERRFI1	2.5	0.00150
AC093001.1	2.5	0.01155
APOL6	2.5	0.00325
METRN	2.5	0.00135
PLXND1	2.5	0.00080
CMSS1	2.5	0.02790
POLE2	2.5	0.02035
AC093323.1	2.5	0.00020
NRM	2.5	0.00700

SHANK3	2.4	0.01460
PDZD4	2.4	0.00845
NRCAM	2.4	0.00045
C2CD4C	2.4	0.00845
COL4A5	2.4	0.01720
AEBP1	2.4	0.03130
SELENOM	2.4	0.04640
RAD54L	2.4	0.03870
MATK	2.4	0.00185
TNFAIP2	2.4	0.01240
H1FX	2.3	0.00005
TCF19	2.3	0.00180
CHGA	2.3	0.00060
FGFR3	2.3	0.00305
H1F0	2.3	0.00010
HES6	2.3	0.01110
RTN4R	2.3	0.02730
LFNG	2.3	0.00315
SGF29	2.3	0.00285
LRFN1	2.3	0.04065
CCDC74A	2.3	0.02460
CDCA4	2.3	0.00225
IFIT1	2.3	0.01000
SULT2B1	2.3	0.01435
PODXL	2.3	0.00150
BIRC5	2.3	0.00190
IFI44	2.3	0.00760
GAS6	2.3	0.02410
FOXO6	2.3	0.03600
NRGN	2.3	0.02660
CRABP2	2.3	0.00075
XRCC3	2.2	0.04310
KYNU	2.2	0.01855
DOK7	2.2	0.00045
WDR76	2.2	0.00895
CDT1	2.2	0.00065
CDCA5	2.2	0.00140
ENDOD1	2.2	0.04435
SEMA3B	2.2	0.00100
MELTF	2.2	0.01710
FAM111B	2.2	0.01305
CHTF18	2.2	0.01390
MCM4	2.2	0.00225
SAMD9	2.2	0.00110
ISG20	2.2	0.04995
RNF223	2.2	0.00395
STC1	2.2	0.02535
NPW	2.2	0.03890
TUBB2B	2.2	0.03795
AL645608.7	2.2	0.04935
MEIS3	2.1	0.01090
SMOX	2.1	0.01570
WDR54	2.1	0.02880
TRIP13	2.1	0.01570
POLD2	2.1	0.00070
TCIRG1	2.1	0.00715

PHLDA1	2.1	0.03535
IFI27	2.1	0.00105
FBXO6	2.1	0.04070
TEDC2	2.1	0.00745
MAP3K20	2.1	0.02365
AC080038.1	2.1	0.01235
NLRC5	2.1	0.02615
RBL1	2.1	0.02220
FN1	2.1	0.00925
CALCR	2.1	0.02825
MSX2	2.1	0.00985
ZNF367	2.1	0.01665
RFC2	2.1	0.00300
GPR153	2.1	0.02800
IRF7	2.1	0.00580
C5	2.1	0.01945
SCN1B	2.0	0.03365
UNC93B1	2.0	0.00160
CXXC5	2.0	0.00075
RASGRP1	2.0	0.01120
MAST4	2.0	0.01235
PTGES2	2.0	0.00175
DDX60L	2.0	0.03150
IFI35	2.0	0.00165
MB21D2	2.0	0.02875
TSEN15	2.0	0.00840
AGK	2.0	0.04040
FSCN1	2.0	0.00685
IFITM3	2.0	0.00040
BRIP1	2.0	0.00070
MAFA	2.0	0.02595
NCAPH2	2.0	0.02970
RND3	2.0	0.03410
ITGB4	2.0	0.01020
SYNE2	2.0	0.00610
BRCA2	2.0	0.03135
TSPAN5	2.0	0.03255
BLM	2.0	0.04890
CIT	2.0	0.00720
C6orf141	1.9	0.01805
MCM2	1.9	0.00290
FADS3	1.9	0.01725
HES4	1.9	0.00840
SLC25A28	1.9	0.03510
TRANK1	1.9	0.03450
ARMC9	1.9	0.02530
AURKB	1.9	0.00760
S100A14	1.9	0.00215
PTPRG-AS1	1.9	0.03505
SLC29A1	1.9	0.00760
H2AFX	1.9	0.00125
IQGAP3	1.9	0.01070
PIP5KL1	1.9	0.01845
TLN2	1.9	0.01565
ZNF787	1.9	0.00330
ZNF185	1.9	0.04810

ASCL2	1.9	0.01560
KIFC1	1.9	0.00440
METRNL	1.9	0.00570
HLA-F	1.9	0.01400
MAD2L2	1.9	0.02475
SSRP1	1.9	0.00330
RELB	1.8	0.02485
FOSL2	1.8	0.00910
ARHGEF19	1.8	0.02990
MALRD1	1.8	0.01860
CDC25A	1.8	0.03945
KCNIP3	1.8	0.03515
SERPINE1	1.8	0.02310
ZWINT	1.8	0.01615
KCNJ3	1.8	0.02790
SATB2	1.8	0.03110
C19orf48	1.8	0.00230
FABP5	1.8	0.01635
GALE	1.8	0.02740
LGALS3BP	1.8	0.00280
ACOT7	1.8	0.02025
UBE2T	1.8	0.01835
AKNA	1.8	0.02140
TUBA1B	1.8	0.03160
DNMBP	1.8	0.05000
IFIT5	1.8	0.00550
STAT1	1.8	0.00560
HAUS5	1.8	0.01585
FANCD2	1.7	0.00840
CDH24	1.7	0.02600
BAG3	1.7	0.00125
TUBB	1.7	0.00270
SAAL1	1.7	0.03940
KIF18B	1.7	0.02395
SUV39H1	1.7	0.02860
CTXN1	1.7	0.01695
SKA3	1.7	0.03975
SHCBP1	1.7	0.02840
MISP3	1.7	0.01490
ZC3H12A	1.7	0.02080
KRT80	1.7	0.00310
JAK2	1.7	0.03640
IGFBP2	1.7	0.01990
KIF1A	1.7	0.00900
CDKN2AIPNL	1.7	0.03420
TAP1	1.7	0.00675
RBBP8	1.7	0.00960
CEBPG	1.7	0.00740
FNDC10	1.7	0.01790
PARP12	1.7	0.01130
CSRP1	1.7	0.00465
C21orf58	1.7	0.04250
LIG1	1.7	0.01235
YBX2	1.7	0.01035
CBX4	1.7	0.00395
OVOL1	1.7	0.03770

MCM3	1.7	0.00555
PRAG1	1.7	0.02720
AC124319.1	1.7	0.01015
MCM7	1.7	0.01480
CENPF	1.7	0.01375
ELF4	1.7	0.03575
DHFR	1.7	0.03115
KLF4	1.6	0.04915
ASB13	1.6	0.03985
C16orf91	1.6	0.03070
ENTPD2	1.6	0.03895
ASF1B	1.6	0.01710
SDC4	1.6	0.00630
NRARP	1.6	0.01650
ECE1	1.6	0.00325
HNRNPD	1.6	0.00530
KIF22	1.6	0.00680
GAMT	1.6	0.03400
ZNF703	1.6	0.00780
TRIB3	1.6	0.01190
USP18	1.6	0.01840
BMP7	1.6	0.01225
TFAP4	1.6	0.01705
FANCA	1.6	0.03045
DEF8	1.6	0.02950
EFHD2	1.6	0.04925
EVL	1.6	0.01330
NUP205	1.6	0.03150
RAB31	1.6	0.01325
GTPBP3	1.6	0.04680
TACC3	1.6	0.03955
RHOD	1.6	0.01105
DKK1	1.5	0.02045
BCAT2	1.5	0.03120
RANBP1	1.5	0.03945
CKS1B	1.5	0.02460
TRIM65	1.5	0.01465
HMGB2	1.5	0.01220
APOL2	1.5	0.01765
PKIB	1.5	0.00955
SLC27A2	1.5	0.04150
MMP15	1.5	0.03640
SFXN2	1.5	0.03145
TMSB10	1.5	0.01000
CEP131	1.5	0.02345
NUP210	1.5	0.01210
WFS1	1.5	0.02190
CBX2	1.5	0.00725
SLC1A4	1.5	0.02225
POLD3	1.5	0.03305
RECQL4	1.5	0.02655
KNTC1	1.5	0.04365
TSPAN15	1.5	0.02485
NCAPG2	1.5	0.01420
NFIX	1.5	0.03505
SEMA4C	1.5	0.01355

FZD1	1.5	0.03040
POP7	1.4	0.02140
HERC6	1.4	0.02320
MAT2A	1.4	0.01740
ESPL1	1.4	0.04080
ASS1	1.4	0.01535
MDK	1.4	0.00915
MKI67	1.4	0.01760
TAGLN2	1.4	0.01365
CBX8	1.4	0.03750
SPTBN1	1.4	0.04675
TRIM21	1.4	0.04720
ZNF48	1.4	0.03345
ABCD1	1.4	0.03680
ATF4	1.4	0.01280
ATP1B1	1.4	0.03475
TLE3	1.4	0.04435
UBE2L6	1.4	0.02150
B2M	1.4	0.02760
HSPB8	1.4	0.01400
HMGB1	1.4	0.02635
FKBP5	1.4	0.03925
CDC42EP1	1.4	0.03960
SRM	1.4	0.02015
PSMC3	1.3	0.01655
OLFM1	1.3	0.04505
HELZ2	1.3	0.02200
ATAD2	1.3	0.01835
ADM2	1.3	0.04415
POFUT1	1.3	0.04680
MRPS2	1.3	0.03040
TUBB4B	1.3	0.01905
HIST1H2BK	1.3	0.03950
IER5L	1.3	0.02000
GPRIN1	1.3	0.03475
ARC	1.3	0.04820
DCLRE1B	1.3	0.02385
TONSL	1.3	0.04865
USP1	1.3	0.04465
CA12	1.3	0.02965
LMNB1	1.3	0.02680
SLC7A5	1.3	0.03320
YDJC	1.3	0.04800
SART1	1.3	0.04375
SYT12	1.3	0.03740
BCAM	1.3	0.03205
LMX1B	1.2	0.04205
CELSR2	1.2	0.03910
TCOF1	1.2	0.04320
SLC25A39	1.2	0.03000
TMEM64	1.2	0.03125
TSKU	1.2	0.03690
SLC7A1	1.2	0.03965
DCXR	1.1	0.04725
CYBA	1.1	0.04275
SH3TC1	1.1	0.02965

PKP3	1.1	0.03420
ADGRG1	1.0	0.04800

Table 5. S9. Shown **is** transcripts with higher levels in specific media at both O_2 levels, or at both O_2 levels in specific media.

Plasmax	**DMEM**	**5% O_2**	**18% O_2**
DHRS2	FGFR4	DLX3	LTB
MX2	IGFBP5	DHRS2	LIF
MSLN	FGFR4	NXPH4	EGR3
KRT17	MGAT4A	PCDH1	LGR4
GSTP1	HNRNPLL	PLK1	TBC1D9
ASCL1	CXCL12	FAM83D	DDX60
SLC15A3	OAT	SAPCD2	COL5A1
S100P	PDCD4	GPT2	CXCL12
ULBP1	PLK2	HIF0	THBS1
IFI6	TRGC1	TMPRSS13	OPTN
CHAC1	FAM102B		ST8SIA4
OASL			COL12A1
IFI44L			FRK
TENT5B			AL133367.1
APOL3			FOS
LGALS3			NPNT
UBA7			BCL2
CAPG			SMAD3
XAF1			TCN1
HIST1H2BO			MSMB
SYNPO			SVIL
SPSB1			TCIM
HIST3H2BB			
ISG15			
CMPK2			
CEBPB			
ACP5			
HMOX1			
VGF			
RSAD2			
MTMR11			
OAS3			
ERRFI1			
APOL6			
NRCAM			
H1FX			
H1F0			
IFIT1			
IFI44			
DOK7			
SAMD9			
ISG20			
MEIS3			
NLRC5			
AKNA			
TAP1			
PARP12			
CEBPG			

CBX4
TRIB3
USP18
APOL2
HERC6
TRIM21
ATF4
HELZ2
KLF4
ADM2
HIST1H2BK
IER5L
C16orf91
ARC
DNMBP
IFIT5
STAT1
SERPINE1
FOSL2
FADS3
TRANK1
PIP5KL1
IFI35
IRF7
MSX2

Table 5. 10S. List of gene with protein IDS that are significantly up -regulated in DMEM at 5% O_2 vs 18% O_2. Threshold is P- value< 0.05 and with greater than 1.2-fold change in expression (Log2FC ≥0.3). * indicates to higher transcript level too.

Gene	Protein	Log2(FC)	P-value
TS101	Isoform 2 of Tumor susceptibility gene 101 protein	1.0	0.03
PTH2	Peptidyl-tRNA hydrolase 2 mitochondrial	0.9	0.04
CEBPZ	CCAAT/enhancer-binding protein zeta	0.9	0.03
YLPM1	Isoform 4 of YLP motif-containing protein 1	0.8	0.03
AFTIN	Isoform 2 of Aftiphilin	0.8	0.01
DPP2	Dipeptidyl peptidase 2	0.8	0.03
ERO1A	ERO1-like protein alpha	0.7	0.02
ALDOA	Fructose-bisphosphate aldolase A	0.6	0.00
SYAM	Alanine--tRNA ligase mitochondrial	0.6	0.01
RFC5	Isoform 2 of Replication factor C subunit 5	0.6	0.04
TPD52	Isoform 2 of Tumor protein D52	0.6	0.01
CYC	Cytochrome c	0.6	0.01
ILVBL	Acetolactate synthase-like protein	0.5	0.01

AP3D1	Isoform 4 of AP-3 complex subunit delta-1	0.5	0.04
SNF5	Isoform B of SWI/SNF-related matrix-associated actin-dependent regulator of chromatin subfamily B member 1	0.5	0.03
ENOA*	Alpha-enolase OS=Homo sapiens	0.5	0.00
TRI37	Isoform 2 of E3 ubiquitin-protein ligase TRIM37	0.5	0.01
P4HA1	Isoform 2 of Prolyl 4-hydroxylase subunit alpha-1	0.5	0.01
HMGB2*	High mobility group protein B2	0.5	0.02
G3P	Glyceraldehyde-3-phosphate dehydrogenase	0.5	0.00
HXK2	Hexokinase-2	0.5	0.03
PGAM1*	Phosphoglycerate mutase 1	0.4	0.00
CDK5	Cyclin-dependent-like kinase 5	0.4	0.03
G6PI	Glucose-6-phosphate isomerase	0.4	0.02
APT	Adenine phosphoribosyltransferase	0.3	0.03
BIEA	Biliverdin reductase A	0.3	0.01
HDHD5	Isoform 1 of Haloacid dehalogenase-like hydrolase domain-containing 5	0.3	0.04
PFKAP*	ATP-dependent 6-phosphofructokinase platelet type	0.3	0.01
KPYM*	Pyruvate kinase PKM	0.3	0.03
PUR1	Amidophosphoribosyltransferase	0.3	0.04
IPO4	Isoform 2 of Importin-4	0.3	0.04

Table 5. 11S. List of gene with protein IDS that are significantly up-regulated in DMEM at 18% O_2 vs 5% O_2. Threshold is P- value< 0.05 and with greater than 1.2-fold change in expression (Log2FC ≥0.3).

Gene	Protein	Log2(FC)	P-value
PM2	Phosphomannomutase 2	0.61	0.02
FAC	Protein FAM3C	0.54	0.01
ZPR1	Zinc finger protein ZPR1	0.50	0.00
RS28	40S ribosomal protein S28	0.41	0.04
IFIT1	Interferon-induced protein with tetratricopeptide repeats	0.40	0.01
TFG	Isoform 2 of Protein TFG	0.40	0.03
AAT	Neutral amino acid transporter B(0)	0.38	0.01
IF4G2	Isoform 2 of Eukaryotic translation initiation factor4 gamma 2	0.38	0.02
RBR	Rab3 GTPase-activating protein non-catalytic subunit	0.34	0.04
HN3	Isoform 2 of Heterogeneous nuclear ribonucleoprotein H3	0.31	0.03
TBB3	Tubulin beta-3 chain	0.30	0.03
FAC1	CAAX prenyl protease 1 homolog	0.30	0.04
SA1	Deoxynucleoside triphosphate triphosphohydrolase SAMHD1	0.29	0.04

ZO1	Isoform Short of Tight junction protein ZO-1	0.29	0.04
INF2	Isoform 2 of Inverted formin-2	0.25	0.02

Table 5. 12S. List of gene with protein IDS that are significantly up-regulated in Plasmax at 5% O_2 vs 18% O_2. Threshold is P- value< 0.05 and with greater than 1.2-fold change in expression (Log2FC ≥0.3).

Gene	Protein	Log2(FC)	P-value
IMA1	Importin subunit alpha-1	0.7	0.00
BOLA1	BolA-like protein 1	0.7	0.00
CAMP3	Isoform 2 of Calmodulin-regulated spectrin-associated protein 3	0.6	0.04
NSL1	Kinetochore-associated protein NSL1 homolog	0.6	0.02
PDS5B	Isoform 2 of Sister chromatid cohesion protein PDS5 homolog B	0.5	0.01
SIR1	Isoform 2 of NAD-dependent protein deacetylase sirtuin-1	0.5	0.04
CALM1	Calmodulin-1	0.5	0.00
MOC2A	Molybdopterin synthase sulfur carrier subunit	0.5	0.01
ALDOA	Fructose-bisphosphate aldolase A	0.5	0.02
FDFT	Squalene synthase	0.5	0.01
RM24	39S ribosomal protein L24 mitochondrial	0.5	0.02
LDHA	Isoform 3 of L-lactate dehydrogenase A chain	0.5	0.01
NUBP2	Cytosolic Fe-S cluster assembly factor NUBP2	0.4	0.04
WRIP1	Isoform 2 of ATPase WRNIP1	0.4	0.04
GEMI5	Gem-associated protein 5	0.4	0.01
TFR1	Transferrin receptor protein 1	0.4	0.00
CSK2B	Casein kinase II subunit beta	0.4	0.04
TRI37	Isoform 2 of E3 ubiquitin-protein ligase TRIM37	0.4	0.03
PGK1	Phosphoglycerate kinase 1	0.4	0.00
DDX3X	Isoform 2 of ATP-dependent RNA helicase DDX3X	0.4	0.04
PAIP2	Polyadenylate-binding protein-interacting protein 2	0.4	0.04
RIR2	Isoform 2 of Ribonucleoside-diphosphate reductase subunit M2	0.3	0.00
RL22	60S ribosomal protein L22	0.3	0.04
DDX5	Probable ATP-dependent RNA helicase DDX5	0.3	0.03
TR112	Multifunctional methyltransferase subunit TRM112-like protein	0.3	0.04
THUM3	THUMP domain-containing protein 3	0.3	0.01
PP2AA	Serine/threonine-protein phosphatase 2A catalytic subunit alpha	0.3	0.02
FAS	Fatty acid synthase	0.3	0.01
SMC2	Structural maintenance of chromosomes protein 2	0.3	0.03

G3P	Glyceraldehyde-3-phosphate dehydrogenase	0.3	0.01
COMT	Isoform Soluble of Catechol O-methyltransferase	0.3	0.01
IF5	Eukaryotic translation initiation factor 5	0.3	0.03
MCM6	DNA replication licensing factor MCM6	0.3	0.02

Table 5. 13S. List of gene with protein IDS that are significantly up-regulated in Plasmax at 18% O_2 vs 5% O_2. Threshold is P- value< 0.05 and with greater than 1.2-fold change in expression (Log2FC ≥0.3). * indicates to higher transcript level too.

Gene	Protein	Log2(FC)	P-value
OSBPL9	Isoform 6 of Oxysterol-binding protein-related protein 9	1.0	0.04
ANXA3	Annexin A3	0.8	0.02
K1C17	Keratin type I cytoskeletal 17	0.7	0.00
MVP	Major vault protein	0.7	0.00
GELS	Isoform 2 of Gelsolin	0.7	0.00
CLUS*	Isoform 2 of Clusterin	0.7	0.02
GABT	4-aminobutyrate aminotransferase mitochondrial	0.7	0.00
ISG15	Ubiquitin-like protein ISG15	0.6	0.00
FAHD1	Isoform 2 of Acylpyruvase FAHD1 mitochondrial	0.6	0.00
DHRS2	Dehydrogenase/reductase SDR family member 2 mitochondrial	0.6	0.01
HSPB8*	Heat shock protein beta-8	0.5	0.01
PCYOX*	Isoform 2 of Prenylcysteine oxidase 1	0.5	0.02
SODM	Isoform 4 of Superoxide dismutase [Mn] mitochondrial	0.5	0.01
SPTB2	Spectrin beta chain non-erythrocytic 1	0.5	0.04
HOOK2	Isoform 2 of Protein Hook homolog 2	0.4	0.01
ECHB	Isoform 2 of Trifunctional enzyme subunit beta mitochondrial	0.4	0.01
SAMH1	Deoxynucleoside triphosphate triphosphohydrolase SAMHD1	0.4	0.01
H2AY	Isoform 1 of Core histone macro-H2A.1	0.4	0.04
CH10	10 kDa heat shock protein mitochondrial	0.4	0.02
LMNA	Prelamin-A/C	0.4	0.02
VDAC2	Isoform 1 of Voltage-dependent anion-selective channel protein 2	0.4	0.01
THIK	3-ketoacyl-CoA thiolase peroxisomal	0.4	0.00
ANM6	Isoform 2 of Protein arginine N-methyltransferase 6	0.4	0.03
ADRO	Isoform Long of NADPH:adrenodoxin oxidoreductase mitochondrial	0.3	0.01
PRDX3	Isoform 2 of Thioredoxin-dependent peroxide reductase mitochondrial	0.3	0.02
HYOU1	Hypoxia up-regulated protein 1	0.3	0.03
SNAA	Alpha-soluble NSF attachment protein	0.3	0.02
QCR1	Cytochrome b-c1 complex subunit 1 mitochondrial	0.3	0.02
ANXA2*	Isoform 2 of Annexin A2	0.3	0.03
PRDX5	Isoform Cytoplasmic+peroxisomal of Peroxiredoxin-5 mitochondrial	0.3	0.04

Table 5. 14S. List of gene with protein IDS that are significantly up-regulated in DMEM vs Plasmax at 5% O_2. Threshold is P- value< 0.05 and with greater than 1.2-fold change in expression (Log2FC ≥0.3). * indicates to higher transcript level too.

Gene	Protein	Log2(FC)	P-value
HSBP1	Heat shock factor-binding protein 1	1.2	0
ZMYM3	Isoform 2 of Zinc finger MYM-type protein 3	1.1	0.04
OAT*	Ornithine aminotransferase mitochondrial	1.1	0
ACOD	Acyl-CoA desaturase	1.1	0
LDHA*	Isoform 3 of L-lactate dehydrogenase A chain	0.8	0
CHD3	Isoform 2 of Chromodomain-helicase-DNA-binding protein 3	0.7	0.02
AT5F1	ATP synthase F(0) complex subunit B1 mitochondrial	0.6	0.01
SF3B4	Splicing factor 3B subunit 4	0.6	0
HXK2	Hexokinase-2	0.6	0
FKBP8	Isoform 2 of Peptidyl-prolyl cis-trans isomerase FKBP8	0.6	0.03
KITH	Thymidine kinase cytosolic	0.6	0.01
ATPK	Isoform 2 of ATP synthase subunit f mitochondrial	0.6	0.02
ALDOC	Fructose-bisphosphate aldolase C	0.6	0.01
RIR2	Isoform 2 of Ribonucleoside-diphosphate reductase subunit M2 O	0.5	0
AGR2	Anterior gradient protein 2 homolog	0.5	0.02
PMYT1	Isoform 3 of Membrane-associated tyrosine- and threonine-specific cdc2-inhibitory kinase	0.5	0.02
IPO11	Isoform 2 of Importin-11	0.5	0.01
PDCD4*	Isoform 2 of Programmed cell death protein 4	0.5	0.04
FIS1	Mitochondrial fission 1 protein	0.5	0
DHX40	Isoform 2 of Probable ATP-dependent RNA helicase DHX40	0.5	0.03
PGK1	Phosphoglycerate kinase 1	0.5	0
F213A	Isoform 2 of Redox-regulatory protein FAM213A	0.4	0.04
SLC27A3	Long-chain fatty acid transport protein 3	0.4	0.03
RPS15	40S ribosomal protein S15	0.4	0.04
FBP1*	Fructose-1 6-bisphosphatase 1	0.4	0.01
IDHP	Isocitrate dehydrogenase [NADP] mitochondrial	0.4	0
P4HA1	Isoform 2 of Prolyl 4-hydroxylase subunit alpha-1	0.4	0.02
RPL7	60S ribosomal protein L7	0.4	0
RPL13	60S ribosomal protein L13	0.4	0
SPC24*	Kinetochore protein Spc24	0.4	0.03
GGYF2	Isoform 2 of GRB10-interacting GYF protein 2	0.4	0.01
ILVBL	Acetolactate synthase-like protein	0.4	0.02
ACBP	Isoform 2 of Acyl-CoA-binding protein	0.4	0.02

HID1	Isoform 2 of Protein HID1	0.4	0.02
DJC10	Isoform 2 of DnaJ homolog subfamily C member 10	0.4	0.04
PFKP*	ATP-dependent 6-phosphofructokinase platelet type	0.3	0.02
RABP2	Cellular retinoic acid-binding protein 2	0.3	0.03
TCPZ	T-complex protein 1 subunit zeta	0.3	0.02
HS90A*	Heat shock protein HSP 90-alpha	0.3	0.01
AIP	AH receptor-interacting protein	0.3	0.01
RPL14	60S ribosomal protein L14	0.3	0.03
NHRF1	Na(+)/H(+) exchange regulatory cofactor NHE-RF1	0.3	0.01
RPL15	60S ribosomal protein L15	0.3	0.04
RPL4	60S ribosomal protein L4	0.3	0.02
AL9A1	4-trimethylaminobutyraldehyde dehydrogenase	0.3	0.03
RPL10A	60S ribosomal protein L10a	0.3	0.04
G3P	Glyceraldehyde-3-phosphate dehydrogenase	0.3	0.01
RAB1B	Ras-related protein Rab-1B	0.3	0.04
RPL35A	60S ribosomal protein L35a	0.3	0.04
RPS24	Isoform 2 of 40S ribosomal protein S24	0.3	0.01
UBP2L	Isoform 2 of Ubiquitin-associated protein 2-like	0.3	0.03
HS90B	Heat shock protein HSP 90-beta	0.3	0
KPYM	Pyruvate kinase PKM	0.3	0.01
SF3B6	Splicing factor 3B subunit 6	0.3	0.04
ATX10	Ataxin-10	0.3	0
DUT	Isoform 2 of Deoxyuridine 5'-triphosphate nucleotidohydrolase	0.3	0.04
COMT	Isoform Soluble of Catechol O-methyltransferase	0.3	0

Table 5. 15S. List of genes with protein IDS that are significantly up-regulated in Plasmax vs DMEM at 5% O_2. Threshold is P- value< 0.05 and with greater than 1.2-fold change in expression (Log2FC ≥0.3). * indicates to higher transcript level too.

Gene	Protein	Log2(FC)	P-value
RO52	E3 ubiquitin-protein ligase TRIM21	1.4	0.01
DHRS2*	Dehydrogenase/reductase SDR family member 2 mitochondrial	1.3	0.00
DTX3L	E3 ubiquitin-protein ligase DTX3L	1.1	0.00
ISG15*	Ubiquitin-like protein ISG15	1.0	0.00
KYNU	Kynureninase	1.0	0.00
IFIT1*	Interferon-induced protein with tetratricopeptide repeats 1	1.0	0.00
UB2L6	Ubiquitin/ISG15-conjugating enzyme E2 L6	0.9	0.00
K1C17	Keratin type I cytoskeletal 17	0.8	0.00
METK2	S-adenosylmethionine synthase isoform type-2	0.8	0.00
TBB3	Tubulin beta-3 chain	0.8	0.00
H10	Isoform 2 of Histone H1.0	0.8	0.01
CAPG*	Isoform 2 of Macrophage-capping protein	0.8	0.00
IFIT3	Interferon-induced protein with tetratricopeptide repeats 3	0.8	0.00
OAS2*	Isoform p69 of 2'-5'-oligoadenylate synthase 2	0.7	0.00
DDX58*	Isoform 2 of Probable ATP-dependent RNA helicase DDX58	0.7	0.00
PCKGM	Phosphoenolpyruvate carboxykinase [GTP] mitochondrial	0.6	0.00
HSPB1	Heat shock protein beta-1	0.6	0.00
AL1B1	Aldehyde dehydrogenase X mitochondrial	0.6	0.01
OAS1	2'-5'-oligoadenylate synthase 1	0.6	0.03
STAT1*	Signal transducer and activator of transcription 1-alpha/beta	0.6	0.00
PARP9*	Isoform 2 of Poly [ADP-ribose] polymerase 9	0.6	0.00
ASNS	Isoform 2 of Asparagine synthetase [glutamine-hydrolyzing]	0.6	0.00
RRS1	Ribosome biogenesis regulatory protein homolog	0.6	0.01
ARM10	Isoform 2 of Armadillo repeat-containing protein 10	0.6	0.00
PARP14*	Isoform 1 of Poly [ADP-ribose] polymerase 14	0.5	0.00
TPSN	Isoform 2 of Tapasin	0.5	0.00
LG3BP	Galectin-3-binding protein	0.5	0.00
SCRB2	Lysosome membrane protein 2	0.5	0.00
HNRPU	Isoform 2 of Heterogeneous nuclear ribonucleoprotein U	0.5	0.02
AT1B1	Isoform 2 of Sodium/potassium-transporting ATPase subunit beta-1	0.5	0.00
SAMH1	Deoxynucleoside triphosphate triphosphohydrolase SAMHD1	0.5	0.00
GABT	4-aminobutyrate aminotransferase mitochondrial	0.5	0.00
SLC3A2*	Isoform 2 of 4F2 cell-surface antigen heavy chain	0.5	0.00
BASI	Isoform 2 of Basigin	0.5	0.02
OAS3*	2'-5'-oligoadenylate synthase 3	0.4	0.04
P5CR3	Pyrroline-5-carboxylate reductase 3	0.4	0.04
RADI	Isoform 5 of Radixin	0.4	0.04
PEBP1	Phosphatidylethanolamine-binding protein 1	0.4	0.00
EPIPL	Epiplakin	0.4	0.00

CSK2B	Casein kinase II subunit beta	0.4	0.01
CN37	Isoform CNPI of 2' 3'-cyclic-nucleotide 3'-phosphodiesterase	0.4	0.03
CRK	Adapter molecule crk	0.4	0.02
H1FX*	Histone H1x	0.4	0.01
HMOX2*	Heme oxygenase 2	0.4	0.01
MOC2A	Molybdopterin synthase sulfur carrier subunit	0.4	0.04
ABRAL	Costars family protein ABRACL	0.4	0.03
LEG1	Galectin-1	0.4	0.02
1433S	14-3-3 protein sigma	0.4	0.00
OTUB1	Ubiquitin thioesterase OTUB1	0.4	0.00
NOP58	Nucleolar protein 58	0.4	0.03
ASSY	Argininosuccinate synthase	0.4	0.00
CBX5	Chromobox protein homolog 5	0.4	0.01
SYSC	Serine--tRNA ligase cytoplasmic	0.4	0.00
MYH14	Isoform 6 of Myosin-14	0.4	0.00
PSME1	Proteasome activator complex subunit 1	0.4	0.01
AATC	Aspartate aminotransferase cytoplasmic	0.4	0.00
TRXR1	Isoform 3 of Thioredoxin reductase 1 cytoplasmic	0.4	0.00
FABP5	Fatty acid-binding protein epidermal	0.3	0.02
BAG3	BAG family molecular chaperone regulator 3	0.3	0.03
ROA0	Heterogeneous nuclear ribonucleoprotein A0	0.3	0.00
ANXA2	Isoform 2 of Annexin A2	0.3	0.01
RN213	Isoform 2 of E3 ubiquitin-protein ligase RNF213	0.3	0.04
RBM14	RNA-binding protein 14	0.3	0.03
AT1A1	Isoform 3 of Sodium/potassium-transporting ATPase subunit alpha	0.3	0.04
TBB6	Tubulin beta-6 chain	0.3	0.02
BCLF1	Isoform 2 of Bcl-2-associated transcription factor 1	0.3	0.04
UGDH	UDP-glucose 6-dehydrogenase	0.3	0.01
CALHM1	Calmodulin-1	0.3	0.04
ROA3	Heterogeneous nuclear ribonucleoprotein A3	0.3	0.02
PSME2	Proteasome activator complex subunit 2	0.3	0.00
DSRAD	Isoform 4 of Double-stranded RNA-specific adenosine deaminase	0.3	0.01
MAP4	Microtubule-associated protein 4	0.3	0.01
6PGD	Isoform 2 of 6-phosphogluconate dehydrogenase decarboxylating	0.3	0.01
SYAC	Alanine--tRNA ligase cytoplasmic	0.3	0.02
TRI25	E3 ubiquitin/ISG15 ligase TRIM25	0.3	0.02
E2AK2	Isoform 2 of Interferon-induced double-stranded RNA-activated protein kinase	0.3	0.02
KCRB	Creatine kinase B-type	0.3	0.01
SYYC	Tyrosine--tRNA ligase cytoplasmic	0.3	0.01
TKT	Isoform 2 of Transketolase	0.3	0.02

Table 5. 16S. List of genes with protein IDS that are significantly up-regulated in DMEM vs Plasmax at 18% O_2. Threshold is P- value< 0.05 and with greater than 1.2-fold change in expression (Log2FC ≥0.3). * indicates to higher transcript level too.

Gene	Protein	Log2(FC)	P-value
IMA1	Importin subunit alpha-1	1.0	0.00
KITH	Thymidine kinase cytosolic	1.0	0.00
OAT	Ornithine aminotransferase mitochondrial	1.0	0.00
ACOD	Acyl-CoA desaturase	1.0	0.00
RPL22L	60S ribosomal protein L22-like 1	0.9	0.02
RIR2	Isoform 2 of Ribonucleoside-diphosphate reductase subunit M2	0.9	0.00
BZW2	Basic leucine zipper and W2 domain-containing protein 2	0.8	0.03
HS90B	Heat shock protein HSP 90-beta	0.8	0.00
DPOLA	DNA polymerase alpha catalytic subunit	0.8	0.03
FDFT	Squalene synthase	0.7	0.00
PMYT1	Isoform 3 of Membrane-associated tyrosine- and threonine-specific cdc2-inhibitory kinase	0.7	0.00
AGR2	Anterior gradient protein 2 homolog	0.7	0.00
ARFP2	Arfaptin-2	0.7	0.01
CND2	Condensin complex subunit 2	0.7	0.01
RPL36A	60S ribosomal protein L36a	0.7	0.03
RIR1	Ribonucleoside-diphosphate reductase large subunit	0.7	0.00
FIS1	Mitochondrial fission 1 protein	0.6	0.00
COMT	Isoform Soluble of Catechol O-methyltransferase	0.6	0.00
DHX40	Isoform 2 of Probable ATP-dependent RNA helicase DHX40	0.6	0.03
SMC4*	Structural maintenance of chromosomes protein 4	0.6	0.00
CSDE1	Isoform 2 of Cold shock domain-containing protein E1	0.6	0.00
RAB1B	Ras-related protein Rab-1B	0.6	0.00
BTF3	Transcription factor BTF3	0.6	0.00
IF5	Eukaryotic translation initiation factor 5	0.6	0.00
SPC24	Kinetochore protein Spc24	0.6	0.01
DDX5	Probable ATP-dependent RNA helicase DDX5	0.6	0.00
DHYS	Deoxyhypusine synthase	0.6	0.03
HAT1	Isoform B of Histone acetyltransferase type B catalytic subunit	0.6	0.05
RL30	60S ribosomal protein L30	0.5	0.00
HPDL*	4-hydroxyphenylpyruvate dioxygenase-like protein	0.5	0.01
TPD53	Isoform 5 of Tumor protein D53	0.5	0.00
F8I2	Factor VIII intron 22 protein	0.5	0.03
UBR7	Putative E3 ubiquitin-protein ligase UBR7	0.5	0.04
CDK1*	Cyclin-dependent kinase 1	0.5	0.01
AAAT	Neutral amino acid transporter B(0)	0.5	0.00
HID1	Isoform 2 of Protein HID1	0.5	0.02
ATX10	Ataxin-10	0.5	0.00
SF3B4	Splicing factor 3B subunit 4	0.5	0.00
RPL11	Isoform 2 of 60S ribosomal protein L11	0.5	0.01
RPL7A	60S ribosomal protein L7a	0.5	0.01
TFR1	Transferrin receptor protein 1	0.5	0.00
DNJA1	DnaJ homolog subfamily A member 1	0.5	0.02
LMAN2	Vesicular integral-membrane protein VIP36	0.5	0.00
RPL7	60S ribosomal protein L7	0.5	0.00
IF4G2	Isoform 2 of Eukaryotic translation initiation factor 4 gamma 2	0.5	0.01
NHRF1	Na(+)/H(+) exchange regulatory cofactor NHE-RF1	0.4	0.00
STK24	Isoform A of Serine/threonine-protein kinase 24	0.4	0.03
HS105	Isoform Beta of Heat shock protein 105 kDa	0.4	0.00
8ODP	Isoform p22 of 7 8-dihydro-8-oxoguanine triphosphatase	0.4	0.03

EHD1	EH domain-containing protein 1	0.4	0.02
RLA2	60S acidic ribosomal protein P2	0.4	0.00
SMC2	Structural maintenance of chromosomes protein 2	0.4	0.00
AHSA1	Activator of 90 kDa heat shock protein ATPase homolog 1	0.4	0.02
CYBP	Calcyclin-binding protein	0.4	0.04
DUT	Isoform 2 of Deoxyuridine 5'-triphosphate nucleotide hydrolase mitochondrial	0.4	0.04
EF1A1	Elongation factor 1-alpha 1	0.4	0.04
RPL13	60S ribosomal protein L13	0.4	0.01
RPL22	60S ribosomal protein L22	0.4	0.03
HS90A	Heat shock protein HSP 90-alpha	0.4	0.00
TCTP	Translationally-controlled tumor protein	0.4	0.00
TELO2	Telomere length regulation protein TEL2 homolog	0.4	0.02
FAS	Fatty acid synthase	0.4	0.00
SSRA	Translocon-associated protein subunit alpha	0.4	0.01
CAPR1	Isoform 2 of Caprin-1	0.4	0.03
PAIP2	Polyadenylate-binding protein-interacting protein 2	0.4	0.03
RPL15	60S ribosomal protein L15	0.4	0.02
MCM2*	DNA replication licensing factor MCM2	0.4	0.01
RL32	60S ribosomal protein L32	0.4	0.02
EF2	Elongation factor 2	0.4	0.00
GGYF2	Isoform 2 of GRB10-interacting GYF protein 2	0.4	0.04
MCM6*	DNA replication licensing factor MCM6	0.3	0.01
TR112	Multifunctional methyltransferase subunit TRM112-like protein	0.3	0.04
RPL4	60S ribosomal protein L4	0.3	0.01
UBP2L	Isoform 2 of Ubiquitin-associated protein 2-like	0.3	0.04
MCM7*	DNA replication licensing factor MCM7	0.3	0.01
IPO7	Importin-7	0.3	0.03
GTF2I	Isoform 2 of General transcription factor II-I	0.3	0.02
CBSL	Cystathionine beta-synthase-like protein	0.3	0.01
EIF3D	Isoform 2 of Eukaryotic translation initiation factor 3 subunit D	0.3	0.04
HSP7C	Heat shock cognate 71 kDa protein	0.3	0.04
MCM3*	Isoform 2 of DNA replication licensing factor MCM3	0.3	0.01
TCPB	T-complex protein 1 subunit beta	0.3	0.01
THUM3	THUMP domain-containing protein 3	0.3	0.03
IF4A1	Eukaryotic initiation factor 4A-I	0.3	0.05
XPO2	Isoform 3 of Exportin-2	0.3	0.02
RPL21	60S ribosomal protein L21	0.3	0.04
TCPE	T-complex protein 1 subunit epsilon	0.3	0.03
MCM4*	DNA replication licensing factor MCM4	0.3	0.02
EIF3H	Eukaryotic translation initiation factor 3 subunit H	0.3	0.03
RPL6	60S ribosomal protein L6	0.3	0.03
EIF3B	Eukaryotic translation initiation factor 3 subunit B	0.3	0.02
PSB6	Proteasome subunit beta type-6	0.3	0.02
PUR2	Trifunctional purine biosynthetic protein adenosine-3	0.3	0.03

Table 5. 17 S. List of gene with protein IDS that are significantly up-regulated in Plasmax vs DMEM at 18% O_2. Threshold is P- value< 0.05 and with greater than 1.2-fold change in expression (Log2FC ≥0.3). * indicates to higher transcript level too.

Accession	Protein	Log2(FC)	P-value
MX2*	Isoform 2 of Interferon-induced GTP-binding protein Mx2	2.1	0.02
DHRS2*	Dehydrogenase/reductase SDR family member 2 mitochondrial	1.6	0.00
RPC3	DNA-directed RNA polymerase III subunit RPC3	1.5	0.02
IFIT5*	Interferon-induced protein with tetratricopeptide repeats 5	1.5	0.01
ISG15*	Ubiquitin-like protein ISG15	1.4	0.00
KYNU*	Kynureninase	1.4	0.00
PLD3	Phospholipase D3	1.3	0.03
K1C17	Keratin type I cytoskeletal 17	1.2	0.00
H10	Isoform 2 of Histone H1.	1.2	0.00
TYPH	Isoform 2 of Thymidine phosphorylase	1.2	0.03
CK068	Isoform 2 of UPF0696 protein C11orf68	1.2	0.03
CAPG*	Isoform 2 of Macrophage-capping protein	1.0	0.00
GABT	4-aminobutyrate aminotransferase mitochondrial	1.0	0.00
NMI	N-myc-interactor	0.9	0.01
MVP	Major vault protein	0.9	0.00
UBT2L6*	Ubiquitin/ISG15-conjugating enzyme E2 L6	0.9	0.00
OAS2	Isoform p69 of 2'-5'-oligoadenylate synthase 2	0.9	0.00
SAMD9*	Sterile alpha motif domain-containing protein 9	0.8	0.04
IFIT3*	Interferon-induced protein with tetratricopeptide repeats 3	0.8	0.00
ODO1	2-oxoglutarate dehydrogenase mitochondrial	0.8	0.03
DPP2	Dipeptidyl peptidase 2	0.8	0.04
DYL2	Dynein light chain 2 cytoplasmic	0.8	0.01
ANXA3	Annexin A3	0.8	0.04
DDX58	Isoform 2 of Probable ATP-dependent RNA helicase DDX58	0.7	0.00
GELS	Isoform 2 of Gelsolin	0.7	0.00
TPSN	Isoform 2 of Tapasin	0.7	0.00
CYC	Cytochrome c	0.7	0.00
ANXA2	Isoform 2 of Annexin A2	0.7	0.00
RAP2B	Ras-related protein Rap-2b	0.7	0.02
LGAL3BP*	Galectin-3-binding protein	0.7	0.00
PCKGM	Phosphoenolpyruvate carboxykinase [GTP] mitochondrial	0.7	0.00
RHOG	Rho-related GTP-binding protein RhoG	0.7	0.00
H2AY	Isoform 1 of Core histone macro-H2A.1	0.7	0.00
RPR1B	Regulation of nuclear pre-mRNA domain-containing protein 1B	0.7	0.04
TMED2	Transmembrane emp24 domain-containing protein 2	0.6	0.02
AT131	Manganese-transporting ATPase 13A1	0.6	0.04
HSPB1	Heat shock protein beta-1	0.6	0.00
NAGK	Isoform 2 of N-acetyl-D-glucosamine kinase	0.6	0.05
PRPF3	U4/U6 small nuclear ribonucleoprotein Prp3	0.6	0.03
CLIC4	Chloride intracellular channel protein 4	0.6	0.02
H2AZ	Histone H2A.Z	0.6	0.04
RNF213	Isoform 2 of E3 ubiquitin-protein ligase RNF213	0.6	0.00
NAMPT	Nicotinamide phosphoribosyltransferase	0.6	0.04
MAT2B	Isoform 2 of Methionine adenosyltransferase 2 subunit beta	0.6	0.00
MYH14	Isoform 6 of Myosin-14	0.6	0.00
METK2	S-adenosylmethionine synthase isoform type-2	0.6	0.00
SAMHD1	Deoxynucleoside triphosphate triphosphohydrolase SAMHD1	0.6	0.00
STAT1*	Signal transducer and activator of transcription 1-alpha/beta	0.6	0.00
TBB3	Tubulin beta-3 chain	0.6	0.00
ATP1B1*	Isoform 2 of Sodium/potassium-transporting ATPase subunit beta-1	0.6	0.00

CLIC3*	Chloride intracellular channel protein 3	0.6	0.02
FAHD1	Isoform 2 of Acylpyruvase FAHD1 mitochondrial	0.6	0.01
PARP9	Isoform 2 of Poly [ADP-ribose] polymerase 9	0.6	0.00
PSME1	Proteasome activator complex subunit 1	0.6	0.00
AP4A	Bis(5'-nucleosyl)-tetraphosphatase [asymmetrical]	0.6	0.05
SHLB2	Endophilin-B2	0.6	0.02
NDUA8	NADH dehydrogenase [ubiquinone] 1 alpha subcomplex subunit 8	0.6	0.04
UGDH	UDP-glucose 6-dehydrogenase	0.6	0.00
OAS3*	2'-5'-oligoadenylate synthase 3	0.5	0.03
PCYOX	Isoform 2 of Prenylcysteine oxidase 1	0.5	0.02
ECI1	Enoyl-CoA delta isomerase 1 mitochondrial	0.5	0.04
HMGB2*	High mobility group protein B2	0.5	0.01
EPIPL	Epiplakin	0.5	0.00
SYSC	Serine--tRNA ligase cytoplasmic	0.5	0.00
M2OM	Mitochondrial 2-oxoglutarate/malate carrier protein	0.5	0.01
SGPL1	Sphingosine-1-phosphate lyase 1	0.5	0.01
CN37	Isoform CNPI of 2' 3'-cyclic-nucleotide 3'-phosphodiesterase	0.5	0.03
NLTP	Isoform SCP2 of Non-specific lipid-transfer protein	0.5	0.02
GSDMD	Gasdermin-D	0.5	0.04
DDX17	Probable ATP-dependent RNA helicase DDX17	0.5	0.01
ADRO	Isoform Long of NADPH:adrenodoxin oxidoreductase mitochondrial	0.5	0.00
OTUB1	Ubiquitin thioesterase OTUB1	0.5	0.00
IFIT1	Interferon-induced protein with tetratricopeptide repeats 1	0.5	0.01
NB5R1	NADH-cytochrome b5 reductase 1	0.5	0.03
CBX5	Chromobox protein homolog 5	0.4	0.01
PDXK	Pyridoxal kinase	0.4	0.04
CDC42	Cell division control protein 42 homolog	0.4	0.02
ANXA4	Annexin A4	0.4	0.01
LEG1	Galectin-1	0.4	0.02
ASS1*	Argininosuccinate synthase	0.4	0.00
G6PD	Isoform Long of Glucose-6-phosphate 1-dehydrogenase	0.4	0.03
PON2	Isoform 1 of Serum paraoxonase/arylesterase 2	0.4	0.01
TSN	Translin OS=Homo sapiens	0.4	0.02
ANM6	Isoform 2 of Protein arginine N-methyltransferase 6	0.4	0.02
H1FX*	Histone H1x	0.4	0.02
ETFB	Electron transfer flavoprotein subunit beta	0.4	0.04
SMCA5	SWI/SNF-related matrix-associated actin-dependent regulator of chromatin subfamily A member 5	0.4	0.02
THIK	3-ketoacyl-CoA thiolase peroxisomal	0.4	0.00
TRI37	Isoform 2 of E3 ubiquitin-protein ligase TRIM37	0.4	0.03
SYYC	Tyrosine--tRNA ligase cytoplasmic	0.4	0.00
BAG3*	BAG family molecular chaperone regulator 3	0.4	0.03
TP53B	Isoform 2 of TP53-binding protein 1	0.4	0.03
NH2L1	NHP2-like protein 1	0.4	0.01
CBX3	Chromobox protein homolog 3	0.4	0.04
AT1A1	Isoform 3 of Sodium/potassium-transporting ATPase subunit alpha-1	0.4	0.04
APT	Adenine phosphoribosyltransferase	0.4	0.02
VDAC1	Voltage-dependent anion-selective channel protein 1	0.4	0.01
IVD	Isovaleryl-CoA dehydrogenase mitochondrial	0.4	0.02
THTR	Thiosulfate sulfurtransferase	0.4	0.03
HOOK2	Isoform 2 of Protein Hook homolog 2	0.4	0.04
TRA2B	Isoform 3 of Transformer-2 protein homolog beta	0.4	0.03
THIL	Acetyl-CoA acetyltransferase mitochondrial	0.4	0.00
ARK72	Aflatoxin B1 aldehyde reductase member 2	0.4	0.01
CLIC1	Chloride intracellular channel protein 1	0.3	0.01
CIRBP	Isoform 2 of Cold-inducible RNA-binding protein	0.3	0.03

MBB1A	Isoform 2 of Myb-binding protein 1A	0.3	0.03
TF3C3	General transcription factor 3C polypeptide 3	0.3	0.02
ASNS	Isoform 2 of Asparagine synthetase [glutamine-hydrolyzing]	0.3	0.01
LONM	Lon protease homolog mitochondrial	0.3	0.01
ACON	Aconitate hydratase mitochondrial	0.3	0.01
HEAT6	HEAT repeat-containing protein 6	0.3	0.02
VDAC2	Isoform 1 of Voltage-dependent anion-selective channel protein 2	0.3	0.02
MAP4	Microtubule-associated protein 4	0.3	0.02
4F2	Isoform 2 of 4F2 cell-surface antigen heavy chain	0.3	0.02
MDHM	Malate dehydrogenase mitochondrial	0.3	0.00
1433B	Isoform Short of 14-3-3 protein beta/alpha	0.3	0.02
PRDX3	Isoform 2 of Thioredoxin-dependent peroxide reductase mitochondrial	0.3	0.02
NT5C	5'(3')-deoxyribonucleotidase cytosolic type	0.3	0.03
PA1B3	Platelet-activating factor acetylhydrolase IB subunit gamma	0.3	0.02
TKT	Isoform 2 of Transketolase	0.3	0.02
|1433S	14-3-3 protein sigma	0.3	0.02
6PGD	Isoform 2 of 6-phosphogluconate dehydrogenase decarboxylating	0.3	0.03
ISOC2	Isochorismatase domain-containing protein 2	0.3	0.02
TRXR1	Isoform 3 of Thioredoxin reductase 1 cytoplasmic	0.3	0.02
ROA0	Heterogeneous nuclear ribonucleoprotein A0	0.3	0.02
E2AK2	Isoform 2 of Interferon-induced double-stranded RNA-activated protein kinase	0.3	0.03
DECR	Isoform 2 of 2 4-dienoyl-CoA reductase mitochondrial	0.3	0.01
HNRPC	Isoform C1 of Heterogeneous nuclear ribonucleoproteins C1/C2	0.3	0.02
PSME2	Proteasome activator complex subunit 2	0.3	0.03
AATC	Aspartate aminotransferase cytoplasmic	0.3	0.03
ACTN1	Alpha-actinin-1	0.3	0.04

REFERENCES

Abbas, M., Moradi, F., Hu, W., Regudo, K. L., Osborne, M., Pettipas, J., Atallah, D. S., Hachem, R., Ott-Peron, N., & Stuart, J. A. (2021). Vertebrate cell culture as an experimental approach - limitations and solutions. Comparative biochemistry and physiology. Part B, Biochemistry & molecular biology, 254, 110570.

Ackermann, T., & Tardito, S. (2019). Cell Culture Medium Formulation and Its Implications in Cancer Metabolism. Trends in cancer, 5(6), 329–332.

Adelman, R., Saul, R. L., & Ames, B. N. (1988). Oxidative damage to DNA: relation to species metabolic rate and life span. Proceedings of the National Academy of Sciences, 85(8), 2706-2708.

Al-Ani, A., Toms, D., Kondro, D., Thundathil, J., Yu, Y., & Ungrin, M. (2018). Oxygenation in cell culture: Critical parameters for reproducibility are routinely not reported. PLoS One, 13(10), e0204269.

Alderton, W. K., Cooper, C. E., & Knowles, R. G. (2001). Nitric oxide synthases: structure, function and inhibition. Biochemical journal, 357(3), 593-615.

Alexander, C., Votruba, M., Pesch, U. E., Thiselton, D. L., Mayer, S., Moore, A., & Wissinger, B. (2000). OPA1, encoding a dynamin-related GTPase, is mutated in autosomal dominant optic atrophy linked to chromosome 3q28. Nature genetics, 26(2), 211-215.

Al Hamed, R., Bazarbachi, A. H., & Mohty, M. (2020). Epstein-Barr virus-related post-transplant lymphoproliferative disease (EBV-PTLD) in the setting of allogeneic stem cell transplantation: a comprehensive review from pathogenesis to forthcoming treatment modalities. Bone marrow transplantation, 55(1*), 25-39.*

Allison, S. J., Knight, J. R., Granchi, C., Rani, R., Minutolo, F., Milner, J., & Phillips, R. M. (2014). Identification of LDH-A as a therapeutic target for cancer cell killing via (i) p53/NAD(H)-dependent and (ii) p53-independent pathways. Oncogenesis, 3(5), e102.

Alvarez, S. W., Sviderskiy, V. O., Terzi, E. M., Papagiannakopoulos, T., Moreira, A. L., Adams, S., Sabatini, D. M., Birsoy, K., & Possemato, R. (2017). NFS1 undergoes positive selection in lung tumours and protects cells from ferroptosis. Nature, 551(7682), 639–643.

Álvarez-Lario, B., & Macarrón-Vicente, J. (2010). Uric acid and evolution. Rheumatology, 49(11), 2010-2015.

Anderson, E. J., & Neufer, P. D. (2006). Type II skeletal myofibers possess unique properties that potentiate mitochondrial H2O2 generation. American Journal of Physiology-Cell Physiology, 290(3), C844-C851.

Anand, R., Wai, T., Baker, M. J., Kladt, N., Schauss, A. C., Rugarli, E., & Langer, T. (2014). The i-AAA protease YME1L and OMA1 cleave OPA1 to balance mitochondrial fusion and fission. Journal of Cell Biology, 204(6), 919-929.

Aquilano, K., Vigilanza, P., Baldelli, S., Pagliei, B., Rotilio, G., and Ciriolo, M.R. (2010). Peroxisome proliferator-activated receptor gamma co-activator 1alpha (PGC-1alpha) and sirtuin 1 (SIRT1) reside in mitochondria: possible direct function in mitochondrial biogenesis. J. Biol.Chem. 285, 21590–21599.

Arganda-Carreras, I. (2009). Registration and 3D reconstruction of histological sections: application to mammary gland development.

Arnold, S., de Araujo, G. W., & Beyer, C. (2008). Gender-specific regulation of mitochondrial fusion and fission gene transcription and viability of cortical astrocytes by steroid hormones. J Moll Endocrinol, 41(5), 289-300.

Ashburner, M., Ball, C. A., Blake, J. A., Botstein, D., Butler, H., Cherry, J. M., & Harris, M. A. (2000). Gene ontology: tool for the unification of biology.Nature genetics, 25(1), 25-29
.

Bach, D., Naon, D., Pich, S., Soriano, F. X., Vega, N., Rieusset, J., & Zorzano, A. (2005). Expression of Mfn2, the Charcot-Marie-Tooth neuropathy type 2A gene, in human skeletal muscle: effects of type 2 diabetes, obesity, weight loss, and the regulatory role of tumor necrosis factor α and interleukin-6. Diabetes, 54(9), 2685-2693.

Bachetti, T., Comini, L., Curello, S., Bastianon, D., Palmieri, M., Bresciani, G., & Ferrari, R. (2004). Co-expression and modulation of neuronal and endothelial nitric oxide synthase in human endothelial cells.Journal of molecular and cellular cardiology, 37(5), 939-945.

Bagshaw, O. R., Balardo, C. J., Bland, N. A., Pardiwalla, N., Samuel, I. A., Zoso, S. L., & Stuart, J. A. (2021). Impaired mitochondrial dynamics in disease. In Mitochondrial Dysfunction and Nanotherapeutics (pp. 57-90). Academic Press.

Ban, T., Heymann, J. A. W., Song, Z., Hinshaw, J. E., & Chan, D. C. (2010). OPA1 disease alleles causing dominant optic atrophy have defects in cardiolipin-stimulated GTP hydrolysis and membrane tubulation. Human Molecular Genetics, 19(11), 2113–2122.

Ban, T., Ishihara, T., Kohno, H., Saita, S., Ichimura, A., Maenaka, K., & Ishihara, N. (2017). Molecular basis of selective mitochondrial fusion by heterotypic action between OPA1 and cardiolipin. Nature cell biology, 19(7), 856-863.

Bánfi, B., Molnár, G., Maturana, A., Steger, K., Hegedûs, B., Demaurex, N., and Krause, K.H. (2001). A Ca2+-activated NADPH Oxidase in Testis, Spleen, and Lymph Nodes. J. Biol. Chem. 276, 37594–37601.

Bartel, D. P. (2009). MicroRNAs: target recognition and regulatory functions. cell,136(2), 215-233.

Chen, M., & Manley, J. L. (2009). Mechanisms of alternative splicing regulation: insights from molecular and genomics approaches. Nature reviews Molecular cell biology,10(11), 741-754.

Baur, J. A., & Sinclair, D. A. (2006). Therapeutic potential of resveratrol: the in vivo evidence. Nature reviews Drug discovery, 5(6), 493-506.

Bauzá-Thorbrügge, M., Rodríguez-Cuenca, S., Vidal-Puig, A., Galmés-Pascual, B. M., Sbert-Roig, M., Gianotti, M., & Proenza, A. M. (2019). GPER and ERα mediate estradiol enhancement of mitochondrial function in inflamed adipocytes through a PKA dependent mechanism. The Journal of Steroid Biochemistry and Molecular Biology, 185, 256-267.

Bedard, K., & Krause, K. H. (2007). The NOX family of ROS-generating NADPH oxidases: physiology and pathophysiology. Physiological reviews, 87(1), 245-313.

Biancur, D. E., Paulo, J. A., Małachowska, B., Del Rey, M. Q., Sousa, C. M., Wang, X., & Kimmelman, A. C. (2017). Compensatory metabolic networks in pancreatic cancers upon perturbation of glutamine metabolism. Nature communications,*8*(1), 1-15.

Birsoy, K., Possemato, R., Lorbeer, F. K., Bayraktar, E. C., Thiru, P., Yucel, B., Wang, T., Chen, W. W., Clish, C. B., & Sabatini, D. M. (2014). Metabolic determinants of cancer cell sensitivity to glucose limitation and biguanides. Nature, 508(7494), 108–112.

Block, K., Gorin, Y., & Abboud, H. E. (2009). Subcellular localization of Nox4 and regulation in diabetes. Proceedings of the National Academy of Sciences, 106(34), 14385-14390.

Boonstra, J. J., Tilanus, H. W., & Dinjens, W. N. (2015). Translational research on esophageal adenocarcinoma: from cell line to clinic. Diseases of the Esophagus, *28*(1), 90-96.

Borrás, C., Sastre, J., García-Sala, D., Lloret, A., Pallardó, F. V., & Viña, J. (2003). Mitochondria from females exhibit higher antioxidant gene expression and lower oxidative damage than males. Free radical biology and medicine, 34(5), 546-552.

Boveris, A., & Chance, B. (1973). The mitochondrial generation of hydrogen peroxide. General properties and effect of hyperbaric oxygen. Biochemical Journal, 134(3), 707-716.

Bowers, J. L., Tyulmenkov, V. V., Jernigan, S. C., & Klinge, C. M. (2000). Resveratrol acts as a mixed agonist/antagonist for estrogen receptors α and β. Endocrinology, 141(10), 3657-3667.

Brand, M. D. (2016). Mitochondrial generation of superoxide and hydrogen peroxide as the source of mitochondrial redox signaling. Free Radical Biology and Medicine, 100, 14-31.

Brann, D., Raz, L., Wang, R., Vadlamudi, R., & Zhang, Q. (2012). Oestrogen signalling and neuroprotection in cerebral ischaemia. Journal of neuroendocrinology, 24(1), 34-47.

Brown, M. F., Gratton, T. P., & Stuart, J. A. (2007). Metabolic rate does not scale with body mass in cultured mammalian cells.American Journal of Physiology-Regulatory, Integrative and Comparative Physiology, 292(6), R2115-R2121.

Brown, D. I., & Griendling, K. K. (2009). Nox proteins in signal transduction. Free Radical Biology and Medicine, 47(9), 1239-1253.

Brunelle, J. K., Bell, E. L., Quesada, N. M., Vercauteren, K., Tiranti, V., Zeviani, M., Chandel, N. S. (2005). Oxygen sensing requires mitochondrial ROS but not oxidative phosphorylation. Cell metabolism, 1(6), 409-414.

Buettner, G. R. (1993). The spin trapping of superoxide and hydroxyl free radicals with DMPO (5, 5-dimethylpyrroline-N-oxide): more about iron. Free radical research communications, 19(sup1), s79-s87.

Bylund-Fellenius, A. C., Walker, P. M., Elander, A., Holm, S., Holm, J., & Schersten, T. (1981). Energy metabolism in relation to oxygen partial pressure in human skeletal muscle during exercise. Biochemical Journal, 200(2), 247-255.

Cannon, M. J., Schmid, D. S., & Hyde, T. B. (2010). Review of cytomegalovirus seroprevalence and demographic characteristics associated with infection

Cantor, J. R., & Sabatini, D. M. (2012). Cancer cell metabolism: one hallmark, many faces. Cancer discovery, 2(10), 881-898.

Cantor, J. R., Abu-Remaileh, M., Kanarek, N., Freinkman, E., Gao, X., Louissaint, A., Jr, Lewis, C. A., & Sabatini, D. M. (2017). Physiologic Medium Rewires Cellular Metabolism and Reveals Uric Acid as an Endogenous Inhibitor of UMP Synthase. Cell, 169(2), 258–272.e17.

Capllonch-Amer, G., Llado, I., Proenza, A. M., Garcia-Palmer, F. J., & Gianotti, M. (2014). Opposite effects of 17-estradiol and testosterone on mitochondrial biogenesis and adiponectin synthesis in white adipocytes.J Mol Endocrinol, 52(2), 203-214.

Cardile, V., Chillemi, R., Lombardo, L., Sciuto, S., Spatafora, C., & Tringali, C. (2007). Antiproliferative activity of methylated analogues of E-and Z-resveratrol. Zeitschrift für Naturforschung C, 62(3-4), 189-195.

Carreau, A., Hafny-Rahbi, B. El, Matejuk, A., Grillon, C., and Kieda, C. (2011). Why is the partial oxygen pressure of human tissues a crucial parameter? Small molecules and hypoxia. J. Cell. Mol.Med. 15, 1239–1253.

Carrera, S., de Verdier, P. J., Khan, Z., Zhao, B., Mahale, A., Bowman, K. J., & Macip, S. (2010). Protection of cells in physiological oxygen tensions against DNA damage-induced apoptosis. Journal of Biological Chemistry, 285(18), 13658-13665.

Cassidy-Stone, A., Chipuk, J. E., Ingerman, E., Song, C., Yoo, C., Kuwana, T., & Nunnari, J. (2008). Chemical inhibition of the mitochondrial division dynamin reveals its role in Bax/Bak-dependent mitochondrial outer membrane permeabilization. Developmental cell,14(2), 193-204.

Chan, D. C. (2012). Fusion and fission: interlinked processes critical for mitochondrial health. Annual review of genetics, 46, 265-287.

Chandel, N. S., McClintock, D. S., Feliciano, C. E., Wood, T. M., Melendez, J. A., Rodriguez, A. M., & Schumacker, P. T. (2000). Reactive oxygen species generated at mitochondrial complex III stabilize hypoxia-inducible factor-1α during hypoxia: a mechanism of O2 sensing. Journal of Biological Chemistry, 275(33), 25130-25138.

Chandrasekera, P. C., & Pippin, J. J. (2014). Of rodents and men: species-specific glucose regulation and type 2 diabetes research. ALTEX-Alternatives to animal experimentation, 31(2), 157-176.

Checa, J., & Aran, J. M. (2020). Reactive Oxygen Species: Drivers of Physiological and Pathological Processes. Journal of inflammation research, *13*, 1057–1073.

Chen, H., Chomyn, A., & Chan, D. C. (2005). Disruption of fusion results in mitochondrial heterogeneity and dysfunction. Journal of Biological Chemistry, 280(28), 26185-26192.

Chen, F., Qian, L. H., Deng, B., Liu, Z. M., Zhao, Y., & Le, Y. Y. (2013). Resveratrol protects vascular endothelial cells from high glucose–Induced apoptosis through Inhibition of NADPH oxidase activation–driven oxidative stress. CNS neuroscience & therapeutics, 19(9), 675-681.

Chen, K. H., Dasgupta, A., Ding, J., Indig, F. E., Ghosh, P., & Longo, D. L. (2014). Role of mitofusin 2 (Mfn2) in controlling cellular proliferation. The FASEB Journal, 28(1), 382-394.

Chen, Y., Zhao, Q., Yang, X., Yu, X., Yu, D., & Zhao, W. (2019). Effects of cobalt chloride on the stem cell marker expression and osteogenic differentiation of stem cells from human exfoliated deciduous teeth. Cell Stress and Chaperones, 24(3), 527-538.

Chen, H., Detmer, S. A., Ewald, A. J., Griffin, E. E., Fraser, S. E., & Chan, D. C. (2003). Mitofusins Mfn1 and Mfn2 coordinately regulate mitochondrial fusion and are essential for embryonic development. The Journal of cell biology, 160(2), 189-200.

Chen, Y., & Dorn, G. W. (2013). PINK1-phosphorylated mitofusin 2 is a Parkin receptor for culling damaged mitochondria. Science, 340(6131), 471-475.

Chen J. (2016). The Cell-Cycle Arrest and Apoptotic Functions of p53 in Tumor Initiation and Progression. Cold Spring Harbor perspectives in medicine, 6(3), a026104.

Cipolat, S., De Brito, O. M., Dal Zilio, B., & Scorrano, L. (2004). OPA1 requires mitofusin 1 to promote mitochondrial fusion. Proceedings of the National Academy of Sciences of the United States of America, 101(45), 15927–15932.

Circu, M. L., & Aw, T. Y. (2010). Reactive oxygen species, cellular redox systems, and apoptosis. Free Radical Biology and Medicine, 48(6), 749-762.

Civiletto, G., Varanita, T., Cerutti, R., Gorletta, T., Barbaro, S., Marchet, S., & Zeviani, M. (2015). Opa1 overexpression ameliorates the phenotype of two mitochondrial disease mouse models. Cell metabolism, 21(6), 845-854.Current opinion in chemical biology, 12(5), 483-490.

Cole, S. P. (2014). Multidrug resistance protein 1 (MRP1, ABCC1), a "multitasking" ATP-binding cassette (ABC) transporter. Journal of Biological Chemistry, 289(45), 30880-30888.

Davidson, S. M., Jonas, O., Keibler, M. A., Hou, H. W., Luengo, A., Mayers, J. R., & Vander Heiden, M. G. (2017). Direct evidence for cancer-cell-autonomous extracellular protein catabolism in pancreatic tumors. Nature medicine, 23(2), 235-241.

Davies, H., Bignell, G. R., Cox, C., Stephens, P., Edkins, S., Clegg, S., & Futreal, P. A. (2002). Mutations of the BRAF gene in human cancer. Nature, 417(6892), 949-954.

Delettre, C., Griffoin, J. M., Kaplan, J., Dollfus, H., Lorenz, B., Faivre, L., & Hamel, C. P. (2001). Mutation spectrum and splicing variants in the OPA1 gene. Human genetics, 109(6), 584-591.

de Oliveira, M. R., Nabavi, S. F., Manayi, A., Daglia, M., Hajheydari, Z., & Nabavi, S. M. (2016). Resveratrol and the mitochondria: From triggering the intrinsic apoptotic pathway to inducing mitochondrial biogenesis, a mechanistic view. Biochimica et Biophysica Acta (BBA)-General Subjects, 1860(4), 727-745.

De Paepe, B., & Van Coster, R. (2017). A critical assessment of the therapeutic potential of resveratrol supplements for treating mitochondrial disorders. Nutrients, 9(9), 1017.

del Mar Blanquer-Rosselló, M., Hernández-López, R., Roca, P., Oliver, J., & Valle, A. (2017). Resveratrol induces mitochondrial respiration and apoptosis in SW620 colon cancer cells. Biochimica et Biophysica Acta (BBA)-General Subjects, 1861(2), 431-440.

Demetrius, L. (2005). Of mice and men: when it comes to studying ageing and the means to slow it down, mice are not just small humans. EMBO reports, 6(S1), S39-S44.

Detmer, S. A., & Chan, D. C. (2007). Functions and dysfunctions of mitochondrial dynamics. Nature reviews Molecular cell biology, 8(11), 870-879.

Diebold, I., Petry, A., Hess, J., and Görlach, A. (2010). The NADPH oxidase subunit NOX4 is a new target gene of the hypoxia-inducible factor-1. Mol. Biol. Cell 21, 2087–2096.

Dobin, A., Davis, C. A., Schlesinger, F., Drenkow, J., Zaleski, C., Jha, S., & Gingeras, T. R. (2013). STAR: ultrafast universal RNA-seq aligner. Bioinformatics, 29(1), 15-21.

Dolinsky, V. W., Rogan, K. J., Sung, M. M., Zordoky, B. N., Haykowsky, M. J., Young, M. E., & Dyck, J. R. (2013). Both aerobic exercise and resveratrol supplementation attenuate doxorubicin-induced cardiac injury in mice. American Journal of Physiology-Endocrinology and Metabolism, 305(2), E243-E253.

Druker, B. J., Tamura, S., Buchdunger, E., Ohno, S., Segal, G. M., Fanning, S., & Lydon, N. B. (1996). Effects of a selective inhibitor of the Abl tyrosine kinase on the growth of Bcr–Abl positive cells. Nature medicine, 2(5), 561-566.

Eagle, H. (1955). Nutrition needs of mammalian cells in tissue culture. Science 122, 501–514.

Engelman, J. A., Zejnullahu, K., Mitsudomi, T., Song, Y., Hyland, C., Park, J. O., & Jänne, P. A. (2007). MET amplification leads to gefitinib resistance in lung cancer by activating ERBB3 signaling. science, 316(5827), 1039-1043.

Earle, W. R., ING, T., Straus, N. P., BRowN, M. F., & SHELToN, E. M. M. A. (1943). Changes Seen in the Living Cells. Journal, 4, 165.

Eiyama, A., & Okamoto, K. (2015). PINK1/Parkin-mediated mitophagy in mammalian cells.Current opinion in cell biology, 33, 95-101.

Elbaz-Alon, Y., Eisenberg-Bord, M., Shinder, V., Stiller, S. B., Shimoni, E., Wiedemann, N., Geiger, T., & Schuldiner, M. (2015). Lam6 Regulates the Extent of Contacts between Organelles.Cell reports, 12(1), 7–14.

Edfors, F., Danielsson, F., Hallström, B. M., Käll, L., Lundberg, E., Pontén, F., & Uhlén, M. (2016). Gene-specific correlation of RNA and protein levels in human cells and tissues. Molecular systems biology, 12(10), 883.

Elbaz-Alon, Y., Rosenfeld-Gur, E., Shinder, V., Futerman, A. H., Geiger, T., & Schuldiner, M. (2014). A dynamic interface between vacuoles and mitochondria in yeast. Developmental cell, 30(1), 95–102.

Elkalaf, M., Anděl, M., and Trnka, J. (2013). Low glucose but not galactose enhances oxidative mitochondrial metabolism in C2C12 myoblasts and myotubes. PLoS One 8, e70772

Elsea, S. H., & Lucas, R. E. (2002). The mousetrap: what we can learn when the mouse model does not mimic the human disease. ILAR journal, 43(2), 66-79.

Engelfried, K., Vorgerd, M., Hagedorn, M., Haas, G., Gilles, J., Epplen, J. T., & Meins, M. (2006). Charcot-Marie-Tooth neuropathy type 2A: novel mutations in the mitofusin 2 gene (MFN2). BMC medical genetics, 7(1), 1-7.

Eura, Y., Ishihara, N., Yokota, S., & Mihara, K. (2003). Two mitofusin proteins, mammalian homologues of FZO, with distinct functions are both required for mitochondrial fusion. Journal of biochemistry, 134(3), 333-344.

Bathke, J., Konzer, A., Remes, B., McIntosh, M., & Klug, G. (2019). Comparative analyses of the variation of the transcriptome and proteome of Rhodobacter sphaeroides throughout growth. BMC genomics, 20(1), 1-13.

Farrell, H. E., & Stevenson, P. G. (2019). Cytomegalovirus host entry and spread. Journal of General Virology, 100(4), 545-553.

Felty, Q., Xiong, W. C., Sun, D., Sarkar, S., Singh, K. P., Parkash, J., & Roy, D. (2005). Estrogen-induced mitochondrial reactive oxygen species as signal-transducing messengers. Biochemistry, 44(18), 6900-6909.

Ferguson, S. M., & De Camilli, P. (2012). Dynamin, a membrane remodeling GTPase. Nature reviews Molecular cell biology, 13(2), 75-88.

Fernandez-Marcos, P. J., & Auwerx, J. (2011). Regulation of PGC-1α, a nodal regulator of mitochondrial biogenesis.The American journal of clinical nutrition, 93(4), 884S–90.

Ferrick, D. A., Neilson, A., & Beeson, C. (2008). Advances in measuring cellular bioenergetics using extracellular flux. Drug discovery today, 13(5-6), 268-274.

Filadi, R., Pendin, D., & Pizzo, P. (2018). Mitofusin 2: from functions to disease. Cell death & disease, 9(3), 1-13.

Fiocchetti, M., Ascenzi, P., & Marino, M. (2012). Neuroprotective effects of 17β-estradiol rely on estrogen receptor membrane initiated signals. Frontiers in physiology, 3, 73.

Fonseca, J., Moradi, F., Valente, A. J., & Stuart, J. A. (2018). Oxygen and glucose levels in cell culture media determine resveratrol's effects on growth, hydrogen peroxide production, and mitochondrial dynamics. Antioxidants, 7(11), 157.

Forrester, S. J., Kikuchi, D. S., Hernandes, M. S., Xu, Q., & Griendling, K. K. (2018). Reactive oxygen species in metabolic and inflammatory signaling. Circulation research, 122(6), 877-902.

Förstermann, U., & Sessa, W. C. (2012). Nitric oxide synthases: regulation and function. European heart journal, 33(7), 829-837.

Forsyth, N. R., Musio, A., Vezzoni, P., Simpson, A. H. R., Noble, B. S., & McWhir, J. I. M. (2006). Physiologic oxygen enhances human embryonic stem cell clonal recovery and reduces chromosomal abnormalities. Cloning and stem cells, 8(1), 16-23.

Franco, A., Kitsis, R. N., Fleischer, J. A., Gavathiotis, E., Kornfeld, O. S., Gong, G.,& Chen, Y. (2016). Correcting mitochondrial fusion by manipulating mitofusin conformations. Nature, 540(7631), 74-79.

Freshney, R. I. (2015). Culture of animal cells: a manual of basic technique and specialized applications. John Wiley & Sons.

Frezza, C., Cipolat, S., De Brito, O. M., Micaroni, M., Beznoussenko, G. V., Rudka, T., & Scorrano, L. (2006). OPA1 controls apoptotic cristae remodeling independently from mitochondrial fusion.Cell, 126(1), 177-189.

Galiniak, S., Aebisher, D., & Bartusik-Aebisher, D. (2019). Health benefits of resveratrol administration. Acta biochimica polonica, 66(1), 13-21.

Galmes-Pascual, B. M., Nadal-Casellas, A., Bauza-Thorbrügge, M., Sbert-Roig, M., Garcia-Palmer, F. J., Proenza, A. M., & Llado, I. (2017). 17β-estradiol improves hepatic mitochondrial biogenesis and function through PGC1B.*J*. Endocrinol, 232, 297-308.

Gehm, B. D., McAndrews, J. M., Chien, P. Y., & Jameson, J. L. (1997). Resveratrol, a polyphenolic compound found in grapes and wine, is an agonist for the estrogen receptor. Proceedings of the National Academy of Sciences, 94(25), 14138-14143.

Gertz, M., Nguyen, G. T. T., Fischer, F., Suenkel, B., Schlicker, C., Fränzel, B., & Steegborn, C. (2012). A molecular mechanism for direct sirtuin activation by resveratrol. PloS one, 7(11), e49761.

Gey, G. O., & Gey, M. K. (1936). The maintenance of human normal cells and tumor cells in continuous culture: I. Preliminary report: cultivation of mesoblastic tumors and normal tissue and notes on methods of cultivation. The American Journal of Cancer, 27(1), 45-76.

Giorgio, M., Migliaccio, E., Orsini, F., Paolucci, D., Moroni, M., Contursi, C., & Pelicci, P. G. (2005). Electron transfer between cytochrome c and p66Shc generates reactive oxygen species that trigger mitochondrial apoptosis. Cell, 122(2), 221-233.

Gnaiger, E. (2001). Bioenergetics at low oxygen: dependence of respiration and phosphorylation on oxygen and adenosine diphosphate supply. Respir. Physiol. 128, 277–297.

Golikov, M. V., Karpenko, I. L., Lipatova, A. V., Ivanova, O. N., Fedyakina, I. T., Larichev, V. F., &
Ivanov, A. V. (2022). Cultivation of Cells in a Physiological Plasmax Medium Increases Mitochondrial Respiratory Capacity and Reduces Replication Levels of RNA Viruses. Antioxidants, 11(1), 97.

Gomes, L. C., Di Benedetto, G., & Scorrano, L. (2011). During autophagy mitochondria elongate, are spared from degradation and sustain cell viability. Nature cell biology, 13(5), 589-598.

Graham, K.A., Kulawiec, M., Owens, K.M., Li, X., Desouki, M.M., Chandra, D., and Singh, K.K. (2010). NADPH oxidase 4 is an oncoprotein localized to mitochondria. Cancer Biol. Ther. 10, 223–231.

Grandemange, S., Herzig, S., & Martinou, J. C. (2009). Mitochondrial dynamics and cancer. Seminars in cancer biology, 19(1), 50–56.

Gregg, J.L., Turner, R.M., Chang, G., Joshi, D., Zhan, Y., Chen, L., and Maranchie, J.K. (2014). Nadph oxidase nox4 supports renal tumorigenesis by promoting the expression and nuclear accumulation of hif2a. Cancer Res. 74, 3501–3511.

Griendling, K. K., Touyz, R. M., Zweier, J. L., Dikalov, S., Chilian, W., Chen, Y. R., & Bhatnagar, A. (2016). Measurement of reactive oxygen species, reactive nitrogen species, and redox dependent signaling in the cardiovascular system: a scientific statement from the American Heart Association. Circulation research, 119(5), e39-e75.

Grivennikova, V. G., Kareyeva, A. V., & Vinogradov, A. D. (2018). Oxygen-dependence of mitochondrial ROS production as detected by Amplex Red assay. Redox biology, 17, 192-199.

Gruber, C. J., Tschugguel, W., Schneeberger, C., & Huber, J. C. (2002). Production and actions of estrogens. New England Journal of Medicine, 346(5), 340-352.

Gui, D. Y., Sullivan, L. B., Luengo, A., Hosios, A. M., Bush, L. N., Gitego, N., Davidson, S. M., Freinkman, E., Thomas, C. J., & Vander Heiden, M. G. (2016). Environment Dictates Dependence on Mitochondrial Complex I for NAD+ and Aspartate Production and Determines Cancer Cell Sensitivity to Metformin. Cell metabolism, 24(5), 716–727.

Gupta, V., & Krishan, A. (1982). Effect of oxygen concentration on the growth and drug sensitivity of human melanoma cells in soft-agar clonogenic assay. Cancer research, 42(3), 1005-1007.

Gupte, A. A., Pownall, H. J., & Hamilton, D. J. (2015). Estrogen: an emerging regulator of insulin action and mitochondrial function. Journal of diabetes research, 2015.

Habler, O.P., and Messmer, K.F. (1997). The physiology of oxygen transport. Transfus. Sci. 18, 425–435.

Halliwell, B. (2003). Oxidative stress in cell culture: An under-appreciated problem? FEBS Lett. 540, 3–6.

Halliwell, B. (2014). Cell culture, oxidative stress, and antioxidants: avoiding pitfalls. Biomedical journal, 37(3), 99.

Halliwell, B., & Gutteridge, J. M. (2015). Free radicals in biology and medicine. Oxford university press, USA.

Handy, D. E., & Loscalzo, J. (2012). Redox regulation of mitochondrial function. Antioxidants & redox signaling, 16(11), 1323-1367.

Harris, M. A. (2004). The gene ontology (GO) database and informatics resource: WCB.

Hayes, J. D., Dinkova-Kostova, A. T., & Tew, K. D. (2020). Oxidative Stress in Cancer.Cancer Cell.

Hayflick, L., and Moorhead, P.S. (1961). The serial cultivation of human diploid cell strains. Exp.Cell Res. 25, 585–621

Hewitt, S. C., & Korach, K. S. (2018). Estrogen receptors: new directions in the new millennium. Endocrine reviews, 39(5), 664-675.

Hilenski, L.L., Clempus, R.E., Quinn, M.T., Lambeth, J.D., and Griendling, K.K. (2004). Distinctsubcellular localizations of Nox1 and Nox4 in vascular smooth muscle cells. Arterioscler. Thromb. Vasc. Biol. 24, 677–683.

Hima, S., & Sreeja, S. (2015). Regulatory role of estrogen-induced reactive oxygen species in the modulatory function of UCP 2 in papillary thyroid cancer cells. IUBMB life, 67(11), 837-846.

Hirayama, A., Kami, K., Sugimoto, M., Sugawara, M., Toki, N., Onozuka, H., & Soga, T. (2009). Quantitative metabolome profiling of colon and stomach cancer microenvironment by capillary electrophoresis time-of-flight mass spectrometry. Cancer research, 69(11), 4918-4925.

Hirschey, M. D., DeBerardinis, R. J., Diehl, A., Drew, J. E., Frezza, C., Green, M. F., Jones, L. W., Ko, Y. H., Le, A., Lea, M. A., Locasale, J. W., Longo, V. D., Lyssiotis, C. A., McDonnell, E., Mehrmohamadi, M., Michelotti, G., Muralidhar, V., Murphy, M. P., Pedersen, P. L.,

Poore, B., Target Validation Team (2015). Dysregulated metabolism contributes to oncogenesis. Seminars in cancer biology, 35 Suppl, S129–S150.

Hock, M. B., & Kralli, A. (2009). Transcriptional control of mitochondrial biogenesis and function. Annual review of physiology, 71, 177–203.

Hoffman, D.L., and Brookes, P.S. (2009). Oxygen sensitivity of mitochondrial reactive oxygen species generation depends on metabolic conditions. J. Biol. Chem. 284, 16236–16245.

Hoffman, D.L., Salter, J.D., and Brookes, P.S. (2007). Response of mitochondrial reactive oxygen species generation to steady-state oxygen tension: implications for hypoxic cell signaling. Am. J.Physiol. Heart Circ. Physiol. 292, H101-8.

Holland, H. D. (2006). The oxygenation of the atmosphere and oceans. Philosophical Transactions of the Royal Society B: Biological Sciences, 361(1470), 903-915.

Holmström, K.M., and Finkel, T. (2014). Cellular mechanisms and physiological consequences of redox-dependent signalling. Nat. Rev. Mol. Cell Biol. 15, 411–421.

Howitz, K. T., Bitterman, K. J., Cohen, H. Y., Lamming, D. W., Lavu, S., Wood, J. G., Zipkin, R. E., Chung, P., Kisielewski, A., Zhang, L. L., Scherer, B., & Sinclair, D. A. (2003). Small molecule activators of sirtuins extend Saccharomyces cerevisiae lifespan. Nature, 425(6954), 191–196.

Huang, B. K., & Sikes, H. D. (2014). Quantifying intracellular hydrogen peroxide perturbations in terms of concentration. Redox biology, 2, 955-962.

Huang, Y. L., Lin, Y. C., Lin, C. C., Chen, W. M., Chen, B., & Lee, H. (2018). High Glucose Induces VEGF-C Expression via the LPA1/3-Akt-ROS-LEDGF Signaling Axis in Human Prostate Cancer PC-3 Cells. Cellular physiology and biochemistry. International journal of experimental cellular physiology, biochemistry, and pharmacology, 50(2), 597–611.

Huang, D. W., Sherman, B. T., & Lempicki, R. A. (2009). Systematic and integrative analysis of large gene lists using DAVID bioinformatics resources. Nature protocols, 4(1), 44-57.

Hui, S., Ghergurovich, J. M., Morscher, R. J., Jang, C., Teng, X., Lu, W., & White, E. (2017). Glucose feeds the TCA cycle via circulating lactate. Nature, 551(7678), 115-118.

Ivanovic Z. (2009). Hypoxia or in situ normoxia: The stem cell paradigm. Journal of cellular physiology, 219(2), 271–275.

Jagannathan, L., Cuddapah, S., & Costa, M. (2016). Oxidative stress under ambient and physiological oxygen tension in tissue culture. Current pharmacology reports, 2(2), 64-72.

Jang, M., Cai, L., Udeani, G. O., Slowing, K. V., Thomas, C. F., Beecher, C. W., & Moon, R. C. (1997). Cancer chemopreventive activity of resveratrol, a natural product derived from grapes. Science, 275(5297), 218-220.

Jensen, P. K. (1966). Antimycin-insensitive oxidation of succinate and reduced nicotinamide-adenine dinucleotide in electron-transport particles II. Steroid effects. Biochimica et Biophysica Acta (BBA)-Enzymology and Biological Oxidation, 122(2), 167-174.

Jheng, H. F., Tsai, P. J., Guo, S. M., Kuo, L. H., Chang, C. S., Su, I. J.,& Tsai, Y. S. (2012). Mitochondrial fission contributes to mitochondrial dysfunction and insulin resistance in skeletal muscle. Molecular and cellular biology, 32(2), 309-319.

Jones, D.P., and Sies, H. (2015). The Redox Code. Antioxid. Redox Signal. 23, 734–746.

Juan SH, Chen JJ, Chen CH, Lin H, Cheng CF, Liu JC, Hsieh MH, Chen YL, Chao HH, Chen TH, et al. (2004) 17-Estradiol inhibits cyclic strain-induced endothelin-1 gene expression within vascular endothelial cells. Am J Physiol Heart Circ Physiol 287:H1254–H1261.

Kamata, T. (2009). Roles of Nox1 and other Nox isoforms in cancer development. Cancer Sci. 100, 1382–1388.

Kamerkar, S. C., Kraus, F., Sharpe, A. J., Pucadyil, T. J., & Ryan, M. T. (2018). Dynamin-related protein 1 has membrane constricting and severing abilities sufficient for mitochondrial and peroxisomal fission. Nature communications, 9(1), 1-15.

Kanki, T., Ohgaki, K., Gaspari, M., Gustafsson, C.M., Fukuoh, A., Sasaki, N., Hamasaki, N., and Kang, D. (2004). Architectural role of mitochondrial transcription factor A in maintenance of human mitochondrial DNA. Mol. Cell. Biol. 24, 9823–9834.

Keeley, T. P., & Mann, G. E. (2019). Defining physiological normoxia for improved translation of cell physiology to animal models and humans. Physiological reviews, 99(1), 161-234.

Kelley, D. E., He, J., Menshikova, E. V., & Ritov, V. B. (2002). Dysfunction of mitochondria in human skeletal muscle in type 2 diabetes. Diabetes,51(10), 2944-2950.

Kelly, D. P., & Scarpulla, R. C. (2004). Transcriptional regulatory circuits controlling mitochondrial biogenesis and function. Genes & development, 18(4), 357-368.

Kim, Seung Wook, Sun-Jin Kim, Robert R. Langley, and Isaiah J. Fidler. Modulation of the cancer cell transcriptome by culture media formulations and cell density. International journal of oncology 46, no. 5 (2015): 2067-2075.

Kim, E. Y., Chung, T. W., Han, C. W., Park, S. Y., Park, K. H., Jang, S. B., & Ha, K. T. (2019). A Novel Lactate Dehydrogenase Inhibitor, 1-(Phenylseleno)-4-(Trifluoromethyl) Benzene, Suppresses Tumor Growth through Apoptotic Cell Death. Scientific reports, 9(1), 3969.

Kipp, J. L., & Ramirez, V. D. (2001). Effect of estradiol. diethylstilbestrol, and resveratrol on F0F1-ATPase activity from mitochondrial preparations of rat heart, liver, and brain. Endocrine, 15(2), 165-175.

Klinge CM(2008). Estrogenic control of mitochondrial function and biogenesis. J Cell Biochem 105(6):1342-1351.

Klinge, C. M. (2001). Estrogen receptor interaction with estrogen response elements. Nucleic acids research, 29(14), 2905-2919.

Klingenberg, M (2008). The ADP and ATP transport in mitochondria and its carrier. Biochimica et Biophysica Acta (BBA) Biomembranes, vol. 1778(10), 1978–2021.

Koopman, W. J., Visch, H. J., Smeitink, J. A., & Willems, P. H. (2006). Simultaneous quantitative measurement and automated analysis of mitochondrial morphology, mass, potential, and motility in living human skin fibroblasts. Cytometry Part A: the journal of the International Society for Analytical Cytology, 69(1), 1-12.

Kratzer, J. T., Lanaspa, M. A., Murphy, M. N., Cicerchi, C., Graves, C. L., Tipton, P. A., & Gaucher, E. A. (2014). Evolutionary history and metabolic insights of ancient mammalian uricases. Proceedings of the National Academy of Sciences, 111(10), 3763-3768.

Kröncke, K. D., Fehsel, K., & Kolb-Bachofen, V. (1998). Inducible nitric oxide synthase in human diseases. Clinical and experimental immunology, 113(2), 147–156.

Kulkarni, S. S., Joffraud, M., Boutant, M., Ratajczak, J., Gao, A. W., Maclachlan, C., & Cantó, C. (2016). Mfn1 deficiency in the liver protects against diet-induced insulin resistance and enhances the hypoglycemic effect of metformin. Diabetes, 65(12), 3552-3560.

Kumar, R., Zakharov, M. N., Khan, S. H., Miki, R., Jang, H., Toraldo, G., & Jasuja, R. (2011). The dynamic structure of the estrogen receptor. Journal of amino acids, 2011.

Kuroda, J., Nakagawa, K., Yamasaki, T., Nakamura, K., Takeya, R., Kuribayashi, F., ImajohOhmi, S., Igarashi, K., Shibata, Y., Sueishi, K., et al. (2005). The superoxide-producing NAD(P)Hoxidase Nox4 in the nucleus of human vascular endothelial cells. Genes Cells 10, 1139–1151.

Ikeda, K., Shiba, S., Horie-Inoue, K., Shimokata, K., & Inoue, S. (2013). A stabilizing factor for mitochondrial respiratory supercomplex assembly regulates energy metabolism in muscle. Nature communications, 4(1), 1-9.

Labbé, K., Murley, A., & Nunnari, J. (2014). Determinants and functions of mitochondrial behavior. Annual review of cell and developmental biology, 30, 357-391.

Lagouge, M., Argmann, C., Gerhart-Hines, Z., Meziane, H., Lerin, C., Daussin, F., Messadeq, N., Milne, J., Lambert, P., Elliott, P., et al. (2006). Resveratrol improves mitochondrial function and protects against metabolic disease by activating SIRT1 and PGC-1alpha. Cell 127, 1109–1122.

Langley, R. R., & Fidler, I. J. (2011). The seed and soil hypothesis revisited—The role of tumor-stroma interactions in metastasis to different organs. International journal of cancer, 128(11), 2527-2535.

Lagranha, C. J., Silva, T. L. A., Silva, S. C. A., Braz, G. R. F., da Silva, A. I., Fernandes, M. P., & Sellitti, D. F. (2018). Protective effects of estrogen against cardiovascular disease mediated via oxidative stress in the brain. Life sciences, 192, 190-198.

Lagziel, S., Gottlieb, E., & Shlomi, T. (2020). Mind your media. Nature Metabolism, 1-4.

Lagziel, S., Lee, W. D., & Shlomi, T. (2019). Inferring cancer dependencies on metabolic genes from large-scale genetic screens. BMC biology, 17(1), 1-11.

Lane, A. N., Higashi, R. M., & Fan, T. W. (2019). Metabolic reprogramming in tumors: Contributions of the tumor microenvironment. Genes & diseases, 7(2), 185–198.

Larrea, D., Pera, M., Gonnelli, A., Quintana–Cabrera, R., Akman, H. O., Guardia-Laguarta, C., & Giacomello, M. (2019). MFN2 mutations in Charcot–Marie–Tooth disease alter mitochondria-associated ER membrane function but do not impair bioenergetics. Human molecular genetics, 28(11), 1782-1800.

Le Corre, L., Chalabi, N., Delort, L., Bignon, Y. J., & Bernard-Gallon, D. J. (2005). Resveratrol and breast cancer chemoprevention: molecular mechanisms. Molecular nutrition & food research, 49(5), 462-471.

Le, A., Cooper, C. R., Gouw, A. M., Dinavahi, R., Maitra, A., Deck, L. M., Royer, R. E., Vander Jagt, D. L., Semenza, G. L., & Dang, C. V. (2010). Inhibition of lactate dehydrogenase A induces oxidative stress and inhibits tumor progression. Proceedings of the National Academy of Sciences of the United States of America, 107(5), 2037–2042.

Lee, J. E., Westrate, L. M., Wu, H., Page, C., & Voeltz, G. K. (2016). Multiple dynamin family members collaborate to drive mitochondrial division. Nature, 540(7631), 139-143.

Lee, S. R., An, E. J., Kim, J., & Bae, Y. S. (2020). Function of NADPH oxidases in diabetic nephropathy and development of nox inhibitors. Biomolecules & therapeutics, 28(1), 25.

Leitman, D. C., Paruthiyil, S., Yuan, C., Herber, C. B., Olshansky, M., Tagliaferri, M., & Speed, T. P. (2012). Tissue-specific regulation of genes by estrogen receptors. In Seminars in reproductive medicine (Vol. 30, No. 01, pp. 14-22). Thieme Medical Publishers.

Leonard, A. P., Cameron, R. B., Speiser, J. L., Wolf, B. J., Peterson, Y. K., Schnellmann, R. G., & Rohrer, B. (2015). Quantitative analysis of mitochondrial morphology and membrane potential in living cells using high-content imaging, machine learning, and morphological binning. Biochimica et Biophysica Acta (BBA)-Molecular Cell Research, 1853(2), 348-360.

Levin, E. R. (2009). Plasma membrane estrogen receptors. Trends in Endocrinology & Metabolism, 20(10), 477-482.

Lewis, S. C., Uchiyama, L. F., & Nunnari, J. (2016). ER-mitochondria contacts couple mtDNA synthesis with mitochondrial division in human cells. Science, 353(6296).

Liesa, M., & Shirihai, O. S. (2013). Mitochondrial dynamics in the regulation of nutrient utilization and energy expenditure. Cell metabolism, 17(4), 491–506.

Liesa, M., Palacín, M., & Zorzano, A. (2009). Mitochondrial dynamics in mammalian health and disease. Physiological reviews, 89(3), 799-845.

Lin, C. Y., Vega, V. B., Thomsen, J. S., Zhang, T., Kong, S. L., Xie, M., & Yeo, A. (2007). Whole-genome cartography of estrogen receptor α binding sites. PLoS Genet, 3(6), e87.

Linkert, M., Rueden, C. T., Allan, C., Burel, J. M., Moore, W., Patterson, A., & Tarkowska, A. (2010). Metadata matters: access to image data in the real world. Journal of Cell Biology, 189(5), 777-782.

Lin, X., David, C. A., Donnelly, J. B., Michaelides, M., Chandel, N. S., Huang, X., & Shen, Y. (2008). A chemical genomics screen highlights the essential role of mitochondria in HIF-1 regulation. Proceedings of the National Academy of Sciences, 105(1), 174-179.

Liu, A. M., Qu, W. W., Liu, X., & Qu, C. K. (2012). Chromosomal instability in in vitro cultured mouse hematopoietic cells associated with oxidative stress. American journal of blood research, 2(1), 71.

Liu, T., Li, N., Yan, Y. Q., Liu, Y., Xiong, K., Liu, Y., & Liu, Z. D. (2020). Recent advances in the anti-aging effects of phytoestrogens on collagen, water content, and oxidative stress. Phytotherapy Research, 34(3), 435-447.

Liu, Y. J., McIntyre, R. L., Janssens, G. E., & Houtkooper, R. H. (2020). Mitochondrial fission and fusion: A dynamic role in aging and potential target for age-related disease. Mechanisms of Ageing and Development, 186, 111212.

Liu, Z., Jia, X., Duan, Y., Xiao, H., Sundqvist, K. G., Permert, J., & Wang, F. (2013). Excess glucose induces hypoxia-inducible factor-1α in pancreatic cancer cells and stimulates glucose metabolism and cell migration. Cancer biology & therapy, 14(5), 428–435.

Liu, X., Sun, J., Yuan, P., Shou, K., Zhou, Y., Gao, W., & Yang, J. (2019). Mfn2 inhibits proliferation and cell-cycle in Hela cells via Ras-NF-κB signal pathway. Cancer cell international, 19(1), 1-9.

López-Lluch, G., Irusta, P. M., Navas, P., & de Cabo, R. (2008). Mitochondrial biogenesis and healthy aging. Experimental gerontology, 43(9), 813-819.

López-Rodríguez, D. M., Kirillov, V., Krug, L. T., Mesri, E. A., & Andreansky, S. (2019). A role of hypoxia-inducible factor 1 alpha in Murine Gammaherpesvirus 68 (MHV68) lytic replication and reactivation from latency. PLoS pathogens, 15(12), e1008192.

Losón, O. C., Song, Z., Chen, H., & Chan, D. C. (2013). Fis1, Mff, MiD49, and MiD51 mediate Drp1 recruitment in mitochondrial fission. Molecular biology of the cell, 24(5), 659-667.

Lu, J., Tan, M., & Cai, Q. (2015). The Warburg effect in tumor progression: mitochondrial oxidative metabolism as an anti-metastasis mechanism. Cancer letters, 356(2), 156-164.

Lucey, B. P., Nelson-Rees, W. A., & Hutchins, G. M. (2009). Henrietta Lacks, HeLa cells, and cell culture contamination. Archives of pathology & laboratory medicine, 133(9), 1463-1467.

Maddalena, L. A., Selim, S. M., Fonseca, J., Messner, H., McGowan, S., & Stuart, J. A. (2017). Hydrogen peroxide production is affected by oxygen levels in mammalian cell culture. Biochemical and biophysical research communications, 493(1), 246-251.

Mailloux R. J. (2015). Teaching the fundamentals of electron transfer reactions in mitochondria and the production and detection of reactive oxygen species. Redox biology, 4, 381–398.

Mailloux R. J. (2018). Mitochondrial Antioxidants and the Maintenance of Cellular Hydrogen Peroxide Levels. Oxidative medicine and cellular longevity, 2018, 7857251.

Mailloux, R. J., & Harper, M. E. (2012). Mitochondrial proticity and ROS signaling: lessons from the uncoupling proteins. Trends in Endocrinology & Metabolism, 23(9), 451-458.

Maleki, J., Nourbakhsh, M., Shabani, M., Korani, M., Nourazarian, S. M., Dahaghi, M. R. O., & Moghadasi, M. H. (2015). 17β-estradiol stimulates generation of reactive species oxygen and nitric oxide in ovarian adenocarcinoma cells (OVCAR 3). Iranian journal of cancer prevention, 8(3).

Marcinek, D.J., Ciesielski, W.A., Conley, K.E., and Schenkman, K.A. (2003). Oxygen regulation and limitation to cellular respiration in mouse skeletal muscle in vivo. Am. J. Physiol. Heart Circ.Physiol. 285, H1900-8.

Martignoni, M., Groothuis, G. M., & de Kanter, R. (2006). Species differences between mouse, rat, dog, monkey and human CYP-mediated drug metabolism, inhibition and induction. Expert opinion on drug metabolism & toxicology, 2(6), 875-894.

Mas-Bargues, C., Viña-Almunia, J., Inglés, M., Sanz-Ros, J., Gambini, J., Ibáñez-Cabellos, J. S., & Borrás, C. (2017). Role of p16INK4a and BMI-1 in oxidative stress-induced premature senescence in human dental pulp stem cells. Redox biology,12, 690-698.

Mattingly, K. A., Ivanova, M. M., Riggs, K. A., Wickramasinghe, N. S., Barch, M. J., & Klinge, C. M. (2008). Estradiol stimulates transcription of nuclear respiratory factor-1 and increases mitochondrial biogenesis. Molecular Endocrinology, 22(3), 609-622.

McKee, T. J., & Komarova, S. V. (2017). Is it time to reinvent basic cell culture medium? American journal of physiology. Cell physiology, 312(5), C624–C626.

McKeown, S. R. (2014). Defining normoxia, physoxia and hypoxia in tumours—implications for treatment response. The British journal of radiology,87(1035), 20130676.

Meacham, C. E., & Morrison, S. J. (2013). Tumour heterogeneity and cancer cell plasticity. Nature, 501(7467), 328–337.

Meitzler, J. L., Makhlouf, H. R., Antony, S., Wu, Y., Butcher, D., Jiang, G.,.& Doroshow, J. H. (2017). Decoding NADPH oxidase 4 expression in human tumors.Redox biology, 13, 182-195.

Meng, X., Zhou, J., Zhao, C. N., Gan, R. Y., & Li, H. B. (2020). Health Benefits and Molecular Mechanisms of Resveratrol: A Narrative Review. Foods (Basel, Switzerland), 9(3), 340.

Metcalf D. (2008). Hematopoietic cytokines. Blood, 111(2), 485–491.

Mihaylova, M. M., Cheng, C. W., Cao, A. Q., Tripathi, S., Mana, M. D., Bauer-Rowe, K. E.,& Yilmaz, Ö. H. (2018). Fasting activates fatty acid oxidation to enhance intestinal stem cell function during homeostasis and aging. Cell stem cell, 22(5), 769-778.

Milanesi, L., Vasconsuelo, A., de Boland, A. R., & Boland, R. (2009). Expression and subcellular distribution of native estrogen receptor β in murine C2C12 cells and skeletal muscle tissue. Steroids, 74(6), 489-497.

Miller AA, Drummond GR, Mast AE, Schmidt HH, and Sobey CG (2007) Effect of gender on NADPH-oxidase activity, expression, and function in the cerebral circulation: role of estrogen. Stroke 38:2142–2149.

Mirabelli, P., Coppola, L., & Salvatore, M. (2019). Cancer cell lines are useful model systems for medical research. Cancers 11, 1098.

Mitchell, P. (1966). Chemiosmotic coupling in oxidative and photosynthetic phosphorylation. 445-502.

Mitra K, Wunder C, Roysam B, Lin G, Lippincott-Schwartz J. (2009).A hyperfused mitochondrial state achieved at G1-S regulates cyclin E buildup and entry into S phase. Proc Natl Acad Sci USA 106:11960-11965.

Monje, P., & Boland, R. (2001). Subcellular distribution of native estrogen receptor α and β isoforms in rabbit uterus and ovary. Journal of cellular biochemistry, 82(3), 467-479.

Moor, A. N., Flynn, J. M., Gottipati, S., Giblin, F. J., & Cammarata, P. R. (2005). 17β-estradiol stimulates MAPK signaling pathway in human lens epithelial cell cultures preventing

collapse of mitochondrial membrane potential during acute oxidative stress. Mitochondrion, 5(4), 235-247.

Moradi, F., Moffatt, C., & Stuart, J. A. (2021). The Effect of Oxygen and Micronutrient Composition of Cell Growth Media on Cancer Cell Bioenergetics and Mitochondrial Networks. Biomolecules, 11(8), 1177.

Moradi, F., Fiocchetti, M., Marino, M., Moffatt, C., & Stuart, J. A. (2021). Media composition and O2 levels determine effects of 17β-estradiol and selective estrogen receptor modulators on mitochondrial bioenergetics and cellular reactive oxygen species. American Journal of Physiology-Cell Physiology, 321(7), C72-C81.

Moreno, A. J., Moreira, P. I., Custódio, J. B., & Santos, M. S. (2013). Mechanism of inhibition of mitochondrial ATP synthase by 17β− Estradiol.Journal of bioenergetics and biomembranes, 45(3), 261-270.

Motylewska, E., Stasikowska, O., & Mełeń-Mucha, G. (2009). The inhibitory effect of diarylpropionitrile, a selective agonist of estrogen receptor beta, on the growth of MC38 colon cancer line. Cancer Letters, 276(1), 68-73.

Muir, A., Danai, L. V., Gui, D. Y., Waingarten, C. Y., & Vander Heiden, M. G. (2017). Environmental cystine drives glutamine anaplerosis and sensitizes cells to glutaminase inhibition. bioRxiv, 126631.

Munro, D., & Treberg, J. R. (2017). A radical shift in perspective: mitochondria as regulators of reactive oxygen species. Journal of Experimental Biology, 220(7), 1170-1180.

Murley, A., & Nunnari, J. (2016). The Emerging Network of Mitochondria-Organelle Contacts. Molecular cell,61(5), 648–653.

Murphy, M.P. (2009). How mitochondria produce reactive oxygen species. Biochem. J. 417, 1– 13.

Nagashima, S., Tábara, L. C., Tilokani, L., Paupe, V., Anand, H., Pogson, J. H., & Prudent, J. (2020). Golgi-derived PI (4) P-containing vesicles drive late steps of mitochondrial division. Science, 367(6484), 1366-1371.

Narendra, D., Tanaka, A., Suen, D.-F., and Youle, R.J. (2008). Parkin is recruited selectively to impaired mitochondria and promotes their autophagy. J. Cell Biol. 183, 795–803.

Nicholls, D. G. (2008). Forty years of Mitchell's proton circuit: From little grey books to little grey cells. Biochimica et Biophysica Acta (BBA)-Bioenergetics, 1777(7-8), 550-556.

Nickel, A. G., Von Hardenberg, A., Hohl, M., Löffler, J. R., Kohlhaas, M., Becker, J., & Maack, C. (2015). Reversal of mitochondrial transhydrogenase causes oxidative stress in heart failure. Cell metabolism, *22*(3), 472-484.

.

Nilsen, J., & Brinton, R. D. (2004). Mitochondria as therapeutic targets of estrogen action in the central nervous system. Current Drug Targets-CNS & Neurological Disorders, 3(4), 297-313.

Nisimoto, Y., Diebold, B. A., Cosentino-Gomes, D., & Lambeth, J. D. (2014). Nox4: a hydrogen peroxide-generating oxygen sensor. Biochemistry, 53(31), 5111-5120.

Nolfi-Donegan, D., Braganza, A., & Shiva, S. (2020). Mitochondrial Electron Transport: Oxidative Phosphorylation, Mitochondrial Oxidant Production, and Methods of Measurement. Redox Biology, 101674.

Okoh, V. O., Felty, Q., Parkash, J., Poppiti, R., & Roy, D. (2013). Reactive oxygen species via redox signaling to PI3K/AKT pathway contribute to the malignant growth of 4-hydroxy estradiol-transformed mammary epithelial cells. PloS one, 8(2), e54206.

Olichon, A., Baricault, L., Gas, N., Guillou, E., Valette, A., Belenguer, P., & Lenaers, G. (2003). Loss of OPA1 perturbates the mitochondrial inner membrane structure and integrity, leading to cytochrome c release and apoptosis. Journal of Biological Chemistry, 278(10), 7743-7746.

Orallo, F., Álvarez, E., Camiña, M., Leiro, J. M., Gómez, E., & Fernández, P. (2002). The possible implication of trans-resveratrol in the cardioprotective effects of long-term moderate wine consumption. Molecular pharmacology, 61(2), 294-302.

Oshima, N., Ishida, R., Kishimoto, S., Beebe, K., Brender, J. R., Yamamoto, K., Urban, D., Rai, G., Johnson, M. S., Benavides, G., Squadrito, G. L., Crooks, D., Jackson, J., Joshi, A., Mott, B. T., Shrimp, J. H., Moses, M. A., Lee, M. J., Yuno, A., Lee, T. D., Neckers, L. M. (2020). Dynamic Imaging of LDH Inhibition in Tumors Reveals Rapid In Vivo Metabolic Rewiring and Vulnerability to Combination Therapy. Cell reports, 30(6), 1798–1810.e4.

Parrinello, S., Samper, E., Krtolica, A., Goldstein, J., Melov, S., & Campisi, J. (2003). Oxygen sensitivity severely limits the replicative lifespan of murine fibroblasts. Nature cell biology, 5(8), 741–747.

Palomera-Avalos, V., Griñán-Ferré, C., Puigoriol-Ilamola, D., Camins, A., Sanfeliu, C., Canudas, A. M., & Pallàs, M. (2017). Resveratrol Protects SAMP8 Brain Under Metabolic Stress: Focus on Mitochondrial Function and Wnt Pathway. Molecular neurobiology, 54(3), 1661–1676.

Panday, A., Sahoo, M. K., Osorio, D., & Batra, S. (2015). NADPH oxidases: an overview from structure to innate immunity-associated pathologies.Cellular & molecular immunology, 12(1), 5-23.

Panza, S., Santoro, M., De Amicis, F., Morelli, C., Passarelli, V., D'Aquila, P., & Aquila, S. (2017). Estradiol via estrogen receptor beta influences ROS levels through the transcriptional regulation of SIRT3 in human seminoma TCam-2 cells. Tumor Biology, 39(5), 1010428317701642.

Parascandolo, A., & Laukkanen, M. O. (2019). Carcinogenesis and reactive oxygen species signaling: Interaction of the NADPH oxidase NOX1–5 and superoxide dismutase 1–3 signal transduction pathways. Antioxidants & redox signaling, 30(3), 443-486.

Parkash, J., Felty, Q., & Roy, D. (2006). Estrogen exerts a spatial and temporal influence on reactive oxygen species generation that precedes calcium uptake in high-capacity mitochondria: implications for rapid nongenomic signaling of cell growth. Biochemistry, 45(9), 2872-2881.

Park, D. W., Baek, K., Kim, J. R., Lee, J. J., Ryu, S. H., Chin, B. R., & Baek, S. H. (2009). Resveratrol inhibits foam cell formation via NADPH oxidase 1-mediated reactive oxygen species and monocyte chemotactic protein-1. Experimental & molecular medicine, 41(3), 171-179.

Parrinello, S., Samper, E., Krtolica, A., Goldstein, J., Melov, S., & Campisi, J. (2003). Oxygen sensitivity severely limits the replicative lifespan of murine fibroblasts. Nature cell biology, 5(8), 741-747.

Peng, K., Tao, Y., Zhang, J., Wang, J., Ye, F., Dan, G., & Zou, Z. (2016). Resveratrol regulates mitochondrial biogenesis and fission/fusion to attenuate rotenone-induced neurotoxicity. Oxidative medicine and cellular longevity, 2016.

Peng, K., Tao, Y., Zhang, J., Wang, J., Ye, F., Dan, G., Zhao, Y., Cai, Y., Zhao, J., Wu, Q., Zou, Z., Cao, J., & Sai, Y. (2016). Resveratrol Regulates Mitochondrial Biogenesis and Fission/Fusion to Attenuate Rotenone-Induced Neurotoxicity.

Pertea, M., Pertea, G. M., Antonescu, C. M., Chang, T. C., Mendell, J. T., & Salzberg, S. L. (2015). StringTie enables improved reconstruction of a transcriptome from RNA-seq reads. Nature biotechnology, 33(3), 290-295.

Pires, A. O., Neves-Carvalho, A., Sousa, N., & Salgado, A. J. (2014). The secretome of bone marrow and Wharton jelly derived mesenchymal stem cells induces differentiation and neurite outgrowth in SH-SY5Y cells. Stem cells international, 2014.

Piperigkou, Z., Manou, D., Karamanou, K., & Theocharis, A. D. (2018). Strategies to target matrix metalloproteinases as therapeutic approach in cancer. Methods Mol Biol, 1731, 325-348.

Plitzko, B., & Loesgen, S. (2018). Measurement of oxygen consumption rate (OCR) and extracellular acidification rate (ECAR) in culture cells for assessment of the energy metabolism. Bio-protocol, 8(10), e2850-e2850.

Prabakaran, S., Lippens, G., Steen, H., & Gunawardena, J. (2012). Post-translational modification: nature's escape from genetic imprisonment and the basis for dynamic information encoding. Wiley Interdisciplinary Reviews: Systems Biology and Medicine, *4*(6), 565-583.

Quinlan, C.L., Perevoshchikova, I. V., Hey-Mogensen, M., Orr, A.L., and Brand, M.D. (2013). Sites of reactive oxygen species generation by mitochondria oxidizing different substrates. Redox Biol. 1, 304–312.

Radi, R. (2018). Oxygen radicals, nitric oxide, and peroxynitrite: Redox pathways in molecular medicine. Proceedings of the National Academy of Sciences, 115(23), 5839-5848.

Rao, A. K., Dietrich, A. K., Ziegler, Y. S., & Nardulli, A. M. (2011). 17β-Estradiol-mediated increase in Cu/Zn superoxide dismutase expression in the brain: a mechanism to protect neurons from ischemia. The Journal of steroid biochemistry and molecular biology, 127(3-5), 382-389.

Razmara, A., Duckles, S. P., Krause, D. N., & Procaccio, V. (2007). Estrogen suppresses brain mitochondrial oxidative stress in female and male rats. Brain research, 1176, 71-81.

Rehman, J., Zhang, H. J., Toth, P. T., Zhang, Y., Marsboom, G., Hong, Z., Salgia, R., Husain, A. N., Wietholt, C., & Archer, S. L. (2012). Inhibition of mitochondrial fission prevents cell cycle progression in lung cancer. The FASEB Journal, 25(5), 2175–2186.

Rehman, J., Zhang, H. J., Toth, P. T., Zhang, Y., Marsboom, G., Hong, Z., & Archer, S. L. (2012). Inhibition of mitochondrial fission prevents cell cycle progression in lung cancer. The FASEB Journal, 26(5), 2175-2186.

Rengasamy, A., & Johns, R. A. (1996). Determination of Km for oxygen of nitric oxide synthase isoforms. Journal of Pharmacology and Experimental Therapeutics, 276(1), 30-33.

Rezende F, Lowe O, Helfinger V, Prior K-K, Walter M, Zukunft S, Fleming I, Weissmann N, Brandes RP, Schroder K (2016) Unchanged NADPH oxidase activity in Nox1-Nox2-Nox4 triple knockout mice – what do NADPH-stimulated chemiluminescence assays really detect? Antiox Redox Signal 24:392-399.

Rezende F, Prior K-K, Lowe O, Wittig I, Strecker V, Moll F, Helfinger V, Schnutgen F, Kurrle N, Wempe F, Walter M, Zukunft S, Luck B, Fleming I, Weissmann N, Brandes RP, Schroder K (2017). Cytochrome P450 enzymes but not NADPH oxidases are the source of NADPH-dependent lucigenin chemiluminescence in membrane assays. Free Radic Biol Med 102:57-66.

Robb, E. L., & Stuart, J. A. (2011). Resveratrol interacts with estrogen receptor-β to inhibit cell replicative growth and enhance stress resistance by upregulating mitochondrial superoxide dismutase. Free Radical Biology and Medicine, 50(7), 821-831.

Robb, E. L., & Stuart, J. A. (2014). The stilbenes resveratrol, pterostilbene and piceid affect growth and stress resistance in mammalian cells via a mechanism requiring estrogen receptor beta and the induction of Mn-superoxide dismutase.Phytochemistry, 98, 164-173.

Rodriguez, A. E., Ducker, G. S., Billingham, L. K., Martinez, C. A., Mainolfi, N., Suri, V., & Chandel, N. S. (2019). Serine metabolism supports macrophage IL-1β production. Cell metabolism, 29(4), 1003-1011.

Ronda, A. C., Vasconsuelo, A., & Boland, R. (2013). 17β-estradiol protects mitochondrial functions through extracellular-signal-regulated kinase in C2C12 muscle cells. Cellular Physiology and Biochemistry, 32(4), 1011-1023.

Rossignol, R., Gilkerson, R., Aggeler, R., Yamagata, K., Remigton, S.J., and Capaldi, R.A. (2004). Energy substrate modulates mitochondrial structures and oxidative capacityin cancer cells. Cancer Res. 64, 985–993.

Rossiter, N. J., Huggler, K. S., Adelmann, C. H., Keys, H. R., Soens, R. W., Sabatini, D. M., & Cantor, J. R. (2021). CRISPR screens in physiologic medium reveal conditionally essential genes in human cells. Cell Metabolism, 33(6), 1248-1263

Sabouny, R., & Shutt, T. E. (2020). Reciprocal Regulation of Mitochondrial Fission and Fusion. Trends in Biochemical Sciences.

Salazar-Roa, M., & Malumbres, M. (2017). Fueling the Cell Division Cycle.Trends in cell biology, 27(1), 69–81.

Saito, H., Hammond, A. T., & Moses, R. E. (1995). The effect of low oxygen tension on the in vitro-replicative life span of human diploid fibroblast cells and their transformed derivatives. Experimental cell research, 217(2), 272-279.

Sastre-Serra J, Nadal-Serrano M, Pons DG, Roca P, Oliver J (2013). The over-expression of Erbeta modifies estradiol effects on mitochondrial dynamics in breast cancer cell line. Int J Biochem Cell Biol 45:1509-1515.

Sastre-Serra J, Nadal-Serrano M, Pons DG, Roca P, Oliver J. (2012). Mitochondrial dynamics is affected by 17beta-estradiol in the MCF-7 breast cancer cell line. Effects on fusion and fission related genes. Int J Biochem Cell Biol 44(11):1901-1905.

Savoia, P., Raina, G., Camillo, L., Farruggio, S., Mary, D., Veronese, F., & Grossini, E. (2018). Anti-oxidative effects of 17 β-estradiol and genistein in human skin fibroblasts and keratinocytes. Journal of dermatological science, 92(1), 62-77.

Sbert-Roig, M., Bauzá-Thorbrügge, M., Galmés-Pascual, B. M., Capllonch-Amer, G., García-Palmer, F. J., Lladó, I., & Gianotti, M. (2016). GPER mediates the effects of 17β-estradiol in cardiac mitochondrial biogenesis and function. Molecular and cellular endocrinology, 420, 116-124.

Sbert-Roig, M., Galmes-Pascual, B. M., Proenza, A. M., Llado, I., Gianotti, M., & Garcia-Palmer, F. J. (2014). Estradiol stimulates mitochondrial biogenesis and adiponectin expression in skeletal muscle. J Endocrinol, 221(3), 391-403.

Schieke, S. M., Ma, M., Cao, L., McCoy, J. P., Liu, C., Hensel, N. F., & Finkel, T. (2008). Mitochondrial metabolism modulates differentiation and teratoma formation capacity in mouse embryonic stem cells. Journal of Biological Chemistry, 283(42), 28506-28512.

Schindelin, J., Arganda-Carreras, I., Frise, E., Kaynig, V., Longair, M., Pietzsch, T., & Tinevez, J. Y. (2012). Fiji: an open-source platform for biological-image analysis. Nature methods, 9(7), 676-682.

Schmid, S. L., & Frolov, V. A. (2011). Dynamin: functional design of a membrane fission catalyst. Annual review of cell and developmental biology, 27, 79-105.

Sebastián, D., Hernández-Alvarez, M. I., Segalés, J., Sorianello, E., Muñoz, J. P., Sala, D.,& Zorzano, A. (2012). Mitofusin 2 (Mfn2) links mitochondrial and endoplasmic reticulum function with insulin signaling and is essential for normal glucose homeostasis. Proceedings of the National Academy of Sciences, 109(14), 5523-5528.

Semenza G. L. (2014). Hypoxia-inducible factor 1 and cardiovascular disease. Annual review of physiology, 76, 39–56.

Sena, L. A., & Chandel, N. S. (2012). Physiological roles of mitochondrial reactive oxygen species. Molecular cell, 48(2), 158–167.

Schilder, Y. D., Heiss, E. H., Schachner, D., Ziegler, J., Reznicek, G., Sorescu, D., & Dirsch, V. M. (2009). NADPH oxidases 1 and 4 mediate cellular senescence induced by resveratrol in human endothelial cells. Free Radical Biology and Medicine, 46(12), 1598-1606.

Shanmugasundaram, K., Nayak, B. K., Friedrichs, W. E., Kaushik, D., Rodriguez, R., & Block, K. (2017). NOX4 functions as a mitochondrial energetic sensor coupling cancer metabolic reprogramming to drug resistance. Nature communications, 8(1), 1-16.

Sheng, Y., Abreu, I. A., Cabelli, D. E., Maroney, M. J., Miller, A. F., Teixeira, M., & Valentine, J. S. (2014). Superoxide dismutases and superoxide reductases. Chemical reviews, 114(7), 3854-3918.

Sheu, S. J., Liu, N. C., Ou, C. C., Bee, Y. S., Chen, S. C., Lin, H. C., & Chan, J. Y. (2013). Resveratrol stimulates mitochondrial bioenergetics to protect retinal pigment epithelial cells from oxidative damage. Investigative Ophthalmology & Visual Science, 54(9), 6426-6438.

Shoemaker, R. H. (2006). The NCI60 human tumour cell line anticancer drug screen. Nature Reviews Cancer, 6(10), 813-823.

Schug, Z. T., Peck, B., Jones, D. T., Zhang, Q., Grosskurth, S., Alam, I. S., & Gottlieb, E. (2015). Acetyl-CoA synthetase 2 promotes acetate utilization and maintains cancer cell growth under metabolic stress. Cancer cell, 27(1), 57-71.

Shutt, T., Geoffrion, M., Milne, R., & McBride, H. M. (2012). The intracellular redox state is a core determinant of mitochondrial fusion. EMBO reports, 13(10), 909-915.

Siekevitz, P. (1957). Powerhouse of the cell. Scientific American, 197(1), 131-144.

Sies, H. (2017). Hydrogen peroxide as a central redox signaling molecule in physiological oxidative stress: Oxidative eustress. Redox Biol. 11, 613–619.

Sies, H., & Jones, D. P. (2020). Reactive oxygen species (ROS) as pleiotropic physiological signalling agents. Nature reviews Molecular cell biology, 21(7), 363-383.

Simpson, E., & Santen, R. J. (2015). Celebrating 75 years of oestradiol. Journal of molecular endocrinology, 55(3), T1.

Spurlock, B., Gupta, P., Basu, M. K., Mukherjee, A., Hjelmeland, A. B., Darley-Usmar, V., & Mitra, K. (2019). Mito-SinCe2 Approach to Quantify Relationships between Mitochondrial Dynamics and Energetics status. bioRxiv, 537373.

Starkov, A. A., Fiskum, G., Chinopoulos, C., Lorenzo, B. J., Browne, S. E., Patel, M. S., & Beal, M. F. (2004). Mitochondrial alpha-ketoglutarate dehydrogenase complex generates reactive oxygen species.The Journal of neuroscience, the official journal of the Society for Neuroscience, 24(36), 7779–7788.

Steger C (1998). An unbiased detector of curvilinear structures. IEEE 1. Transactions on pattern analysis and machine intelligence, 20(2), 113-1257059966.

Stirone C, Duckles SP, Krause DN, Procaccio V. Estrogen increases mitochondrial efficiency and reduces oxidative stress in cerebral blood vessels (2005). Molecular pharmacology., 68, 959–965.

Storch TG. Oxygen concentration regulates 5-azacytidine-induced myogenesis in C3H/10T1/2cultures. Biochim Biophys Acta. 1990 Nov 12; 1055(2):126-9.

Strehlow, K., Rotter, S., Wassmann, S., Adam, O., Grohé, C., Laufs, K., & Nickenig, G. (2003). Modulation of antioxidant enzyme expression and function by estrogen. Circulation research, 93(2), 170-177.

Stuart, J. A., & Robb, E. L. (2013). Bioactive polyphenols from wine grapes (Vol. 457). New York, NY: Springer.

Stuart, J. A., Aibueku, O., Bagshaw, O., & Moradi, F. (2019). Hypoxia inducible factors as mediators of reactive oxygen/nitrogen species homeostasis in physiological normoxia. Medical hypotheses, 129, 109249.

Stuart, J. A., Fonseca, J., Moradi, F., Cunningham, C., Seliman, B., Worsfold, C. R., Dolan, S., Abando, J., & Maddalena, L. A. (2018). How Supraphysiological Oxygen Levels in Standard Cell Culture Affect Oxygen-Consuming Reactions. Oxidative medicine and cellular longevity, 2018, 8238459.

Sullivan, M. R., Danai, L. V., Lewis, C. A., Chan, S. H., Gui, D. Y., Kunchok, T., Dennstedt, E. A., Vander Heiden, M. G., & Muir, A. (2019). Quantification of microenvironmental metabolites in murine cancers reveals determinants of tumor nutrient availability. eLife, 8, e44235.

Taguchi, N., Ishihara, N., Jofuku, A., Oka, T., & Mihara, K. (2007). Mitotic phosphorylation of dynamin-related GTPase Drp1 participates in mitochondrial fission. Journal of Biological Chemistry, 282(15), 11521-11529.

Teixeira, F. G., Panchalingam, K. M., Anjo, S. I., Manadas, B., Pereira, R., Sousa, N., & Behie, L. A. (2015). Do hypoxia/normoxia culturing conditions change the neuroregulatory profile of Wharton Jelly mesenchymal stem cell secretome? Stem Cell Research & Therapy, 6(1), 1-14.

Tilokani, L., Nagashima, S., Paupe, V., & Prudent, J. (2018). Mitochondrial dynamics: Overview of molecular mechanisms. In Essays in Biochemistry; 62(3), 341-360.

Timpano, S., Guild, B.D., Specker, E.J., Melanson, G., Medeiros, P.J., Sproul, S.L.J., and Uniacke, J. (2019). Physioxic human cell culture improves viability, metabolism, and mitochondrial morphology while reducing DNA damage. FASEB J. fj201802279R.

Tormos, K. V., Anso, E., Hamanaka, R. B., Eisenbart, J., Joseph, J., Kalyanaraman, B., & Chandel, N. S. (2011). Mitochondrial complex III ROS regulate adipocyte differentiation. Cell metabolism, 14(4), 537-544.

Torres, M. J., Ryan, T. E., Lin, C. T., Zeczycki, T. N., & Neufer, P. D. (2018). Impact of 17β-estradiol on complex I kinetics and H2O2 production in liver and skeletal muscle mitochondria. Journal of Biological Chemistry, 293(43), 16889-16898.

Tarazona, S., Furió-Tarí, P., Turrà, D., Pietro, A. D., Nueda, M. J., Ferrer, A., & Conesa, A. (2015). Data quality aware analysis of differential expression in RNA-seq with NOISeq R/Bioc package. Nucleic acids research, 43(21), e140-e140.

Tremblay, G. B., Tremblay, A., Labrie, F., & Giguère, V. (1999). Dominant activity of activation function 1 (AF-1) and differential stoichiometric requirements for AF-1 and-2 in the estrogen receptor α-β heterodimeric complex. Molecular and cellular biology, 19(3), 1919-1927.

Trevisan, R., Mello, D. F., Uliano-Silva, M., Delapedra, G., Arl, M., & Dafre, A. L. (2014). The biological importance of glutathione peroxidase and peroxiredoxin backup systems in bivalves during peroxide exposure. Marine environmental research,*101*, 81-90.

Trinh, H. V., Grossmann, J., Gehrig, P., Roschitzki, B., Schlapbach, R., Greber, U. F., & Hemmi, S. (2013). iTRAQ-based and label-free proteomics approaches for studies of human adenovirus infections. International journal of proteomics, 2013.

Truong, V.-L., Jun, M., and Jeong, W.-S. (2018). Role of resveratrol in regulation of cellular defense systems against oxidative stress. Biofactors 44, 36–49.

Tsai, C. C., Chen, Y. J., Yew, T. L., Chen, L. L., Wang, J. Y., Chiu, C. H., & Hung, S. C. (2011). Hypoxia inhibits senescence and maintains mesenchymal stem cell properties through down-regulation of E2A-p21 by HIF-TWISBlood, The Journal of the American Society of Hematology, 117(2), 459-469.

Van Buul, J. D., Fernandez-Borja, M., Anthony, E. C., & Hordijk, P. L. (2005). Expression and localization of NOX2 and NOX4 in primary human endothelial cells. Antioxidants & redox signaling, 7(3-4), 308–317.

Van Gent, D. C., Hoeijmakers, J. H., & Kanaar, R. (2001). Chromosomal stability and the DNA double-stranded break connection. Nature Reviews Genetics, 2(3), 196-206.

Vaneev, A. N., Gorelkin, P. V., Garanina, A. S., Lopatukhina, H. V., Vodopyanov, S. S., Alova, A. V., & Erofeev, A. S. (2020). In vitro and in vivo electrochemical measurement of reactive oxygen species after treatment with anticancer drugs. Analytical Chemistry, 92(12), 8010-8014.

Varanita, T., Soriano, M. E., Romanello, V., Zaglia, T., Quintana-Cabrera, R., Semenzato, M., & Viscomi, C. (2015). The OPA1-dependent mitochondrial cristae remodeling pathway controls atrophic, apoptotic, and ischemic tissue damage. Cell metabolism, 21(6), 834-844.

Villa, A., Vegeto, E., Poletti, A., & Maggi, A. (2016). Estrogens, neuroinflammation, and neurodegeneration. Endocrine reviews, 37(4), 372-402.

Vogel, C., & Marcotte, E. M. (2012). Insights into the regulation of protein abundance from proteomic and transcriptomic analyses. Nature reviews genetics, 13(4), 227-232.

Vono, R., Jover Garcia, E., Spinetti, G., & Madeddu, P. (2018). Oxidative stress in mesenchymal stem cell senescence: regulation by coding and noncoding RNAs. Antioxidants & Redox Signaling, 29(9), 864-879.

Voorde, J. V., Ackermann, T., Pfetzer, N., Sumpton, D., Mackay, G., Kalna, G., & Tardito, S. (2019). Improving the metabolic fidelity of cancer models with a physiological cell culture medium. Science advances, 5(1), eaau7314.

Wagner T., & Hiner, M.Thorstenwagner/ij-ridgedetection: 2017 Ridge Detection 1.4. 0

Wallerath, T., Deckert, G., Ternes, T., Anderson, H., Li, H., Witte, K., & Förstermann, U. (2002). Resveratrol, a polyphenolic phytoalexin present in red wine, enhances expression and activity of endothelial nitric oxide synthase. Circulation, 106(13), 1652-1658.

Wallerath, T., Li, H., Gödtel-Ambrust, U., Schwarz, P. M., & Förstermann, U. (2005). A blend of polyphenolic compounds explains the stimulatory effect of red wine on human endothelial NO synthase. Nitric oxide, 12(2), 97-104.

Wallerath, T., Poleo, D., Li, H., & Förstermann, U. (2003). Red wine increases the expression of human endothelial nitric oxide synthase: a mechanism that may contribute to its beneficial cardiovascular effects. Journal of the American College of Cardiology, 41(3), 471-478.

Walsh, G. (2018). Biopharmaceutical benchmarks 2018. Nature biotechnology, 36(12), 1136-1145.

Wang, C. Y., Liu, L. N., & Zhao, Z. B. (2013). The role of ROS toxicity in spontaneous aneuploidy in cultured cells. Tissue and Cell, 45(1), 47-53.

Wang, J., Green, P. S., & Simpkins, J. W. (2001). Estradiol protects against ATP depletion, mitochondrial membrane potential decline and the generation of reactive oxygen species induced by 3-nitroproprionic acid in SK-N-SH human neuroblastoma cells. Journal of neurochemistry, 77(3), 804-811.

Wang, W., He, Q., Yan, W., Sun, J., Chen, Z., Liu, Z., Lu, Z., Hou, J., Shao, Y., Zhou, X., & Wang, A. (2017). High glucose enhances the metastatic potential of tongue squamous cell carcinoma via the PKM2 pathway. Oncotarget, 8(67), 111770–111779.

Weiskirchen, S., & Weiskirchen, R. (2016). Resveratrol: how much wine do you have to drink to stay healthy? Advances in Nutrition, 7(4), 706-718.

Wenger, R.H., Kurtcuoglu, V., Scholz, C.C., Marti, H.H., and Hoogewijs, D. (2015). Frequently asked questions in hypoxia research. Hypoxia 3, 35–43.

Westermann B (2010). Mitochondrial fusion and fission in cell life and death. Nature Rev Moll Cell Biol 11(12):872-884.

Willems PH, Rossignol R, Dieteren CE, Murphy MP, Koopman WJ (2015) Redox homeostasis and mitochondrial dynamics. Cell Metab 22:207-218.

Wong, H. S., Dighe, P. A., Mezera, V., Monternier, P. A., & Brand, M. D. (2017). Production of superoxide and hydrogen peroxide from specific mitochondrial sites under different bioenergetic conditions. Journal of Biological Chemistry, 292(41), 16804-16809.

Wu, Z., Liu, B., E, C., Liu, J.J., Zhang, Q., L Resveratrol inhibits the proliferation of human and apoptosis. Mol. Med. Rep. 11, 400–404.

Xia, N., Daiber, A., Förstermann, U., & Li, H. (2017). Antioxidant effects of resveratrol in the cardiovascular system. British journal of pharmacology, 174(12), 1633-1646.

Xie, H., Hanai, J., Ren, J. G., Kats, L., Burgess, K., Bhargava, P., Signoretti, S., Billiard, J., Duffy, K. J., Grant, A., Wang, X., Lorkiewicz, P. K., Schatzman, S., Bousamra, M., 2nd, Lane, A. N., Higashi, R. M., Fan, T. W., Pandolfi, P. P., Sukhatme, V. P., & Seth, P. (2014). Targeting lactate dehydrogenase-a inhibits tumorigenesis and tumor progression in mouse models of lung cancer and impacts tumor-initiating cells. Cell metabolism, 19(5), 795–809.

Xu, Z., Huang, B., Liu, J., Wu, X., Luo, N., Wang, X., & Pan, X. (2018). Combinatorial anti-proliferative effects of tamoxifen and naringenin: The role of four estrogen receptor subtypes. Toxicology, 410, 231-246.

Yang, S. H., Sarkar, S. N., Liu, R., Perez, E. J., Wang, X., Wen, Y., & Simpkins, J. W. (2009). Estrogen receptor β as a mitochondrial vulnerability factor. Journal of Biological Chemistry, 284(14), 9540-9548.

Yao, T., & Asayama, Y. (2017). Animal-cell culture media: History, characteristics, and current issues. Reproductive medicine and biology, 16(2), 99-117.

Yao, X., Wigginton, J. G., Maass, D. L., Ma, L., Carlson, D., Wolf, S. E., & Zang, Q. S. (2014). Estrogen-provided cardiac protection following burn trauma is mediated through a reduction in mitochondria-derived DAMPs. American Journal of Physiology-Heart and Circulatory Physiology, 306(6), H882-H894.

Youle, R. J., & Van Der Bliek, A. M. (2012). Mitochondrial fission, fusion, and stress. Science, 337(6098), 1062-1065.

Yu, R., Jin, S. B., Lendahl, U., Nistér, M., & Zhao, J. (2019). Human Fis1 regulates mitochondrial dynamics through inhibition of the fusion machinery. The EMBO journal, 38(8), e99748.

Zhang, L., Pang, S., Deng, B., Qian, L., Chen, J., Zou, J., & Le, Y. (2012). High glucose induces renal mesangial cell proliferation and fibronectin expression through JNK/NF-κB/NADPH oxidase/ROS pathway, which is inhibited by resveratrol. The international journal of biochemistry & cell biology, 44(4), 629-638.

Zhang, J., & Zhang, Q. (2019). Using Seahorse Machine to Measure OCR and ECAR in Cancer Cells. Methods in molecular biology (Clifton, N.J.), 1928, 353–363.

Zhao, H., Niu, Q., Li, X., Liu, T., Xu, Y., Han, H., & Wang, Z. (2012). Long-term resveratrol consumption protects ovariectomized rats chronically treated with D-galactose from developing memory decline without effects on the uterus. Brain research, 1467, 67-80.

Zhao, R. Z., Jiang, S., Zhang, L., & Yu, Z. B. (2019). Mitochondrial electron transport chain, ROS generation and uncoupling. International journal of molecular medicine, 44(1), 3-15.

Zhou, Q., Huang, G., Yu, X., & Xu, W. (2018). A novel approach to estimate ROS origination by hyperbaric oxygen exposure, targeted probes and specific inhibitors. Cellular Physiology and Biochemistry, 47(5), 1800-1808.

Zhou, J., Pei, Y., Chen, G., Cao, C., Liu, J., Ding, C., & Niu, G. (2018). SPC24 Regulates breast cancer progression by PI3K/AKT signaling. Gene, 675, 272-277.

Zhou, T., Li, Y., Yang, L., Tang, T., Zhang, L., & Shi, J. (2017). Annexin A3 as a prognostic biomarker for breast cancer: a retrospective study. BioMed research international, 2017.